THE INFLUENCE OF AMINO ACID PROPERTIES ON THE ADSORPTION OF PROTEINS AND PEPTIDES TO STAINLESS STEEL SURFACES

A thesis submitted

in partial fulfilment of the requirements for the Degree of

Doctor of Philosophy

in Chemical and Process Engineering

University of Canterbury

New Zealand

NEHA CHANDRASEKARAN

March 2014

To my beloved Master, spiritual guide, teacher and friend Baba Gurinder Singh Dhillon

Abstract

Stainless steel (SS) is the material of choice in a number of process industries ranging from food and dairy to pharmaceuticals. Adsorption phenomena on SS surfaces are of paramount importance in these industries. For example, protein adsorption constitutes a major issue in process equipment, as the associated surface fouling decreases the efficiency of the overall process and leads to an increase in operational costs because of the need for regular cleaning. In addition, the adsorption of proteins at solid–liquid interfaces is an important research field with relevance in biosensor and biomaterial applications.

The primary aim of this thesis was to understand the underlying adsorption properties of selected protein onto SS surfaces and to identify the influence of specific amino acids on bio-fouling. Protein adsorption experiments were carried out on 316 grade SS sensors using a quartz crystal microbalance with dissipation (QCM-D). The proteins consisted of milk proteins (α-lactalbumin, β-lactoglobulin, α-casein, β-casein, κ-casein and bovine serum albumin), blood proteins (cytochrome-c, haemoglobin and myoglobin) and proteins of industrial and medical relevance (α-chymotrypsinogen, human recombinant insulin, lysozyme and papain). The adsorption characteristics of the test proteins were studied and an empirical correlation relating the amount of protein adsorbed to their physical properties was proposed. Adsorption onto a SS surface was followed on the QCM-D in real time and the amounts adsorbed calculated using the Sauerbrey model. In addition, the binding kinetics was modelled using different theoretical models to describe the adsorption mechanism. In all the proteins tested, the conformational change model was found to fit considerably well the adsorption data. Finally, the data collected were used to identify the physical properties of proteins that induce surface binding, with hydrophobic and aromatic amino acids having the most effect on binding.

A second aspect investigated in the present work was the determination of hydration water present in the adsorbed layer. In fact, water molecules, solvated ions and other small molecules in the vicinity of the surface all play an important role in protein adsorption and often constitute a large fraction of the total measured adsorbed mass. The fraction of water present on SS surfaces along with adsorbed proteins was determined using fluorescently labelled proteins through a comparative study that included QCM-D experiments as well as fluorescent light intensity measurements. The results were similar for all proteins tested, indicating that 32-45.8% of the total mass adsorbed composed of water.

One last aspect considered in this thesis was the influence of the putative adhesive amino acid 3, 4-dihydroxyphenylalanine (DOPA). DOPA residues are present in high levels in the adhesive proteins from marine mussels, hence are thought to facilitate surface attachment. The role of DOPA residues in mediating protein adhesion on SS surfaces was studied using QCM-D. Two repetitive peptide motifs extracted from the sequence of the mussel foot protein mefp-5, KGYKYYGGSS and KGYKYY, were selected for this study. The two peptides contained unmodified tyrosine (Y) residues, which were chemo-enzymatically modified to DOPA using mushroom tyrosinase. Adsorption of the two sequences on SS surfaces was tested before and after modification of tyrosine residues to DOPA. Conversion was linearly related to the incubation time of the peptide fragments with mushroom tyrosinase, Amount of DOPA formed was 70-99% of the tyrosine content in the peptides. QCM-D adsorption experiments on the DOPA-modified sequences revealed four-fold greater adhesion than for unmodified mefp-5 motifs, indicating the paramount role that DOPA has on the adsorption of peptides on 316 grade stainless steel.

Conferences and Publications

The adsorption of proteins on stainless steel surfaces was the main subject of this thesis. Modification of tyrosine to DOPA in peptide sequences and its influence on adhesion was also studied. The following papers and presentations have resulted from this work to date.

1) Chandrasekaran, N., Dimartino, S. and Fee, C.J. (2013) *Study of the adsorption of proteins on stainless steel surfaces using QCM-D.* Chemical Engineering Research and Design, **91**, 1674-83, September 2013.
2) Chandrasekaran, N., Dimartino, S. and Fee, C.J. (2012) *Adsorption of proteins on stainless steel surfaces.* Wellington, New Zealand: Chemeca2012, 23-26 September 2012. (Conference Contribution - Paper in published proceedings)
3) Chandrasekaran, N., Dimartino, S. and Fee, C.J. (2013) *Comparative study of dairy protein-associated water and its adsorption effects on stainless steel surfaces by fluorescent labelling and QCM-D*, (Conference presentation Chemeca2013)

Acknowledgements

"Although the road is never ending, take a step and keep walking – Rumi"

The end of the PhD journey has lead me to a new journey with a lot of learning and gratitude for everyone who has been a part of my life to make this dream turn into reality.

Conan,

You have been my role model throughout my PhD. Words would not do justice to thank you for your guidance and support to make this happen. I have learnt not only academically, but also learnt to unveil myself with your inspiration on leadership, time management and dedication.

Simone,

Your advice of "*Non Scholæ sed Vitæ Discimus*" – "*We do not learn for the school, but for life*" would remain embedded in my heart forever. Thank you very much for being an inspirational guide, good friend and support throughout this journey.

The research would not be successful without the guidance of Rayleen who has stretched herself and helped me immensely in the research. I would like to extend my warm gratitude to my research group mates Kannan, Prasanna, Balaji and Anton for their friendship during the happy and tough days of my research. John Abrahmanson, thank you for your advice on writing and constant encouragement during my whole thesis. The support received from Charlotte, Diandree and Swami for being there for me always will remain very close to my heart. Neeru and Lucas, thank you for the unconditional love, support and care through my writing phase.

The research would be incomplete without the guidance of Prof. Steven Gieseg, Biochemistry, School of Biological Sciences for the on the HPLC. Tejraj Janmale, thank you for your guidance through my experiments with the HPLC, for being my closest friend and extending your love and care through the past couple of years. Your constant encouragement, motivation and positive vibes have been very supportive.

My deepest gratitude to my beloved extended family who has put up with me through my anxieties – Grandpa, Grandma, Badimum, Ajay and Ashwin uncle, Bindu and Seema aunty, Nandu aunty, Hari uncle, Adhithi, Manikanth Kadri, Chandhoke cousins – Nikhil, Ayush, Aanchal, Anuditta, Aakarshan, Avyukth, Ayaan and Anika. To all my lovely girlfriends across

the sea, Subhapriya, Kadamabari and Janani to remain a strong pillar of support through this journey – thank you. Warren and Ethel, thank you for your love and encouragement from time to time.

This thesis would not have been possible without the unconditional support and immense love by my parents – Balu Chandrasekaran and Arthi Chandrasekaran. Both of you have been a pillar of support for me by moulding me to face the challenges – I could never thank you enough for inspiring, supporting and being there for me in every step of the way. My best friend, lovely little sister, angel and my research group mate now – Shradha Chandrasekaran, I would never be able to thank you for your encouragement and love throughout this phase. You are the best sister and I am blessed to have you as my sibling.

To my beloved Master, Gurinder Singh Dhillon – You have been the highest power of protection and love during this journey. You held me by my hand throughout the rough and tough roads, making me a stronger person and helping me to get back on track when things seemed impossible. Your optimism, humbleness, grace and presence have been there with me every single day. Expressing my love and gratitude in words for You, Master, would never be enough. I do not owe you this thesis alone but my very life.

Table of contents

List of Figures

List of Tables

Symbols and Abbreviations

Symbols

Ar	Cross-sectional area, m^2
Ala	Alanine
c	concentration of protein in solution, mg/mL
c*	Interfacial concentration of protein, mg/mL
c_{Tyr}^{in}	Initial concentration of tyrosine, mg/mL
c_{Tyr}^{fin}	Final concentration of tyrosine, mg/mL
c_{DOPA}^{fin}	Final concentration of DOPA, mg/mL
C_{SPR}	SPR instrument constant
d_f	Thickness, m
d_n/d_c	Refractive index change per unit protein concentration
Da	Damköhlar number
D_{expt}	Experimental diffusivity of protein, cm^2/s
D_{theo}	Theoretical diffusivity of protein, cm^2/s
Di	Diffusivity of protein, cm^2/s
ΔD	dissipation change, dimensionless
Glu	Glutamic acid
$E_{dissipated}$	Energy dissipated during one oscillation
E_{stored}	Energy stored in the oscillating system
Δf	resonant frequency change, Hz
f_0	fundamental frequency of the quartz sensor, Hz
Phe	Phenylalanine
Fe	Iron
Gly	Glycine
Ile	Isoleucine
k_a	Adsorption rate constant
k_d	Desorption rate constant
k_f	Constant for final adsorbed mass

K	Overall adsorption factor
K_d	Langmuir dissociation constant, mg/mL
Leu	Leucine
$L.a$	Area of the sensor, 0.00015 m^2
Δm_{SPR}	Surface mass density, mg/m^2
Δm	mass change on quartz sensor, mg/m^2
Met	Methionine
Mn	Manganese
Mo	Molybdenum
n	Overtone of the acoustic oscillation, dimensionless
η_f	Refractive index
n_0	Refractive index measured in bulk
η_f	Film shear elastic modulus
Ni	Nickel
$[PS]_{rev}$	Protein-substrate complex, reversibly bound on the surface
$[PS]_{irr}$	Protein-substrate complex, irreversibly bound on the surface
Pro	Proline
Ph	Phosphorus
q	Amount of protein adsorbed on the surface, mg/m^2
q_{irr}	irreversible concentration of protein on surface, mg/m^2
$q_{m,\mathrm{irr}}$	maximum irreversible concentration of protein on surface, mg/m^2
q_{tot}	total concentration of protein on surface, mg/m^2
dq/dt	Change in adsorption with respect to time, $mg/(m^2.s)$
Q	Flowrate, 0.1 mL/min
t	Time, s
t_f	Film mass transfer, s
t_r	Reaction time, s
t_q	thickness of the quartz sensor, m
Ti	Titanium

v_0	Velocity, m/s
Val	Valine
Trp	Tryptophan
Tyr (Y)	Tyrosine
α_1,α_2	Reaction orders for adsorption and desorption reactions respectively
β	Factor compensating for the decrease in the SPR signal with distance from the gold substrate in SPR
ρ_q	specific density of the quartz sensor, kg/m^3
ρ_{pq}	protein charge density, elementary charge/kDa
ρ_f	Effective film density, kg/m^3
ρ_{max}	Surface protein concentration at complete coverage, mg/m^2
ρ_t	Amount of protein adsorbed at *t*, mg/m^2
ρ_e	Equilibrium amount of protein adsorbed, mg/m^2
$d\rho/dt$	Rate of change in surface concentration, mg/(m^2·s)
υ_q	shear wave velocity of the quartz sensor, m/s
μ_f	Film shear viscosity, kg/(s.m)
δ_f	Film thickness, m
ψ	Ratio of reflection coefficients for parallel and polarized light
Δ	Difference in phase change between parallel and perpendicular light
Γ	Surface mass density, mg/m^2
χ	Conversion factor
3-D	3-Dimensional

Abbreviations

AA	Amino acids
AFM	Atomic force microscopy
ASA	Accessible surface area
BSA	Bovine serum albumin
BSM	Bovine submaxillary gland mucin
CIP	Cleaning-in-place
DMSO	di-methyl sulfoxide
DOPA	3,4- dihydroxyphenylalanine
DLS	Dynamic light scattering
FITC	Fluorescein iso-thiocyanate
HCl	Hydochloric acid
HPLC	High performance liquid chromatography
HSA	Human serum albumin
IgG	Immunoglobulin
MAPs	Mussel adhesive proteins
mefp	*Mytilus edulis* foot protein
MW	Molecular weight
NMR	Surface nuclear magnetic resonance
OWLS	Optical waveguide lightmode spectroscopy
PCA	Principal component analysis
PEG	Poly(ethylene) glycol
QCM-D	Quartz crystal microbalance with Dissipation
RU	Resonance units
SEC	Size exclusion chromatography
SPR	Surface plasmon resonance
TCA	Tricholoroacetic acid
TE	Transverse electric
TFA	Trifluoroacetic acid
ToF-SIMS	Time-of-flight secondary ion spectrometry
TM	Transverse magnetic
XPS	X-ray photoelectron spectroscopy

Chapter 1 - Introduction

1-1 Background and significance

Protein adsorption on surfaces is a major issue in the chemical and process industries. Proteins are identified as the major components in deposits formed on the surfaces of food and biotechnology processing equipment as well as biomedical devices. Adsorbed proteins form a bio-layer detrimental to the quality standards in industrial production, and are often associated with biological contamination as well as efficiency loss in industrial equipment. Considerable effort and costs are devoted to cleaning and maintenance of fouled process equipment, with direct implications in the process economy (Changani *et al.*, 1997).

Implantable bio-medical devices are also extremely sensitive to protein adsorption, and the risk of infections and/or rejection of prostheses are highly correlated to the presence of a bio-fouling layer (Jeurnink *et al.*, 1996c). Protein adsorption and subsequent deposition occurs rapidly on membranes employed in biomedical equipment for the treatment of blood and blood fractions (example, hemodialysis, plasmapheresis, plasma fractionation and leukofiltration), usually within seconds to minutes after the first blood contact (Sun *et al.*, 2003, Anand *et al.*, 2010). This leads to a drastic change in membrane characteristics and affects the efficiency of the entire process (Yang and Etzel, 2003).

In the present work the aim was to improve understanding of protein adsorption on 316 grade stainless steel (SS) surfaces. Protein adsorption onto material surfaces has been extensively investigated by a variety of techniques, including ellipsometry (Höök *et al.*, 2002), optical waveguide lightmode spectroscopy (OWLS) (Höök *et al.*, 2002), atomic force microscopy (AFM) (Mulheran and Kubiak, 2009), surface plasmon resonance (SPR) (Goda and Miyahara, 2012b) and quartz crystal microbalance with dissipation (QCM-D) (Chandrasekaran *et al.*, 2012, Goda *et al.*, 2012a, Goda and Miyahara, 2012b, Höök *et al.*, 2002, Mulheran and Kubiak, 2009, Otzen *et al.*, 2003, Ngadi *et al.*, 2012). Amongst these, the QCM-D offers a precise

and reliable way to characterize surface adsorption in real-time and in aqueous solutions (Shen *et al.*, 2001).

In this thesis, adsorption experiments were carried out on a set of proteins relevant to the food, dairy, and biomedical industries, comprising eleven proteins characterized by different physicochemical properties. The amount of protein adsorbed on SS was determined using QCM-D. The possibility of monitoring the adsorption process in real time, in situ, allows an opportunity to study the adsorption kinetics and develop suitable models to describe the adsorption and desorption phenomena.

In addition to the adsorbed protein, QCM-D measurements measure water (or any solvent or liquid molecules) that may couple as an additional mass via hydration or entrapment in the cavities of the adsorbed layer. This means that the layer sensed is essentially a combination of protein and water molecules on the surface of the SS sensor. The typical amount of coupled water has been shown in different systems to vary significantly depending upon the nature of the film, mass uptake and protein characteristics (Schreiber and Haimovich, 1983).

Other authors have quantified typical water and protein mass fractions using independent experimental techniques on two different sensors to study the amount of water present in the protein adsorbed layer. In this study, a new technique was developed to determine the fractions of adsorbed protein and associated water on a single sensor by using fluorescently labelled proteins. The mass of protein adsorbed was measured by comparing flourescence light intensity (through a calibration curve relating light intensity to dry mass adsorbed) with the wet mass as determined by QCM-D. Because the dry and wet mass experiments were performed on the same sensor surface, this comparison offers an improved accuracy and reliability for estimating the water content in the protein adsorbed layers.

A solution to combat fouling of surfaces in dairy and other process industries may be to develop a functional biofilm that would adhere strongly to the surface of SS and, at the same time, create a barrier to repel proteins. Ngadi (2009) and others have studied the use of synthetic polymers, mainly poly(ethylene glycol), to create a protein-repellent coating but often such coatings require surface preparation and are unstable.

On the other hand, there are many examples of very effective natural adhesives, such as the glue produced by large kelps to allow them to cling to a rocky shoreline (Dimartino *et al.*, 2013) and plant adhesives for self-healing and protection against defects in wood (Keckes *et al.*, 2003, Schreiber *et al.*, 2005). Given the natural tendency for proteins to bind to surfaces and the tenacity of some natural protein-based adhesives, it was hypothesized that a coating inspired by nature might spontaneously bind, prove to be very stable, and offer a platform for subsequent PEG modification.

"Bio-inspired coatings" are synthetic coatings designed to mimic the surface characteristics of selected biological species. The objective of creating biomimetic adhesives lies in replicating the original interaction between an organism and a surface, whether the surface is of biological or non-biological origin (Silverman and Roberto, 2007). This research is an inspiration from the sea mussels that are able to adhere strongly to wet surfaces through specialized adhesive plaques, namely the mussel threads. The amino acid 3,4-dihydroxyphenylalanine (DOPA) is found in large quantities in mussel adhesive proteins (MAPs) and so it is hypothesized that it strongly contributes to bio-adhesion under water (Lee *et al.*, 2011, Waite *et al.*, 2005). DOPA is formed through hydroxylation of tyrosine residues by a polyphenoloxidase enzyme (Silverman and Roberto, 2007) and are thought to be crucial for both the adhesive and cohesive properties of mussel foot proteins (Wilke and Börner, 2012). Another remarkable characteristic of DOPA is its structural simplicity: DOPA and its analogues are small and are therefore easily incorporated into materials destined for adhesion to a wide variety of substrates (Brubaker and Messersmith, 2012).

In this study, the aim was to test the hypothesis that conversion of tyrosine to DOPA would increase surface adsorption. Two particularly interesting peptide sequences, KGYKYYGGSS and KGYKYY, taken from the full protein sequence of *Mytilius edulis* foot protein 5 (mefp-5) were specifically considered. These peptide fragments were chosen because of their high content of tyrosine residues, 50% and 30%, respectively, providing a good basis to study the effect of the conversion of tyrosine to DOPA on adsorption. The peptide sequences were chemo-enzymatically modified by hydroxylating tyrosine residues to DOPA using mushroom tyrosinase. The

percentage conversion of tyrosine to DOPA was determined and correlated to adsorption of the motifs on SS surface using QCM-D. Increased adsorption of the modified peptide sequences on SS was observed and quantified. Although not tested in the current work, the chosen sequences, once modified, can potentially be functionalized with PEG and used as a coating on surfaces thus presenting a promising approach towards the development of anti-fouling adhesive biofilms, inspired by mussel peptides that could potentially be used in various applications in the food and pharmaceuticals industries.

1-2 Thesis Rationale and objectives:

The overall objective of this study was to obtain a deeper understanding of protein adsorption on the surface of grade 316 SS and this was achieved by adsorption studies performed using QCM-D. The specific objectives were as follows:

1) The key objective was to improve understanding of the adsorption of proteins (food, dairy and commercial) on SS surfaces, using QCM-D as a measurement tool. After attaining knowledge on the amount of adsorbed proteins on the surface, relationships were identified between the various physical properties and their relative adsorbed masses. To fully understand protein adsorption, the contribution of water to QCM-D measurements must be determined, so a second objective was to estimate the amount of hydration water embedded within an adsorbed layer of proteins on a SS surface. To meet this secondary aim, two independent experimental methods were applied in parallel, on a single SS sensor surface. QCM-D offers a precise and reliable way to characterise real-time surface adsorption in aqueous solutions but gives the total mass constituting the adsorbed layer, including water molecules in the hydration layer (Chandrasekaran *et al.*, 2013). On the other hand, fluorescence excited from fluorescently labelled proteins depends only on the amount of protein present and is independent of the associated water. Fluorescence thus offers a method to estimate only the fraction of protein adsorbed on the surface, excluding any water contribution (Rodahl *et al.*, 1996a). Using this approach to account for associated water, the actual protein mass adsorbed

could be determined, providing an improved quantitative, comparative study between the various protein adsorption behaviours.

2) Taking inspiration from the marine world, another focus of the study was on developing a biofilm that would spontaneously bind to SS surfaces and to provide further insights into protein adsorption on SS surfaces using two particularly interesting peptide fragments, KGYKYYGGSS (Peptide I) and KGYKYY (Peptide II), taken from the full protein sequence of mefp-5. QCM-D was used to compare their adsorption onto SS surfaces before and after modification of tyrosine residues to DOPA using mushroom tyrosinase. Here, modification was carried out through chemo-enzymatic modification of tyrosine residues to DOPA using mushroom tyrosinase. A high rate of conversion to DOPA, with up to 97.6% of the tyrosine residues converted, was obtained for the chosen peptide fragments and significant increases in adsorption was observed after conversion.

1-3 Thesis organization

The remainder of this thesis is organized as follows:

Chapter 2: This chapter includes relevant background and a review of previous work on fouling, protein adsorption mechanisms on surfaces, fouling of SS, QCM-D measurements and mussel foot proteins for adhesive applications.

Chapter 3: In this chapter the adsorption behaviour of proteins onto SS grade 316 surfaces is explored using QCM-D. The chapter consists of four major parts: (1) experimental work on adsorption of commercially obtained proteins, using QCM-D, (2) development and application of a new technique combining fluorescence and QCM-D measurements on a single sensor to determine the relative contributions of water and protein to the mass of the adsorbed layer, (3) exploring the various parameters affecting protein adsorption, including the use of principal component analysis to examine the influence of amino acid characteristics found on the surface of proteins and determining an empirical equation to assess their adsorption and (4) kinetic models that describe reversible and irreversible protein adsorption.

Chapter 4: In this chapter, the main aim was to provide further insights into adsorption on SS of two particularly interesting mussel peptide sequences, KGYKYYGGSS and KGYKYY, taken from the full protein sequence of mefp-5. These peptide fragments were chosen because of their high content of tyrosine residues, 50% and 30%, respectively, providing a good basis to study the effect of the conversion of tyrosine to DOPA on adsorption. The peptide sequences were therefore chemo-enzymatically modified by hydroxylating tyrosine residues to DOPA using mushroom tyrosinase. The percentage conversion of tyrosine to DOPA was determined and correlated to adsorption of the motifs on SS surfaces using QCM-D. Significantly increased adsorption of the modified peptide sequences to SS was observed and quantified, thus identifying a promising approach towards the development of strongly adhesive biofilms, inspired by mussel peptides that could potentially be used in various applications in the food and pharmaceuticals industries.

Chapter 5: Conclusions and future recommendations are summarized in this chapter.

Chapter 2 - Literature Review

2-1 Introduction to fouling

In many processing industries, fouling of heat transfer surfaces is a major contributing factor towards reduction in process efficiencies and performance with respect to time. Fouling is a prevalent problem in the dairy, food processing plants and pharmaceutical industries (Changani *et al.*, 1997). Fouling of heat exchangers has been investigated extensively for years (Bansal and Chen, 2005). This fouling is a serious concern as it reduces heat transfer efficiency, increases pressure drop and eventually affects the economy of the processing plant. As a result of fouling and deposition of milk proteins on the surface, there is a possibility of deterioration of product quality through microbial contamination because fluids used in the process are not heated to the required temperature for sterilization. Protein adsorbed on medical instruments prompt the adhesion of bacteria and hence spoil the sanitary state of the surface (Sakiyama *et al.*, 2004).

Processing over 13 billion litres of milk every year in New Zealand means that the efficiency of the heating process is of paramount importance (Bansal and Chen, 2006, Changani *et al.*, 1997). Fouling related costs include over-sizing of heat exchangers, extra fuel consumption, additional equipment requirements, lost productivity, manpower and environmental conditions (Bansal and Chen, 2006, Ramachandra *et al.*, 2005). Total fouling costs equate to 0.25% of the gross national product (GNP) for developed countries such as USA, and 0.15% of the GNP for industrialized countries such as New Zealand (Ramachandra *et al.*, 2005). This would amount to approximately 300 million NZD expenditure towards fouling and maintenance by industries belonging to the food production sector in New Zealand (Economics, 2013).

2-1-1 Importance of fouling in dairy industries

Fouling in dairy and food processing industries is more severe than in other industries and involves rigorous and expensive cleaning steps that must be performed regularly (Changani *et al.*, 1997, Bansal and Chen, 2006). Fouling on a stainless steel (SS) surface begins with the adsorption of proteins, followed by the deposition of protein

on top of the initially adsorbed layer. The main difference between adsorption and deposition is that adsorption of proteins refers to the process of proteins adhering to the bare surface, during which the protein becomes unfolded and attached by strong polar bonds. Deposition refers to the adherence of proteins on previously attached proteins, forming a multi-layer of adsorbed proteins on the surface (Jeurnink *et al.*, 1996a). Studies have also shown that an increase in deposit and thus in fouling occurs upon heating of aged skim milk because of the action of proteolytic enzymes produced by bacteria in milk (Jeurnink *et al.*, 1996b). The action of these enzymes decreases the heat stability of the milk, indicating that there may be a relationship between the heat stability and the amount of deposit (Visser and Jeurnink, 1997).

Increased fouling resistances and therefore decreased heat transfer coefficients, decreased processing times; and increased frequency and duration of cleaning cycles are other effects resulting from fouling (Ramachandra *et al.*, 2005). Daily cleaning is often needed in food plants using cleaning-in-place (CIP) systems. Two types of CIP treatment are currently in place in the milk processing industries: two-stage cleaning, which involves consecutive alkali and acid wash treatments; or single-stage cleaning, using formulated detergents as well as chelating compounds (Changani *et al.*, 1997). In dairy industries, about 80% of the total production costs have been attributed to fouling and cleaning of the dairy process equipment (Bansal and Chen, 2006). Quality issues arising from fouling are equally important and there have been instances in the past of shutdown of dairy and process plants due to concerns in the product quality and contamination (Bansal and Chen, 2006). For example, in a heat exchanger, fouling depends on bulk and surface processes. The steps include denaturation and aggregation of proteins, followed by the transport of aggregated proteins to the surface.

Milk is a complex biological fluid that contains a number of components. Its average composition in weight % is: water – 87.5, total solids – 13.0 (fat – 3.9, lactose – 4.8, proteins – 3.4 (casein – 2.6, β-lactoglobulin – 0.32, α-lactalbumin – 0.12), minerals – 0.8) and small quantities of other miscellaneous species (Bansal and Chen, 2005). Out of these, β-lactoglobulin is known to contribute predominantly in fouling (Changani *et al.*, 1997, Bansal and Chen, 2005, Lalande *et al.*, 1984). Dairy fouling is simplified

to two stages: calcium phosphate fouling and whey protein fouling. The first step involves the deposition of calcium ions on the surface causing calcium phosphate fouling. This is then followed by the deposition of aggregated protein molecules on the surface, resulting in whey protein fouling (Visser and Jeurnink, 1997). Of the milk proteins, β-casein is known to form complexes with κ-casein, either at the surface of casein micelles or in the serum, and hence is no longer available for the fouling reaction. The calcium content in milk from various animal sources varies greatly. The effect of the calcium content present in milk is directly proportional to fouling of surfaces, such as the walls of the heat exchangers (Jeurnink *et al.*, 1996c).

Several researchers have studied the relationship between the denaturation and unfolding of whey proteins and fouling (Dannenberg and Kessler, 1988, Bennett, 2007, Manji and Kakuda, 1986, Hiddink *et al.*, 1986). Lalande *et al*. (1984) anticipated the spread of a deposit of β-lactoglobulin along a heat transfer surface using the kinetic data on denaturation of the particular protein given by Lyster (Lyster, 1970, Hillier and Lyster, 1979). De Jong *et al*. (1997) proposed a fouling model based on the denaturation kinetics of β-lactoglobulin. Fouling of surfaces was found to be proportional to the heating temperature of the milk in the process. From these studies, it was concluded that preheating the bulk of the solution strongly influenced the rate of deposition of the milk proteins on the surface leading to interpretation that the deposition process is measured by the bulk reactions rather than surface reactions (Jeurnink *et al.*, 1996c).

As mentioned above, factors such as aggregation and denaturation of proteins are found to have a direct influence on the fouling of surfaces. Apart from these properties, there has been little work relating the physical properties of individual dairy proteins to their propensity to foul surfaces. In Chapter 3 of this thesis, other physical properties such as molecular weight (MW), charge on the surface of the protein and surface accessible amino acid residues are explored in terms of its adsorption to SS surface.

2-1-2 Choice of SS for adsorption studies (ISSF, 2010)

In addition to its use in food industries, SS is widely used in biomedical applications because of its high corrosion resistance and durability (Sakiyama *et al.*, 1998). SS is

one of the most widely used materials for a variety of applications. Being an alloy, there is a possibility of formation of various oxides on its surface. This in turn leads to changes in the mechanical, chemical and physical properties of SS. The specific composition of 316 SS is iron (Fe), 16-18% chromium (Cr), 10-14% nickel (Ni), 2-3% molybdenum (Mo) and smaller amounts of manganese (Mn), silicon (Si) and phosphorus (P) (Anand *et al.*, 2010, Corporation, 2007). SS corrosion resistance to a large extent, is due to the Cr-rich oxide layer that acts as a barrier against diffusion of ions between the alloy and the solution phase that it is in contact with (Donik *et al.*, 2009). The Cr-oxide layer is related to the denaturation process. It has been shown that the diffusion of hydroxide ions occurs in the foulant layer with disengagement of protein aggregates and deposits near the surface.

It was possible to quantify the rate of deposition by relating it to the concentration of activated molecules in solution, using a model for the denaturation and aggregation of β-lactoglobulin (Manji and Kakuda, 1986). SS defined by the oxide layer interacts with the protein with polar interactions, bonding with charged groups in the protein, hydrogen bonding between the amine groups in the protein and the metal oxide and interactions with the carboxyl and hydroxyl groups of the protein. Bansal *et al*. (2007) studied the interaction of whey proteins with SS. The X-ray Photoelectron Spectroscopy (XPS) analysis used in this study showed increased intensity of carbon, oxygen and nitrogen as a result of protein deposition on the surface. Further, analysis of this study showed the bonding of carbon and oxygen groups on the SS played a significant role at the interface. SS being a polar, hydrophilic surface influenced the rate of deposition of whey proteins on the surface. In the initial few minutes, there was maximum deposition of the proteins and the deposition gradually decreased . These studies showed that surface chemistry also influences deposition of whey proteins on the surfaces of SS based on the interactions of the functional groups of the proteins with the oxide layer formed on SS (Premathilaka *et al.*, 2007).

The level of hygiene needed during the manufacture of dairy products has increased so that the nutritional quality of the product is preserved (Lundin *et al.*, 2012). The modern-day dairy industry requires clean, corrosive-resistant SS equipment to meet the needs of the milk product consumers. Earlier adsorption studies on 316 grade SS

and chromium show limited release of metal during protein adsorption (Lundin *et al.*, 2012) . 316 grade SS is used in dairy industries, this has been the choice of SS in this thesis too for studying the protein adsorption phenomena.

2-1-3 Fouling by protein adsorption on SS

Protein adsorbed on the equipment surface is one of the main components of fouling and is found to be a severe problem for the food industry (Murray and Deshaires, 2000). Protein adsorption and desorption behaviour on surfaces has been extensively researched to provide a better understanding of the mechanism and kinetics of formation and removal of fouling deposits. Protein adsorption is the first step in the integration of implanted devices or attachment to tissues in biomedical applications. In nano-technology, protein-surface interactions are important for the arrangement of protein constructs, such as sensors and activators (Gray, 2004). The adsorption of proteins at solid-liquid interfaces has also been extensively studied by various researchers (Wahlgren and Arnebrant, 1991). Lalande *et al*. (1984) reported that protein deposits in milk processing plants constitutes about 50% of the fouling. Dairy proteins such as β-lactoglobulin and α-lactalbumin are the two major whey proteins present in bovine milk. These proteins are found to denature relatively quickly at high temperatures to expose their core, which contains reactive sulfhydryl groups. The denatured protein molecules then react with other protein molecules such as caseins and form aggregates. β-lactoglobulin contains two disulfide bridges and one free thiol group, which is "buried" in the interior of the molecule. Upon an increase in temperature, a conformational change occurs, making the free thiol group accessible for disulfide-thiol exchange reactions. This in turn leads to aggregation by interaction between the intermolecular bonds between β-lactoglobulin molecules (Jeurnink *et al.*, 1996a). Studies on β-lactoglobulin adsorption on SS particles have shown that there is an adsorption of the protein to SS due to the free sulfhydryl groups (Sakiyama *et al.*, 1998, Ngadi *et al.*, 2008).

Studies on adsorption of β-casein, lysozyme and apo-α-lactalbumin performed by Ngadi *et al*. (2009) showed that the adsorption of these proteins to SS was governed by diffusion-reaction mechanisms. Ngadi *et al*. (2009) reported that β-casein is expected to have a monolayer on the SS surface. The viscoelastic properties such as

density, viscosity, elasticity, and thickness of the adsorbed protein layer are correlated to the frequency changes (Δf) and dissipation factor from the QCM-D responses, based on the Voigt model (Liu and Kim, 2009). The mass calculated by the Voigt model ranged from 7 – 19 mg/m^2. The area occupied by this adsorbed layer on the sensor surface (termed as "surface density") was determined to be 2.3 mg/m^2, approximately 4-5 times the dry mass of the protein. The conclusion drawn was that multi-layers of β-casein were formed due to the hydrophobic and electrostatic interactions to the surface. The conformational changes of the protein are expected to reveal the negatively charged surface of the protein to the negatively charged surface and hence causing repulsion in the adsorption experiments.

Ngadi *et al*. (2009) also studied the adsorption of lysozyme on SS. Lysozyme showed fully irreversible adsorption even after 30 minutes buffer wash. The Voigt mass was estimated to be 4-16 mg/m^2. The surface density was found to be 3 mg/m^2 forming multi-layers due to conformational changes and aggregation. Kim *et al*. (2002) studied the irreversible adsorption of lysozyme on mica surfaces. The force-volume data determined a single layer of lysozyme adsorbed to the surface. Once adsorbed on the surface, conformational changes were observed due to protein-surface interactions. The study also revealed the importance ofhydrophobic attraction and electrostatic repulsion in adsorption.

There are two types of α-lactalbumin – holo-α-lactalbumin (native form with calcium present) and apo-α-lactalbumin (calcium depleted). Adsorption of α-lactalbumin in its native form on SS was another protein studied by Ngadi *et al* (2009). The study showed the Voigt mass of 4-16 mg/m^2, surface density of 3 mg/m^2 and irreversible adsorption of the protein on SS surface, with 5 to 12 times greater adsorption when compared to the dry mass. Also the adsorption induced structural changes causes irreversibility of the protein on the SS surface. Bettoni (2001) studied conformational changes caused by the conversation of the holo-to apo-α-lactalbumin due to the exposure of the interior hydrophobic groups to interact with the surface. Cabilio *et al*. (2000) studied the native α-lactalbumin and the carboxylate groups responsible for interaction with the surface. Out of the 21 carboxyl groups present on the acidic amino acids of the protein, four of them were bound to the calcium in its native

structure and the remaining 17 carboxyl groups were available for surface binding to occur. In the apo- form all 21 carboxylate groups bind to the surface causing increased binding when compared with the native form.

Adsorption and desorption of other proteins such as bovine serum albumin (BSA) and gelatin have also been studied and shown to exhibit different behaviour on solid surfaces during adsorption due to the structure of the respective proteins. Once proteins deposit on the surface, reactions occur that lead to removal of the top metal layer from the surface, thus commencing the adhesion of micro-organisms that can be extremely difficult to remove (Murray and Deshaires, 2000). Earlier studies have also reported that fouling on surfaces is caused by aggregation of protein molecules (Bansal and Chen, 2005, Bansal and Chen, 2006). Studies also identified the functional groups of the proteins as well as the amount of fouling occurring on SS, detected by XPS and ellipsometry by knowing the intensity of the functional groups. Those with lower intensity were found to be buried in the interior of the fouled surface (Premathilaka *et al.,* 2007). The above mentioned studies have provided knowledge of dairy proteins adsorbed on surfaces and the mechanisms governing them. Few of the proteins have been explored from the viewpoint of the exterior surface properties of the protein and interactions with the surface. In this thesis, the main aim was to study the various physio-chemical properties of proteins such as MW, charge of the protein and surface amino acid side chains and their influence on adsorption.

2-2 Protein structure

Proteins are complex bio-molecules comprising amino acid residues, linked by peptide bonds, in defined sequences. Each amino acid contains an acidic carboxyl group (carboxyl terminus) and basic amine group (amino terminus), which form a covalent peptide bond during translation of the DNA code in protein synthesis by the ribosome. Proteins are also known as “amphiphilic molecules” that contain hydrophobic, hydrophilic, polar, non-polar and charged (both positive and negative) regions.

The shape a protein folds into is known as the native state of the protein. The structure of protein molecules is organized into four different levels: primary, secondary, tertiary, and quaternary (Fig. 2) (Bi *et al.*, 1984). The structure of protein molecules is responsible for its contribution towards biological function. Proteins are found to be stable at their individual isoelectric points (pH = pI). Changes in a protein's structure are caused when denaturation occurs and hence proteins lose their activity, which can be regained if the protein regains its native state. Several factors such as increase in temperature, pressure or a change in pH can easily provoke denaturate the protein (Ngadi *et al.*, 2012).

Proteins are classified into two categories: 'soft' and 'hard' proteins. The 'soft' proteins display large conformational changes upon adsorption. Examples include BSA, human serum albumin (HSA), immunoglobulin (IgG), α-lactalbumin, β- casein and haemoglobin. 'Hard' proteins undergo limited or no structural rearrangements during adsorption because of their high internal cohesion. Examples of hard proteins include α-chymotrypsinogen, ribonuclease (RNase), cytochrome-c, lysozyme and β-lactoglobulin (Ngadi, 2009).

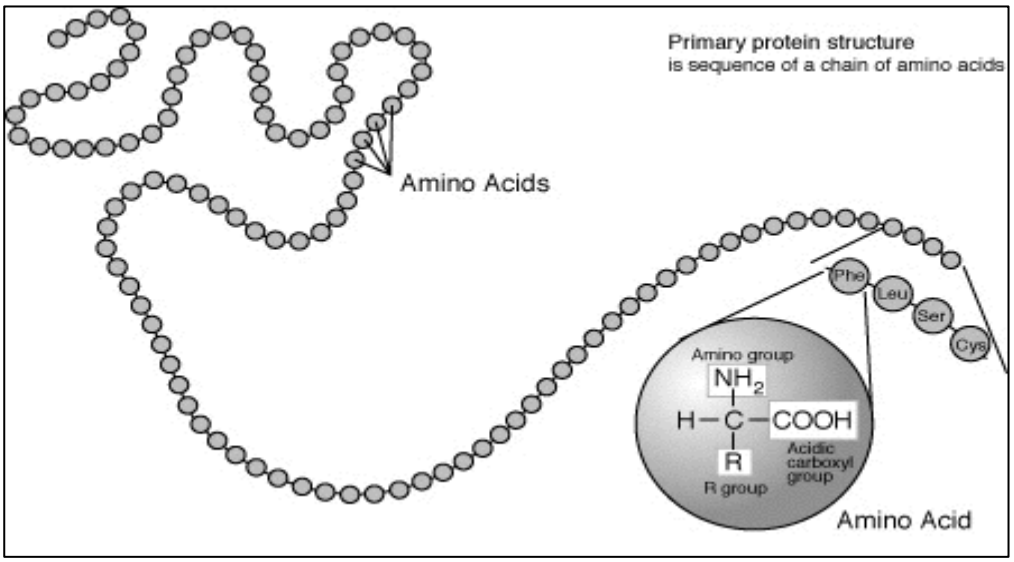

Figure 2-1: Primary protein structure (continuous chain of amino acid residues) (Ngadi, 2009)

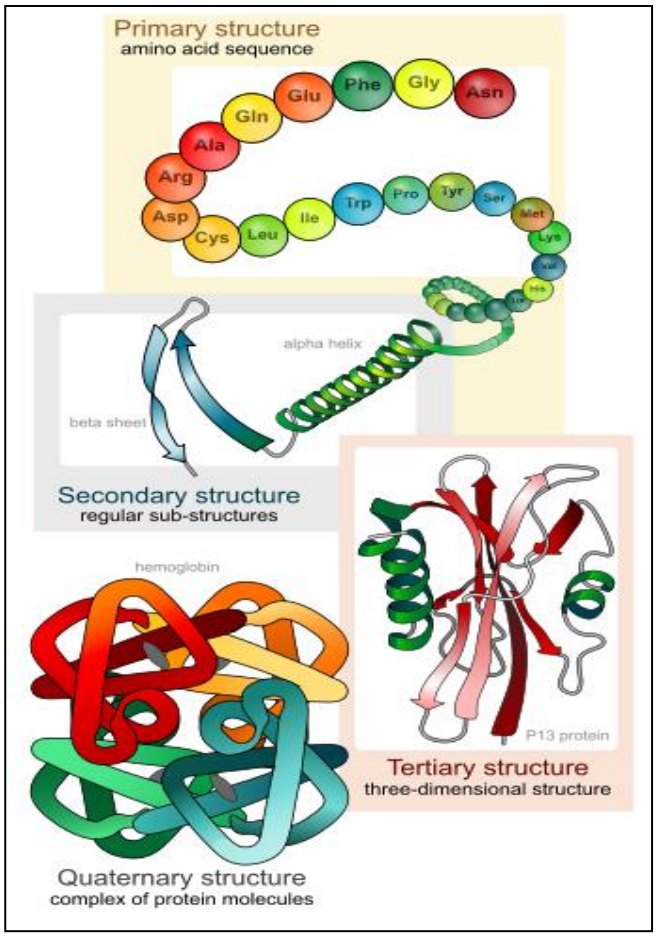

Figure 2-2: Protein in the four predominant structures (Ngadi, 2009)

2-3 Protein adsorption on surfaces

Progress on understanding protein adsorption has been considerable over the past few years but the concept of interfacial adsorption behaviour of proteins remains unclear. This is largely because of the higher complexity of protein adsorption that poses experimental difficulties such as varying MW, charge and structural forms of proteins. Theoretical understanding of proteins and their intrinsic processes have been studied previously (Malmsten, 1998). Interaction of proteins with SS also triggers release of metal species from these materials and mixing of these metal species with milk can induce potential adverse health effects. The interaction of the proteins with solid surfaces is not only a fundamental phenomenon but is also a key phenomenon to several important and novel applications, as mentioned earlier. The interaction of proteins with the surfaces involves both the binding and unfolding of proteins (Bi *et al.*, 1984).

The desire to control, predict and understand the protein adsorption on SS surfaces has been the ultimate goal of Chapter 3 of this thesis. This also involved goals of studying surface coverage and kinetic details of the protein-surface interactions.

2-3-1 Parameters affecting protein adsorption

Several parameters affect surface adsorption of proteins. Briefly, these include the MW, size of the protein, hydrodynamic radius, charge of the protein, and the influence of the amino acids present on the exterior surface of the folded proteins that can readily adsorb to the surface. Other factors, such as temperature and pH also influence adsorption (Bi *et al.*, 1984). The phenomena of protein adsorption on surfaces are complicated due to conformational changes of proteins and folding. However, specific characteristics of the protein are also important in surface adsorption. For example, the charged and hydrophilic/hydrophobic residues displayed on the surface of a protein are closely related to its structural and biological functions, and are seldom homogeneously distributed. The presence of "patches" of similar amino acidic residues can trigger or inhibit interactions with solid surfaces, generating specific peculiarities in the adsorption behaviour (Lins *et al.*, 2003, Bansal and Chen, 2006, Rabe *et al.*, 2011). Other protein characteristics that influence the nature of adsorption include the charge on the protein during adsorption, size exclusion effects and surface aggregation (Rabe *et al.*, 2011). The solvent also plays a crucial role in the adsorption process. For example, relatively high ionic strengths can stabilize proteins in solution, thus preventing aggregation and formation of insoluble protein deposits on surfaces (Höök *et al.*, 1998b, Otzen *et al.*, 2003). In addition, the pH of the buffer determines the charge state of both the biomolecules and the surface, thus facilitating or preventing the adsorption interaction (MacRitchie, 1972, Nakanishi *et al.*, 2001, Petrone and McQuillan, 2011). The properties of the buffer also influence the release of metal ions from the SS surface in different ways, either directly (dissolution of ions) or indirectly (by changing the extent of adsorption of proteins) (Lundin *et al.*, 2012). The possibility of adsorption of potential-determining species present in solutions should also be considered. Protein adsorption is further complicated by the physicochemical properties of the metallic substrate such as surface composition (including the presence of a passivating layer of metal oxides), surface microstructure and the presence of active sites or residual materials from

previous processing conditions (Jeurnink *et al.*, 1996c, Visser and Jeurnink, 1997, Rodahl *et al.*, 1996a). It is clear that the intrinsic properties of the protein–solvent–surface triplet will determine the overall extent and physical nature of protein adsorption.

Studies have been performed on different properties of proteins and their influence on adsorption. Until now, there has been no approach taken to bring all the different properties of the protein and try determining a new way of relating them. In this thesis, an empirical relationship is proposed to evaluate the mass constituting the adsorbed layer only from the knowledge of the physical properties of the proteins. This relation gives an understanding of the adsorption of proteins with relation to its MW and charge of the protein in the buffer.

Another tool to study the different variables and its influence on adsorption was performed by principal component analysis (PCA). This is an eigenvector-based technique to determine new axes that span the directions of greatest variation in a multivariate data set. The main aim of the technique is to reduce the dimensionality of the data by projecting the data onto new axes (called principal components, PCs). The PCs are usually linear combinations of the variables. The major variation patterns in the data set are studied by using axis rotation in PCA (Sanni *et al.*, 2002). In Chapter 3, PCA is explored to study different parameters of the different proteins to find a relation between them with respect to adsorption. Several examples of the use of PCA are mentioned here. Jufang *et al*. (2004) Wu (2004) studied modelling using PCA for the adsorption of eight organic compounds on activated carbon having varying shape and sizes. Adsorption of compounds was analysed by time-of-flight secondary ion mass spectrometry (ToF-SIMS) data, that showed variation in peak intensity of the protein samples (Muramoto *et al.*, 2011). Once adsorption occurred, the ToF-SIMS showed different composition of amino acids on the surface. Because the same 20 amino acids are present in all proteins, the difference in the relative intensities of the amino acid fragments in the ToF-SIMS spectra contained information of the adsorbed proteins. To analyse the results, PCA was used. To date, PCA has not been used with respect to the different physio-chemical properties of the proteins and their influence

on adsorption. This is the first time this technique has been implemented in the thesis.

2-3-1-1 Physiochemical properties of proteins

Protein adsorption is a complex process mainly because of the diverse nature of proteins as mentioned earlier and the surface properties (such as chemical property, density and architecture). Other factors include:

(i) Temperature: The temperature of milk in the heat exchanger is one of the most important factors controlling fouling. Chen and Bala (1998) studied the effect of fouling with respect to surface and bulk temperatures in whole and skim milk, and whey proteins. The study resulted in identifying fouling to be caused due to the increase in temperature. If the surface temperature was below 68°C, no fouling was found to occur even when the bulk temperature was higher than 84°C. Preheating of milk resulted in denaturation and aggregation of proteins that in turn resulted in lower fouling in heat exchangers. The main effect of pre-heating was on β-lactoglobulin and its association with caseins resulting in micelle formation and hence fouling (Bansal and Chen, 2006). Studies have reported that protein adsorption is usually found to be higher at high temperature than the room temperature due to denaturation of the proteins (Jackler *et al.*, 2002). In this thesis the temperature in the experiments were maintained at 22°C, to prevent denaturation of the proteins.

(ii) pH and Ionic strength: pH as well as ionic strength are the main contributors to determine the electrostatic attraction or repulsion in adsorption of proteins on surfaces. Some studies have reported that the adsorption is decreased if both the protein and the surface are electrostatically neutral. In general the pH of the solution alters the charge of the protein with respect to the pI of the individual proteins. The pI of the protein represents the iso-electric point of the protein. If the pI is greater than the pH of the solution, the protein is positively charged and vice versa when the pI is lower than the pH of the solution. For example, α-lactalbumin was found to have the same properties at

both high and low pH (pH 2 and pH 11) due to the absence of calcium at these pH's (Cabilio *et al.*, 2000). Lysozyme for example, has a pI of 11 and at a pH of 7.5, the molecule becomes positively charged and that helps in the adsorption to chromium and SS (Lundin *et al.*, 2012). Ionic strength is often found to be associated with the thickness of the diffused ion layer from the surface. If the pH is far from the pI, the effect of the ionic strength disappears gradually and the protein adsorption no longer depends on pH (Höök *et al.*, 1998a).

(iii) **Concentration and size of the protein:** Higher protein concentration results in increased adsorption on surfaces and a saturated monolayer is formed quickly (Roach *et al.*, 2005, Vörös, 2004, Baujard-Lamotte *et al.*, 2008). After the initial protein monolayer is established, additional protein molecules tend to adsorb on the first layer and form a multilayer (Fig. 2-3). The protein-protein interactions occur by hydrophobic, hydrophilic and ionic interactions or by covalent bonding. In solution, the concentration of proteins appears to have an effect on the denaturation state of a protein. At low concentrations, a protein can maximize interactions with the surface both by its orientation on the surface as well as by unfolding that leads to denaturation and irreversible adsorption of the protein at the surface (Ngadi, 2009). At higher concentrations of the protein in solution, the supply rate of proteins to the surface increases and the surface will be filled with adsorbed proteins in a shorter time span. Therefore, the surface mass density adsorbed becomes greater as the adsorbed protein adsorbs to the surface. A small protein generally adsorbs more than a large protein and is more compact, with a higher mass surface density than a larger protein (Ngadi, 2009, Vörös, 2004).

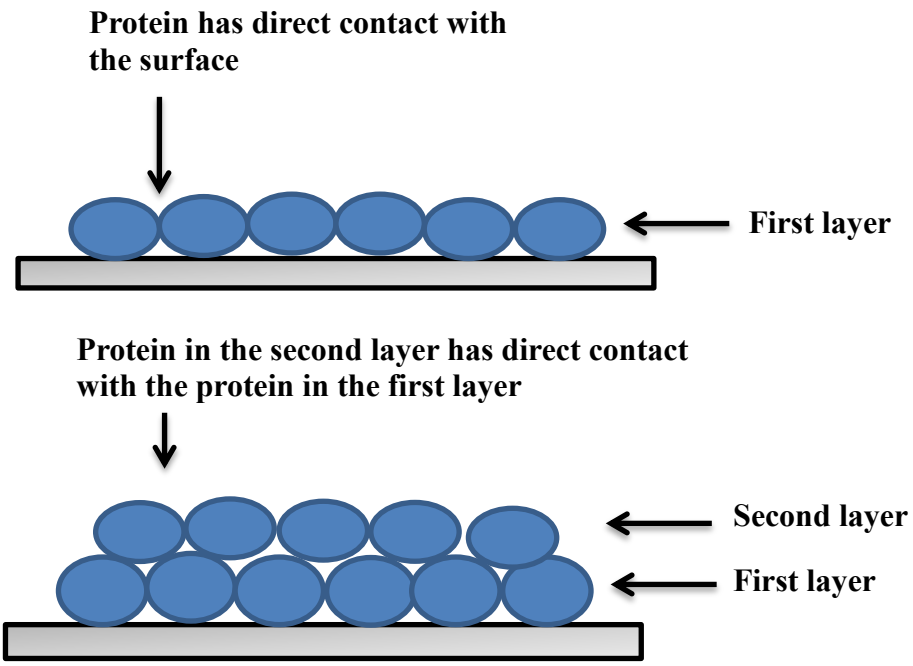

Figure 2-3: Illustration of protein-surface interaction in monolayer and multilayer (reproduced from (Ngadi, 2009))

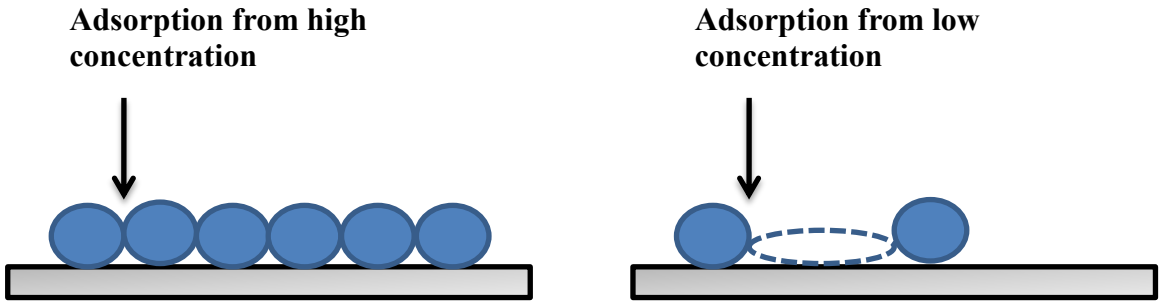

Figure 2-4: Illustration of adsorption from higher concentration and from low concentration onto surface with the same area (reproduced from (Ngadi, 2009)

2-3-1-2 Protein-solvent interactions

Protein adsorption onto a material surface has been extensively investigated by a variety of techniques, including ellipsometry (Höök *et al.*, 2002), OWLS (Höök *et al.*, 2002), AFM (Mulheran and Kubiak, 2009), SPR (Goda and Miyahara, 2012b) and

QCM-D (Höök *et al.*, 2002, Otzen *et al.*, 2003, Mulheran and Kubiak, 2009, Goda *et al.*, 2012a, Goda and Miyahara, 2012b, Chandrasekaran *et al.*, 2012). Amongst these, the QCM-D offers a precise and reliable way to characterise surface adsorption in real-time and in aqueous solutions (Shen *et al.*, 2001, Rodahl *et al.*, 1996a). Use of the QCM-D equipped with quartz sensors coated with SS represents an ideal and convenient tool to investigate "wet" (proteins and water molecules) mass adsorbed by proteins on a 316 grade SS surface.

2-3-1-3 Contribution by surface amino acids towards adsorption

Amino acids are the building blocks of proteins and peptides. Investigation of their behaviour on surfaces is an essential and key step towards understanding protein adsorption on surfaces (Lins *et al.*, 2003). Apart from their role in protein-surface interactions, amino acids offer exciting opportunities for functioning of solid surfaces due to their multi-functionality and tendency for self-organization (Pászti *et al.*, 2008).

Studies on bonding of amino acids to metal surfaces has used modern surface science methods. The situation seems to be very different in wet environments used for QCM-D. In general, the interaction between individual amino acids and the metal surfaces is almost zero in solution phase. For example, studies have shown that there was no adsorption of glycine or glutamine on a TiO_2 surface (Pászti *et al.*, 2008).

Additional simulation studies have helped improve understanding of the interactions of the various types of amino acid residues on metallic surfaces. Some studies have shown that acidic amino acids, aspartic acid (Asp, D) and glutamic acid (Glu, E) bind strongly to titanium (Ti) surfaces (Pászti *et al.*, 2008). Other studies have shown that multiple lysine (K) residues show a weaker affinity to metal surfaces, even when the surface is negatively charged (Imamura *et al.*, 2007). When adsorption of amino acids occurs at polar or charged surfaces, it tends to involve hydroxyl transfer reactions that are irreversible (Trudeau and Hore, 2010). Desorption can involve breaking the bonds in the molecule (Trudeau and Hore, 2010). On the other hand, reversible adsorption of amino acids on a non-polar surface is largely driven by hydrophobic interaction between the amino acids and the surface.

The role of water as a solvent is also crucial in physisorption of amino acids. While polar and hydrophilic surfaces can reversibly adsorb all amino acids in vacuum, they have difficulty in adsorbing reversibly in aqueous solutions (Trudeau and Hore, 2010). This implies that the role of water as a solvent is crucial in physisorption of individual amino acid residues in a protein, and it helps in determining the adsorbed structure of the proteins (Trudeau and Hore, 2010).

2-3-2 Phenomena of protein adsorption

From a general perspective, adsorption of proteins on solid surfaces is a complex phenomenon. Protein adsorption has been described by several independent researchers (Hlady and Buijs, 1996, Draeger, Dietschweiler and Sander, Imamura *et al.*, 2008, Hedberg *et al.*, 2012b). Regardless of the nature of the protein and the surface considered, the adsorption process generally follows a few basic steps (Bird, 2002):

(i) Transport of proteins from the bulk solution phase towards the interfacial region of the surface: The first step in protein adsorption is driven by the Brownian motion occurring in the solution and a gradient diffusion of protein molecules to the surfaces. This step is dependent on the conditions such as MW of the protein and its respective size, charge of the protein, temperature and concentration of the sample and flow rate that has been set in the experiments.

(ii) Initial attachment of protein to the surface (initial protein-surface interaction): The next step in protein adsorption involves the protein molecules interacting with the surface for a sufficiently long time to achieve adsorption. The interaction strength between the protein and the surface determines the residence time for the initial attachment of the molecules. There are several means by which adsorption occurs, such as random site interaction (unordered binding), ordered adsorption, an adsorption island or a cluster formation of proteins. The random site interaction usually involves low coverage of proteins on the surface, while at moderate coverage the ordered structure of proteins or their islands are formed. In the case of a mixture of proteins, the protein with the highest concentration usually dominates the

initial adsorption and will gradually be replaced (displaced) by the higher affinity protein species. The initial adsorption of proteins on surfaces is dominated by smaller proteins and then replaced by larger proteins, because the larger protein has a greater surface area, leading to a higher affinity from the bulk solution phase towards the surface compared with a smaller protein.

(iii) Conformational changes of proteins on the surface: During the process of adsorption, some of the adsorbed protein molecules undergo conformational changes (Fig. 2-5) or may be denatured due to experimental conditions such as the temperature or pH of the solution. This might result in a change in the interaction energy of the proteins with the surface, resulting in an increased residence time and a stronger binding. This is because a denatured protein spreads more broadly over a surface compared with a native protein. Denaturation is found to be more predominant on a hydrophobic surface than a hydrophilic surface because protein-surface interactions allow hydrophobic residues of proteins to readily contact with the surface (Kim *et al.*, 2002). The structural properties of the protein also influence the adsorption and conformational integrity of adsorbed protein molecules on the surface.

(iv) The detachment of adsorbed protein from the surface: If the binding between proteins and the surface is weak (physical adsorption) then the proteins may be easily desorbed back into the solution near the surface. Protein adsorption is usually only partially reversible because proteins undergo structural changes during adsorption and are attached by many molecular segments to the surface (Fant *et al.*, 2000, Baujard-Lamotte *et al.*, 2008, Kim and Lund, 1998, Chandrasekaran *et al.*, 2012). Experimental conditions such as changing the pH or increasing the ionic strength can affect the charge of the proteins and hence its interaction to the surfaces, thus promoting desorption (Cabilio *et al.*, 2000).

(v) Transport of proteins from the surface: The final step of the adsorption phenomena is the reverse of the first step. Here, the desorbed protein has an altered structure compared with the native state of the protein. In many cases, the desorbed proteins become reabsorbed to the surface (Ngadi, 2009).

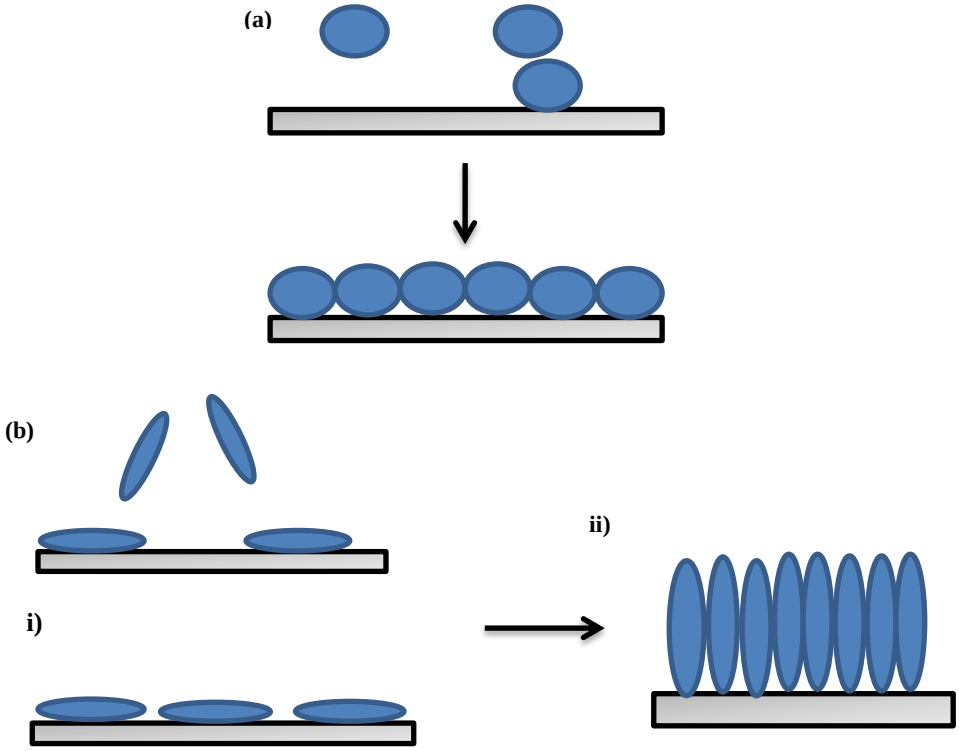

Figure 2-5: Schematic to show (a) a globular protein, whose conformation may be distorted on interaction with the surface and (b) a rod-like protein undergoing multistage adsorption process where (i) initially the protein adsorbs with its long axis parallel to the surface and (ii) rearrangement of protein molecules occurs to increase a protein-protein interaction (reproduced from (Roach *et al.*, 2005)).

The protein then begins to interact with the surface through a combination of forces, mainly electrostatic, van der Waals and hydrophobic interactions. Finally, all co-operating forces attain a certain state of equilibrium that concludes the protein adsorption process. Once adsorption has taken place, the protein can follow two possible alternatives: if adsorption is fully reversible, then the biomolecule follows exactly the same steps in reverse, leading to surface desorption and return to the liquid phase. However, the proximity of the protein backbone to the surface can trigger other interactions previously hindered by steric or spatial constraints, thus creating a more stable and stronger interaction with the surface (Yang and Etzel, 2003, Roach *et al.*, 2005). In this case, protein conformation changes from its native state, a process that usually leads to denaturation and loss of biological function. In some cases, the protein molecules can unfold, denature and/or aggregate before they

start migrating towards the surface, phenomena that mainly depend on the nature of the protein itself and the physical conditions of the solution. Surface adsorption and conformational change may also occur simultaneously (Höök *et al.*, 1998b, Shen *et al.*, 2001).

2-3-3 Kinetics of protein adsorption

Many attempts have been made to describe the adsorption kinetics of proteins onto solid surfaces, from Langmuir-type adsorption models to surface-exchange reaction denaturation models (Kim and Lund, 1998). If the adsorption process is entirely reversible, the protein molecules can desorb completely and return to the liquid phase. However, conformational changes subsequent to protein adsorption reported in earlier studies indicate the formation of a stable and stronger interaction with the surface (Roach *et al.*, 2005).

Studies on a variety of surfaces including titanium and methylated silica have predicted the process of protein adsorption. From this adsorption process, the kinetics and equilibrium interaction along with the extent of protein conformational changes has been studied (Imamura *et al.*, 2008, Wahlgren and Arnebrant, 1991). Numerous models have been proposed to account for the behaviour of protein adsorption. For example, the Langmuir model has been used to describe adsorption of proteins with different isoelectric points and sizes to titanium surfaces (Imamura *et al.*, 2008). The Temkin isotherm was used to describe protein adsorption to metal-chelating ligands (Johnson and Arnold, 1995). A somewhat different model of continuous energetic heterogeneity for a protein-surface interaction has been proposed to explain the logarithmic-like adsorption kinetics of IgG and HSA on a quartz surface and the Freundlich-like character of human serum albumin adsorption (Kulik *et al.*, 2008).

Among other approaches, the random sequential adsorption model has been used to predict both the partial irreversibility of protein adsorption and the clustering of proteins at surfaces as well as to explain antibody binding to antigen-coated surfaces (Rahn and Hallock, 1995). The fact that charge, size, temperature and the type of amino acids interacting with the surface influence desorption of the proteins adds to the complexity of protein adsorption kinetics (Kim and Lund, 1998).

In this study, three different kinetic models – Langmuir, Freundlich and the conformational change model were studied. Although Langmuir and Freundlich are strictly applicable only for reversible adsorption, an additional hypothesis concerning the use of Langmuir kinetics for irreversible adsorption was also studied in this thesis.

2-3-3-1 Langmuir Model

The Langmuir model, derived by Langmuir in 1916, is one of the simplest adsorption models and is frequently used to describe the kinetics of protein adsorption (Brusatori and Van Tassel, 1999, Cosman *et al.*, 2005). The kinetic equation for the Langmuir model can be written in terms of surface concentration ρ, as:

$$\frac{d\rho}{dt} = k_a C_0(\rho_{max} - \rho_t) - k_d \rho_t \qquad (1)$$

where, ρ_{max} is the surface concentration of protein corresponding to a complete surface coverage, ρ_t is the amount of protein adsorbed onto the surface at time *t*, C_0 is the protein concentration in the bulk liquid phase , *t* is the time, and k_a and k_d are adsorption and desorption rate constants, respectively. As time approaches infinity, there will be no change observed in the rate of change in surface concentration of the protein ($\frac{d\rho}{dt} = 0$), indicating the attainment of equilibrium conditions, a condition that corresponds to an equilibrium amount of protein adsorbed (ρ_e). This equilibrium value depends on the specific bulk protein solution concentration of the experiment and can be calculated from the following expression obtained by rearranging Eq. (1) in equilibrium conditions:

$$\rho_e = \rho_{max} \frac{C_0}{C_0 + K_d} \qquad (2)$$

A major limitation of the Langmuir equation for protein systems was that it assumes reversible adsorption, whilst many studies have shown the irreversible character of the adsorption process on realistic time scales.

2-3-3-2 Freundlich Model

The Freundlich Adsorption kinetic equation is mathematically expressed as:

$$\frac{d\rho}{dt} = k_a\rho^{\alpha_1} - k_d\rho^{\alpha_2} \quad (3)$$

At equilibrium conditions, the equation reduces to:

$$\rho_e = K_D^f C_0{}^{\alpha} \quad (4)$$

where α_1, α_2 are the reaction orders for the adsorption and desorption reactions, respectively, $\alpha = \frac{\alpha 1}{\alpha 2}$ and $K_D^f = \left(\frac{k_a}{k_d}\right)^{\frac{1}{\alpha_2}}$

The Freundlich isotherm is known to be applicable only within certain concentration limits because, given an exponential distribution of binding sites, the number of sites increases indefinitely with a decreasing association constant, implying that there are an infinite number of sites (Umpleby II *et al.*, 2001).

2-3-3-3 Conformational Change Kinetic Model

The rate at which a ligand reaches equilibrium is determined not only by the association rate constant and the protein concentration, but also by the dissociation constant. An alternative approach is to measure the association and dissociation constant in a single experiment. In this approach, protein at a specific concentration is passed through the QCM-D flow modules and the total binding at multiple time intervals measured. The dissociation is initialized with the start of the buffer wash and the dissociation measured is included along with the equilibrium Langmuir surface concentration. The approach yields an alternative, continuous evaluation of the adsorption and desorption phases (Gillard *et al.*, 2006). The protein concentration and time, t_0, at which the dissociation phase starts, are the input parameters in this model. This model follows the scheme (Motulsky, 1999):

$$P + S \rightleftharpoons PS_{rev} \quad (5)$$

$$P + S \rightarrow PS_{irr} \quad (6)$$

In this equation, the formation of $[PS]_{rev}$ (protein-substrate complex, reversibly bound on the surface) and $[PS]_{irr}$ (protein-substrate intermediate with irreversibly bound protein on the surface) are assumed to have an association rate constant (k_a) of similar magnitude and the dissociation constant (k_d) for $[PS]_{rev}$. When the

$[PS]_{rev}$ does not readily return to its native $[P]$ state, then the dissociation is minimal and can be neglected, hence the rate of change equation is given by:

$$-\frac{d[C_0]}{dt} = \frac{d[C_0S]_{rev}}{dt} = \frac{d[C_0S]_{irr}}{dt} = k_aP \tag{7}$$

The integrated forms of the equations (when dissociation is neglected) are given by:

$$[C_0] = [C_0]\, e^{(-k_at)} \tag{8}$$

$$[C_0S]_{rev} = [C_0]\,(1 - e^{-k_at}) \tag{9}$$

Equation (16) is the rate constant obtained when the dissociation of $[PS]_{rev}$ is also taken into account in the expression for the rate of formation of $[PS]_{rev}$. Equations (14) to (20) show the step-by-step calculation required to solve the kinetics of protein adsorption; in this case there is no assumption of the protein being reversibly bound to the surface. Equations (12) to (14) are used in equation (15) that gives the solution for calculation of the association phase of the binding of protein. C_0 and $Dissociation\,(t(0))$ are the initial conditions. Once the protein binding is saturated (a steady state) on the QCM-D sensor, the buffer is injected. This step represents the the start of protein dissociation.

Step 1: $$k_{ob} = [C_0]\frac{k_a}{k_d} \tag{10}$$

Step 2: $$K_D = \frac{k_d}{k_a} \tag{11}$$

Step 3: $$\rho_e = \rho_{max}\frac{[C_0]}{[C_0] + K_D} \tag{12}$$

Step 4: $$[PS]_{rev} = \rho_e\left(1 - e^{(-k_{ob}t)}\right), t < t(0) \tag{13}$$

Step 5: $$Y\big(t(0)\big) = \rho_e\left(1 - e^{\left(-k_{ob}t(0)\right)}\right), t \geq t(0) \tag{14}$$

Step 6: $$Dissociation\ of\ [PS]_{rev} = Y\big(t(0)\big)(1 - e^{\left(-k_{ob}t(0)\right)}) \tag{15}$$

Step 7: $$Y = If\ (X < t(0), Association, Dissociation) + [PS]_{irr} \tag{16}$$

where $[PS]_{irr}$ denotes the protein-substrate intermediate with irreversible protein bound to the surface, in units of the mg/m^2.

2-3-4 Techniques for measurement of protein adsorption

To date, several techniques based on different principles such as optical adsorption, refractive index changes, radio-labeling, electromechanical microbalances, fluorescence markers and many others have been used to study protein adsorption on different surfaces (Höök *et al.*, 2002, Jordan and Fernandez, 2008). Other techniques that have been explored for measuring protein adsorption are the QCM-D, AFM, XPS, surface-nuclear magnetic resonance (NMR) and other optical techniques, such as, OWLS and SPR. A number of the optical techniques such as ellipsometry, OWLS, SPR and XPS are described briefly below.

2-3-4-1 Atomic Force Microscopy (AFM)

AFM is a scanning probe technique for analyzing surface topography and protein adsorbed on surfaces. It directly measures the real-space topography of surfaces on a nanometer scale and detects the spatial distribution of adsorbed proteins. The AFM force measurements measure interaction forces between protein and protein-resistant layers (Hemmerlé *et al.*, 1999).

The AFM has a sharp tip at the end of the cantilever. The interaction between the tip and the surface occurs when the tip is brought close to the surface and high resolution images can be obtained when the tip is scanned through the entire surface. Three imaging modes as shown in Fig. 2-6 are used to produce the images of the sample surface:

(1) **Contact mode:** In the contact mode, the tip of the AFM probe is in permanent physical contact with the sample.

(2) **Tapping mode:** Here the probe is oscillated such that the tip contacts the sample intermittently. The resonance frequency controls the probe-sample interaction force. This mode is generally applied to soft films.

(3) **Non-contact mode:** The force applied by the AFM probe to the sample is reduced in the non-contact mode. This mode allows easy and productive image of delicate samples (Ngadi, 2009).

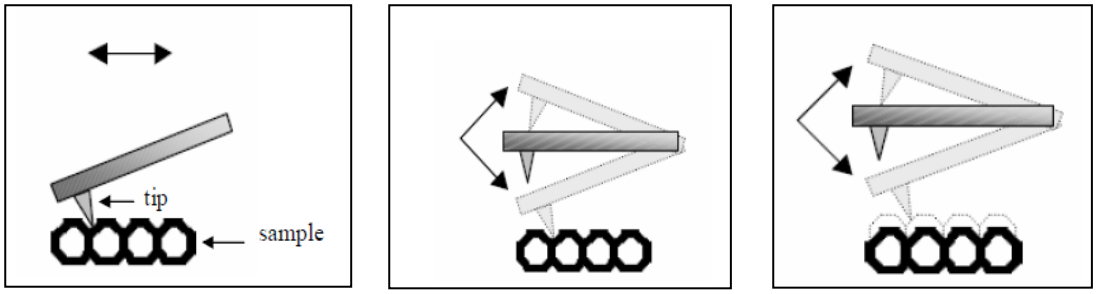

(a) (b) (c)

Figure 2-6: AFM Imaging Modes: (a) Contact-mode, (b) Tapping mode and (c) Non-contact mode (Ngadi, 2009)

AFM provides a 3-dimensional (3-D) surface profile with high resolution and does not require any pretreatment of the surface, thus not affecting the sample for analysis. The disadvantage of the AFM is that it can only probe a maximum height of 10-20 μm (Lee *et al.*, 2006a, Lee *et al.*, 2006b). The low scanning speed of the AFM is also one of its disadvantages, inducing thermal drift and distortions in the image (Khulbe *et al.*, 2008). As a topographical scanning technique, AFM does not help to understand the nature of the adsorbed film and its sharp tip could damage the adsorbed layer (King *et al.*, 2009).

Recent studies suggest that high-speed AFM provides quick and reliable information about the structural changes in biomolecules during adsorption onto the surfaces. High-resolution and high-speed capabilities of this recently developed AFM could be used in the imaging of secondary structures on adsorbed protein onto surfaces. It also has the capacity to accurately measure changes in the water layer structure at protein surfaces and detects small interactions of water with the protein's active site which is not possible to study these phenomena by using conventional high-speed AFM (Ando *et al.*, 2008). Minimal contact force exerted along with high precision positioning of the probe used in high speed AFM techniques allows accurate imaging of the biological samples (Zou *et al.*, 2004, Ren and Zou, 2014).

2-3-4-2 Ellipsometry

Ellipsometry, is one of the most extensively used optical techniques for measuring the thickness, d_f and the refractive index, n_f of the adsorbed layer.

The basic principle behind this technique is that the polarization state of an incident light beam is changed upon reflection at a planar surface. This occurs due to changes in the dielectric properties of the interfacial region. These changes in the interface are brought about by the changes in the amplitude and phases of the oscillating parallel and perpendicular vector components of the electric field. A change in the state of polarization is described by the ellipsometric angles, ψ and Δ, where ψ represents the ratio of the reflection coefficients for parallel and perpendicular polarized light with respect to the analyzer position and Δ is the difference in phase change between parallel and perpendicular light with respect to the polarizer position (Azzam and Bashara, 1977, Arwin, 2000). The surface mass density, Γ (mass per unit area) is then calculated using the Feijter's formula (De Feijter *et al.*, 1978):

$$\Gamma = d_f \frac{n_f - n_0}{\frac{dn}{dc}} \qquad (17)$$

where, d_n/d_c is the refractive index change per unit protein concentration (protein specific) while n_0 is the refractive index measured in bulk. Also d_f and n_f can be calculated directly from the measurements in change in polarization.

Characterization using ellipsometry has been used to study biological samples and also offers the possibility to quantify adsorption and desorption processes on surfaces. One of the merits to ellipsometry is that compared with the other techniques, studies have shown the determination of layer thickness and orientation of the adsorbed non-symmetrical shaped proteins can be derived (Arwin, 2000).

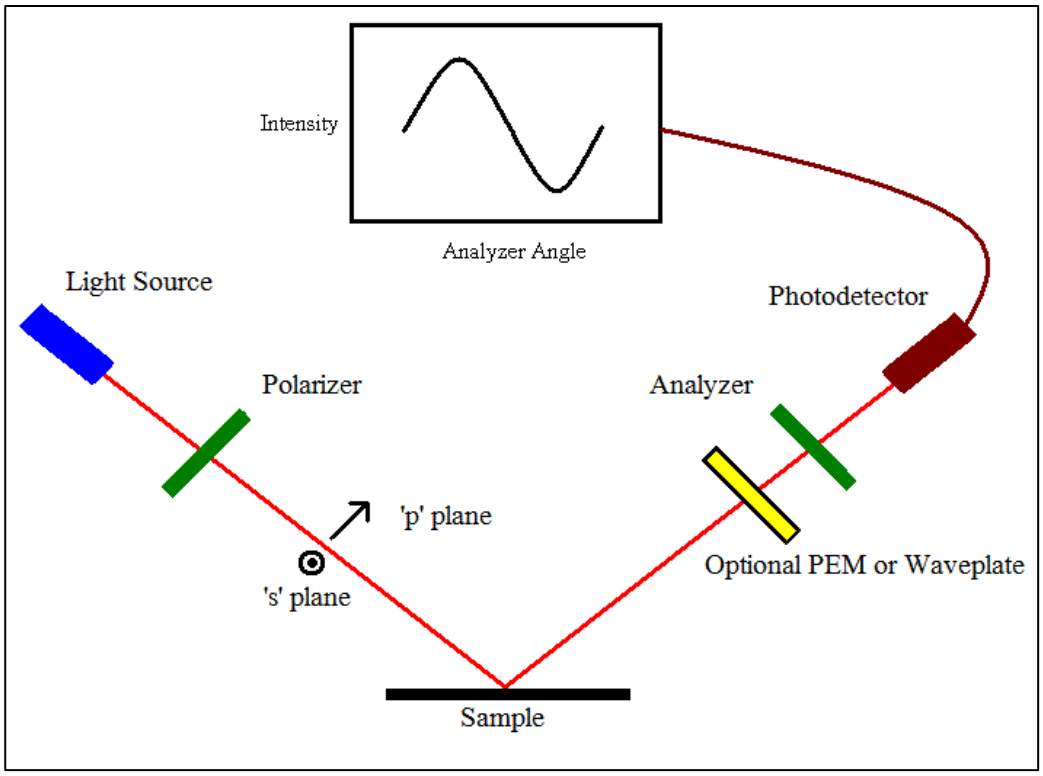

Figure 2-7: Principle of Ellipsometry (Brockman, 2007)

Ellipsometry provides information on adsorbed proteins and other bio-molecules on surfaces and the properties of these adsorbed films. Being an optical technique, the disadvantage of this technique is that only the adsorbed molecules are detected by ellipsometry and not any solvent or water that is trapped in between the adsorbed layers.

2-3-4-3 Optical Waveguide Lightmode Spectroscopy (OWLS)

The OWLS technique is based on the use of He-Ne laser coupled into a planar waveguide via optical grating (Tiefenthaler and Lukosz, 1989).

The variation principle behind OWLS is that, the angle of the incident light beam excites the different guided transverse electric (TE) and transverse magnetic (TM) modes and this when coupled with the light intensity is measured with the help of a photo detector. Measuring the shift of these in coupling angles allows the monitoring of the macromolecules adsorbed above the grating surface.

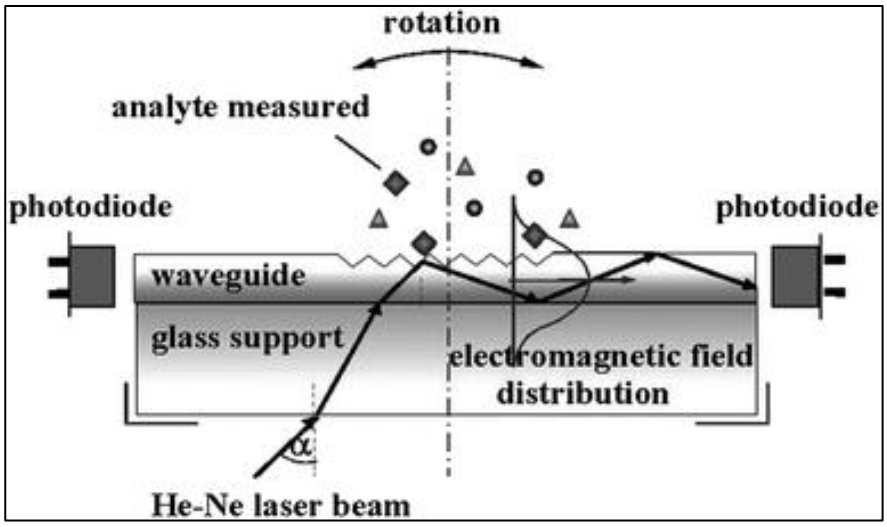

Figure 2-8: Principle of OWLS (Székács, 2009)

The variables d_f and n_f of thin (<50nm) and homogenous adsorbed layers can be determined from the phase shifts between TE and TM (Tiefenthaler and Lukosz, 1989). The surface mass density of the adsorbed layer is then calculated in a similar manner to ellipsometry using the Feijter's formula (De Feijter *et al.*, 1978).

A merit to OWLS in comparison with the ellipsometry technique is that the light beam does not have to pass through the solution to interact with the surface. Hence, the changes in the optical properties of the solution do not affect the measurement of the adsorbed layer. The disadvantage of this technique is that only highly transparent surfaces can be investigated and not opaque surfaces (Ngadi, 2009). OWLS relies on the refractive indices of the proteins in the solution, the measured adsorbed mass includes the mass of the proteins and not that of the water (or solvent) that is trapped between the adsorbed particles.

2-3-4-4 Surface Plasmon Resonance (SPR)

SPR spectroscopy is an optical technique that is sensitive to changes in the refractive index of the thin films assembled on a noble-metal surface (Jönsson and Johansson, 2004) .

SPR utilizes surface plasmon polarization excitations that consist of charge-density waves propagating along the interface between a metal and a dielectric material (prism), to sense the local refractive index in the liquid close to the gold surface. This

phenomenon occurs when an incident beam of p-polarized light of a given angle is passed through a prism. The photon-plasmon surface electromagnetic waves are created at this metal-dielectric interface and these waves then propagate parallel to the metal dielectric interface and the associated optical electric field decays exponentially away from the surface with a typical decay length of 200 nm. The detector continuously records the position of the reduced light intensity and calculates the SPR angle of the reflected light reported in resonance units (RU) (Ngadi, 2009).

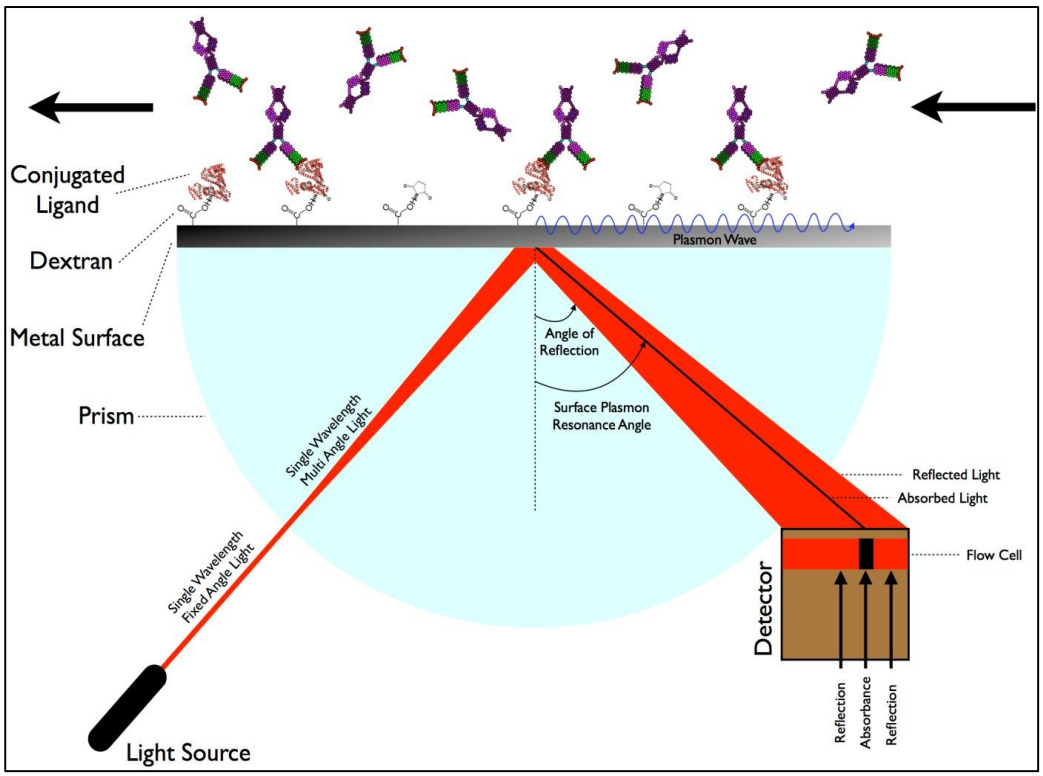

Figure 2-9: Principle work of a SPR (Sabban, 2011)

As adsorption of proteins occurs on top of a surface, the angle of the SPR is changed in accordance to it. The change in the SPR angle is proportional to the mass adsorbed at the surface according to,

$$\Delta m_{SPR} = \frac{C_{SPR} * \Delta RU}{\beta} \tag{18}$$

where Δm_{SPR} is the surface mass density adsorbed, C_{SPR} is a factor that contains an instrument constant, ΔRU is the measured change in response units, and β is a factor

that compensates for the decrease in the SPR signal with distance from the gold substrate (Ngadi *et al.*, 2008).

SPR helps in evaluating the kinetics of the adsorbed layer but only for compact and dense adsorbed layers. SPR, being an optical technique, greatly limits the determination of the film thickness. The adsorbed mass determined by the SPR is based on the difference in refractive index between the adsorbed proteins and other bio-molecules and water displaced by the biomolecules upon adsorption. This means that water trapped between the protein adsorbed layers is not included in the determination of the mass.

2-3-4-5 X-ray Photoelectron Spectroscopy (XPS)

XPS is a quantitative surface characterization technique. The principle behind XPS is the bombardment of the sample surface with x-rays resulting in the removal of electrons from atoms in the material (Premathilaka *et al.*, 2007). The element is analyzed by the binding energy of the ejected electrons providing the elemental composition of the surface in general. In XPS, electrons are released from the sample by the process of photoemission. An electron is ejected from an atomic energy level by an X-ray photon and its energy is analyzed by the spectrometer. The XPS process is represented in Fig. 2-10 for the emission of an electron from the 1s shell of an atom.

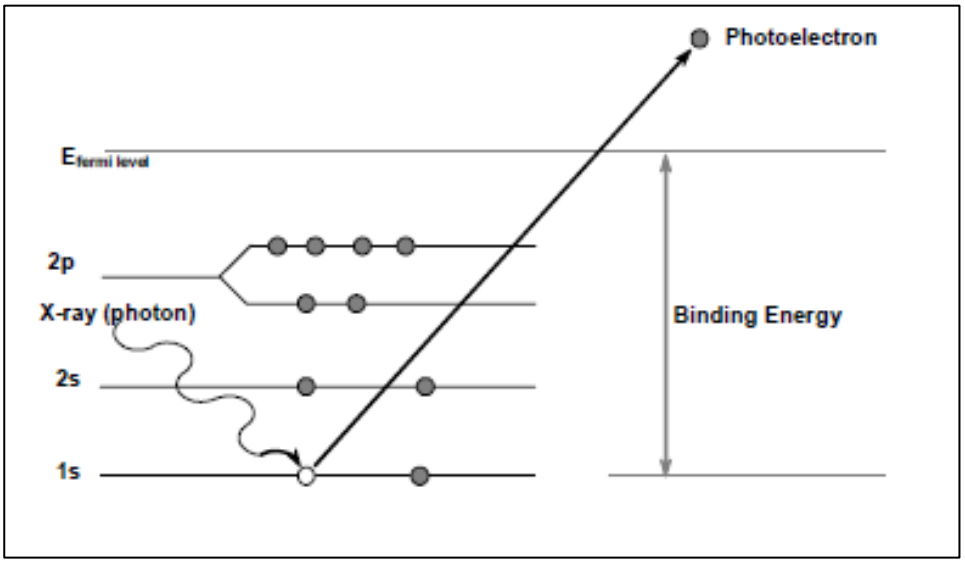

Figure 2-10: Principle of XPS

The main advantage of XPS is that it detects both the chemical state on surfaces and is also quantitative. XPS is capable of detecting the difference in chemical and oxidation states between samples. One of the major limitations of the XPS is that only ~10 μm of the surface area can be measured and the samples must be compatible with the ultrahigh vacuum environment. Because XPS is a surface technique, it is limited to measurements of elements having atomic numbers of 3 or greater, making it unable to detect hydrogen or helium (Andrade, 1985).

2-3-5 Quartz Crystal Microbalance - Dissipation

The core part of this research work uses of the QCM-D technique to monitor the protein adsorption on surfaces in the aqueous phase. Although optical techniques like the ones mentioned above are used to estimate dry protein mass, QCM-D determines the total "wet" (protein and water molecules) mass adsorbed on the surface (Yu *et al.*, 2012, Gray, 2004).

QCM-D is an experimental approach capable of measuring changes in adsorbed mass and viscoelastic properties of adsorbed material via differences in the frequency and decay of oscillation, respectively (Rodahl and Kasemo, 1996). QCM-D is an instrument that has become widely used to study soft and solvated surfaces. This technique includes a mass sensing device with the ability to measure very small mass changes, either a monolayer or a single layer of atoms on a quartz crystal (sensor) in real-time. Hence, QCM-D is a rapid tool for studying protein adsorption kinetics in aqueous solution (Shen *et al.*, 2001). The possibility of monitoring the kinetics of adsorption allows an opportunity to model the adsorption and desorption with rate equations.

The basis of QCM-D operation relates to the quartz's property of piezoelectricity. The QCM-D sensor is made of a thin piezoelectric quartz crystal, sandwiched between a pair of metal electrodes that establishes an electric current across the diameter of the crystal (Höök, 1997). The resonant frequency of the oscillating crystal surface is related to the total oscillating mass adsorbed on the surface over time, while the energy dissipation, shown in Fig. 2-11(*c*) is related to the viscoelastic properties of the oscillating mass on the sensor surface. For viscoelastic masses, such as biomolecules, the change in the adsorbed mass is detected using both frequency and

dissipation changes. For a rigid protein, the change in the adsorbed mass is detected only by the frequency change.

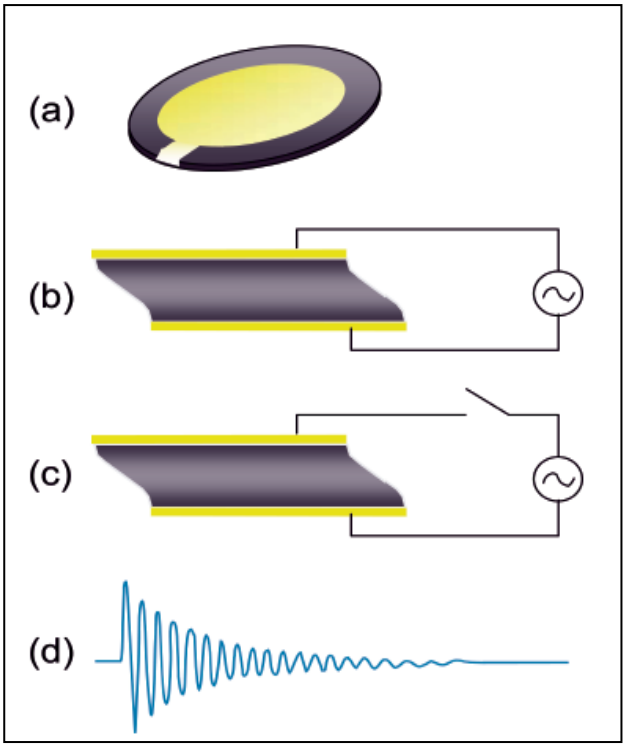

Figure 2-11: The main components in QCM-D where, (a) typical QCM-D sensor with Gold (Au) electrodes, (b) quartz crystal with alternating current applied across electrodes, (c) short circuiting the alternating current and, (d) the oscillatory decay as the quartz disk comes to rest (Dixon, 2008)

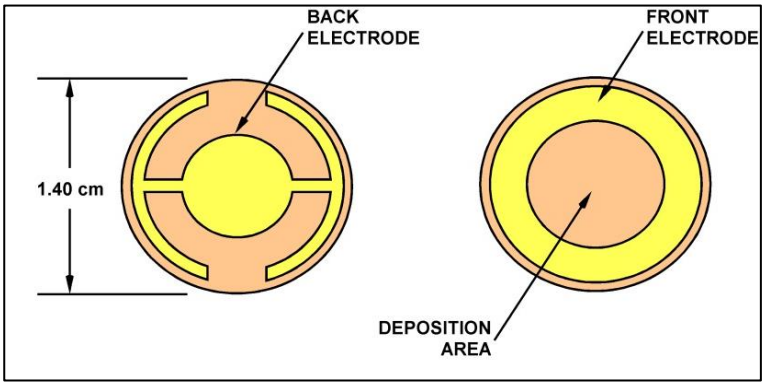

Figure 2-12: Quartz resonator in QCM-D depicts a typical sensor surface (Hellstrom, 2007)

When an AC voltage is applied over the electrodes, the crystal is made to oscillate at its fundamental frequency (f_0). When sufficient voltage is achieved, and the fundamental frequency is attained the resonance is excited. The resonant is measured in terms of maximum amplitude of the signal attained. The shift in the dissipation is measured by the QCM-D system as a result of change in damping of the QCM-D crystal during measurements that occurs when the viscoelastic properties of the adsorbed layer changes. The dissipation factor is defined as follows (Ngadi, 2009):

$$\Delta D = \frac{E_{dissipated}}{2\prod E_{stored}} \tag{19}$$

where $E_{dissipated}$ is the energy dissipated during one oscillation and E_{stored} is the energy stored in the oscillating system. The QCM hence measures simultaneously changes in resonance frequency, f and dissipation, D (the frictional and viscoelastic energy losses in the system) due to adsorption and desorption of bio-molecules on the sensor surface. Change in frequency corresponds to the mass adsorbed while changes in the dissipation are related to the shear viscous losses brought about by the adsorbed layers, and thus provide information that helps to identify structural differences between different adsorbed systems, or structural changes in the same type of molecule, or aggregation of molecules during the adsorption process (Q-Sense).

The main advantages of QCM-D are that the acoustic basis of the technique allows measurement of thicker films of adsorbed proteins than thinner layers of bio-molecules. It also detects subtle changes in the solution – surface interface, that could be due to density – viscosity changes or viscoelastic changes in the adsorbed interfacial material (Marx, 2003). The change in frequency acquired with QCM-D measure water coupled as an inherent mass, and/or entrapment in cavities in the adsorbed film and the layer is sensed as a "hydrogel" composed of the macromolecules and coupled water. The additional information contained in energy dissipation data from QCM-D increases the capacity for an in-depth analysis of the adsorbed layers (Q-Sense). The major disadvantages of the QCM-D are the need of large sample volumes for experimentation and the measured adsorbed mass is the average mass across the sensor surface (Garg *et al.*, 2011).

2-3-5-1 Data Interpretation of QCM-D

The QCM-D result can be analyzed either using the Sauerbrey model or the Kelvin-Voigt viscoelastic model (Voigt model). Both the models are present in Q Tools (provided by Q-Sense, ATA Scientific, Tarren Point, NSW, Australia). These models are briefly described below:

Sauerbrey Model

Prediction of linear relationship between the deposited mass per unit area (Δm) and the measured Δf was derived by Sauerbrey (1959). The relationship is as follows:

$$\Delta m = -\frac{\rho_q v_q \Delta f}{2 f_0^2 n} = -\frac{\rho_q t_q \Delta f}{f_0 n} = -C\frac{\Delta f}{n} \qquad (20)$$

where, ρ_q, v_q and t_q are the specific density, the shear wave velocity and the thickness of the quartz sensor, respectively, and n is the number of the overtone (n = 1, 3, 5, 7, 9…). For a 5 MHz quartz crystal, the constant *C* is equal to 17.7 ng/cm^{2}Hz (Malmström *et al.*, 2007). The Sauerbrey model is valid only when the adsorbed layer of biomolecules is rigid and viscoelastic effects are negligible, as the main assumption in this model is that the resulting change in the resonant frequency is directly proportional to the mass adsorbed on the surface, with no change in dissipation energy. In case of the material adsorbed behaving as a viscous layer, energy dissipation affects the change in measured resonance frequency and the Sauerbrey model underestimates the actual mass of the adlayer. A good method to characterize the rigid and viscoelastic properties of the layer adsorbed is to evaluate the $\Delta D/\Delta f$ ratio, from the slope of a ΔD vs. Δf plot. As a rule of thumb, if only a small dissipation shift is observed, i.e. $\Delta D/(-\Delta f/n) << 4*10^{-7}$ Hz^{-1} for a 5 MHz sensor, then viscoelastic dissipation of energy can be neglected and the Sauerbrey model can be safely used for interpretating of the data (Irwin *et al.*, 2005, Stengel *et al.*, 2005b, Reviakine *et al.*, 2011).

Kelvin-Voigt Viscoelastic Model (Voigt Model)

In some cases, the adsorbed film does not form a rigid layer (for example, very hydrated layers) and in these situations the Sauerbrey Model becomes invalid. Figure

2-13 represents the adsorbed layer formed on the sensor surface. For films that are 'soft' and not fully coupled to the oscillation of the crystal, the Sauerbrey Model underestimates the mass of the film on the sensor surface and in this case the Voigt model is implemented for calculation on thickness of the adsorbed layer on the surface (Malmström *et al.*, 2007, Stengel *et al.*, 2005b, Irwin *et al.*, 2005).

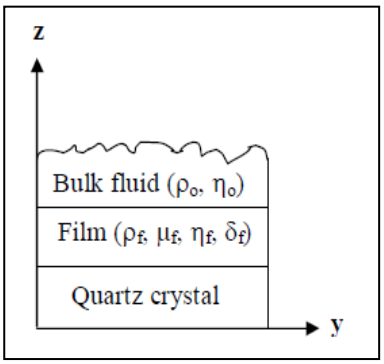

Figure 2-13: System modeled by the Kelvin-Voigt Viscoelastic Model. The quartz crystal is covered by a thin film that can be described by ρ_f, μ_f, η_f and δ_f under no slip conditions. The film is covered by a semi-infinite Newtonian fluid with ρ_0 and η_0 properties.

In brief, the Voigt-based viscoelastic model consists of four parameters; effective film density (ρ_f), film shear viscosity (μ_f), film shear elastic modulus (η_f), and the film thickness (δ_f). As the viscous layers (adsorbed films) give rise to different penetration depths of the harmonic acoustic frequencies, multiple frequencies are thus simultaneously fitted to calculate the values of ρ_f, μ_f, η_f and δ_f. The mass of the layer M_{voigt} is obtained as a product of the fitted value of thickness, δ_{voigt} with the estimated effective layer density.

2-3-5-2 Water content in protein adsorbed layers

As mentioned earlier, QCM-D detects the total adsorbed mass that includes water molecules trapped in the adsorbed protein layers. It is essential to detect the percentage of water in these layers for accurate determination of the protein adsorbed on the surface. The typical amount of coupled water involved has been previously studied by different techniques on the basis of the nature of the film, mass uptake and protein characteristics (Schreiber and Haimovich, 1983).

Other authors have combined two different and independent experimental techniques on two different sensor surfaces to study the amount of hydration water present in this protein adsorbed layer; for example, one sensor in QCM-D and another in SPR. Although attempts are made to keep conditions comparable between the two systems, nonetheless, the results from subtracting the ("dry") mass from the optical technique from the ("wet") mass of the QCM-D to determine the protein and water fractions may not be entirely accurate. Usually, these are QCM-D for the determination of the wet mass and SPR or ellipsometry to estimate the dry mass. For example, using QCM-D and SPR, the adsorption of ferritin on gold surfaces was studied by Caruso *et al*. (1997), who determined that 43% of the adsorbed layers were water. Yugi *et al*. (2012) also compared SPR and QCM-D results and found that ~25-67% was associated water. Anand *et al*. (2010) considered blood proteins on various metallic surfaces and found that, on average, ~58% was associated water. Independent studies by Heiden *et al*. (2007) reported that more than 90% of the mass detected on the QCM-D sensor was due to trapped water molecules. In addition to QCM-D and SPR, Höök *et al*. (2002a) used ellipsometry to study adsorption of proteins on titanium oxide surfaces. On comparison of the QCM-D wet mass to the dry mass obtained by ellipsometry, they found that 34-56% of these adsorbed layers was associated water.

The main drawback in the above mentioned analysis is that different surfaces that have been utilized to compare dry and wet mass of proteins adsorbed. The above mentioned studies detect and compare masses on separate principles. For example, SPR is an optical technique and the dry mass obtained is compared with the QCM-D, an acoustic technique for wet mass. This causes uncertainty and inconsistency. On the other hand, in this study, the wet and dry mass analyses are being performed independently using the same SS sensor surface through the QCM-D and the fluorescent microscope. .

2-4 Bio-inspired coatings development

After protein adsorption was studied in depth, the aim of the thesis was to study a particular adhesive available in nature and test its adhesiveness to SS. The focus was on one particular post-translational modification of tyrosine to DOPA in peptide fragments. The peptide fragments were produced synthetically, while the conversion

of tyrosine to DOPA was performed chemo-enzymatically using mushroom tyrosinase. The adsorption of these modified peptide fragments, compared with their unmodified counterparts are reported in detail in Chapter 4. Below, is a review of related work on bio-inspired adhesives, as these provide a background to the study of bio-inspired coatings.

Nature has been developing adhesives for millions of years in its own way. The earliest reported uses of adhesives were caulking ships with tars and sealing jars of spices with asphalt by the Phoenicians (Creton and Papon, 2003). Naturally available adhesives that have already been exploited for many technical applications include casein, latex rubber, tree gum, and adhesives of natural textiles, production of paper and sealing of jars (Rischka *et al.*, 2010). The industrial development of adhesive was first observed in the 15^{th} century. Although the application of natural adhesives still plays a vital role, modern adhesives have been associated with the development of synthetic polymers in the 20^{th} century (Creton and Papon, 2003). "Bio-inspired coatings" are named after their origin – from biological species. There have been various proven applications of adhesion obtained from the biologicals including the use of plant based adhesives for self-healing (Keckes *et al.*, 2003, Schreiber *et al.*, 2005). On the other hand, animals producing sticky compounds defend themselves against predators and to hunt their prey (Voigt and Gorb, 2008, Flammang, 2006). The key interest of the bio-mimetic coatings is the interaction between the material and a surface, whether the surface is of biological or non-biological origin (Silverman and Roberto, 2007). The choice for this study was mussel foot protein. Instead of studying natural mussel protein (that contributes to adhesion) we used specific fragments of the mussel proteins to study adsorption on SS (Section 2-5-1), in particular after modification of tyrosine residues to DOPA.

2-4-1 Marine adhesives

The biological adhesives are broadly categorized into four genera: freshwater caddisfy larva, sandcastle worms, acorn barnacles and blue mussels. These are categorized on the basis of the broad range of function of the adhesives – mechanistic features and unique adsorption characteristics. The caddisfy larvae make use of the sticky underwater silk to exploit their habitats, whereas the sandcastle worms live in

tubes that have been assemble by sand, shell fragments and underwater proteinaceous glue. Acorn barnacles glue their base plate to the rocks. Mussels hang on with a handful of high-tech threads that mitigate the mechanical mismatch between hard rock and the soft invertebrate. Other examples include snails, brown algae (kelp), tubeworms and starfishes (Stewart *et al.*, 2011).

2-4-2 Special characteristic features of mussel adhesives

Mussel attachment to varied surfaces (Fig. 2-14) has been one of the earliest observed means of bio adhesion. Freshwater mussels or molluscs, of the subfamily *Dresisena* adhere to temporarily or permanently in an aqueous environment to a variety of surfaces (Francisco and Heather, 2010). They use a proteinaceous secretion called "byssus" that enables a strong, durable adhesion. The term "byssus" (Greek – "bysso" for flax linen) was coined accidently by Aristotle (Ehrlich, 2010). Mussel byssi originate from a root that is attached to the byssal reactor muscle and a stem that extends from the root. Byssal threads terminate into byssal plaques (Francisco and Heather, 2010).

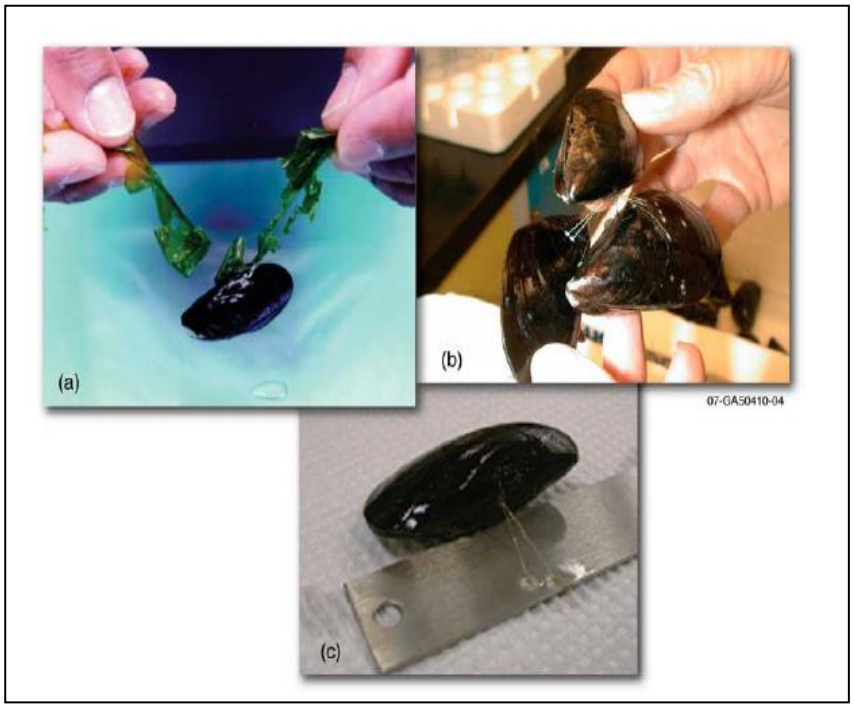

Figure 2-14: Mussel attachment to (a) Seaweed, (b) Other mussels and (c) SS (Silverman and Roberto, 2007)

The first description of the mollusc byssus was done in 1711. The work described that the byssal thread of *Mytilus edulis* displayed different morphology throughout the length of the byssus. They emerged from the mussel as the proximal thread and attached to the surfaces at the distal thread and plaque. Byssal threads range from 2 to 4 cm long and 0.1 mm in diameter. They have a flexible and soft core that is enclosed within a hardened sheath or cuticle. The core has three unique collagens – precol C, precol D and precol NG. They also contain the five major proteins (termed *Mefp* – *Mytilus edulis* foot proteins 1 to 5). Table 2-1 lists the different foot proteins contributing to the adhesive properties of mussels.

Table 2-1: Byssal protein adhesive properties (Francisco and Heather, 2010)

Biological Classification			**Adhesive materials classification**	
Byssus	**Region**	**Mussel proteins identified**	**Function**	**Curing mechanism**
Plaque	Primer layer	fp-3,5,6	Primer plaque/ primer	Couple with inorganic (metals) and organics
	Plaque foam	fp-2	Stabilize	Inter- and intra-molecular cross-linking
	Thread collagen anchor	fp-4		
Thread	Thread sheath (cuticle)	fp-1	Varnish/coating	Inter- and intra-molecular cross-linking
		Polyphenol oxidase		Oxidation
	Thread core	distal precol –D	Rigid	Inter-and intra-molecular cross-linking
		proximal precol-PTMP-1	Elastic Rigid	
		Non-gradient Precol-NG	Rigid and elastic	

This byssal thread and adhesive plaque is formed by the secretion of the liquid protein from within the gland. Solidification of this secreted liquid occurs rapidly and provides a stable attachment (Silverman and Roberto, 2007, Ehrlich, 2010, Francisco and Heather, 2010). The bysuss thread holds the animal firmly to the substrate against the activity of waves and predators. Each byssal thread has the potential to withstand a tensile force of 0.25 N, and nearly double this magnitude if it is dry. The molluscs has therefore developed effective strategies to survive turbulent and windy shores (Ehrlich, 2010).

2-4-2-1 Importance of 3, 4-dihydroxyphenylalanine (DOPA) in adhesion

Nature impressively demonstrates the use of polyphenolic compounds in different materials. Different marine organisms use these compounds as adhesives (Rischka *et al.*, 2010). The reactive functional moiety of interest is frequently a special phenolic-based structure, DOPA that has the ability to react in different ways with itself or with other functional groups (Yu *et al.*, 1999, Rischka *et al.*, 2010). 'Catechols' are phenolic compounds that contain hydroxyl groups in the ortho position and are useful in chemical linkage or chelation (Rischka *et al.*, 2010). DOPA has played a double role in marine adhesion, being important for both the cohesive and adhesive properties of the mussel adhesive. DOPA shows specific interactions with metal and metal oxide surfaces. Cross-linking between DOPA molecules also play an important role in adhesion. Earlier adsorption studies have shown the nature of aggregated adsorbed layers of mussel proteins (due to the presence of DOPA) on surfaces (Haemers *et al.*, 2003).

Mytilus edulis foot protein-1 was the first of the polyphenolic proteins to be identified (Waite and Tanzer, 1981). The primary location of the Mefp-1 is in the byssal threads and it has a molecular mass of 115 kDa and 897 amino acids. Mefp-1 protein is mainly built from two building blocks of 71 deca-peptides containing the amino acid residues AKSTYP`P``TYK, that comprises of the major consensus repeat and the 12 deca-peptides of AKPTYK (here three post-translational modifications have been observed: Y represents DOPA – conversion of tyrosine to DOPA, P` represents trans-2, 3-cis-3, 4-dihydroxyproline, and P`` represents trans-4-hydroxy-L-proline). *Mefp-1* proteins constitutes over 10-15 mol% DOPA content (Francisco and Heather, 2010,

Silverman and Roberto, 2007, Ehrlich, 2010). *Mefp-1* requires oxidation of tyrosine residues by enzymes such as catechol oxidase, tyrosinase, or sodium periodate for conversion to the reactive DOPA residues required for strong adhesion. This particular adhesive protein is now commercially produced and available from several companies (Silverman and Roberto, 2007).

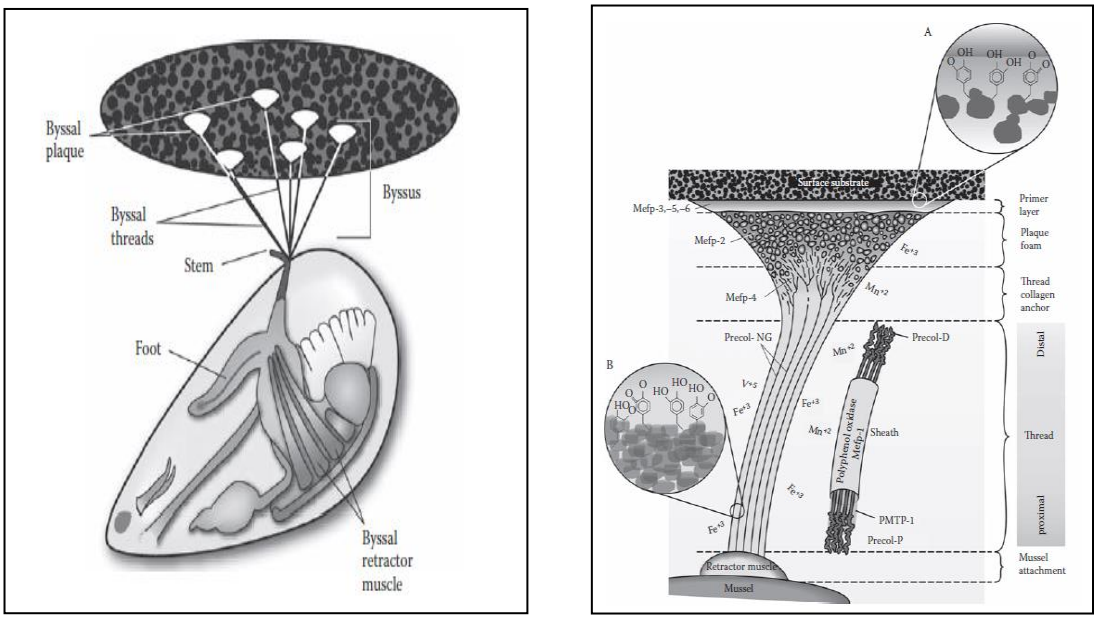

Figure 2-15: (a) Anatomy of *Mytilus edulis* and byssus structures (Silverman and Roberto, 2007) and (b) location of adhesive-related proteins identified in *Mytilus edulis* (Silverman and Roberto, 2007)

Mefp-2 is found in the byssal plaques, constituting 25-40% of the plaque proteins. Unlike *Mefp-1*, this protein is smaller and has a molecular mass of 42–47 kDa. Only 2–3% of DOPA is found in *Mefp-2* and there is no hydroxylation of proline to trans-2, 3-cis-3, 4-dihydroxyproline or trans-4-hydroxy-L-proline. The stabilization role in the byssus has been suggested to occur due to the high cysteine content (6 to 7 mol %) in the *Mefp-2* (Ehrlich, 2010, Silverman and Roberto, 2007).

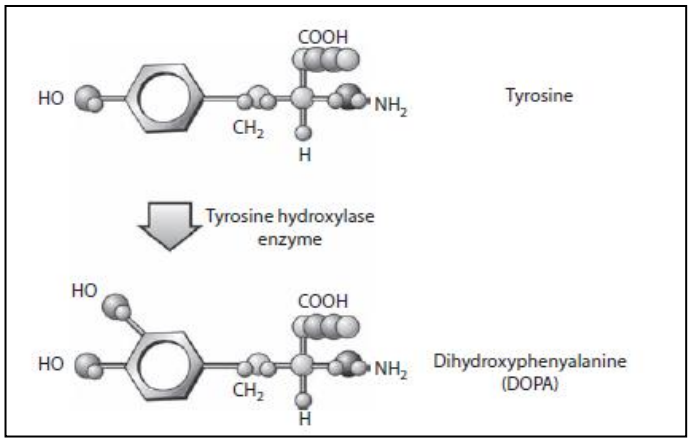

Figure 2-16: Hydroxylation of tyrosine residues in *Mytilus edulis* (Silverman and Roberto, 2007)

Mefp-3 is the smallest of the byssal adhesive proteins identified and has a molecular mass of ~ 5 to 7 kDa; it contains no repeats and has over 20 to 25 mol% of DOPA residues in its composition. The molecular mechanism for the binding of Mefp-3 to substrates has still not been completely explored, although it is predicted that the influence of factors such as exposure time to surfaces, water temperature and age of the animal plays a key role in expression levels of the protein (Silverman and Roberto, 2007).

Mefp-4 is found in the bulk adhesive of the plaque, having a MW of 79 kDa. This protein contains very high amounts of levels of glycine, arginine and histidine and about 5% of DOPA in its sequence (Silverman and Roberto, 2007, Ehrlich, 2010).

Mefp-5 is one of the most recently discovered adhesive proteins. It is relatively small having a MW of 9.5 kDa comprising of 74 residues and 27% DOPA content (Ehrlich, 2010, Silverman and Roberto, 2007). Mefp-5 is found to be rich in non-aromatic residues – lysine and glycine represent 65% of the composition. Mefp-5 also has the highest DOPA content - one in four amino acids of the sequence is DOPA (Ehrlich, 2010).

A newly discovered protein *Mefp-6*, that could possibly explain the link between DOPA-rich proteins and plaque proteins has been identified. It has a MW of 11.6 kDa and higher tyrosine content than DOPA (Silverman and Roberto, 2007).

2-5 Synthetic production of DOPA in fragments

2-5-1 Choice of study fragments

Development of synthetic polymers has been a potential source for functionally equivalent adhesives found in nature. *Mefp-5* is the least polymorphic of the plaque proteins with abundant of glycine and lysine amino acid residues(Lee *et al.*, 2011). In addition to DOPA, there is potential involvement of lysine in adsorption(Yu *et al.*, 1999). In this study we have chosen fragments of the whole protein (mefp-5) because of the presence of DOPA. Two fragments containing 50% and 30% tyrosine respectively, KGYKYY and KGYKYYGGSS have been chosen for chemo-enzymatic modification. They were subjected to chemical modification for formation of DOPA residues and the adhesion properties were studied using QCM-D.

2-5-1 Chemo-enzymatic modification of tyrosine to DOPA

Waite *et al*. (2000) studied the adhesive properties of natural mussel substances in detail. Although natural extraction has been initially used to isolate mussel adhesive protein for commercial purposes, this process is labor-intensive and requires around 10,000 mussels for 1 mg of protein (Dodson *et al.*, 1979). There have been attempts to express functional and economical mussel adhesive proteins, but these have failed in many instances due to the presence of the highly biased amino acid composition (five amino acids comprise ~89% of the total amino acids in *mefp*-1), different codon usage between mussel and other expression systems (problem in utilizing transfer RNA (tRNA)), and the small amount of adhesive produced (Hwang *et al.*, 2004). The focus of this study is to explore adsorption of fragments of *mefp-5* having higher amounts of tyrosine, 50% and 30% respectively (KGYKYY and KGYKYYGGSS), obtained from synthetic production. These fragments were then subjected to mushroom tyrosinase to modify tyrosine to DOPA residues.

2-5-2 Analysis of DOPA produced by high performance liquid chromatography (HPLC)

Tyrosinase (EC 1.14.18.1) is a copper-containing oxido-reductase catalyzing two sequential reactions: hydroxylation of monophenols to *o*-diphenols (cresolase activity) and the subsequent oxidation of *o*-diphenols to *o*-quinones (catecholase

activity), both requiring molecular oxygen as the oxidizing agent (Xu *et al.*, 2012, Taylor, 2002). Mushroom tyrosinase was employed for hydroxylating tyrosine-containing sequences in peptides to DOPA. Ito *et al*. (1984) have a simple and rapid method for quantificating of DOPA produced from chemo-enzymatic conversion using tyrosinase at 0, 30, 60 and 120 minutes with BSA. Gieseg *et al*. (1984) also followed a similar approach of incubating proteins with tyrosinase for modification to occur at 0, 1, 2.5, 4 and 6 hours with bovine insulin.

2-5-3 Adsorption of modified and unmodified fragments

The function of the mussel adhesive thread is to hold the animal firmly to the substrate against the activity of waves and predators. It is therefore important that it is not only strong but also able to absorb energy imparted by breaking waves and strong surges. Each byssus thread can withstand a tensile force of about 0.25 N (Ehrlich, 2010). The role of DOPA in the mussel adhesives has been best understood as it related to solidification of the secreted adhesive liquids, a process that derives from protein crosslinking reactions giving rise to highly cross linked bulk protein matrix. DOPA residues are found to interact with organic and inorganic surfaces through π electron interactions (Waite, 1976). DOPA is also capable of both donating and accepting hydrogen bonds, which allows DOPA to compete well with water bonding to hydrophilic and polar surfaces (Lee *et al.*, 2006a).

In this study, the main differences in adsorption of the modified and unmodified fragments of the *mefp-5* proteins are explored. Earlier results have shown the adsorption of complete *mefp* fragments to surfaces. For example, DOPA residues can form coordinate metal ion complexes with SS and titanium, thus increasing the interaction of DOPA with the surface (Monahan and Wilker, 2003, Sever *et al.*, 2003).

Chapter 3 - Protein adsorption studies on stainless steel sensors using a quartz crystal microbalance with dissipation

Introduction

In this chapter the adsorption behaviour of proteins onto SS grade 316 surfaces is explored using QCM-D. The chapter consists of four major parts: (1) experimental work on adsorption of commercially obtained proteins, using QCM-D, (2) development and application of a new technique combining fluorescence and QCM-D measurements on a single sensor to determine the relative contributions of water and protein to the mass of the adsorbed layer, (3) exploring the various parameters affecting protein adsorption, including the use of principal component analysis to examine the influence of amino acid characteristics found on the surface of proteins and determining an empirical equation to assess their adsorption and (4) kinetic models that describe reversible and irreversible protein adsorption.

3-1 Materials and methods

3-1-1 Materials

All test proteins (α-lactalbumin, β-lactoglobulin, α-casein, β-casein, κ-casein, bovine serum albumin, cytochrome-c, haemoglobin, myoglobin, α-chymotrypsinogen, human recombinant insulin, lysozyme and papain), fluorescein iso-thiocyanate (FITC), ammonia, hydrogen peroxide, di-methyl sulfoxide (DMSO), Trizma salt and sodium carbonate salt was purchased from Sigma Aldrich (Sydney, Australia). Decon-90 was purchased from Decon Laboratories, UK and MilliQ water was obtained from Merck Millipore (Billerica, MA). SS sensors were purchased from Q-Sense (ATA Scientific, Tarren point, NSW, Australia).

3-1-2 Methods

The QCM-D E4 system obtained from Q-Sense, was used for adsorption studies. Experimentation and analysis were performed using QSoft^{TM} and QTools^{TM} to control the system and analyse data, respectively, both provided by Q-Sense. The peristaltic pump used to feed fluids through the QCM-D system was obtained from Ismatec IPC-N Pump (IDEX Health & Science, Wertheim, Germany). A UV Ozone chamber (Bioforce Nano from Q-Sense (Gotenberg, Sweden)) is used for irradiating the sensors. A Nanodrop^{TM} Spectrophotometer A280 nm (Thermo Scientific, DE, USA) was used for quantification of proteins. A Nano-Zetasizer (Malvern, UK) was used for determining diameter of the protein. A HiTrap desalting column (GE Healthcare Life Sciences, Connecticut, USA) was used for buffer exchange. For the fluorescent work, a Leica DM500 microscope was used for fluorescent images and ImageJ software for analysis.

3-1-3 Protein adsorption studies on stainless steel using QCM-D

3-1-3-1 Buffer solution

10 mM Tris buffer (pH 7.5) was prepared by dissolving 1.2 g of Trizma salt (MW 121.4 g/mol) in 1 L MilliQ water. The buffer was degassed prior to loading on the QCM-D.

3-1-3-2 Sample Preparation

The test proteins in this study were divided into three groups: milk proteins (α-lactalbumin, β-lactoglobulin, α-casein, β-casein, κ-casein and bovine serum albumin), blood proteins (cytochrome-c, haemoglobin and myoglobin) and proteins of industrial and medical relevance (α-chymotrypsinogen, human recombinant insulin, lysozyme and papain). Protein solutions at desired concentrations (0.1, 0.25, 0.5, 0.75, 1, 1.5 and 2 mg/mL) were prepared in 10 mM Tris buffer (pH 7.5). Quantification of protein samples was performed using the Nanodrop^{TM} Spectrophotometer A280 nm.

3-1-3-3 QCM-D Experimental Method

All experiments were run in triplicate. Experiments were carried out at 22°C using clean stainless steel coated quartz sensors mounted in a Q-Sense E4 system equipped with four measuring chambers. Q-Sense sensor crystals used in the experiments were coated with SS grade 316, characterized by an isoelectric point of ~ 3-4. The detailed chemical composition of the metal surfaces, XPS survey reports, roughness data, and metal deposition methods of the SS coating on the sensor crystals were extensively reported in Anand *et al*. (2010). The solutions were fed to the QCM-D system using a peristaltic pump at a flow rate of 0.1 mL/min. The adsorption tests include a preliminary equilibration with pure Tris buffer to obtain the signal baseline. Equilibration was followed by the adsorption step, where protein solutions were recycled at known concentrations through the flow cells until stable frequency and dissipation signals were obtained. Subsequently, a desorption step was carried out using plain Tris buffer to monitor removal/desorption of the protein from the surface. This step was continued until stable signals were obtained. The frequency and dissipation signals were recorded using QSoft™ control software and further analysed by applying the Sauerbrey model on QTools™ software (both programs supplied with the QCM-D instrument).

The SS sensors were cleaned at the end of each experiment with 1% Decon-90 prepared in MilliQ water. A second *ex situ* cleaning of the SS sensors was performed between experiments using Pirhana solution (5:1:1 mixture of MilliQ water, ammonia (25%) and hydrogen peroxide (30%)), followed by a MilliQ water rinse. Sensors were then dried using nitrogen gas and UV irradiated using a UV Ozone chamber for 10 minutes.

3-1-4 QCM-D data interpretation using the Sauerbrey model

The Sauerbrey model assumes that the adsorbed layer was rigidly coupled to the sensor and viscoelastic effects are negligible. Following this assumption, the resulting change in the resonant frequency, Δf, was directly proportional to the mass accumulated onto the surface, Δm, accordingly to the following relationship (Sauerbrey, 1959):

$$\Delta m = -\frac{\rho \nu \Delta f}{2 f_0 n} = -\frac{\rho t \Delta f}{f_0 n} = -C\frac{\Delta f}{n} \quad (21)$$

Where the adsorbed material behaves as a viscoelastic layer, energy dissipation affects the change in measured resonance frequency and the Sauerbrey model underestimates the actual mass of the adsorbed layer. A good indication of whether the adsorbed layer was rigid or viscoelastic can be attained through evaluation of the dimensional ratio $\Delta D/(-\Delta f/n)$, obtained from the slope of a ΔD vs. Δf plot. As a rule of thumb, if the dissipation shift observed with respect to the frequency change was small, then viscoelastic dissipation of energy can be neglected and the Sauerbrey model can be safely used for interpretating of the QCM-D data (Irwin *et al.*, 2005, Stengel *et al.*, 2005a, Reviakine *et al.*, 2011). For a 5 MHz sensor, the adsorbed layer can be assumed rigid when $\Delta D/(-\Delta f/n) << 4\times10^{-7}$ Hz^{-1} (Reviakine *et al.*, 2011).

3-1-5 Determination of water in the adsorbed layers (Fluorescent labelling of proteins)

3-1-5-1 Buffer solution

100 mM carbonate buffer (pH 9) was prepared by dissolving 10.6 g of sodium carbonate salt (MW 105.99 g/mol) in 1 L MilliQ water.

3-1-5-2 Sample Preparation

All the protein solutions were prepared in 100 mM carbonate buffer (pH 9) at a concentration of 1 mg/mL and labelled with FITC. The labelling was performed by adding 50 µL of freshly prepared FITC solution (1 mg of FITC in 1 mL of DMSO) to 1 mL of protein solution at room temperature for 3 hours. After this step, carbonate buffer was exchanged to Tris pH 7.5 using a 5 mL HiTrap desalting column.

3-1-5-3 Experimental Protocol

Adsorption experiments were carried out using a QCM-D as described in Section 3-1-3-3. Briefly, the adsorption tests included a preliminary equilibration with pure Tris buffer followed by the adsorption step, where labelled protein solutions were pumped into the flow cells until stable frequency and dissipation signals were obtained. The

total wet mass of protein adsorbed onto the SS sensor was calculated from the frequency and dissipation signals as recorded using QSoft™ control software and further analysed applying the Sauerbrey model on QTools™ software (QCM-D experiments and analysis as described above) (Sauerbrey, 1959). At the end of the adsorption experiments, the SS sensors were removed from the flow cells, dried for 2 – 3 hours and fluorescent images were obtained using a Leica DM500 microscope under 1X magnification for 2.2 seconds. Fluorescence intensity calculations were performed using ImageJ software.

To obtain a calibration curve to correlate the amount of dry protein on the SS surface with fluorescent intensity, 0.25 µL of protein solutions at different concentrations (0.015 – 2 mg/mL) were spotted on a new sensor surface and dried for 2 – 3 hours. Fluorescent images were obtained and processed as above to obtain fluorescent intensity data.

3-2 Results and discussion

3-2-1 Adsorption of commercial proteins on SS using QCM-D

The objective of the work presented here was to provide information on the adsorption behaviour of selected proteins present in milk and blood fractions as well as other proteins of industrial and medical relevance.

For consistency and to allow for a direct comparison between the different experiments, the pH of the Tris buffer was set to 7.5 in all tests, a value chosen as a compromise between the fluids commonly treated in the food and biomedical industries: the pH of milk is 6.5–7.1 (Anema *et al.*, 2004); the pH of egg is 7.3–8.5 (Scott and Silversides, 2000); the pH of blood/plasma is 7.35–7.45 (Waugh and Grant, 2010).

Figure 3-1 shows a time profile for the frequency and dissipation signals of a typical experiment. After the initial equilibration step with pure saline buffer (point A in Fig. 3-1), introduction of the protein solution (point B in Fig. 3-1) caused a large drop in the frequency signal, followed by a slower frequency decrease. The first abrupt signal change is associated with rapid protein adsorption over the SS sensor surface as the

result of: i) maximum mass transport rate through the boundary layer above the SS surface, in which the protein concentration in the liquid in contact with the surface was practically zero at the beginning of the loading step, and ii) complete availability of the sensor surface to bind the protein molecules introduced. About 80% of total adsorption occured in the first 10 min of the loading stage. This is further explored in Section 3-2-1-1.

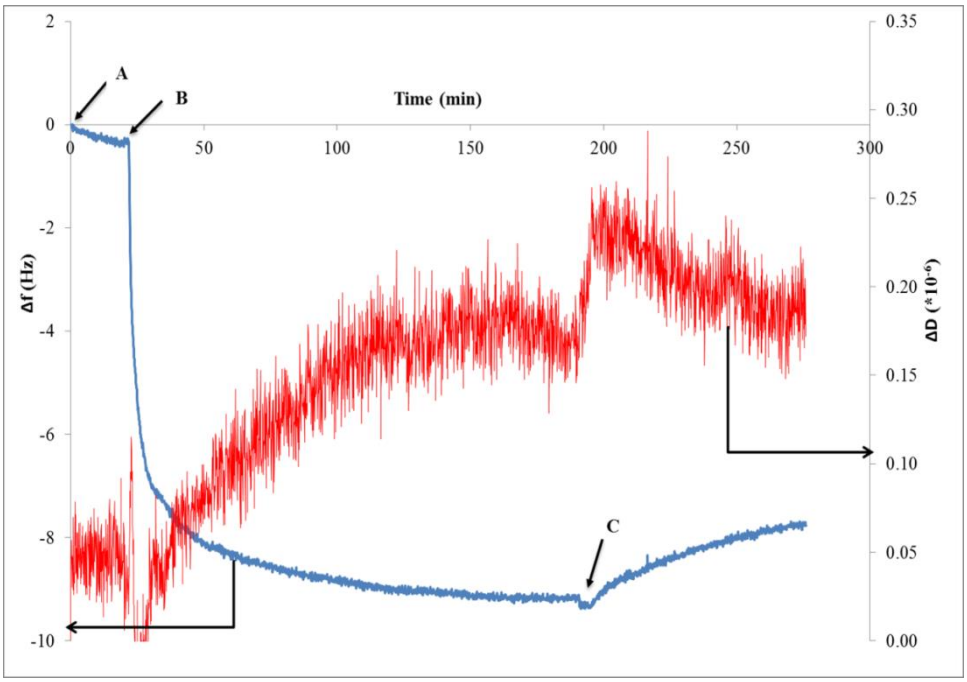

Figure 3-1: Representative example of a QCM-D adsorption experiment. Signals for the run carried out with β-lactoglobulin at a concentration of 0.25 mg/mL and 7th overtone. A: equilibration with pure Tris buffer at pH 7.5; B: protein load; C: desorption in absence of protein (buffer).

3-2-1-1 Study on primary adsorption on SS and protein adsorption factor

Because of the design of the QCM-D flow chamber, primary adsorption is likely limited by protein diffusion through the boundary layer rather than the surface reaction in itself (Höök, 1997). This was supported by the observation that, under the experimental conditions employed, the flow regime in the measuring chamber was laminar, with values for the Reynolds number in the order of 0.1–1. The Reynolds number was calculated with the following equation and values.

$$Reynolds\ Number = \frac{QD_H}{\nu A} \quad (22)$$

where Q is the flowrate (0.100 mL/min, D_H is the diameter of the sensor (1.4 cm), ν is the kinematic viscosity (0.01 cm^2/s) and A is the area of the sensor (1.54 cm^2).

On the other hand, the flow conditions commonly used in industrial practice are fully turbulent, implying thinner boundary layers and faster kinetics for overall adsorption (diffusion + surface reaction). These points clearly indicate that initial protein adsorption was effectively an instantaneous process compared with the time scales involved in industrial practice. Protein adsorption continued to occur, but more slowly in the following few hours as shown by the decrease in the frequency (Fig. 3-1). The time needed to reach surface saturation depended mainly on protein type rather than protein concentration but in all cases it occurred between a lower limit of about 40 minutes for β-lactoglobulin and an upper limit of 4.5 hours for blood proteins (Refer Appendix I – Fig. A-11). During this stage, the protein molecules already adsorbed can desorb from the surface and return back in solution or shuffle and rearrange in the attempt to achieve lower energy configurations, as well as change their local conformation. The dynamic changes occurring make available additional adsorption sites on the surface, resulting in the slow but steady adsorption necessary for complete surface saturation. In this final condition, a dynamic equilibrium was reached between the new biomolecules adsorbing on the surface and the proteins leaving the SS surface. To evaluate the nature of the interaction between protein molecules and the SS surface, pure Tris buffer was used as a washing step in the QCM-D following the adsorption step. During this stage, a fraction of the proteins previously adsorbed desorbs from the sensor surface, with an associated gain in the frequency signal (point C in Fig. 3-1). However, regardless of the duration of the washing, the frequency signal did not approach the zero baseline. This observation was further tested in an experiment in which the washing stage lasted more than 48 hours. Hence, for the system investigated and the proteins used, protein adsorption on SS was a combination of both reversible and non-reversible adsorption.

In the first ten minutes of adsorption, the frequency change was large (Fig 3-1) corresponding to the maximum adsorption of proteins on the surface (refer Eq. (22)). To further understand the adsorption, these first ten minutes of adsorption were studied in detail. The protein adsorption factor, *K*, defined as the sum of the mass transfer and surface reaction in series was also determined at 50%, 60%, 70%, 80%, 50%<x<70% and 50%<x<80% of the first 10 minutes for five test proteins. This range was selected to understand which part of the primary adsorption in the first ten minutes was responsible for the maximum coverage of proteins on the surface.

To study protein mass transfer study the bulk solution phase to the surface, both reversible and irreversible Langmuir kinetics were considered;

Reversible kinetics cen be described by:

$$\frac{dq}{dt} = (k_a \times c^* \times (q_m - q)) - (k_d \times q) \quad (23)$$

and

Irreversible kinetics can be described by:

$$\frac{dq}{dt} = k_a \times c^* \times (q_m - q) \quad (24)$$

where, q was the amount of protein adsorbed, q_m was the maximum adsorbed protein on the surface, $\frac{dq}{dt}$ was the change in adsorption with respect to time, c^* was the interfacial concentration in the liquid phase, k_a was the adsorption constant and k_d was the desorption constant.

At the beginning of adsorption, we can neglect the desorption effects. Also we have $q << q_m$; hence Eq. (24) can be rewritten as follows:

$$\frac{dq}{dt} = k_a \times c^* \times q_m \quad (25)$$

The value of c^* was determined by the boundary layer mass transport of the protein, where flux of protein travelling through boundary layer was equal to the amount of protein adsorbing;

$$k_f \times (c - c^*) = k_a \times c^* \times q_m \quad (26)$$

Rearranging,

$$c^* = \frac{c}{\frac{q_m k_a}{k_f}+1} = \frac{c}{Da+1} \quad (27)$$

where, k_f was the constant for the final adsorbed mass on the sensor and *Da* represents the Damköhlar number (Da = $\frac{q_m k_a}{k_f} = \frac{t_f}{t_r}$) and represents the ratio between the characteristic time for film mass transfer and reaction time.

If, $Da >> 1$, then $t_f >> t_r$, mass transfer was film controlled and $c^* = 0$ and

if, $Da << 1$, then $t_f << t_r$, mass transfer was reaction controlled and $c^* = c$

It is worth noting that c^* is a value generated as a compromise between the velocity boundary layer mass transfer and reaction rate for times close to zero. This would not be valid at longer times. In fact at longer times, the r.h.s of Eq. (23) must take into account other effects such as desorption and a surface that was not totally free. Under this approximation, i.e., t = 0; Eq. (27) can be rewritten as follows:

$$\frac{dq}{dt} = \frac{c}{\frac{1}{k_f}+\frac{1}{k_a q_m}} = Kc \quad (28)$$

where; $K = \frac{1}{\frac{1}{k_f}+\frac{1}{k_a q_m}}$ (29)

K represents the overall adsorption factor of proteins and was the result of two resistances in series: mass transfer (k_f) and surface reaction (k_a).

In Eq. (28), *dq/dt* represents the initial slope of the measurements; if a linear relationship occurs between the slope, *dq/dt*, and protein concentration in the liquid phase, c_0, then we can immediately evaluate the overall adsorption, *K*. Once *K* is determined, k_a can be determined from knowledge of q_m and the evaluation of k_f through the available mass transfer correlations.

To evaluate k_f, the sensor surface was considered here as a laminar plate and hence the mass transfer for the sensor was considered as follows (Incropera and DeWitt, 2001),

$$\frac{kL}{D} = 0.646 \times \left(\frac{Lv_0}{\nu}\right)^{\frac{1}{3}} \times \left(\frac{\nu}{D}\right)^{\frac{1}{3}} \quad (30)$$

where, $k = k_f$, D was the diffusivity of the protein (experimental (D_{expt}) and theoretical (D_{theo})), $L.a$ was the area of the sensor (0.00015 m^2) and velocity, v_0 , was calculated as follows:

$$v_0 = \frac{Q}{A} \quad (31)$$

where, Q was the flowrate (0.1 mL/min) and $Ar = L.a$ was the cross-sectional area (area of the sensor).

The diffusivities of the proteins to be used in Eq. (30) were calculated experimentally (D_{expt}) and compared with the theoretical values (D_{theo}) (Tyn and Gusek, 1990) along with a constant for the finally adsorbed mass on the SS sensor, k_f (Table 3-1). It can be seen here that D_{expt} was approximately equal to D_{theo}. Similarly, $k_{f,expt}$ was equal to $k_{f,theo}$.

Table 3-1: Experimental and theoretical diffusivities

Protein	**D_{expt} ($*10^7$) cm^2/s)**	**D_{theo} ($*10^7$) cm^2/s)**	**$1/k_{f,expt}$ ($*10^7$) (cm/s)**	**$1/k_{f,theo}$ ($*10^7$) (cm/s)**
α-lactalbumin	10.6	11.6	5.2	4.9
β-lactoglobulin	7.8	8.1	6.3	6.2
α-casein	11.2	11.8	4.3	4.8
β-casein	1.4	1.25	2.0	2.2
α-chymotrypsinogen	10.2	9.3	5.3	5.6

Figure 3-2 shows protein adsorption factor values at 50%, 60%, 70%, 80%, 50%<x<70%, 50%<x<80% for four out of the five test proteins, excluding beta-

lactoglobulin. α-lactalbumin and α-chymotrypsinogen followed a similar trend of increase in protein adsorption factor during the first ten minutes. This higher protein adsorption factor to the SS surface is due to the immediate adsorption of the proteins on the surface, which could be due to the change in the binding sites of these protein as temperature and time of adsorption onto the SS surface increased (Corredig, 2004). α-casein and β-casein had higher protein adsorption factors compared to α-lactalbumin and α-chymotrypsinogen. One of the reasons that could contribute to a higher protein adsorption factor is the self-association characteristics of the caseins. At increased ionic strength and pH 7.5, the casein monomers exist in a rapid equilibrium to the oligomers and so the adsorption factor of these proteins on the SS surface increases with formation of the oligomers (McSweeney, 2013). The protein adsorption factor for β casein at 80% of maximum adsorption is almost five times that of α-casein. The reason for β-casein having a very high adsorption factor could be its aggregation and the corresponding formation of oligomers present at pH 7.5 (McSweeney, 2013). Although equilibrium exists between the monomers at oligomers at pH 7.5, there was a continuous distribution between the monomer and the largest polymer at 22°C. There was a shift in equilibrium towards increasing the number of monomers in the solution so there are many more monomers accumulate to aggregate and move from the bulk solution phase to the surface - adsorbing to the SS compared with the polymers. Eventually this increases the protein adsorption (Cosman *et al.*, 2005).

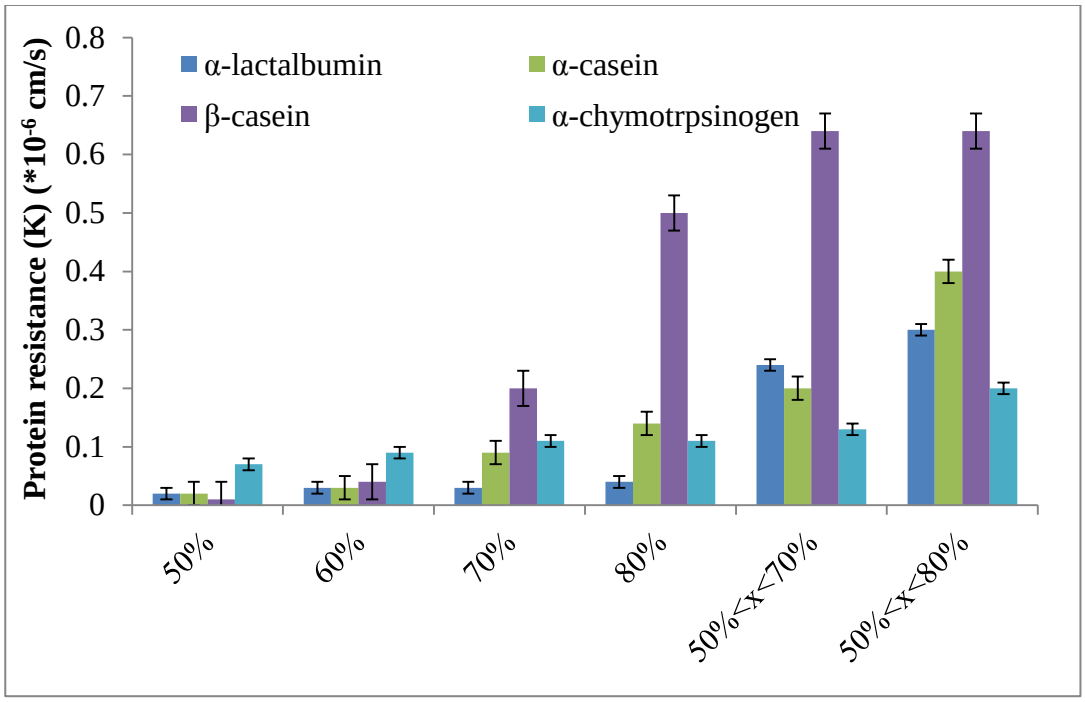

Figure 3-2: Comparison of protein adsorption s at 50%, 60%, 70%, 80%, 50%<x<70%, 50%<x<80% of the first ten minutes of adsorption for four test proteins.

β-lactoglobulin on the other hand has a much higher protein adsorption factor than to the other four test proteins. Between 50% and 80% adsorption, the protein adsorption factor $12x10^{-6}$ cm/s (not shown in Fig. 3-2). Binding studies of β-lactoglobulin showed that the protein undergoes several conformation changes between pH 2-9 that could lead to aggregation of the protein and this enhances movement from the bulk solution phase to the SS surface (McSweeney, 2013). Helices content found in the β-lactoglobulin create a compact non-polar core by hydrophobic interactions. Dill *et al*. (1995) also suggested the complication in the protein structure was higher due to the higher helices content and this compactness by means of hydrophobic, ionic and van Der Waals interaction leads to protein folding. Earlier studies have shown that in the pH range 2.5 to 7.5 and at 22°C, β-lactoglobulin dimer formation occurs and hence predominant aggregation (Schmitt *et al.*, 2001). The protein adsorption factor in this study suggests aggregation and conformational change in β-lactoglobulin similar to that reported. Hence, in β-lactoglobulin, most of the protein is present as aggregates that move towards and adsorb on the surfaces rather than being dispersed in the liquid

phase, which contributes to the protein being adsorbed onto SS at much higher levels than the other proteins used.

3-1-3-2 Rigidity of protein adsorbed layers on SS

The dissipation signal decreases slightly between the loading and washing steps (Fig. 3-1). This indicates that the adsorbed layer contributes to the vibrational energy of the QCM-D sensor. Depending on the change in the dissipation signal, the adsorbed layer could be considered as viscoelastic or rigidly coupled to the sensor surface. For this reason, the dissipation signal was used to calculate the $\Delta D/(-\Delta f/n)$ ratio, which was then compared with the 4×10^{-7} Hz^{-1} threshold suggested by Reviakine and also used by other researchers to distinguish between rigid or viscoelastic adsorbed layers (Höök *et al.*, 1998b, Höök *et al.*, 2002, Reviakine *et al.*, 2011).

Table 3-2: Effect of β-lactoglobulin concentration on frequency, dissipation and dimensional ratio at overtone 3 (n =3), for rigid layer rheology, calculated using the Sauerbrey model.

	Concentration (mg/mL)	**Frequency (f) (Hz)**	**Dissipation (D) (x 10^{-7})**	**$\Delta D/(-\Delta f/n)$ (x 10^{-7})**
β- lactoglobulin	0.10	8	5	1.8
	0.25	10	7	2.1
	0.50	10	2	0.6
	0.75	12	4	1.0
	1.00	14	5	1.1
	1.50	11	5	1.4
	2.00	15	8	1.6

For all proteins, the dimensional ratio was $1.5 – 2.2 \times 10^{-7}$ Hz^{-1} (Refer Appendix I: Table A-1). Hence, the layer formed by the adsorbed proteins was considered rigidly coupled to the QCM-D sensors and the Sauerbrey model was considered valid for determining the corresponding surface concentration for the system. Table 3-2 shows

values for frequency and dissipation for overtone 3 (n = 3) for β-lactoglobulin. Overtone 3 was chosen here due to its stable signal for all concentration of the test proteins. All the values fell in the dimensional ratio of 0.6 – 2.1 x 10^{-7} Hz $^{-1}$.

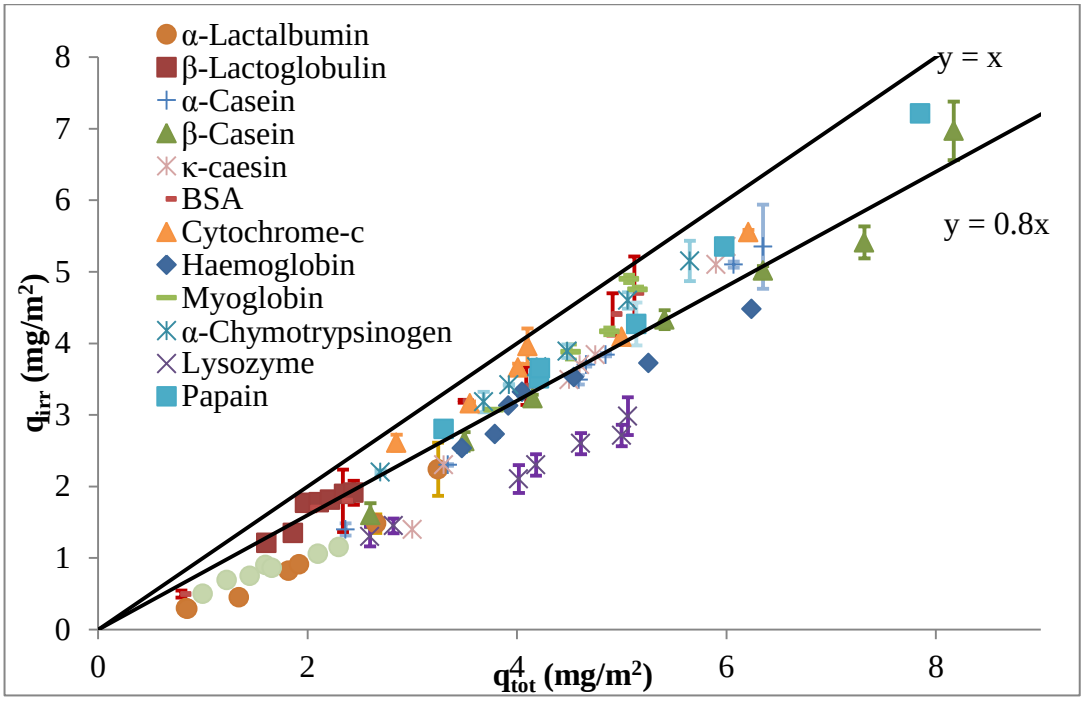

Figure 3-3: Correlation between total protein adsorbed (prior to buffer rinse - q_{tot}) and irreversibly bound protein (after washing – q_{irr}). For the sake of clarity, the lines with equations y = x and y = 0.8x are also included.

During washing, not all the protein molecules previously bound desorb from the sensor surface, indicating simultaneous reversible and irreversible adsorption. The total surface calculated at the end of the adsorption stage, q_{tot} , accounts for both types of surface binding. However during the washing stage only the protein reversibly bound can desorb, so the surface concentration estimated at the end of the washing stage corresponds to the fraction of irreversibly adsorbed molecules, q_{irr}.

The relative extents of total (q_{tot}) and irreversible (q_{irr}) adsorption are shown in Fig. 3-3. The q_{irr}, was around 80% of q_{tot}, during the loading stage, independent of the value and protein type or concentration. This behaviour has been observed in other researchers investigating adsorption of HSA, lysozyme, BSA and bovine

submaxillary gland mucin (BSM), and depicts an adsorption feature common to many proteins (Hedberg *et al.*, 2012b, Lundin *et al.*, 2012). It is likely, that irreversible adsorption was intimately associated to the primary protein layer that forms after the initial interactions were established and, that formed when they were processing in the first 10 minutes of contact at the latest. Therefore, for the times generally considered in the food and biomedical industries, it must be concluded that an adsorbed layer is immediately and ubiquitously present on untreated SS surfaces after contact with any fluid containing proteinaceous species.

3-2-2 Study on dairy protein-associated water and its adsorption effects on SS surfaces by comparison with fluorescent labelling and QCM-D

In QCM-D measurements, water (or any solvent or liquid molecules) may couple as an additional mass via hydration or entrapped in the cavities of the adsorbed layer (Macakova *et al.*, 2007, Anand *et al.*, 2010, Goda and Miyahara, 2012b). This means that the layer sensed was a combination of protein and water molecules on the surface of the SS sensor. The typical amount of coupled water in different systems can vary significantly depending upon the nature of the film, mass uptake and protein characteristics (Schreiber and Haimovich, 1983).

As an alternative technique for comparison of the QCM-D wet mass, dry mass calculated using fluorescent labelling technique has been proposed in the current work. This labelling represents a method to estimate only of protein adsorbed on a surface excluding any water contribution (Rodahl *et al.*, 1996a). FITC was used to attach a fluorescent label to proteins via the amine groups. The isothiocyanate group reacts with amino terminal and primary amines in proteins (Schreiber and Haimovich, 1983). FITC absorbs light maximally at 480 nm and fluoresces maximally at 520 nm. The two techniques measure adsorbed amounts in the same adsorption experiment, but by two independent methods through the QCM-D and the Leica DM500 fluorescent microscope (Leica Microsystems, Germany) as mentioned earlier in Section 3-1-3.

The dairy/milk proteins (α-lactablumin, β-lactoglobulin, α-casein, β-casein, κ-casein) were used in a fluorescent trial. Concentrations of each protein were prepared and 0.25 μL was spotted on the SS sensor surface in two rows. Figure 3-4 is a representative example for dried α-lactablumin. Once spotted, the sensors were allowed to dry in a humid environment at room temperature (22°C) for 2–3 hours (until dried). These were done in triplicate using three different 316 SS grade SS sensors provided by Q-Sense. In Fig. 3-4, the dry spotted protein concentrations have been photographed at an exposure time of 2.2 s. The least concentration (0.015 mg/mL) has the least fluorescence and the fluorescence intensity increased as protein concentration of the spotted protein increases. These experiments allowed the intensity to be correlated with the dry mass of the fluorescent protein adsorbed on the sensor surface (Fig. 3-5).

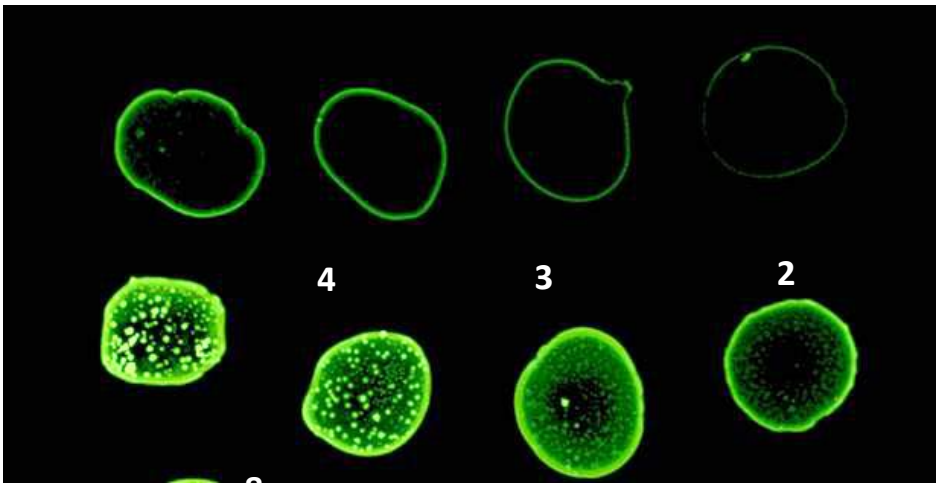

Figure 3-4: Fluorescence of dried α-lactalbumin spots on the SS surface under 1X magnification, exposure time of 2.2s. The spots correspond to (1) 0.015, (2) 0.03125, (3) 0.0625, (4) 0.125, (5) 0.25, (6) 0.5, (7) 1, and (8) 2 mg/mL.

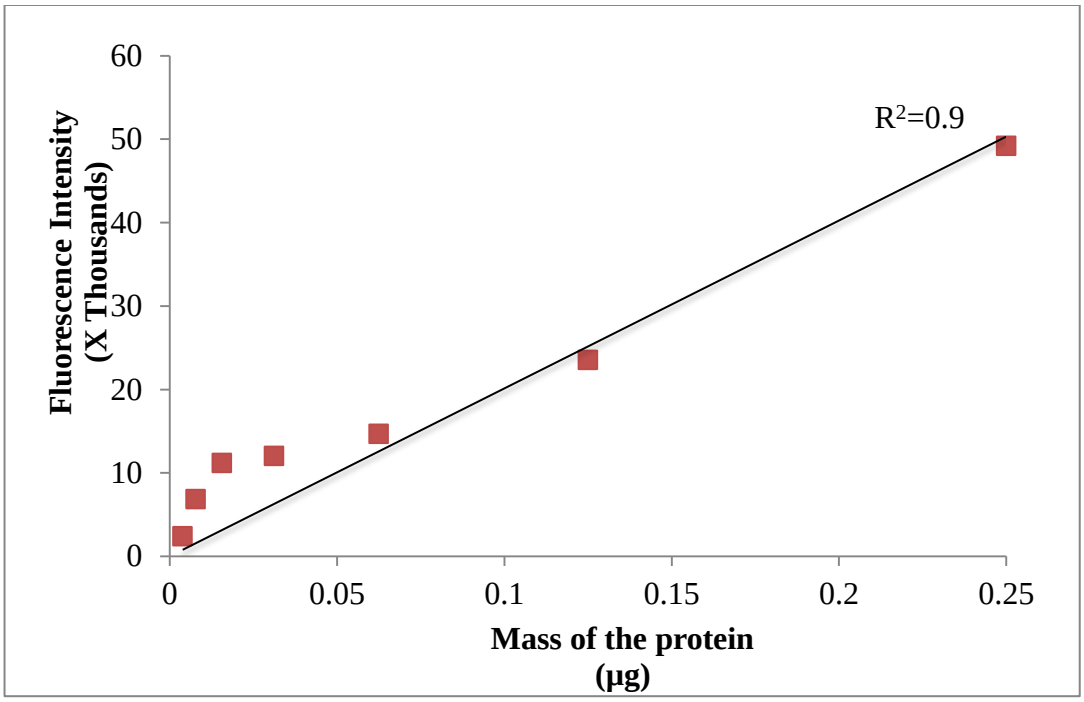

Figure 3-5: Calibration curve of low concentrations of dry mass of alpha-lactalbumin by fluorescent labelling.

Once fluorescence of the dry spots of protein was measured for their fluorescence intensity, the wet concentrations from the QCM-D adsorption experiments were determined. A single 316 SS grade SS sensor was used in the adsorption experiments. The SS sensor was equilibrated with 10 mM Tris buffer until a stable frequency signal was obtained. The protein solution 0.5 mg/mL was passed through the sensor at 0.1 mL/min (22°C). The sensor was then finally re-equilibrated with the buffer solution. The sensors were then carefully removed, wiped with a Kim wipe (Kimberly-Clark®, Texas, US) to remove free water and placed in the humid environment at 22°C and allowed to dry. At the end of adsorption experiments, fluorescent intensity on the QCM-D sensors was measured at an exposure time of 2.2 s under the fluorescence microscope (Fig 3-6). The intensity of this sensor was then plotted on the calibration curve used to estimate the mass of dry protein present on the surface (Table 3-3).

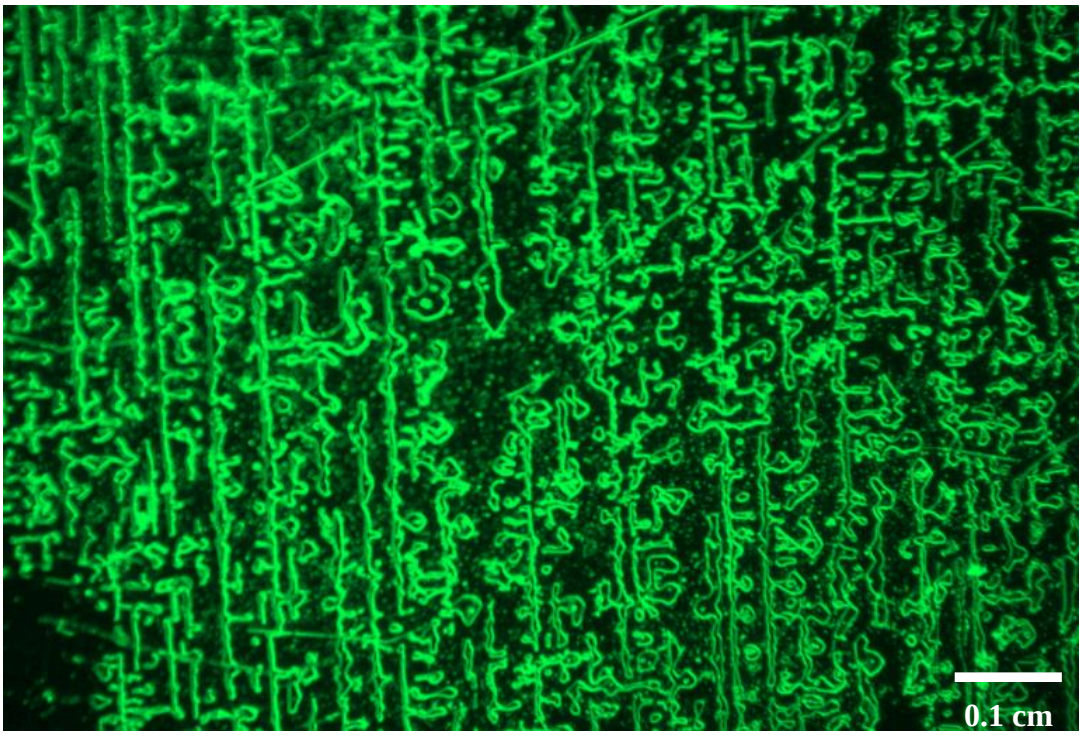

Figure 3-6: Wet mass of α-lactalbumin adsorbed on the SS surface after the adsorption experiments using 0.5 mg/mL. The green fluorescence represents protein and the black spaces represent water (no protein content) at 50X magnification.

The mass of protein and water molecules (adsorption experiments) was compared with mass of the dry protein (calibration of dry spotted proteins) to determine relative content of water and protein in the adsorbed layer. The results summarized in Table 3-3 indicate the hydration water present in the adsorbed layer (QCM-D adsorption experiments) for the test proteins.

Table 3-3: Wet and dry masses of the adsorbed test proteins on SS surface

Protein	Wet mass (mg/mm^2)	Dry mass (mg/mm^2)	Ratio (Wet/dry mass)	Water % in QCM-D adsorption experiments (wet basis)
α-lactalbumin	3.25 ± 0.36	1.76 ± 0.07	1.85	45.8
β-lactoglobulin	5.55 ± 0.50	3.20 ± 0.09	1.68	42.3
α-casein	5.28 ± 0.29	3.30 ± 0.05	1.60	37.5
β-casein	4.80 ± 0.09	3.20 ± 0.06	1.50	33.3
κ-casein	6.62 ± 0.25	4.50 ± 0.08	1.47	32.0

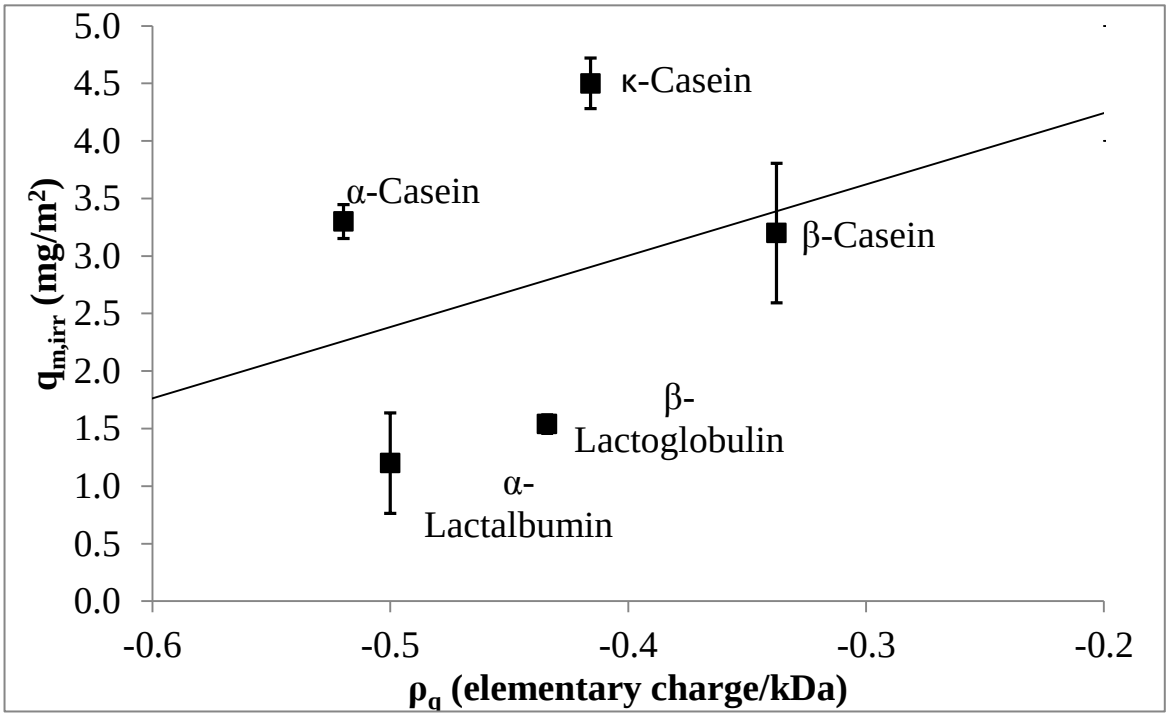

Figure 3-7: Trend of dry irreversible surface concentration with charge density for the proteins tested

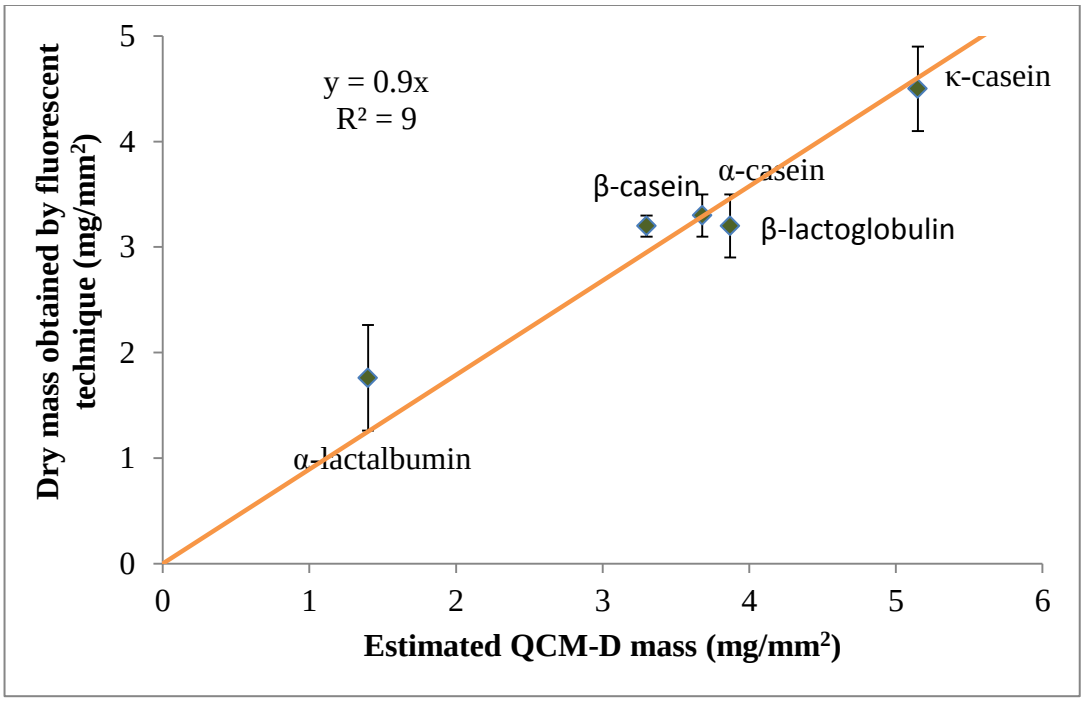

Figure 3-8: Correlation between the estimated dry mass by the QCM-D and fluorescent technique

The estimated QCM-D dry mass was calculated from the fraction mass (ratio of wet/dry mass) obtained from the "wet" mass experiments. There was a direct relationship (R^2=0.9) obtained between the mass estimated by the QCM-D technique and the spot drying fluorescence technique. α-lactalbumin contained the most hydration water, followed by β-lactoglobulin. These two proteins are highly hydrophilic, and would trap the water molecules while adsorbing to the SS surface (Schatzberg, 1967). In contrast, the caseins probably have a tendency to form large aggregates and consequently exclude water molecules (Schatzberg, 1967, Fahmy, 1995, McSweeney, 2013). The amount of water present in the adsorbed layers is than the amount of the protein, irrespective of the protein. Water and protein make almost even contribution to the layer only for the case of α-lactalbumin. The ratio between wet and dry mass was always less than 2 (Table 3-3).

Previously literature used two separate experiments with different sensors to measure the protein and water. The different instrumentations, more importantly with the different topographies of the sensor surfaces, would bias calculations of water content. In this work, the water content was 32% - 45.8% (wet basis), half of that

reports using two different measurements. For the first time, we propose a method determining accurate values for protein adsorption onto surfaces that involve measuring QCM-D and fluorescent measurements on QCM-D, using the same sensor (316 SS grade provided by Q-Sense), hence removing uncertainties about the protein-surface interactions.

3-2-3 Parameters affecting protein adsorption

Finding useful relationships between the physicochemical properties of the proteins and their adsorption behaviour was of paramount importance for predicting the amount of protein adsorbed on a surface without the actual need to perform a complete experiment. Unfortunately, experimentation is extremely difficult because of the multifaceted and complex structure of proteins. As well as the principal properties of molecular weight, hydrodynamic radius, isoelectric point and electrostatic charge, many different specific characteristics, such as 3-D structure and folding, presence of post-translational modifications, repeat motifs, and the abundance of certain amino acids (AA) on the surface differentiate the various protein molecules. In an effort to offer a general yet useful method to predict the adsorbing behaviour of proteins on SS surfaces, the attempt to correlate the concentration irreversibly adsorbed to the main properties of the proteins. Different generic parameters such as, pI, MW, charge, hydrodynamic radius, hydrophobicity factor and surface accessible amino acid composition were considered, but none of these was able to reliably describe the adsorbing attributes of the proteins used. Under the hypothesis that the key factor driving surface fouling was closely related to the protein's electrostatic charge, and that the electrostatic charge was distributed over the entire protein, we propose to define the protein's charge density of a protein, ρ_{pq}, as the ratio between the charge of that protein at the pH of the buffer and the molecular weight of the protein.

Some of the parameters of the test proteins considered in this study are given in Table 3-4. The MW, charge and protein dimensions were considered for producing an empherical relationship and principal component analysis (PCA). The crystal structures of the proteins have been used to study the accessible amino acid residues on the surface and their influence in protein adsorption studies using PCA.

Table 3-4**:** MW, net charge at pH 7.5 and protein data bank (PDB) ID for the proteins tested.

Group	**Proteins**	**MW (kDa)**	**Charge at pH 7.5**	**Protein Dimensions (Å)**	**PDB ID** (Rose *et al.*, 2011)
Milk	**α-lactalbumin**	14.1	-7.0	1.9 (Gast *et al.*, 1998)	1A4V
	β-lactoglobulin	18.2	-7.9	4 (Ngadi, 2009)	1B0O
	α-casein	22.9	-11.9	3.7 (Pessen *et al.*, 1991)	3AT2
	β-casein	23.5	-7.9	2.9 (Pessen *et al.*, 1991)	1QF8
	κ-casein	19.0	-1.2	8.9 (Pessen *et al.*, 1991)	1CK1
	BSA	66.5	-16.6	14.0*4.0*4.0 (Wright and Thompson, 1975)	3V03
Blood	**Cytochrome-c**	11.9	9.1	1 (Banci *et al.*, 1997)	1AKK
	Haemoglobin	16.0	-0.8	1.7 (Fermi *et al.*, 1984)	2HHB
	Myoglobin	17.0	0.3	1.5 (Maurus *et al.*, 1998)	1AZI
Commercial	**α-chymotrypsinogen**	13.9	-2.0	2 (Frigerio *et al.*, 1992)	1ACB
	Human recombinant insulin	5.0	-3.6	1.4 (Bi *et al.*, 1984)	4FG3
	Lysozyme	14.3	7.9	1.8 (Rypniewski *et al.*, 1993)	132L
	Papain	23.4	6.0	1.7 (Janowski *et al.*, 2004, Kamphuis *et al.*, 1984)	9PAP

For many proteins there is a positive linear relationship (R^2= 0.94) between q_{irr} and ρ_{pq} for the majority of the proteins tested (Fig. 3-9), especially for those with negative or slightly positive charge density values. The correlation indicate the relationship of electrostatic attraction forces acting between the protein molecule and the SS surface. As the pH of the buffer (7.5) was higher than the pI of most of the proteins in solution (Table 3-4) the proteins are negatively charged. As the isoelectric point of SS is ~ 3–4 (Anand *et al.*, 2010), the SS surface was negatively charged at the pH used in the experiments. The less negative the protein, the lower the energetic barrier it must overcome to approach the metal surface and the greater the likelihood of establishing other types of stronger and more stable interactions.

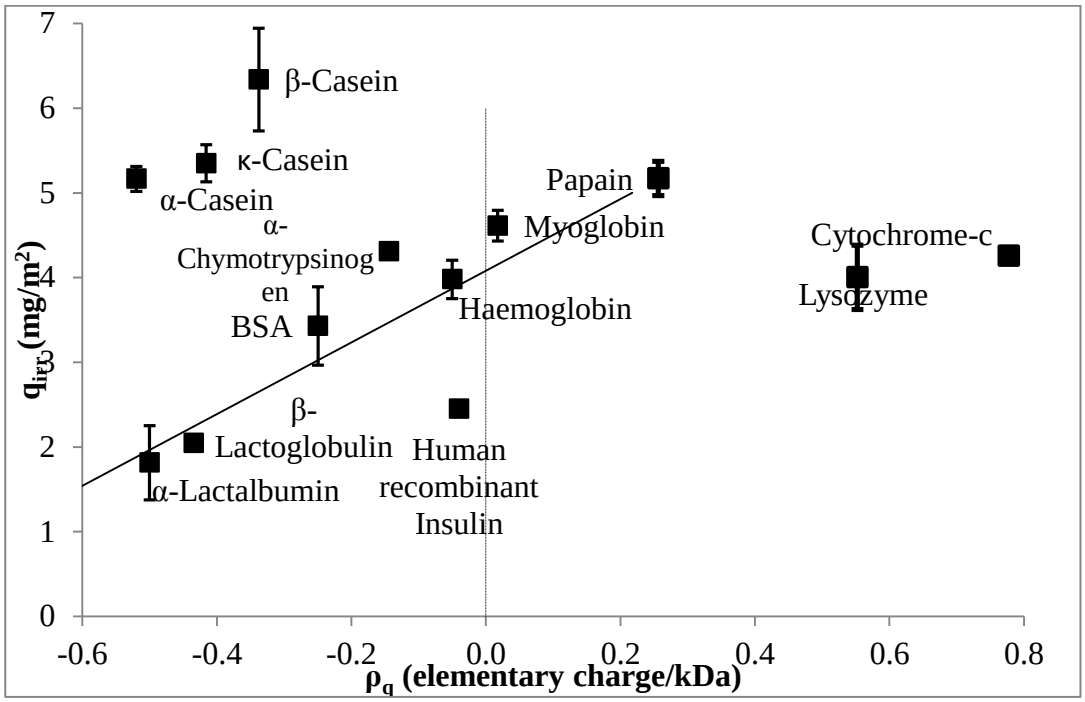

Figure 3-9: Relationship of maximum irreversible surface concentration with protein charge density.

The charge density of positively charged proteins such as cytochrome-c, lysozyme and myoglobin does not affect the adsorbed mass on the sensor surface. With these proteins, the maximum concentration value was between 4 and 5 mg/m^2 was achieved. Lack of effect is probably because the maximum adsorption condition for positively charged proteins corresponds to complete monolayer surface coverage of the sensor surface. According to this hypothesis, the mass/thickness of the adsorbed

layer will be proportional to the molecular weight of the proteins, so larger proteins produce a thicker adsorbed layer or, in other words, a layer characterized by a higher surface concentration.

This relationship exists for the proteins (Fig 3-10) with a maximum adsorption of 4–5 mg/m^2 surface (R^2= 0.83). The minor deviations from this linear correlation are probably due to random, imperfect molecular packing on the surface, that inevitably have small voids that cannot be filled by adsorption of additional protein molecules.

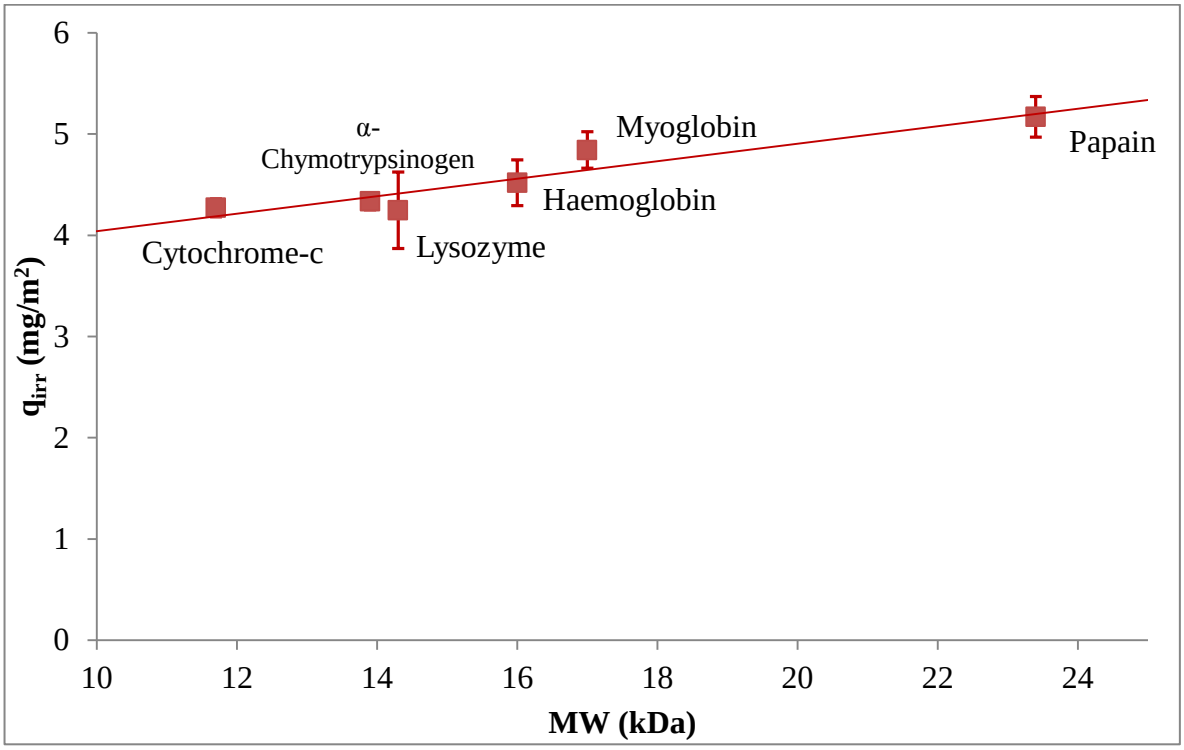

Figure 3-10: Relationship between irreversible surface concentration and molecular weight for the positively charged proteins.

The two linear correlations in Fig. 3-9 and Fig. 3-10 gives the following empirical relationship:

$$q_{m,irr} = \begin{cases} 4.6 + (5.5 \times \rho_q) \text{if } \rho_{pq} < 0.1 \\ 3.2 + (0.1 \times M.W) \text{ if } \rho_{pq} > -0.1 \end{cases}$$

(32)

where molecular weight was in kDa, charge density was in elementary charges per kDa and the resulting surface concentration was in mg/m^2. The maximum error in the

proposed correlation was less than 15% for proteins with $\rho_q < 0.1$, while the maximum error for $\rho_{pq} > -0.1$ was only 7.5%. In the transition zone, i.e. $-0.1 < \rho_q < 0.1$, the two correlations give similar results, with relative errors below 5%.

These simple relationships can be used to estimate the amount of protein irreversibly adsorbed onto SS surfaces from knowledge of only two physical parameters of the protein, namely molecular weight and total charge of the protein. The total maximum protein that will be adsorbed onto SS surfaces can be determined combining Eq. (31) with the observation that on average $q_{irr} = 0.8 \times q_{tot}$. Exceptions to the relationship α- and β-caseins do not fit the model. Even though the caseins were negatively charged, they adsorb at a similar or greater extent than the positively charged proteins. Caseins have a high number of phosphor-substituted serine residues known to have high affinity towards iron oxides (Suci and Geesey, 2001), iron ions (Bernos *et al.*, 1997, Stewart *et al.*, 2011) and chromium oxide-hydroxides (Degenhardt and McQuillan, 1999, Connor and McQuillan, 1999). Release of these metal ions was observed from SS surfaces of biomedical implants (Hedberg *et al.*, 2012a, Lundin *et al.*, 2012)and a passive layer of metal oxides is ubiquitously present on SS surfaces (Lundin *et al.*, 2012, Shi *et al.*, 2012). Caseins can self-associate (Section 3-2-1-1), forming equal numbers of monomers and larger oligomers/polymers. The equilibrium for β-caseins, shifted towards formation of monomers at temperatures higher to 22°C (McSweeney, 2013). These factors could attribute to the increased adsorption of caseins on the SS surfaces.

Proline residues constitute 5–10% of the total amino acid content in caseins, which is significantly higher than the average 3% proline content in the other proteins. Proline residues enhance flexible conformations and favour structural rearrangements following a surface interaction (Yeung *et al.*, 2002). This open structure would both increase the surface area for adsorbing other casein proteins as well as allow rearrangements in the backbone, favouring stronger surface interactions. In addition, caseins self-polymerize through intermolecular hydrophobic forces, favouring aggregation and precipitation of the protein molecules (Imamura *et al.*, 2008). These factors give rise to a thicker and more complex adsorbed layer explaining the higher surface concentration of adsorbed caseins. The example of caseins shows that

deviations from Eq. (31) are possible and must be carefully taken into consideration, especially when the protein being studied was prone to aggregation and precipitation.

3-2-4 Molecular models for surface accessible amino acid types

The calculations for surface accessible area were performed on NetSurfP of the Expasy tool (Swiss Institute of Bioinformatics) (Artimo *et al.*, 2012). The initial step for this analysis, considers all the exposed AA of the particular protein was considered. Once known, the threshold of the relative and absolute accessible surface area of the particular amino acid was taken into account and a 50% threshold of these exposed AA as the basis in this study. After this analysis was performed, the AA was grouped by hydrophobicity, hydrophilicity, basic, acidic and aromatic residues.

To confirm to the data obtained, measurements were performed with the Nano-Zetasizer, and diameters of the proteins were measured using the dynamic light scattering (DLS) principle (Section 3-2-7). The accessible amino acid residues on the surface of the protein were also visualized using VMD software to supplement the PCA results (University of Illinois, United States) (Humphrey *et al.*, 1996). Papain (Fig. 3-11) and other molecules (data not shown) were studied in the similar manner. The various regions are indicated by colour, where:

(a) represents the hydrophilic (green) and hydrophobic (white) residues on the surface of the molecule
(b) represents the charged AA present on the surface and accessible to the surface of SS where acidic (positively charged are red) and basic (negatively charged are blue); and
(c) represents the aromatic (purple) AA present on the surface of the papain molecule.

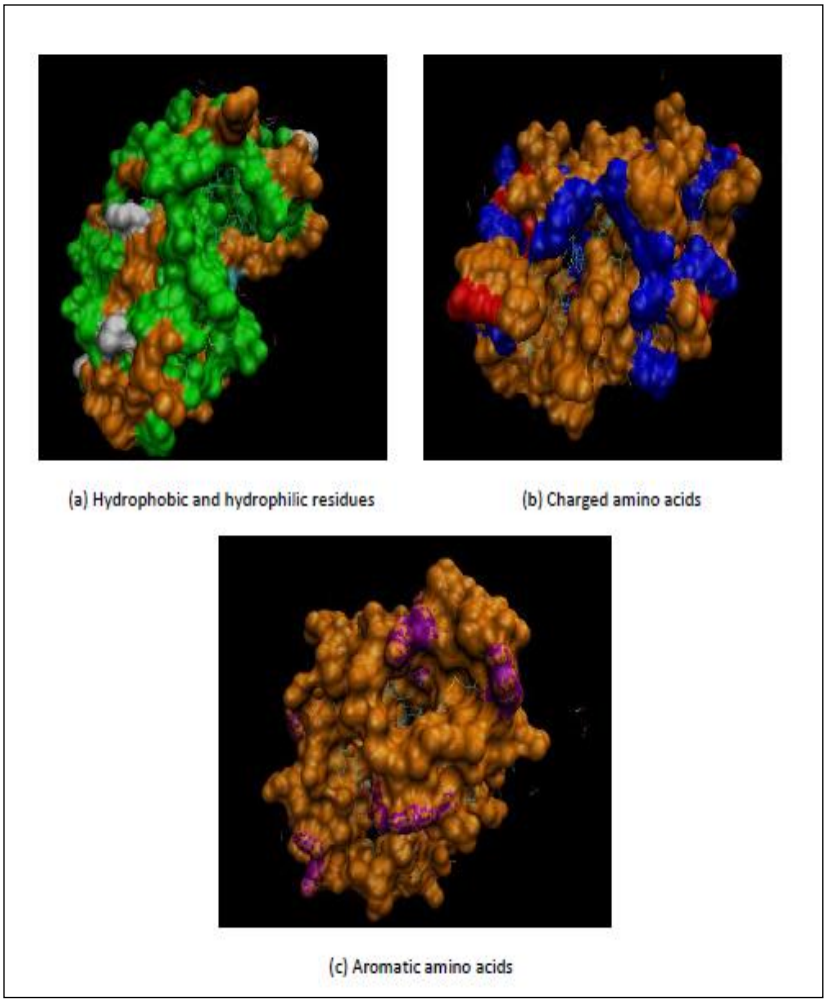

Figure 3-11: Accessible residue types of papain molecule (PDB ID: 9PAP)

3-2-5 Principal component analysis of the relationship between protein properties and adsorption

After developing of the empirical relationship, the physical parameters were determined by PCA to further understand how the physiochemical parameters influence protein adsorption. PCA can be considered as a method which projects observations from a p-dimensional space with p variables to a k-dimensional space (where $k < p$) where the maximum amount of information (information was measured through the total variance of the scatter plots) from the initial dimensions is conserved. If the information associated with the first two or three axes is a sufficient proportion of the total variability of the scatter plot, the observations can be represented on a 2- or 3-D chart, thus making interpretation much easier.

For this analysis, the following parameters were considered: charge of the protein at pH 7.5, protein dimensions and surface accessible amino acid residues (hydrophobic, hydrophilic, acidic, basic and aromatic). The calculations for surface accessible AA were performed using NetSurfP tool in the Swiss Institute of Bioinformatics – Expasy website (Artimo *et al.*, 2012, Lins *et al.*, 2003). The tool needs the sequence of the particular protein in single letter amino acid code. From this sequence, the buried and the exposed AA, relative and absolute accessible surface areas are calculated. As the initial step for this analysis, all exposed AA's of the particular protein are considered. Once known, the threshold of the relative (area of the particular residue with respect to other residues in the protein) and absolute (area of the residue with respect area of the entire protein) accessible surface area of the particular amino acid was taken into account. The 50% threshold of the absolute accessible surface area (ASA) of these exposed AA was used as the basis in this study. The other thresholds tested were 15%, 25% and 75% of the exposed AA but they were not the best for further studies (data not shown). For this analysis to be performed, the AA were grouped by:

1) Hydrophobicity (alanine – Ala (A), glycine – Gly (G), isoleucine – Ile (I), leucine – Leu (L), methionine – Met (M), phenylalanine – Phe (F), proline – Pro (P), tryptophan – Trp (W), tyrosine – Tyr (Y), valine – Val (V)),
2) Hydrophilicity (arginine – Arg (R), asparagine – Asn (N), aspartic acid – Asp (D), cysteine – Cys (C), glutamine – Glu (G), lysine – Lys (K), serine – Ser (S), threonine – Thr (T)),
3) Basic (arginine, lysine, histidine – His (H)),
4) Acidic (aspartic acid, glutamic acid – Glu (E)) and
5) Aromatic acids (aspartic acid, phenylalanine, tryptophan, tyrosine).

β-lactoglobulin is discussed here as an example. Table 3-5 contains the data using the NetSurfP tool. The exposed AA with an absolute surface area (ASA) threshold of 50% was considered. After this analysis, the AA was classified as hydrophobic, hydrophilic, basic, acidic and aromatic residues. The sum of the AA was then calculated for the amino acid residue category. Once this was done, the percentage content of the AA present in each category was calculated using shown in Eq. (33).

Based on 50% of surface area, the percentage of hydrophobic, hydrophilic, basic, acidic and aromatic AA in β-lactoglobulin that are accessible are 54%, 67%, 21%, 37% and 3% respectively.

$$\%\ of\ hydrophobic\ AA\ in\ the\ 50\%\ threshold\ RSA = \frac{Sum\ of\ the\ hydrophobic\ AA\ RSA's}{Total\ number\ of\ AA\ residues} \quad (33)$$

Table 3-5: Exposed AA, RSA and ASA for β-lactoglobulin from NetSurfP (Petersen *et al.*, 2009)

RSA Threshold: 50 %								
AA	**Seq no**	**RSA**	**ASA**		**AA**	**Seq no**	**RSA**	**ASA**
A	34	0.6	61		I	78	0.7	126
A	142	0.8	91		I	147	0.6	102
D	11	0.6	80		I	162	0.6	109
D	33	0.6	83		K	8	0.7	148
D	98	0.5	75		K	77	0.8	159
D	130	0.7	94		K	100	0.6	125
E	51	0.8	135		K	138	0.6	123
E	89	0.5	88		K	141	0.6	125
E	112	0.7	120		L	1	0.6	111
E	114	0.5	91		L	87	0.6	116
E	127	0.7	127		N	63	0.7	106
E	131	0.7	126		P	50	0.8	119
E	134	0.6	105		P	79	0.6	91
E	157	0.7	119		P	113	0.7	96
E	158	0.6	99		P	144	0.7	101
G	9	0.5	42		Q	13	0.7	132
G	64	0.5	41		Q	35	0.6	104
H	161	0.6	101					

A similar analysis was done for all the test proteins used in this study. A PCA was then performed using the XLSTAT tool in Microsoft Excel 2010 (Fahmy, 1995).

The PCA computation used Pearson's correlation matrix, which produces the classical correlation coefficient. The next step is to identify the axes for the plots. To avoid misinterpreting the results, in this study, the variability described by the first two factors was very high (64%).

The correlation matrix shows the correlation between the various data sets chosen for analysis. The protein charge at pH 7.5 is negatively correlated (r = -0.692) to protein dimensions (Table 3-6). We can also see that the charge of the protein has low correlation with the other variables. This means that charge of the does not have a large influence on adsorption effect compared with the other variables and the charge would be dependent on the specific amino acid types that are found in the particular protein.

Table 3-6: Correlation matrix (R^2 values) from PCA analysis

	F1	F2	F3	F4	F5	F6	F7
Protein charge at pH7.5	**1**	-0.7	0.2	-0.3	0.2	-0.5	0.2
Protein Dimensions (Å)	-0.7	**1**	0.2	0.1	0.1	-0.1	0.1
50% Hydrophobic ASA	0.2	0.2	**1**	-0.5	0.3	-0.4	**0.8**
50% Hydrophilic ASA	-0.3	0.1	-0.5	**1**	0.3	0.5	-0.5
50% Basic ASA	0.2	0.1	0.3	0.3	**1**	-0.1	0.0
50% Acidic ASA	-0.5	-0.1	-0.4	0.5	-0.1	**1**	-0.4
50% Aromatic ASA	0.2	0.1	**0.8**	-0.5	0.0	-0.4	

The eigenvalue, indicate the quality of the projection from the N-dimensional initial table (N=8 in this study) to a lower number of dimensions. These values are summarized in Table 3-7. Table 3-7 are related to the fit factors (Table 3-6). The first eigenvalue is 2.815 and represents 40% of the total variability (Table 3-7). If we represent the data on one axis, we can see percentage of total variability of the data. Each eigenvalue corresponds to a factor, and each factor to a dimension. A factor is a linear combination of the initial variables, and all the factors are un-correlated (r=0). The eigenvalues and the corresponding factors are sorted by descending order of the initial variability they represent (converted to %). Protein charge was not highly correlated with most of the factors dimension (r = -0.69).

Table 3-7: Eigen values, variability and cumulative percentages

	F1	F2	F3	F4	F5	F6	F7
Eigenvalue	2.8	1.7	1.2	0.7	0.4	0.1	0.1
Variability (%)	40.2	24.1	17.5	10.1	5.4	1.5	1.1
Cumulative %	40.2	64.3	81.9	91.9	97.3	98.9	100.0

The first two eigenvalues allow us to explain 64% of the initial variability of the data and the first three eigenvalues explain 82% of the variance, confirming that the maps based on the first two or three factors are a good quality projection of the initial multi-dimensional table. Although eight variables were considered, the number of factors was seven here..

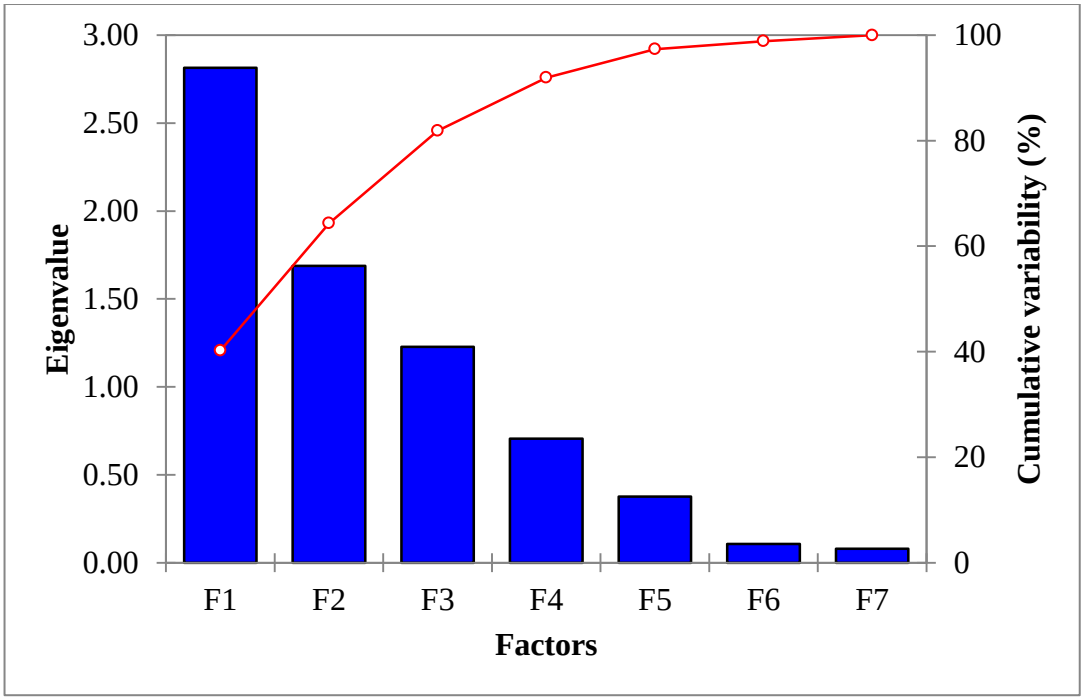

Figure 3-12: Eigenvalues of factors considered and cumulative value

The first map (Fig. 3-13) on correlation circle (on axes F1 and F2) shows a projection of the initial variables in the factors space. When two variables are far from the center, and are close to each other, they are significantly positively correlated (r close to 1). If they are orthogonal, they are not correlated (r close to 0) and if they are opposite each other, they are significantly negatively correlated (r close to -1). When variables

are close to the center some information is carried on other axes, so any interpretation might not be accurate. This can be confirmed by looking at the correlation matrix or by looking at the correlation circle on axes F1 and F3.

Later in Fig. 3-13 the 50% threshold of the absolute surface areas of the hydrophobic and the aromatic amino acid residues and 50% threshold of the absolute surface areas of the hydrophilic and the acidic amino acid residues are positively correlated. On the other hand, protein dimensions are orthogonally placed with respect to the 50% threshold of the absolute surface areas of the hydrophilic and the acidic amino acid residues and hence they are not correlated.

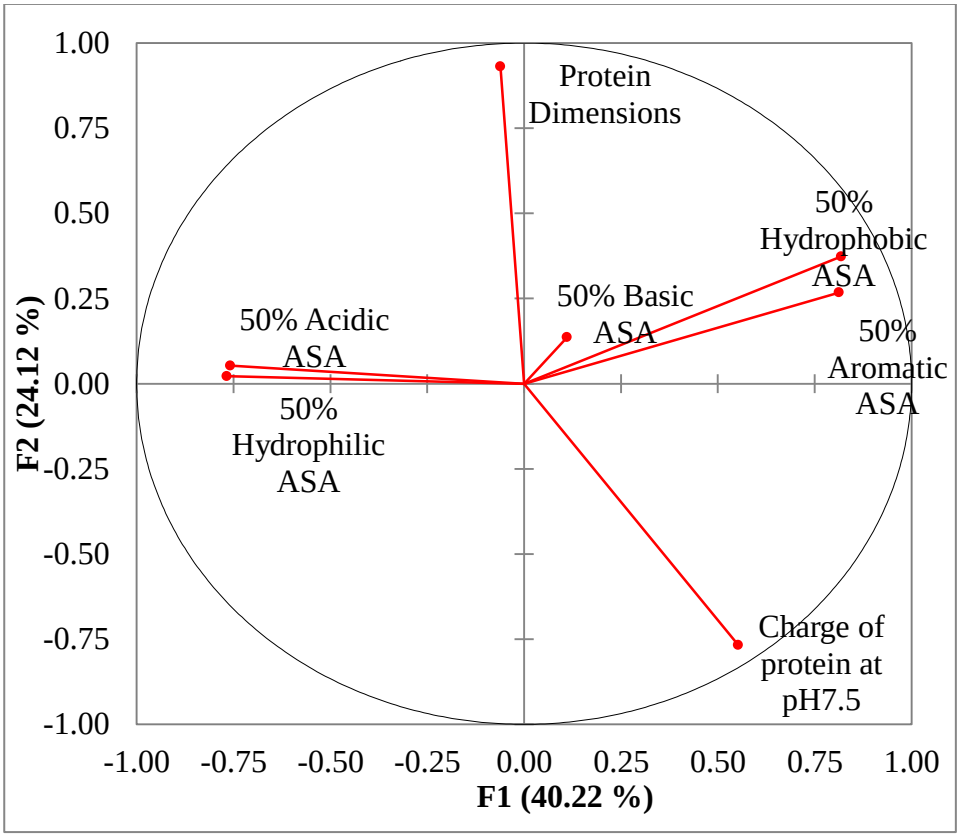

Figure 3-13: Correlation circle for F1 and F2, with variability of 40% and 24%, respectively

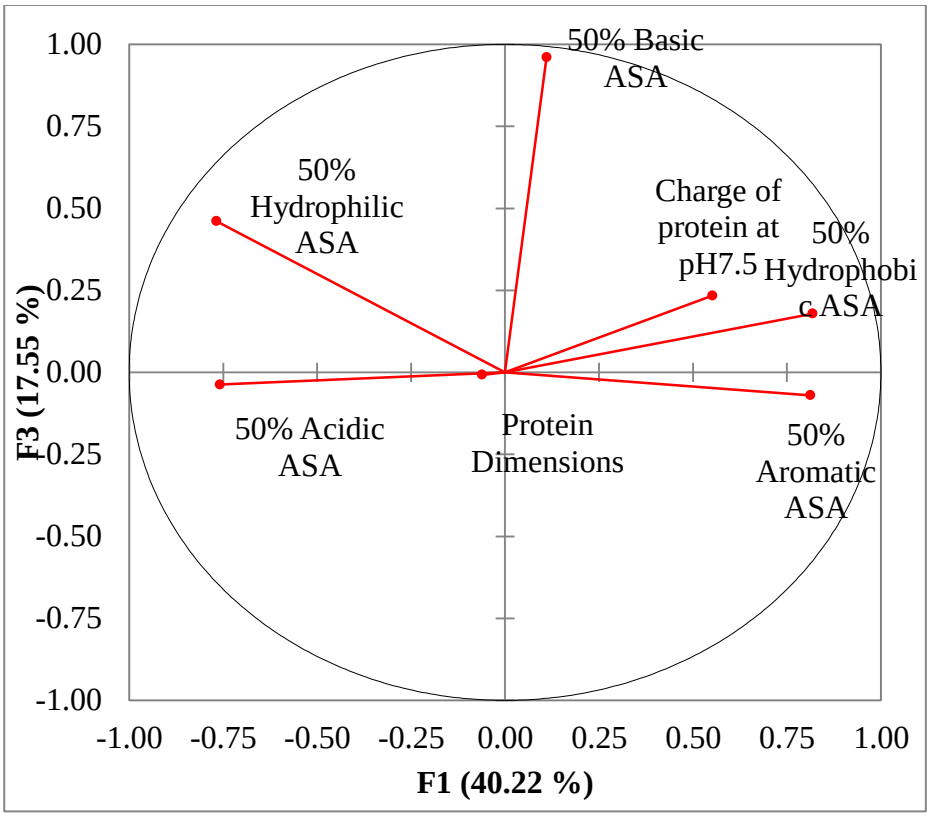

Figure 3-14: Correlation circle for F1 and F3, with variability of 40% and 18%, respectively

The correlation circle shows that the protein charge and the 50% threshold of the absolute surface areas of the hydrophobic amino acid (f = 3) are positively correlated (Fig. 3-14). These trends will be helpful in interpreting the next map. To confirm that a variable was well linked with an axis, the squared cosines were determined (Table 3-8). The greater the squared cosine, the greater is the link with the corresponding axis. The closer the squared cosine of a given variable is to zero, the greater care when interpreting results in terms of trends on the corresponding axis.

Table 3-8: Squared cosines of the variables

	F1	F2	F3	F4	F5	F6	F7
F1	0.305	**0.588**	0.055	0.004	0.002	0.029	0.017
F2	0.004	**0.868**	0.000	0.097	0.000	0.015	0.016
F3	**0.669**	0.139	0.032	0.100	0.016	0.024	0.020
F4	**0.590**	0.000	0.212	0.008	0.177	0.008	0.005
F5	0.012	0.018	**0.923**	0.002	0.029	0.014	0.002
F6	**0.576**	0.003	0.001	0.368	0.038	0.002	0.012
F7	**0.660**	0.072	0.005	0.126	0.115	0.013	0.009

A further step in PCA is to "rotate" the components or data sets. The most common form of rotation is the varimax where reorientation of the axes occurs in the principal component space and the components are analysed and interpreted more easily. In this study, the factor loadings after varimax rotation reflect how much the variable contributes to that particular principal component.

The first factor (Factor 1) explains 40% of the total variance (Table 3-9). The other four significant parameters are: the percentage of the 50% threshold of the absolute surface area accessible for the hydrophobic, hydrophilic, acidic and aromatic amino acid residues. The percentage of accessible hydrophobic residues has a maximum positive loading of 0.818. This indicates the proteins do not bind to the water molecules but aggregate by self-associating with neighbouring protein molecules in the solution and then adsorb to the surface. The percentage of accessible aromatic residues has a maximum positive loading of 0.812, indicating that the higher the aromatic residue contents in a protein the higher would be the binding to the surface. The charge of the protein also has a positive loading (0.552). Several studies on

adsorption have shown that the charge on a protein surface contributes significantly towards protein adsorption (Dietschweiler and Sander, Goda and Miyahara, 2012b). Phenylalanine, tryptophan and tyrosine are the major aromatic groups in proteins and these residues enhance protein folding (Taniguchi).

The percentage of accessible hydrophilic and aromatic amino acid residues have a strong negative loading (-0.768) as does accessible acidic amino acid residues (-0.759) having negative correlation with adsorption. There is a high probability that water molecules are trapped in between the protein layers (Anand *et al.*, 2010). Also, as the surface was negatively charged, the lower the percentage of accessible acidic residues on the surface, the higher the adsorption of the particular protein on the SS surface.

Table 3-9: Factor Loadings for Principle Component Analysis

Properties	**F1**	**F2**	**F3**
Protein charge at pH7.5	**0.552**	-0.767	0.234
Protein Dimensions (Å)	-0.061	**0.931**	-0.008
50% Hydrophobic ASA	**0.818**	0.373	0.179
50% Hydrophilic ASA	-0.768	0.022	0.461
50% Basic ASA	0.111	0.136	**0.961**
50% Acidic ASA	-0.759	0.053	-0.037
50% Aromatic ASA	**0.812**	0.268	-0.070
Eigenvalue	2.815	1.689	1.228
Variability (%)	40	24	18
Cumulative (%)	40	64	82

Factor 2 (24% of the total variance) was associated to the protein dimensions. Protein with larger dimensions probably adsorb more readily to the SS surface than smaller protein molecules.

Factor 3 (18% of the total variance) has a strong positive loading (0.931) and was associated to the percentage of accessible basic/positive residues. At pH 7.5, the SS

surface was negatively charged and has greater affinity proteins that have a higher percentage of positively charged or basic residues on the protein surface.

Overall, protein adsorption on the stainless surface could be attributed to the following three significant factors;

a) Factor 1: Positive correlation to the accessible hydrophobic, aromatic residues and protein charge at pH 7.5

b) Factor 2: Positive correlation to protein dimension

c) Factor 3: Positive correlation to percentage of accessible basic residues

The ultimate result of performing PCA is given in Fig 3-15 gives a 2-D map of the data. BSA is not grouped with the other proteins, indicating that the adsorption of BSA probably is a different mechanism (from Fig. 3-3 and 3-4). As the remaining proteins have in a similar range, it is difficult to interpret adsorption in terms of physiochemical parameters of these proteins from the 2-D plot.

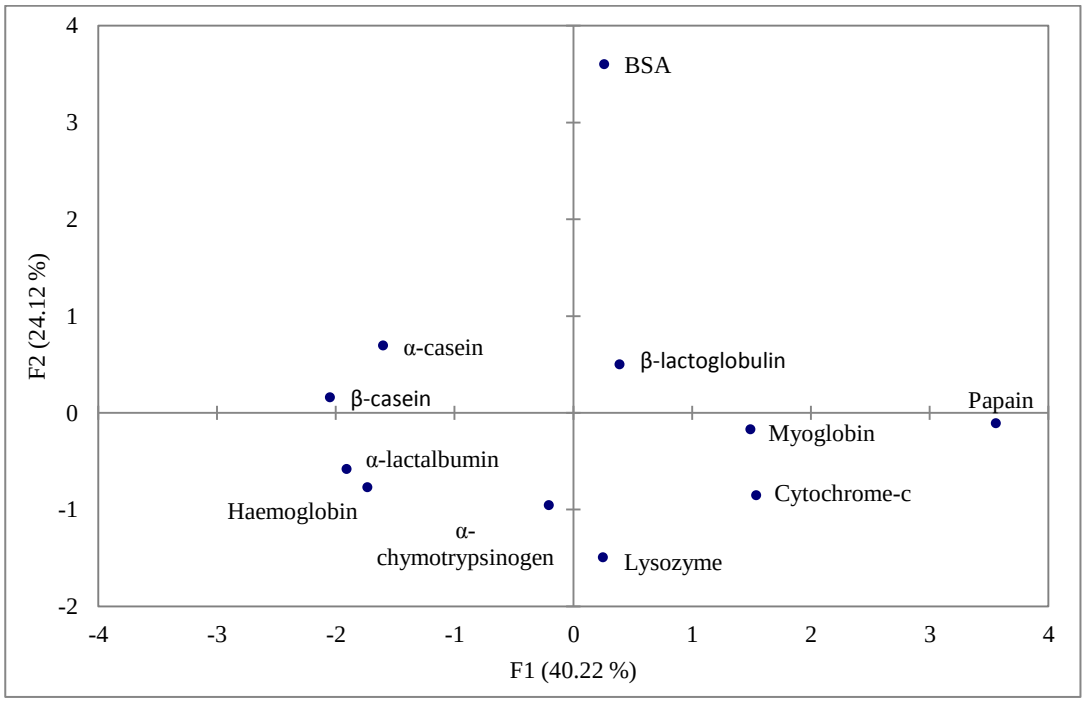

Figure 3-15: 2-D plot of the proteins with the factor loadings

The PCA data plotted in 3-D in Fig. 3-16 PCA. Papain is in Quadrant I and its adsorption is therefore positively correlated with Factors 1 and 3; implying that papain adsorption has features of Factors 1 and 3 but not of Factor 2. Therefore adsorption does not depend on dimension of the protein. On the other hand, lysozyme is in Quadrant III and is positively correlated with Factors 1 and 2 and negatively correlated with Factor 3. This means adsorption does not depend on the basic/positive residues of the protein. α-casein is in Quadrant IV and its adsorption is positively correlated with Factor 1 and negatively correlated with Factor 3. Hence, adsorption depends on the basic/positive residues exposed on the surface that can bind to the negatively charged SS. For example, papain, as can be observed in Fig. 3-16, falls in Quadrant I, having a positive correlation with Factor 1 (aromatic residues). in the PDB micrographs (Fig. 3-11) as papain has very high number of the aromatic residues exposed on the surface, which contribute to the increased adsorption on SS surfaces.

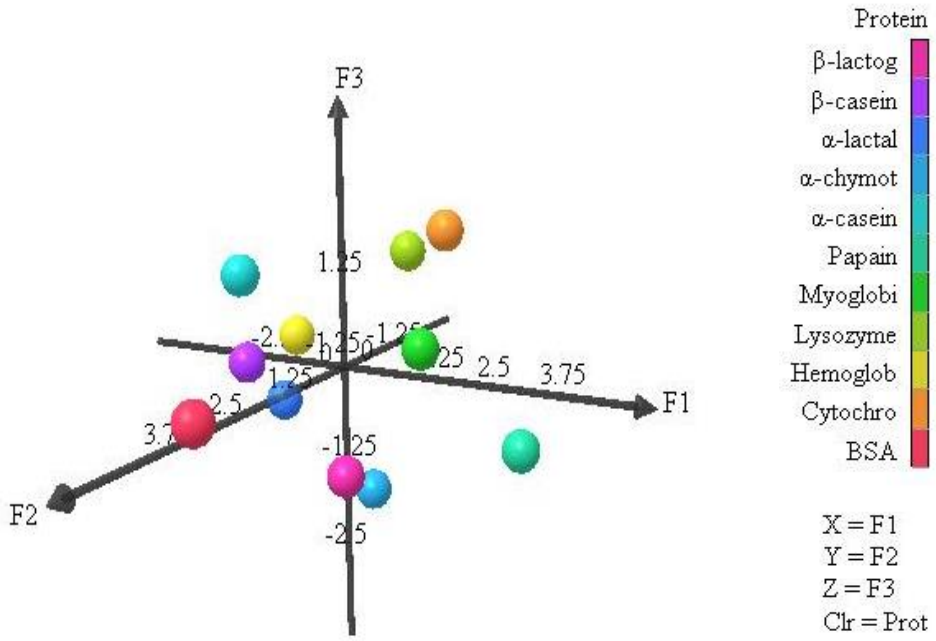

Figure 3-16: 3-D scatter plot for the proteins, their adsorption on SS compared to the factor loadings

PCA gave an insight on how different properties of the proteins affect adsorption and helped categorize them by their individual properties. The proteins studied had different characteristics and therefore were different quadrants. However results

obtained from PCA show that is no general conclusion that could be drawn for the entire set of proteins only for individual properties of individual proteins with respect to few of its properties.

3-2-5 Kinetic models to study reversible and irreversible adsorption on SS sensor surface

After studying protein adsorption and identifying the parameters affecting adsorption onto surfaces, the kinetics of the adsorption mechanism were investigated. Protein adsorption involved both reversible and irreversible kinetics (Fig. 3-1) and that almost 80% of the adsorbed protein was irreversibly bound to the surface. As both reversible and irreversible adsorption occurs, three standard models have been considered – Langmuir, Freundlich and Conformational change kinetic models.

After applying the Sauerbrey model to the data, simple kinetic models were used to describe the experimental adsorption/desorption data. Fitting the Langmuir and Freundlich models were performed using *Origin 8.6 Pro* software.*Graphpad Prism® software* (version 6.0, San Diego, CA) was used for the Conformational change kinetic model.

Data from α-casein adsorption discussed here. Experiments were carried out at concentrations ranging from 0.1 to 2 mg/mL. Once the Sauerbrey analysis had been performed, the mass adsorbed (mg/m^2) was plotted against protein concentration in the feed (mg/mL). The fit of the Langmuir, Freundlich and Conformational change with the data are shown in Fig. 3-17. The fitted values for the three models can be seen in Table 3-10.

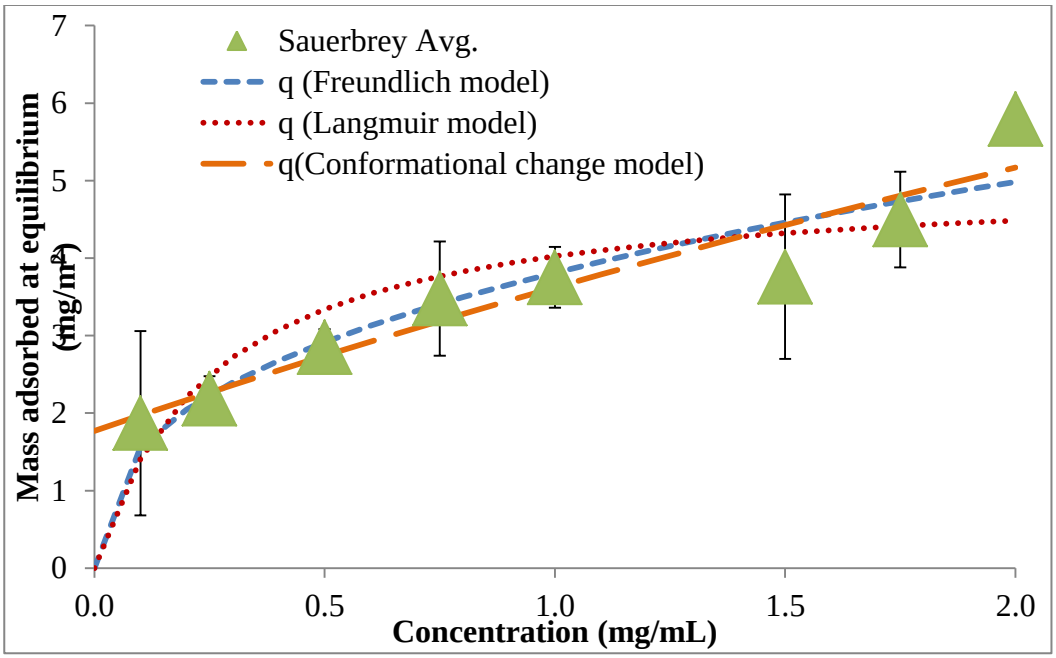

Figure 3-17: Langmuir, Freundlich and Association and Dissociation models for adsorption of α-casein to SS

Table 3-10: Fitted values of Langmuir, Freundlich and Conformational Change models for α–casein adsorption to SS

Langmuir isotherm	ρ_{max} = 506.44 and K_D = 0.25
Freundlich isotherm	ρ_{max} = 381.15 and α = 0.38
Conformational change isotherm	ρ_{max} =177 and K_D = 0.09

The protein adsorption data fits the Freundlich approximation better than the Langmuir isotherm (Appendix I). The Langmuir and Freundlich kinetic models gave reasonable fits for α-casein adsorption using Sauerbrey mass (ng/cm^2), but could not describe protein desorption during washing. This indicates the Langmuir and Freundlich assumptions of reversible protein-surface binding were invalid for the consideration used. There are large differences between protein adsorption and desorption, leading to an apparent irreversible adsorption process. The models do not recognize any change in surface concentration once the maximum surface

concentration has been attained. Other proteins tested also did not fit the two models well.

The k_a, k_d and K_D values of the models are the correlation coefficients (R^2). The k_a values in the Langmuir and Freudlich models are lower to that of the Conformational change model.

The protein molecules irreversibly adsorbed make a primary layer and play a direct role in the overall fouling phenomena as they encourage successive deposition of other biological material. Therefore attention was directed towards the irreversible contribution to total adsorption rather than explaining the reversible binding phenomenon. Also, reversible adsorption accounts for only 20% of total binding.

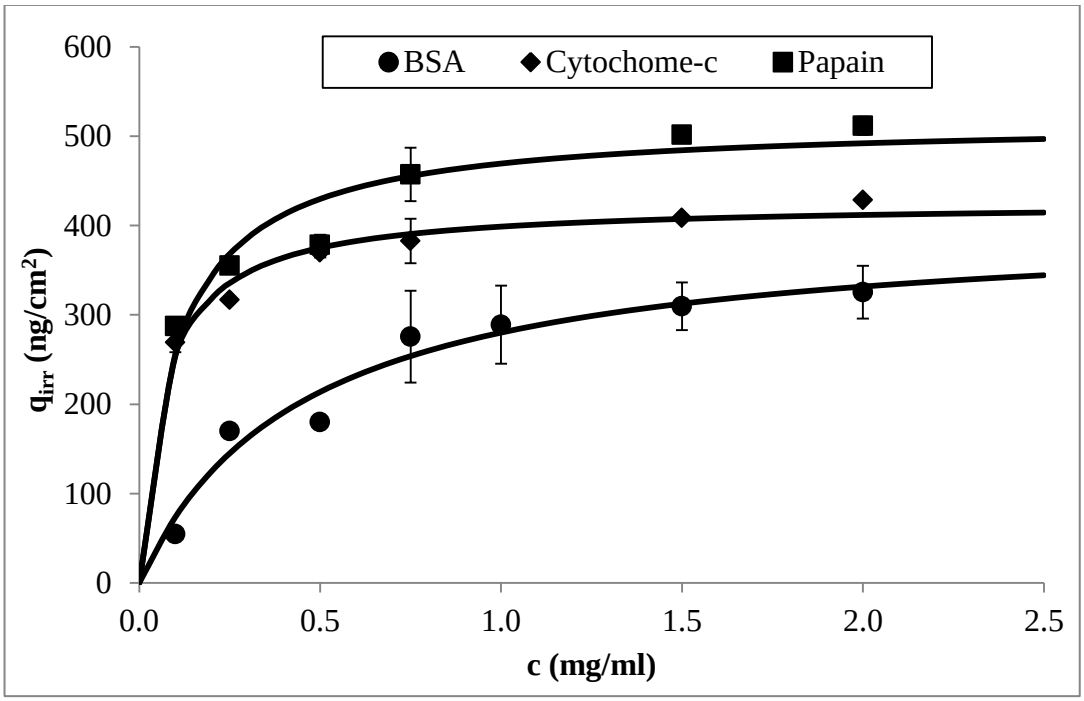

Figure 3-18: Effect of protein concentration on surface for irreversibly adsorbed protein. The Langmuir best-fit curves are also presented.

The calculated surface concentration of protein irreversibly adsorbed on to the QCM-D sensor is asymptotic (Fig. 3-18) for selected proteins belong in the three main classes (milk protein – BSA, blood protein – cytochrome-c and commercial protein – papain). This behaviour is typical of adsorption processes with a saturation limit and included in the Langmuir, Freundlich or Toth adsorption models. Although these

models have been extensively used to model adsorption of proteins on to solid supports (Hlady and Buijs, 1996, Suen, 1996, Dimartino *et al.*, 2011), they are based on completely reversible adsorption. This condition did not exist under the conditions used in this study. However, the mathematical form of the Langmuir model is a convenient tool for estimating the asymptotic value of the adsorbed layer concentration. The Langmuir model relates the amount adsorbed on a surface to the concentration of the same species in solution : where $q_{m,irr}$ and k_d are the two parameters of the Langmuir isotherm and correspond to the maximum amount absorbed on the surface and dissociation constant of the solute–surface interaction, respectively. The Langmuir equation was applied the experimental adsorption data and the parameters are summarized in Table 3-11.

Table 3-11: Langmuir parameters used to describe irreversible adsorption data of the test proteins.

Group	Proteins	q_m (mg/mL) Langmuir for irreversible adsorption	K_d (mg/mL) Langmuir for irreversible adsorption
Milk	α-lactalbumin	181	0.35
	β-lactoglobulin	205	0.08
	α-casein	517	0.28
	β-casein	634	0.35
	BSA	343	0.28
Blood	Cytochrome-c	426	0.07
	Haemoglobin	398	0.08
	Myoglobin	461	0.05
Commercial	α-chymotrypsinogen	431	0.10
	Lysozyme	400	0.37
	Papain	517	0.10

The parameters $q_{m,\mathrm{irr}}$ and K_d listed in Table 3-11 were determined for irreversibly bound protein, even though the Langmuir model assumes a reversible mechanism. The factor K_d of the affinity of a species to adsorb onto a material surface, and in particular it represents the protein concentration of protein in solution for which half the saturation was attained. Therefore, the smaller the K_d, the smaller the concentration in the liquid phase required to foul the surface. The blood proteins investigated all have a relatively low K_d, indicating these proteins are good fouling agents for SS surfaces. This behaviour may be associated with theit high content of positive and metal chelating AA residues (Banci *et al.*, 1997). Caseins have high fouling behaviour (Jeurnink *et al.*, 1996c, De Jong, 1997, Bennett, 2007). Although they have smaller affinity towards the surface, they by a relatively higher maximum adsorption than the blood proteins tested. However, aside from some exceptions all proteins investigated had a narrow range of maximum adsorption and binding affinities. These results of are in agreement with previous studies on protein adsorption onto 316 grade SS surfaces. For example, Ngadi *et al*. (2012) estimated the adsorbed layer produced by α-lactalbumin using the Voigt model, to be about 2.5 mg/m^2. However, the Voigt model overestimates the mass adsorbed when viscoelastic effects are negligible, and the Sauerbrey model offers a more accurate estimate for the adsorbed layer. This observation explains the marginally smaller values determined in the present work. Karlsson *et al*. (2005) measured β-lactoglobulin adsorption by ellipsometry, with surface concentrations in the range of 1 mg/m^2. This value was slightly lower than estimated through QCM-D. The difference is possibly because QCM-D accounts both for the adsorbed protein present onto the surface and associated water molecules embedded in the hydration layer (Section 3-2-2).

3-2-6 Rate of adsorption vs. amount adsorbed

As well as determining the kinetic constants, the different phases involved in adsorption of proteins on the SS surfaces over time were by plotting the rate of adsorption against the mass adsorbed on the surfaces (Fig. 3-19). The rate of adsorption was calculated from experimental data as the ratio between change in

adsorbed mass (Δm) and with time (Δt). This graph indicates that adsorption of proteins occurs in three phases/regimes: (i) the initial adsorption is associated with the dynamics of the protein solution filling the measuring chamber. (ii) The next regime involves interactions between the protein molecules and the surface, with fast adsorption at the beginning of the run characterized by low surface coverage of the proteins, because all binding sites on SS are available for the protein at the start. In other words, the decreased adsorption rate indicated that the incoming proteins have fewer or limited binding sites on SS for adsorption. Some of the protein molecules could be very loosely bound and hence may return solution instead of being adsorbed to the surface. Because the protein solution was recycled, these free unbound proteins return to the solution and are re-introduced for adsorption to SS again. Until the frequency signal becomes stable (Fig. 3-1), the protein molecules try to bind to the SS, once the frequency is stable, no more sites are available for binding. Proteins also bind to water molecules and the QCM-D senses both the protein and the water molecules on the surface. (iii) When the surface is completely saturated with the protein molecules, all the sites available on the surface are occupied by the protein molecules and either a multilayer may start to form or proteins rearrange on the surface to allow further monolayer binding. In this phase, the rate of adsorption (i.e. rate of accumulation/aggregation of proteins on top of the protein layer or rearrangement to enable further surface binding) remains constant.

α-casein was discussed as an example (Fig. 3-19). Lower concentrations resulted in a lower surface coverage. Also, the adsorption rate in the second regime is maximum when only a relatively small surface coverage was attained when working at low concentrations, while the rate remains at the maximum until a higher surface coverage was achieved in the case of high protein concentration in solution. For example when α-casein concentration, at c_0 = 0.1 mg/mL the rate decreases after having reached a maximum surface adsorption rate of 0.04 mg/m^{2}s at 0.5 mg/m^2 adsorbed protein, but when the protein concentration is at 1.75 mg/mL, adsorption rate is a maximum of 0.11 mg/m^{2}s until the mass of protein adsorbed was almost 3.0 mg/m^2. These data suggest that there are other, more subtle, mechanisms associated with adsorption than the simple steric hindrance by the protein already present on the surface.

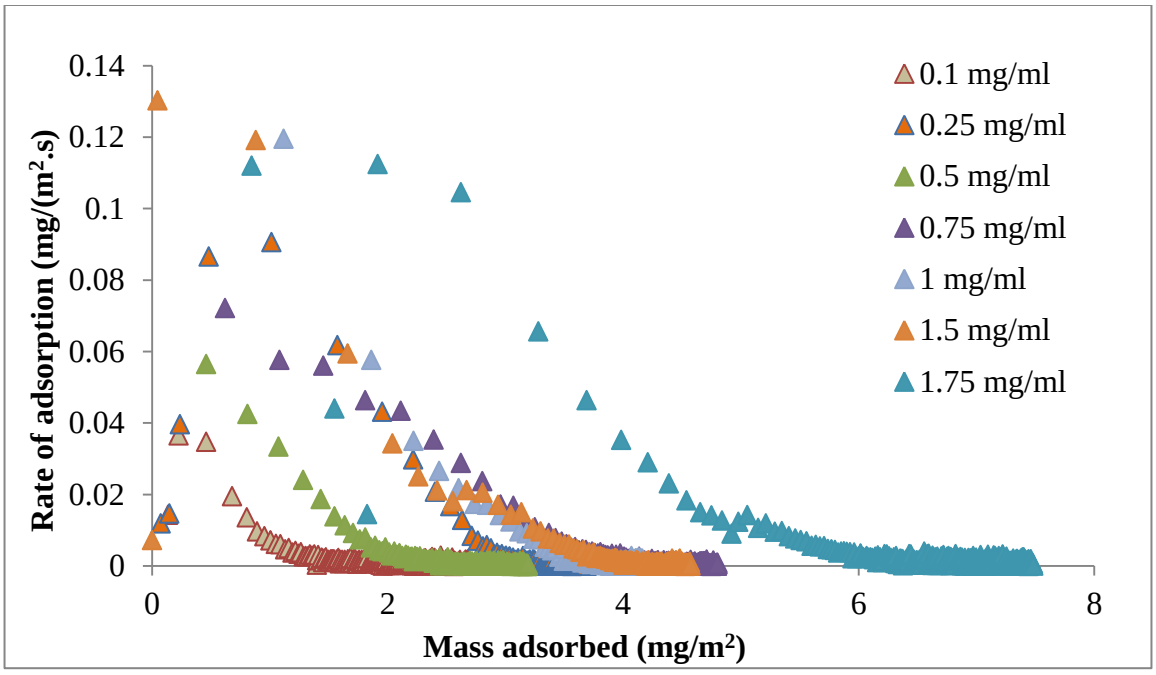

Figure 3-19: Rate of adsorption vs. amount adsorbed (α-casein)

3-2-7 Geometric modeling

After the kinetic fitting adsorption rate was studied at various concentrations test protein, was investigated for the way the protein molecules would orient themselves on the surface. The QCM-D experimental data used the Sauerbrey model for modeling the protein binding to the surface, did not predict the orientation of the protein molecules on the SS surface. The theoretical dimensions of the proteins are already known but, for accuracy, the protein diameters were obtained the Nano-Zetasizer (Table 3-12) and used to calculate the surface coverage. The particle diameter was measuring triplicates at 0.5 mg/mL protein solutions.

Five different models are proposed for orientation (geometric modeling) of the proteins on the surface.

Table 3-11: Nano-Zetasizer measurements (n=3)

Protein	Size: Diameter (nm) (± 0.005 nm)	Published Protein Dimensions (nm)
α-lactalbumin	2.465	2.9 (Pessen *et al.*, 1991)
β-lactoglobulin	4.605	1 (Banci *et al.*, 1997)
α-casein	3.995	3.7 (Pessen *et al.*, 1991)
β-casein	4.734	4.0 (Wright and Thompson, 1975)
BSA	4.665	1.9 (Gast *et al.*, 1998)
Haemoglobin	2.366	1.7 (Fermi *et al.*, 1984)
Myoglobin	2.545	1.5 (Maurus *et al.*, 1998)
α-chymotrypsinogen	2.529	8.9 (Pessen *et al.*, 1991)
Lysozyme	2.529	8.9 (Pessen *et al.*, 1991)

3-2-7-1 Spherical model

The first model approximated protein molecules as spheresand model was the first assumption for geometric modeling. The placement of protein molecules on the surface is shown in Fig. 3-20. The proteins can form a monolayer or multilayer. This model assumes that only protein molecules are adsorbed on the SS surface. Another assumption here is that stable frequency intials, the entire surface is packed with the spherical protein molecules there are no spaces and hence the surface is completely saturated.

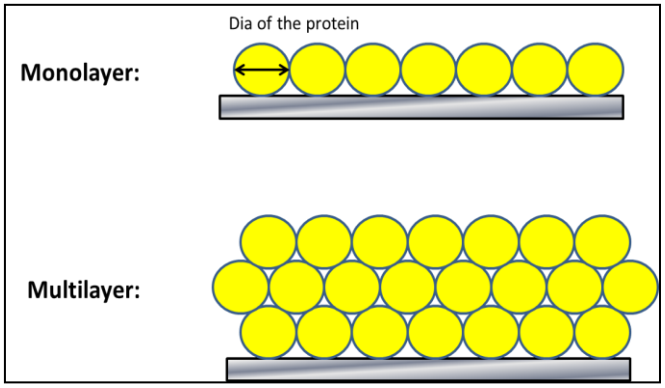

Figure 3-20: Spherical model where the protein molecules are considered as spheres occupying the SS surface

3-2-7-2 Concentric Circle model

The second model assumes water molecules are trapped in the protein layers formed on the surface. The QCM-D detects the adsorbed layer. Although the Sauerbrey

model assumes the surface to be rigid, earlier research shows water in the bound layer on the surface occurs during the adsorption phenomena (Macakova *et al.*, 2007, Anand *et al.*, 2010). This model is an improvement on the spherical model, where the protein molecules are considered as spheres with layer of water surrounding each sphere. The water molecule coats the protein molecule and hence the diameter of the water is greater than that of the protein molecules (Fig 3-21). This did not seem to occur in practice because the diameter of the water molecules was smaller than that of the protein (~ 0.25 nm) (Schatzberg, 1967).

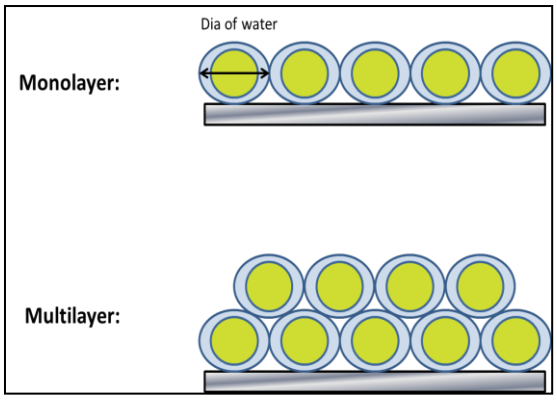

Figure 3-21: Concentric circle model where water molecules surround each spherically arranged protein molecules

3-2-7-3 Cylindrical model

In this third model the protein molecules are considered as cylinders rather than spheres either with top-on orientation where the protein molecules are arranged in a longitudinal manner or end-on orientation where the protein molecules have a latitudinal arrangement (Fig. 3-22). The diameter and height of the protein molecule are considered as two different dimensions rather than the single dimension considered in the first two models.

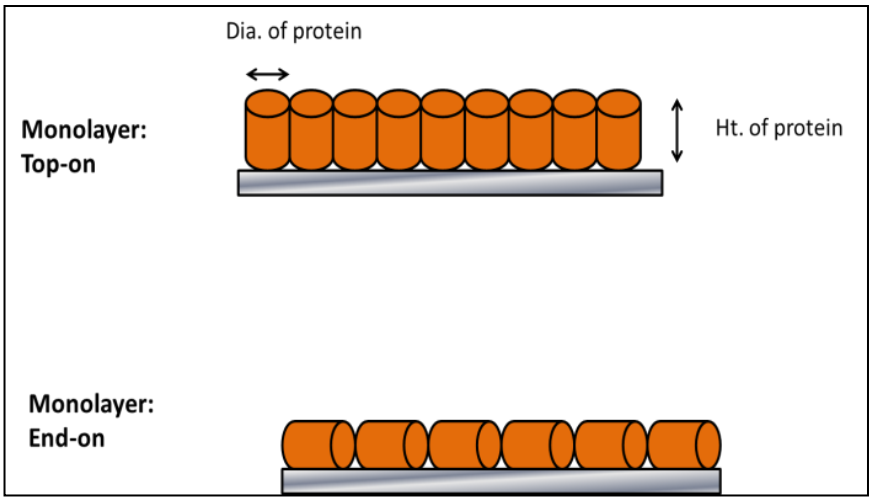

Figure 3-22: Cylindrical model, with top-on orientation and end-on orientation of the protein molecule

3-2-7-4 Truncated cone model

The recently developed truncated model involves coats of hydrodynamically-trapped water that surrounding each adsorbed protein molecule (Reviakine *et al.*, 2011). The protein molecule was considered as a cylinder and the water molecule as a truncated cone, together are considered in this approximation (Fig. 3-23). Further approximations can be performed on this model, (considering the overlapping layers of the liquid trapped and approximation towards angle of attachment of the liquid with the adsorbed protein molecule). This model is a good approximation against the other four models.

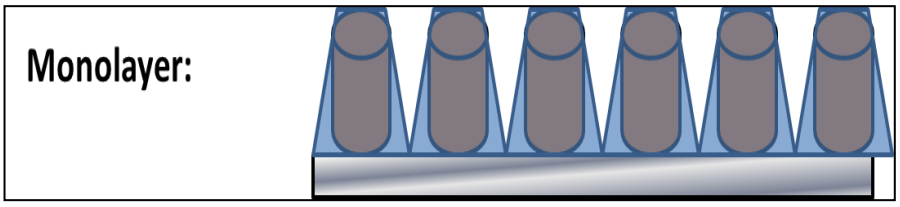

Figure 3-23: Truncated cone model where protein molecules are considered as cylinders and water molecules around them forming a truncated cone (overlapping water molecules between neighboring proteins adsorbed on the surface)

These four models were used to predict surface coverage for different concentration of α-casein. The spherical, concentric and cylindrical models predict very high

coverage (> 1000%) of some protein concentrations, inferring multiple layers would be formed. However, the truncated cone model has comparatively less surface coverage. For example, at the lowest concentration of 0.1 mg/mL of α-casein, only 38% of the entire surface was occupied by the protein molecules. At a higher concentration of 1.5 mg/mL there was 91% of the sensor surface saturated with the protein molecules (Table 3-12). This analysis helps to gain a better understanding regarding the assumption of orientation of protein molecules on the surfaces. Also, this work lead to the determination of the percentage of water in the protein-water adsorbed layers on the SS sensor.

Table 3-12: Surface coverage using the geometric models

Concentration (mg/mL)	**Molecules on sensor surface (*10^{12})**	**Spherical model**	**Concen-tric circle model**	**Cylindrical model (top on orientation)**	**Cylindrical model (end on orientation)**	**Truncated cone model**
0.10	3.16	500	503	182	82	38
0.25	3.70	585	588	212	118	44
0.50	4.82	762	766	277	167	58
0.75	5.88	930	935	338	245	70
1.00	6.34	1003	1009	364	295	76
1.25	6.36	1006	1011	365	315	76
1.50	7.60	1203	1209	437	401	91
1.75	9.79	1550	1557	562	465	117

Chapter 4 - Chemo-enzymatic modification of tyrosine to DOPA and testing its adhesiveness to stainless steel

Introduction

The main aim of the work described is to provide further insights in two particularly interesting peptide sequences, KGYKYYGGSS and KGYKYY, taken from the full protein sequence of the mussel foot protein mefp-5. These peptide fragments were chosen because they have a high content of tyrosine residue content, 50% and 30%, respectively, providing a good basis to study the effect of converting tyrosine to DOPA on adsorption to SS. The peptide sequences were chemo-enzymatically modified by hydroxylating tyrosine residues to DOPA using mushroom tyrosinase. The percentage conversion of tyrosine to DOPA was determined and correlated to adsorption of the motifs on SS surfaces using QCM-D. To confirm the effectiveness of modification of tyrosine residues to DOPA, model proteins lysozyme and insulin were tested before proceeding to testing the peptide sequences. The adsorption of a complete hybrid sequence of mefp-151 (combination of six decapeptides of mefp-1 on either side of one complete sequence of mefp-5), with 32 tyrosine residues and accounting for 4% of the total protein content was also studied (Choi *et al.*, 2012, Waite *et al.*, 1985). This sequence was produced by recombinant methods and was kindly gifted by Professor Hyung Joon Cha, Pohang University, South Korea (Dodson *et al.*, 1979). A high rate of conversion to DOPA, in which up to 97.6% of the tyrosine residues were converted, was obtained for the chosen peptide fragments and significant increases in adsorption observed after conversion.

4-1 Materials and methods

Equipment and reagents are described in Section 3-1-3.

4-1-1 Materials

Human recombinant insulin was purchased from Sigma Aldrich (Sydney, Australia). Peptides I and II (KGYKYYGGSS and KGYKYY respectively, both of which are present in mefp-5) were obtained from GenScript (Piscataway, NJ, USA). The mefp-151 sequence was produced recombinantly and was kindly gifted by Professor Hyung Joon Cha, Pohang University, South Korea (Dodson *et al.*, 1979). Tricholoroacetic anhydride (TCA) was obtained from Merck & Co., Inc. (New Jersey, USA), argon and nitrogen gases were obtained from BOC gases (Christchurch, New Zealand). HPLC-grade acetonitrile was obtained from JT Baker®, Mallinckrodt Baker Inc., (PA, USA), and Decon-90 was purchased from Agar Scientific (Chelmsford, United Kingdom). All other chemicals used in this work, including L-tyrosine, L-DOPA, mushroom tyrosinase (~2000 units/mg), mercaptoacetic acid, phenol, sodium carbonate salt, Trizma salt and anhydrous trifluoroacetic acid (TFA), were obtained from Sigma Aldrich (St. Louis, MO). All buffers were degassed prior to use.

4-1-2 Methods

To separate unreacted tyrosinase, Sephadex™ Peptide size exclusion chromatography (SEC) column 10/300 GL (GE Healthcare Technologies, Uppsala, Sweden) was used for the peptide fragment and a Superdex 75 SEC column was used for lysozyme and human recombinant insulin. Analytical HPLC was carried out on a Shimadzu™ SCL 10A instrument (Shimadzu Corporation, Japan) connected to an Aqua™ C18 column, (250 mm x 4.6 mm ID, 5 μm column, Phenomenex, Auckland, New Zealand) and equipped with a RF-10AXL Shimazdu fluorescence detector Model-1050 (Shimadzu Corporation, Japan). Yasara Biosciences (Vienna, Europe) was used for modeling peptide structure.

4-1-2 Modification of tyrosine to DOPA

Tyrosine residues present in the peptide fragments were converted to DOPA by reaction with mushroom tyrosinase, using methods described by Ito *et al*. (1984) and Gieseg *et al*. (1993). Briefly, 100 nmol/mL of lysozyme, insulin or the peptide fragments were incubated with 200 units/mL of mushroom tyrosinase for 0 (control), 2, 4 and 6 h in a final volume of 1 mL of 100 mM sodium phosphate buffer pH 7.4. (1 tyrosinase unit is defined as the amount of enzyme that produces a 0.001/min increase

in absorbance at 280 nm in a 3-mL reaction mixture containing L-tyrosine at pH 6.5 and 25°C). Reaction was quenched by denaturing the tyrosinase enzyme using 0.5 mL of 5% v/v TCA solution.

4-1-3 Separating unreacted tyrosinase using size exclusion chromatography

After DOPA modification, the samples were pre-filtered through a 0.22 μm syringe filter (25 mm diameter, MS ® PES syringe filter, and injected onto a Sephadex™ Peptide SEC column 10/300 GL (GE Healthcare Technologies, Uppsala, Sweden) for the peptide fragment and a Superdex 75 SEC column for lysozyme and human recombinant insulin. The columns were connected to an AKTAexplorer10 and used to separate unreacted tyrosinase. Briefly, 500 μL of the samples were injected into the system, using 10 mM Tris, pH 7.5 as buffer at a flow rate of 0.25 ml/min. This procedure simultaneously enabled i) separation of the modified proteins and peptide fragments from the mushroom tyrosinase enzyme and ii) buffer exchange from the reaction mixture to Tris buffer. 200 μL protein and peptide samples were collected for subsequent acid hydrolysis.

4-1-4 Gas phase acid hydrolysis

Protein/peptide hydrolysis was carried out on the DOPA-modified samples using acid vapor, following a protocol similar to the one previously described by Ito *et al*. (1984) and Gieseg *et al*. (1993). In brief, 200 μL of the purified protein and peptide fractions after separation of unreacted tyrosinase was placed in a 7.5 mm i.d. glass Durham tube and dried under vacuum overnight. The Durham tube containing the dried protein/peptide sample was then placed into a Pico-Tag vial (Millipore, Bedford, USA) containing 1 mL solution of 6 M hydrochloric acid (HCl), 1% w/v phenol and 50 μL mercaptoacetic acid. Argon was thoroughly flushed through the Pico-Tag vials for 5 minutes to remove any air, then the argon was extracted using a vacuum pump connected to a Speed Vac ® Plus AR system (Savant instruments, New York, USA) for five seconds, ensuring that the vacuum gauge pressure was below 200 mTorr. Acid hydrolysis was eventually carried out by incubating the vials in an oven at 110ºC for 24 h. The samples were then lyophilized using the Speed Vac system connected to a -110ºC freeze trap. The lyophilized samples were re-dissolved

in 200 μL of 0.1% TFA and transferred to Eppendorf tubes for centrifugation at 20,000 × g for 10 minutes. 20 μL of the supernatant (clear liquid overlying the precipitate) was used for high-pressure liquid chromatography (HPLC) analysis of DOPA as described below.

4-1-5 Quantification of DOPA and tyrosine residues

Analytical HPLC was carried out on a Shimadzu™ SCL 10A instrument connected to an Aqua™ C18 column, (250 mm x 4.6 mm ID, 5 μm column) and equipped with a RF-10AXL Shimazdu fluorescence detector Model-1050. The mobile phase consisted of 0.1% (v/v) TFA adjusted to pH 2.5 with 10 M NaOH. 20 μL of the hydrolysate was routinely injected and eluted with using an acetonitrile gradient elution. The gradient began at 100% 0.1% TFA pH 2.5 with 1% acetonitrile where the acetonitrile linearly increased to 15% by 14 min and 50% by 16 min. This was maintained for 7 minutes to clean the column, after which the acetonitrile concentration was returned to 1% by 30 min. The eluted DOPA and tyrosine peaks were detected at approximately 5 and 7 min respectively, at an excitation wavelength of 280 nm and emission wavelength 320 nm. The identities and concentrations of DOPA and tyrosine in the hydrolyzed samples were confirmed using pure amino acids as reference standards. The DOPA and tyrosine standards were diluted with 0.1% (v/v) TFA to final concentrations of 2 and 20 μM respectively. The hydrolyzed samples were injected in triplicate runs. The analysis of reference standards and samples resulted in highly repeatable peak areas with retention times varying within 5% between runs.

4-1-6 Adsorption tests of modified proteins/peptides on stainless steel surfaces

As described earlier in Section 2-5, protein adsorption studies were carried out on unmodified and modified peptide fragments using QCM-D. The dissipation changes observed during adsorption experiments were negligible so the Sauerbrey model was used for quantifying the mass adsorbed.

4-2 Results and discussion

Lysozyme, human recombinant insulin and mefp fragments were modified to DOPA. Lysozyme and human recombinant insulin were chosen for proof of concept as they have three and four residues of tyrosine, respectively. The studies performed with lysozyme and insulin were to check the effectiveness of tyrosinase in forming DOPA from tyrosine. These proteins are easily available and economical for use in this experiment as a proof of concept.

Mefp fragments have a high DOPA content, which aids the adherence of mussels on rock surfaces. Out of the six mefps currently identified, mefp-5 and mefp-6 have been found to be mainly responsible for this adhesion (Waite *et al.*, 2005, Benedict Christine and Picciano Paul, 1989, Lee *et al.*, 2006b). Two synthetic peptides, Peptide I (KGYKYYGGSS) and Peptide II (KGYKYY), were used in the present study. These peptide sequences represent specific fragments of the mussel adhesive protein (mefp-5), and were converted to KGY*KY*Y*GGSS and KGY*KY*Y*, where Y* denotes DOPA. Conversion of tyrosine to DOPA was done using mushroom tyrosinase at reaction times of 2, 4 and 6 h and percentage conversions determined. Adsorption to SS surfaces of the unmodified peptide fragments and those modified by different levels of conversion to DOPA were studied using QCM-D to determine the differences in binding between the two forms. The adsorption of chemo-enzymatically modified fragments and the recombinantly modified mefp-151 sequence were then compared.

4-2-1 Separation of unreacted tyrosinase by size exclusion chromatography

After modification, the unreacted tyrosinase (119 kDa) was separated from lysozyme (14.3 kDa), human recombinant insulin (5 kDa), the Peptide I fragment (1.1 kDa) and Peptide II fragment (0.8 kDa) by size exclusion chromatography (SEC), with simultaneous buffer exchange from the 100 mM sodium phosphate in the original samples to a 10 mM Tris buffer. Fractions of the protein and peptide fragments were collected and subjected to acid hydrolysis for analysis.

Modification of peptide I is discussed as an example. The elution profile for Peptide I showed tyrosinase eluted at approximately 10 minutes and the modified peptide sample eluted at 25–26 minutes (Fig. 4-1). The tyrosinase elution peak increased as reaction time was increased through 2, 4 and 6 h. This discrepancy in the peak heights for the tyrosinase and modified peptides were due to the clogging of the tyrosinase on top of the SEC column. The modified peptide fragments eluted in three of the 0.5 mL fractions, which were pooled before the concentration of the peptide sample using the Nanodrop^{TM} Spectrophotometer by absorbance at A280 nm.

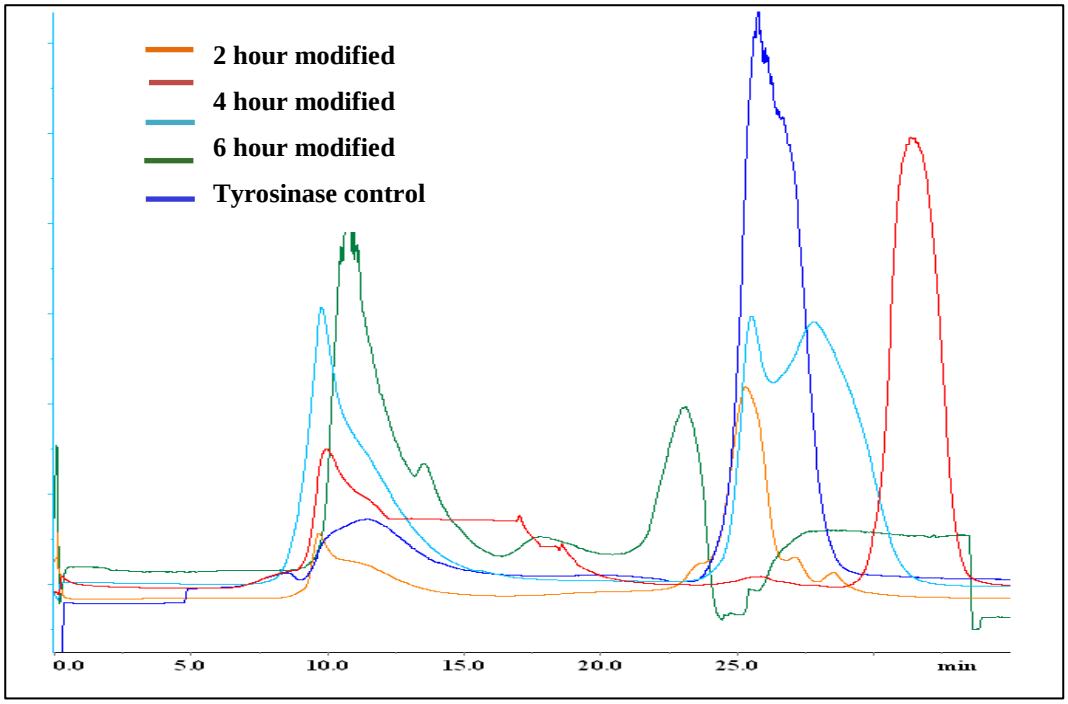

Figure 4-1: Effect of the reaction time on elution for chemo-enzymatically modified Peptide I fragment.

The good separation of the modified fragments from the tyrosinase enabled unreacted tyrosinase to be removed and samples containing modified fragments could then be used for acid hydrolysis, analysis of DOPA and adsorption on SS.

4-2-2 Oxidation of proteins by tyrosinase

4-2-2-1 Lysozyme and human recombinant insulin

For acid hydrolysis, mercaptoacetic acid (reducing agent) was added and oxygen removed by flushing the hydrolysis vessel with an inert gas (argon). The recovery of DOPA was also aided by gas phase hydrolysis, where only the acid vapor came into contact with the protein sample. These steps were essential for detecting DOPA in the hydrolysates because DOPA is labile (Ito *et al.*, 1984, Gieseg *et al.*, 1993). As reaction time with tyrosinase increased, the amount of DOPA formed also increased. At 6 h, 0.5 pmoles DOPA were formed per nmol protein (Fig. 4-2).

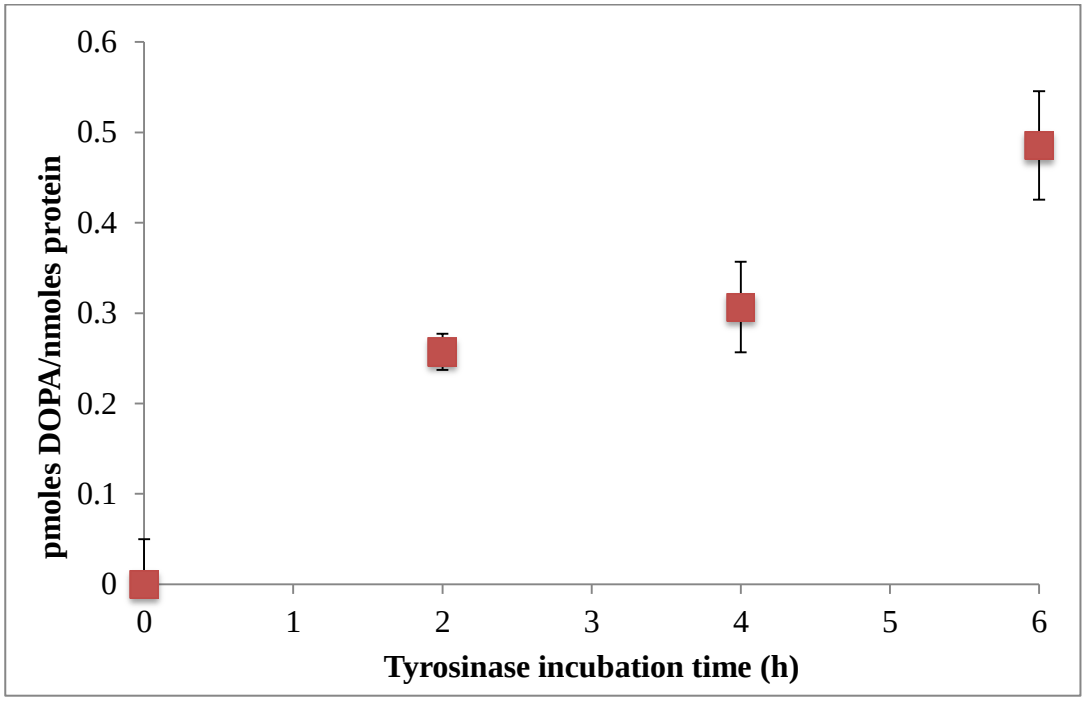

Figure 4-2: Effect of reaction time on DOPA formation in lysozyme.

Almost 18 pmoles of DOPA was formed for every nmol of insulin after 6 h of reaction with tyrosinase. The higher DOPA formation is due to insulin having more of tyrosine residues than lysozyme

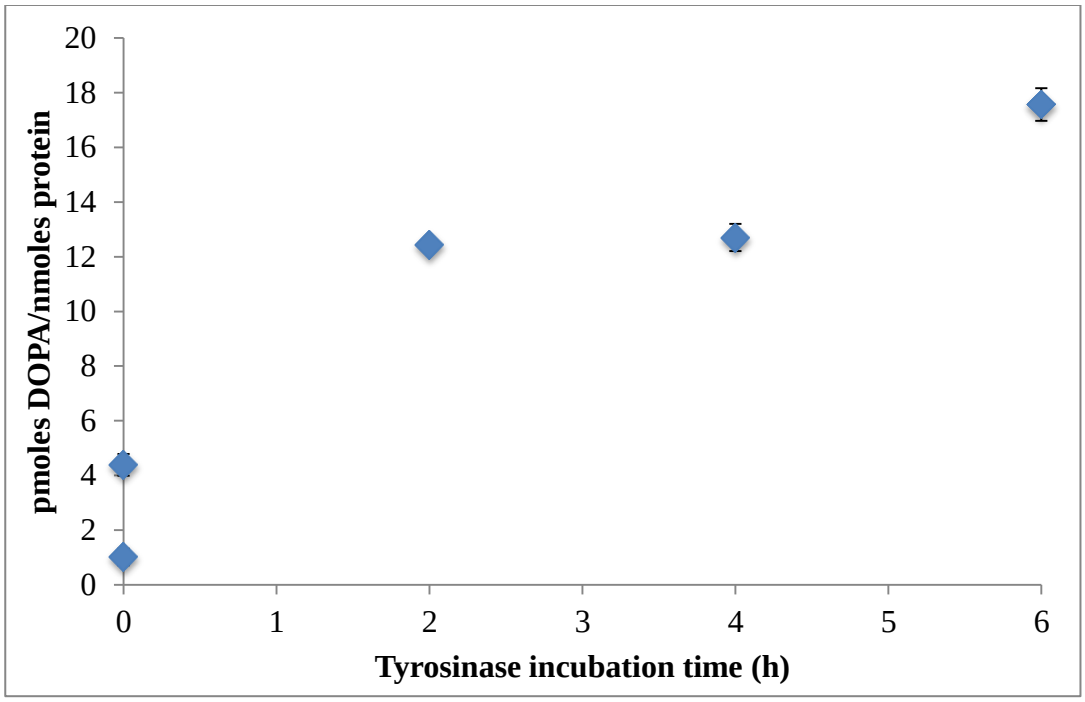

Figure 4-3: Effect of reaction time on DOPA formation in insulin.

4-2-2-2 Peptide fragments

The main focus of this study was to understand the adsorption of modified peptide fragments using tyrosinase. Once lysozyme and insulin had been studied, the focus was moved onto the peptide fragments. The synthetic peptide analogues Peptide I and Peptide II have three tyrosine residues, corresponding to 30% and 50% tyrosine content, respectively. Based on optimum conversion of tyrosine residues to DOPA using mushroom tyrosinase obtained in the previous studies Ito *et al*. 1984 and Gieseg *et al*. 1993, reaction times of 2, 4 and 6 h were chosen for the peptide fragments. The controls for both the peptides were the 0 h samples containing the peptide and tyrosinase in 10 mM Tris buffer. All samples were processed by SEC to remove unreacted and (TCA) deactivated mushroom tyrosinase, before being subjected to acid hydrolysis. The contents were determined of DOPA analysis by reversed-phase HPLC using a fluorescence detector. Pure DOPA and tyrosine were the reference standards. The fluorescence peak areas of DOPA were proportional DOPA concentration in the sample and were quantified against the standard. DOPA eluted at approximately 5 minutes and tyrosine at approximately 7 minutes (Fig. 4-4).

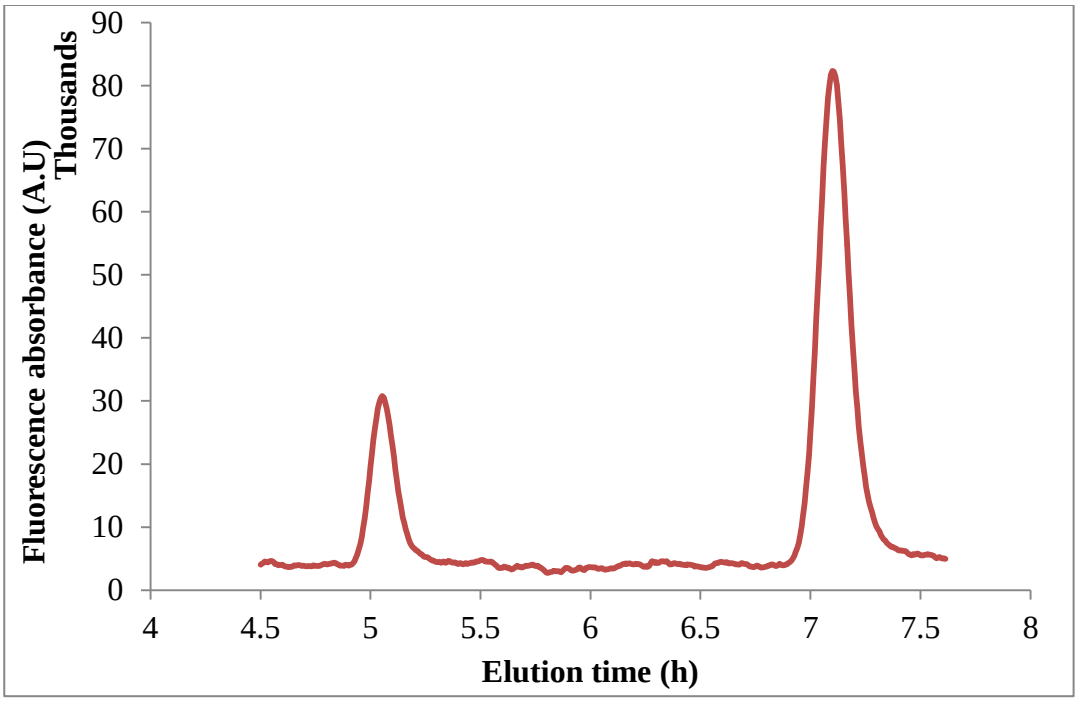

Figure 4-4: HPLC elution profiles for 20 µg/mL tyrosine and 1 µg/mL DOPA

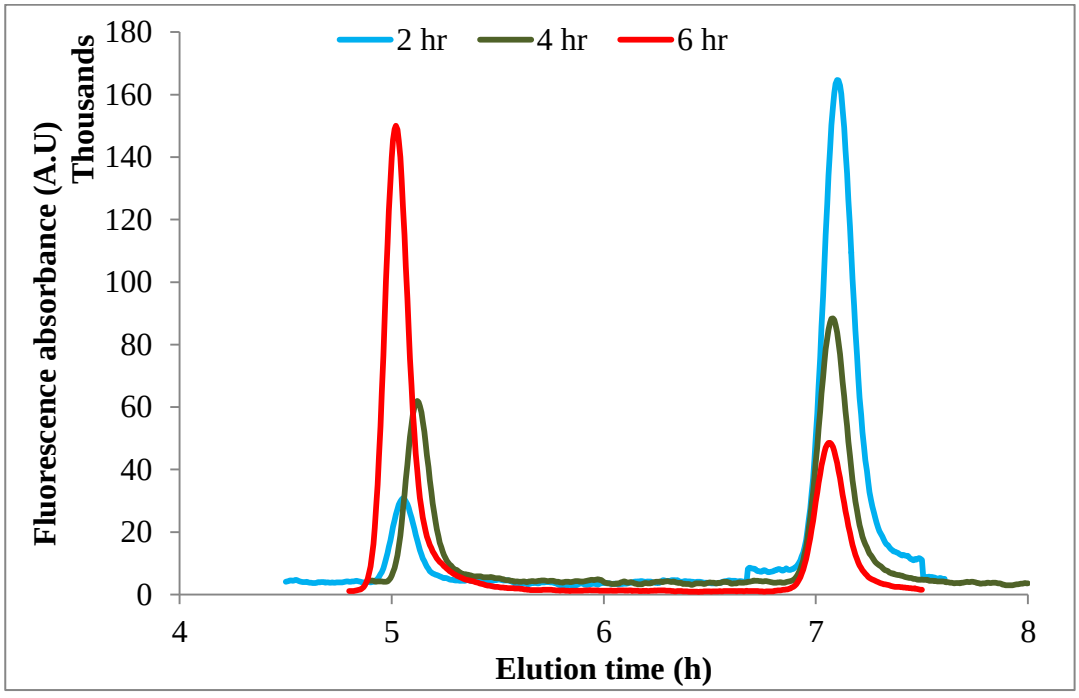

Figure 4-5: Effect of tyrosinase reaction time on elution profile of modified peptide fragment I.

The peptide fragments at 0 time point showed only a single large peak corresponding to tyrosine at approximately 7 minutes (data not shown). The peak at 5 minutes in the elution profiles for peptide II with mushroom tyrosinase indicated DOPA formation (Fig. 4-5). The amount of DOPA formed increased with reaction time.

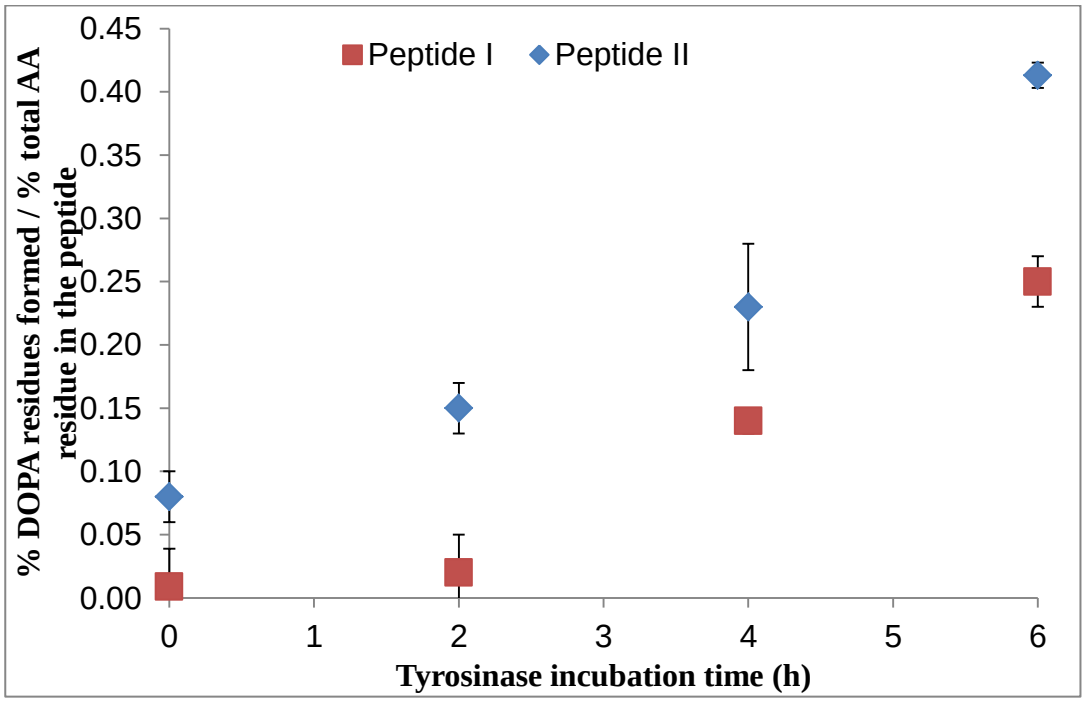

Figure 4-6: Effect of tyrosinase incubation time on DOPA formed in peptide fragments I & II.

The amount of DOPA formed was directly related to tyrosinase reaction time (Fig 4-6). The amount of DOPA formed in Peptide II increased because of the higher content of tyrosine residues. Based on the HPLC analysis of supernatants of acid-hydrolysed peptide fragments for DOPA concentration, it was observed that 0.15 µmole of DOPA was formed per µmole of the Peptide II at 2 h or 0.15 µmol of DOPA formed from 0.5 µmol of tyrosine present in the Peptide II (containing 50% tyrosine), showing that approximately 30% of the tyrosine residues were modified to DOPA at 2 h. At 4 h, approximately 50% of the tyrosine residues were modified and at 6 h about 80% of the tyrosine residues were converted to DOPA in Peptide II. In Peptide I (containing 30% tyrosine), the conversions of tyrosine residues to DOPA was approximately 26%, 57% and 83% at 2, 4 and 6 h, respectively.

The conversion factor represents the amount of DOPA determined from the tyrosine residues present in the sample. For example, after 2 h of incubation Peptide I had ~73% conversion, so out of the 30% tyrosine content (three tyrosine residues in KGYKYYGGSS), at least two of the tyrosine residues were converted to DOPA. After 4 h of incubation, ~2.5 residues were converted (~84% conversion) and finally after 6 h of incubation with the enzyme almost all three tyrosine residues were converted to DOPA (~99%). Similarly, for Peptide II (50% tyrosine containing peptide KGYKYY) after 2 h of incubation out of the three tyrosine residues ~81% were converted to DOPA denoting the formation of two DOPA residues. After 4 h of incubation, ~2.5 residues were converted (~87% conversion) and after 6 h all the three tyrosine residues were converted to DOPA (~97%). As observed, the 6 h modified sample of both the peptides has the maximum conversion of tyrosine to DOPA of ~97-99%.

4-2-4 Protein adsorption studies using QCM-D

Adsorption curves obtained in the QCM-D shows that the maximum adsorption for the insulin was 1 mg/m^2 and this insulin almost completely desorbed from the sensor surface when it is re-equilibrated with the buffer solution. Insulin that was reacted with tyrosinase for 6 h contained DOPA residues and reversibly adsorbed to a maximum of 8 mg/m^2 and adsorbed irreversibly at 2 mg/m^2. Insulin has a lower less tyrosine content (16% of total residues. Therefore, only 3% was found to be converted after 6 h of reaction with tyrosinase; thus there was only a small amount of irreversible adsorbed mass on the sensor. Lysozyme had almost no irreversible adsorbed mass on the surface because only 1% of the tyrosine residues had been converted to DOPA (data not shown).

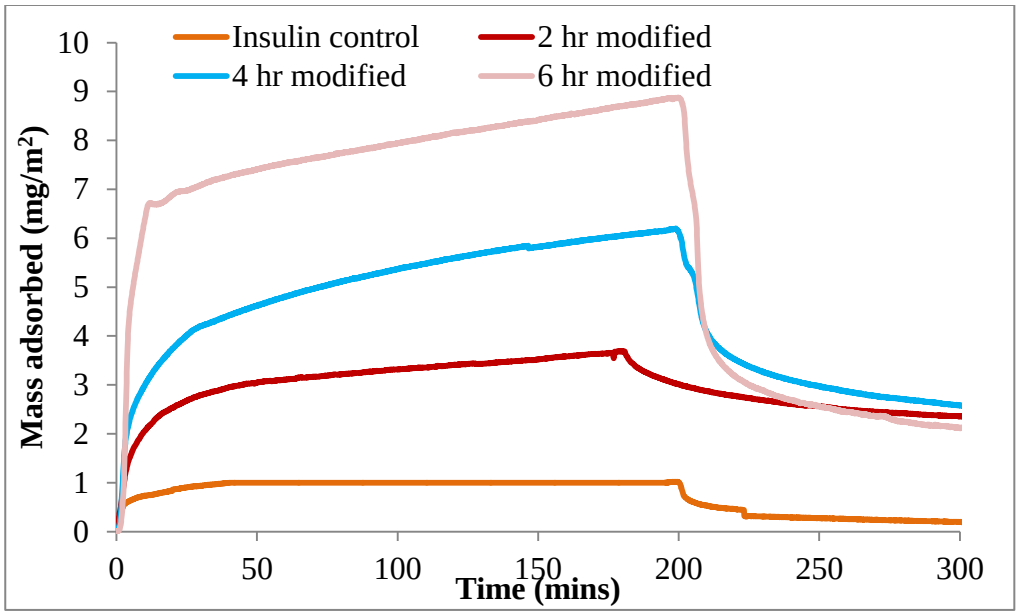

Figure 4-7: Typical QCM-D adsorption curves for insulin (modified and unmodified) on SS sensor surface.

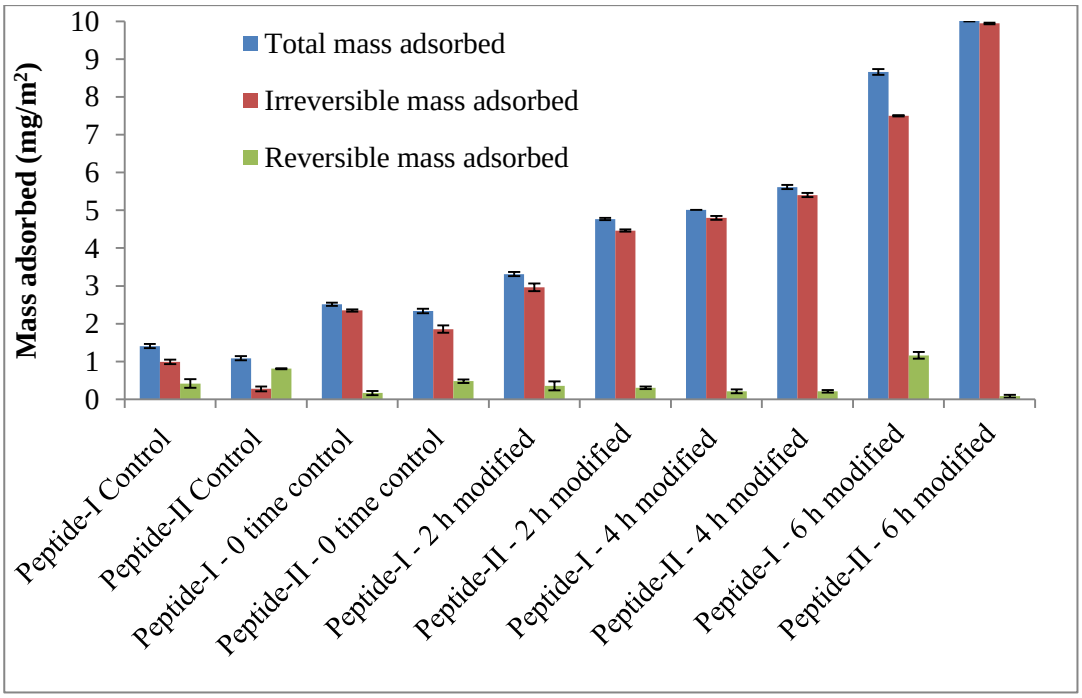

Figure 4 9: Effect of tyrosinase on peptide fragments on SS surfaces. Peptide I and II controls represent the peptide-only samples and the 0 h controls represent peptides and tyrosinase incubated together but immediately.

Figure 4-9 shows that the adsorption behaviours of modified and unmodified peptide samples, both the peptide-only control and 0 h controls differed. This could be attributed to the fact that tyrosinase activity on the peptide fragments at the 0 h time point is rapid and hence some oxidation of the tyrosine residues could take place almost instantaneously, resulting in increased adsorption when compared with the peptide-only control fragments (Fig. 4-7). Surface adsorption increased for peptides as the reaction times of the peptides with tyrosinase increased. For example, Peptide II had similar total and irreversible mass adsorbed and very low reversible mass adsorbed on the sensor surface after 6 h of modification with tyrosinase. Thus, the 6 h modified sample of Peptide II was more strongly adsorbed onto the SS surface than the other samples and it contained a higher percentage of DOPA. Hence, this stronger adhesion was attributed to the presence of higher numbers of DOPA residues in the peptide fragment. Additionally, DOPA residues are known to form coordinate metal ion complexes with, for example, SS and titanium, thus increasing the interaction of DOPA with the surface (Monahan and Wilker, 2003, Sever *et al.*, 2003). Reaction of peptide samples with tyrosinase for 6 h showed almost complete conversion of tyrosine to DOPA (~ 97-99%). When compared with the peptide-only control samples, the adsorption of the 2 h modified samples showed 4-fold increases; 4 h modified samples showed ~ 5-fold increases; and the 6 h modified samples showed ~ 9-fold increases. Catechol moieties in the DOPA residues may also play a major role in the adsorption of the peptides through hydrogen bonding, metal ion chelate complexes or covalent cross-links of DOPA with the metal surface (Waite and Tanzer, 1981).

DOPA in the peptide fragments formed by chemo-enzymatic synthesis was compared to the DOPA formed in the mefp-151 hybrid sequence *in vivo* (post-translational modification). Adsorption of mefp-151 on the SS surfaces was also studied. The mefp-151 adsorption of 5 mg/m^2 on the SS surface was lower than that of the 6 h modified Peptide II sample that adsorbed, which is 8 mg/m^2 irreversibly on the surface. It was observed that the mefp-151 had an equal amount of total and irreversible mass adsorbed on the surface, suggesting that there was no loss of adsorbed mefp-151 on the SS and hence very strong adsorption of the DOPA groups to the metal ions.

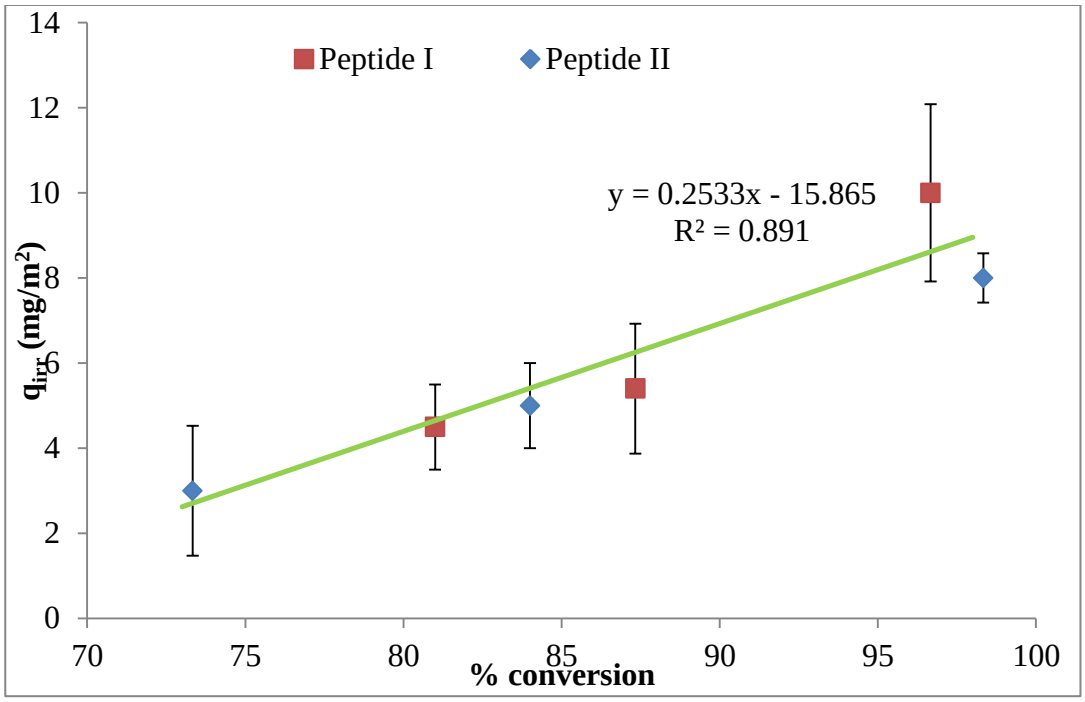

Figure 4-8: Relationship of DOPA content (as percentage converted) on SS.

The irreversibly bound protein (q_{irr}) on the SS surface was was directly related to total % conversion of tyrosine to DOPA (Fig. 4-9). The regression correlation for peptide I was R^2 = 0.93 and for peptide II was R^2=0.99. The overall linear trend for both the peptides is observed to have a R^2 = 0.89. The correlation line had an intercept value of -16 here, which does not make mechanistic sense but the percentage conversion was directly studied only from the 2 h time point onwards. Lower time reactions after 30, 60 and 90 minutes of reaction of the peptides with tyrosinase were not analysed but may have shown a more sensible trend as time approached zero. It is observed that for adsorption on SS studied at 2, 4 and 6 h q_{irr} increased with each consecutive time point. For example, both peptides showed 5 mg/m^2 irreversible adsorption on the surface after 4 h, compared with 10 mg/m^2 after 6 h. The very high increase in the irreversible adsorption of the peptide on the surface is attributed to their DOPA content. When considering the overall trend line, the maximum irreversible adsorption was observed after 6 h, with almost 80-83% conversion from tyrosine to DOPA and the adsorption was four-fold higher than the control sample (containing only tyrosine and no DOPA). DOPA residues have been found to interact with organic and inorganic surfaces through π electron interactions

(Waite, 1976). DOPA is also capable of both donating and accepting hydrogen bonds and this allows DOPA to compete well with water bonding on hydrophilic and polar surfaces (Lee *et al.*, 2006a).

4-2-5 DOPA interaction with surfaces

Hlady (1996) studied adsorption of DOPA on a titanium oxide (TiO_2) surface using AFM. The basic amino acids, which are positively charged at neutral pH, were responsible for adhesion to surfaces. Histidine (H) has the ability of forming metal coordination complexes when pH is higher than the pI of the protein molecules in solution. pH is higher than pI of the protein, the surface is negatively charged, which enhances adsorption of basic amino acid residues (K and R) onto the oxide layer by electrostatic interactions (Hlady and Buijs, 1996). Another cohesive property of DOPA is covalent cross-linking between the DOPA molecules, which the covalent cross-linking promotes formation of triss-dopa-Fe(III) complexes at the interface of the surface (Hlady and Buijs, 1996). The role of DOPA in the adhesion process has also been studied by Yu *et al*. (1999). In this study, the DOPA-K copolymer both with and without the oxidant hydrogen peroxide (H_2O_2) rapidly oxidized, of which decreased the co-polymer's adhesive-forming ability. Cohesive bond failure was observed in slowly oxidized samples which allowed catechol to be the active form of DOPA in surface adhesion (Bitton and Bianco-Peled, 2008). Catechol form strong hydrogen bonds with hydrophilic, polar surfaces such as, SS and titanium. Transition metals are also key reagents in protein cross-linking. The iron center cross links with DOPA residues to form a very strong metal-protein interaction (Wiegemann, 2005). The adhesive property of mussel proteins has been shown to be due to the DOPA-containing peptides.

4.3 Conclusions

In this study, tyrosine residues in two peptide fragments derived from mefp-5, KGYKYYGGSS and KGYKYY, were converted to DOPA by treating them with tyrosinase. These linear peptide fragments showed that all the tyrosine residues could easily be converted to DOPA. The resultant DOPA sidechains could then easily interact with the SS surface. An analysis of the effect of total conversion of tyrosine

to DOPA on adsorption showed that the latter increased as DOPA formation increased with the tyrosinase reaction time The greatest adsorption, 80-83%, was observed after 6 h reaction, an approximately 9-fold increase in adsorption when compared with the control samples. Adsorption studies of tyrosine-containing fragments indicate successful chemo-enzymatic conversion to DOPA and confirmed that DOPA is responsible for a marked increase in adsorption to surfaces.

Chapter 5 - Conclusions and recommendations

5-1 Conclusions

5-1-1 Protein adsorption studies on stainless steel sensors using a quartz crystal microbalance with dissipation

Adsorption behaviour of proteins onto 316 grade SS surfaces was investigated using QCM-D measurements. The proteins formed an adsorbed layer that cannot be removed by simple buffer wash, and more complex cleaning protocols were required to strip the bio-layer irreversibly adsorbed to the surface. This layer is rigidly coupled to the QCM-D sensor and its viscoelastic characteristics can be neglected.

The mass of protein adsorbed is the result of reversible and irreversible adsorption. Data showed that irreversible adsorption was the main contributor, accounting for 80% of the total mass adsorbed. Irreversible adsorption is a relatively fast process, usually occuring in the first few minutes of contact between the protein and the surface. To predict the amount of protein adsorbed on SS, a simple empirical relationship correlating surface concentration, $q_{m,irr}$, to protein charge density, ρ_q, was developed.

Under the operating conditions used in the experiments, the SS surface was negatively charged. Hence, negatively charged proteins adsorbed less due to their charge density, and electrostatic repulsion is the main energetic barrier to overcome for surface adsorption. Positively charged biomolecules could achieve maximum surface coverage, and the mass/thickness of the adsorbed layer is linearly related to the molecular weight of the protein. The research is the first time a simple relationship to estimate the extent of the adsorbed protein layer when SS and protein solutions are in contact has been determined. This developed relationship will allow other characteristics such as reduction in heat transfer coefficient in process equipment in the food industry or decrease in mass transport rates in biomedical devices to be estimated. PCA allowed the contribution of several protein properties (e.g. hydrophobicity, size, charge, presence of specific residues, etc.) on the adsorption prediction to be determined. These properties were correlated to the mass

adsorbed on SS surfaces. However, no clear conclusions could be drawn for the set of proteins used.

A secondary objective of the research was to determine water content in the adsorbed layers. α-lactalbumin had the most hydration water, followed by β-lactoglobulin. These two proteins are highly hydrophilic, and therefore should entrap high water when adsorbing to the SS surface. The casein species used did not produce adsorbed layers with significant water content because they form large aggregates by self-associating with neighbouring protein molecules that exclude water molecules.

Published research on protein adsorption based on the execution of two separate experiments with different sensors, introducing possible bias associated with using different instruments but, more importantly, errors because the sensor surfaces have different topographies and compositions. This thesis describes a new method involving QCM-D and fluorescent measurements on QCM-D to measure surface adsorption, using a single 316 grade SS sensor in a single experiment, to measure total mass adsorbed by QCM-D and protein mass adsorbed by fluorescence intensity simultaneously on a single 316 grade SS sensor. The current research thus measured water content in the adsorbed layer using two methods on a single sensor, resulting in estimates of 32% - 45.8% (wet basis); half of that which most researchers record. This approach removes the uncertainties associated with using differing surfaces for each measurement technique.

5-1-2 Chemo-enzymatic modification of tyrosine to DOPA and testing its adhesiveness to SS

Tyrosine residues in two peptide fragments, KGYKYYGGSS (peptide I) and KGYKYY (peptide II), derived from mefp-5, were converted to DOPA by treating with mushroom tyrosinase for 2, 4 and 6 h. Linear peptide fragments were used so all the tyrosine residues were easily accessible for conversion to DOPA. The DOPA formed could then easily interact with the SS surface. Conversion of tyrosine to DOPA and its effect on adsorption was analysed. As tyrosinase reaction time increased, DOPA formation increased linearly and adsorption of these samples on SS increased. The adsorption studies on tyrosine-containing fragments indicate

successful chemo-enzymatic conversion to DOPA and also confirm that DOPA markedly increases adsorption to surfaces. Peptide II that had been tyrosinase treated for 6 h had total mass adsorbed and very low reversible mass adsorbed on the sensor surface. Thus, Peptide II samples were more strongly adsorbed onto the SS surface than the model proteins used in this study and contained a higher percentage of DOPA. This stronger adhesion was attributed to the of higher DOPA residues in the peptide fragment. Compared with the peptide-only control samples, the adsorption of the 2 h modified samples adsorbed 4-fold, 4 h modified samples showed ~ 5-fold increases; and the 6 h modified samples showed ~ 9-fold increases. The catechol moieties in the DOPA residues may also play a major role in the adsorption of the peptides through hydrogen bonding, metal ion chelate complexes or covalent cross-links of DOPA with the metal surface.

5-2 Recommendations for future work

The following work is recommended for the future:

1) Further experiments could be done to investigate the effect of various factors such as buffer pH and temperature on overall adsorption of peptides/proteins on SS surface.
2) Mussel peptides contain other post-translationally modified amino acids that could possibly contribute to their adhesive properties. For eg. serine to phosphoserine modification is also considered important for adhesion. The recommended peptide fragments could be post-translationally modified and tested for adhesiveness

   I: YHYHSGGSYHGSGYH (15mer peptide) - Partial fragment of core peptide of mefp-5 containing H and S. Serine can be converted to phosphoserine.

   II: GGYKGKYYGKAKKYYYKYKNSGKYKY (26mer peptide) - Partial fragment of mefp - 5 peptide containing G, K and Y (to be converted to DOPA).

III: YHYHSGGSYHGSGYHGGYKGKYYGKAKKYYYKYKNSGKYKY (41mer peptide) - Repetitive fragments containing G, K and DOPA with the influence of H and S.

3) Having identified that there is DOPA-metal interaction, it might be possible to use the peptide fragments containing DOPA to form a bio-film by functionalizing the bio-layer or the fragment, after tethering it to a PEG (poly-ethylene glycol) using other reactive side chains and binding it on to the SS surface,. A bio-inspired adhesive formed in this way could form a stable coating on the SS surfaces and prevent its fouling. This bio-inspired adhesive could be used in several other industries and applications.

References

Anand, G., Zhang, F., Linhardt, R. J. & Belfort, G. 2010. Protein-associated water and secondary structure effect removal of blood proteins from metallic substrates. *Langmuir,* 27**,** 1830-1836.

Ando, T., Uchihashi, T., Kodera, N., Yamamoto, D., Miyagi, A., Taniguchi, M. & Yamashita, H. 2008. High-speed AFM and nano-visualization of biomolecular processes. *European Journal of Physiology,* 456**,** 211-225.

Andrade, J. D. 1985. X-ray photoelectron spectroscopy (XPS)*Surface and interfacial aspects of biomedical polymers.* Springer.

Anema, S. G., Lee, S. K., Lowe, E. K. & Klostermeyer, H. 2004. Rheological properties of acid gels prepared from heated pH-adjusted skim milk. *Journal of Agricultural and Food Chemistry,* 52**,** 337-343.

Artimo, P., Gasteiger, E., Grosdidier, A., Hernandez, C., Ioannidis, V., Kuznetsov, D., Liechti, R., Moretti, S., Mostaguir, K., Redaschi, N., Rossier, G., Jonnalagedda, M., Xenarios, I., Stockinger, H., Arnold, K., Baratin, D., Csardi, G., de Castro, E., Duvaud, S., Flegel, V. & Fortier, A. 2012. ExPASy: SIB bioinformatics resource portal. *Nucleic acids research,* 40**,** W597.

Arwin, H. 2000. Ellipsometry on thin organic layers of biological interest: characterization and applications. *Thin Solid Films,* 377–378**,** 48-56.

Azzam, R. M. A. & Bashara, N. M. 1977. *Ellipsometry and polarized light,* Amsterdam North-Holland Publishing Company.

Banci, L., Bertini, I., Gray, H. B., Luchinat, C., Reddig, T., Rosato, A. & Turano, P. 1997. Solution structure of oxidized horse heart cytochrome c. *Biochemistry,* 36**,** 9867-9877.

Bansal, B. & Chen, X. D. Fouling of heat exchangers by dairy fluids-a review *Proceedings of 6th International Conference on Heat Exchanger Fouling and Cleaning - Challenges and Opportunities,* 2005.

Bansal, B. & Chen, X. D. 2006. A critical review of milk fouling in heat exchangers. *Comprehensive Reviews in Food Science and Food Safety,* 5**,** 27-33.

Baujard-Lamotte, L., Noinville, S., Goubard, F., Marque, P. & Pauthe, E. 2008. Kinetics of conformational changes of fibronectin adsorbed onto model surfaces. *Colloids and Surfaces B: Biointerfaces,* 63**,** 129-137.

Benedict Christine, V. & Picciano Paul, T. 1989. Adhesives from marine mussels*Adhesives from Renewable Resources.* American Chemical Society.

Bennett, H. A. E. 2007. *Aspects of fouling in dairy processing.* Dissertation/Thesis, Massey University

Bernos, E., Girardet, J. M., Humbert, G. & Linden, G. 1997. Role of the *O*-phosphoserine clusters in the interaction of the bovine milk α-*s1*, β-, κ-caseins and the PP3 component with immobilized iron (III) ions. *Biochimica et Biophysica Acta (BBA)-Protein Structure and Molecular Enzymology,* 1337**,** 149-159.

Bi, R. C., Dauter, Z., Dodson, E., Dodson, G., Giordano, F. & Reynolds, C. 1984. Insulin's structure as a modified and monomeric molecule. *Biopolymers,* 23**,** 391-395.

Bird, R. B. 2002. Transport phenomena. *Applied Mechanics Reviews,* 55**,** R1-R4.

Bitton, R. & Bianco-Peled, H. 2008. Novel biomimetic adhesives based on algae glue. *Macromolecular Bioscience,* 8**,** 393-400.

Brockman, J. S. 2007. Kramers-Kronig and Ellipsometry Techniques. *Applied Physics 272* [Online].

Brubaker, C. E. & Messersmith, P. B. 2012. The present and future of biologically inspired adhesive interfaces and materials. *Langmuir,* 28**,** 2200-2205.

Brusatori, M. A. & Van Tassel, P. R. 1999. A kinetic model of protein adsorption/surface-induced transition kinetics evaluated by the Scaled particle theory. *Journal of Colloid and Interface Science,* 219**,** 333-338.

Cabilio, N. R., Omanovic, S. & Roscoe, S. G. 2000. Electrochemical studies of the effect of temperature and pH on the adsorption of α-Lactalbumin at platinum. *Langmuir,* 16**,** 8480-8488.

Chandrasekaran, N., Dimartino, S. & Fee, C. J. Adsorption of proteins on stainless steel surfaces *Chemeca 2012*, 23-26 Sep 2012 2012, Wellington, New Zealand.

Chandrasekaran, N., Dimartino, S. & Fee, C. J. Comparative study of dairy protein-associated water and its adsorption effects on stainless steel surfaces by fluorescent labelling and QCM-D Jones, M. I. & Chen, J. J. J., eds. *NZ Conference of Chemical and Materials Engineering 2013*, 25-26 Nov 2013 2013, University of Auckland, New Zealand. 31-32.

Changani, S. D., Belmar-Beiny, M. T. & Fryer, P. J. 1997. Engineering and chemical factors associated with fouling and cleaning in milk processing. *Experimental Thermal and Fluid Science,* 14**,** 392-406.

Choi, Y. S., Yang, Y. J., Yang, B. & Cha, H. J. 2012. In vivo modification of tyrosine residues in recombinant mussel adhesive protein by tyrosinase co-expression in Escherichia coli. *Microbial Cell Factories,* 11**,** 139.

Connor, P. A. & McQuillan, A. J. 1999. Phosphate adsorption onto TiO_2 from aqueous solutions: An in situ internal reflection infrared spectroscopic study. *Langmuir,* 15**,** 2916-2921.

Corporation, A. S. 2007. 316/316L Stainless steel data sheet

Corredig, M. 2004. Advanced Dairy Chemistry. Volume 1. Dairy Proteins: P.F. Fox and P.L.H. McSweeney, Kluwer Academic/Plenum Publishers, 2003. *Trends in Food Science & Technology,* 15**,** 282.

Cosman, N. P., Fatih, K. & Roscoe, S. G. 2005. Electrochemical impedance spectroscopy study of the adsorption behaviour of α-lactalbumin and β-casein at stainless steel. *Journal of Electroanalytical Chemistry,* 574**,** 261-271.

Creton, C. & Papon, E. 2003. Materials science of adhesives: How to bond things together. *MRS Bulletin,* 28**,** 419-423.

Dannenberg, F. & Kessler, H. G. 1988. Reaction kinetics of the denaturation of whey proteins in milk. *Journal of Food Science,* 53**,** 258-263.

De Feijter, J. A., Benjamins, J. & Veer, F. A. 1978. Ellipsometry as a tool to study the adsorption behavior of synthetic and biopolymers at the air–water interface. *Biopolymers,* 17**,** 1759-1772.

De Jong, P. 1997. Impact and control of fouling in milk processing. *Trends in Food Science & Technology,* 8**,** 401-405.

Degenhardt, J. & McQuillan, A. J. 1999. Mechanism of oxalate ion adsorption on chromium oxide-hydroxide from pH dependence and time evolution of ATR-IR spectra. *Chemical Physics Letters,* 311**,** 179-184.

Dietschweiler, C. & Sander, D. M. *Protein adsorption at solid surfaces*. Institute of Biogeochemistry and Pollutant Dynamics

(IBP), Swiss Federal Institute of Technology (ETH), Zürich.

Dimartino, S., Boi, C. & Sarti, G. C. 2011. A validated model for the simulation of protein purification through affinity membrane chromatography. *Journal of Chromatography A,* 1218**,** 1677-1690.

Dimartino, S., Lir, I., Haber, M. & Azhari, R. 2013. Characterization of biomimetic adhesives from the red alga Gracilaria conferta for biomedical applications*Biological and Biomimetic Adhesives: Challenges and Opportunities.* The Royal Society of Chemistry.

Dixon, M. C. 2008. Quartz crystal microbalance with dissipation monitoring: enabling real-time characterization of biological materials and their interactions. *Journal of Biomolecular Techniques,* 19**,** 151-158.

Dodson, E., Dodson, G., Hodgkin, D. & Reynolds, C. 1979. Structural relationships in the two-zinc insulin hexamer. *Canadian Journal of Biochemistry*, 57**,** 469-479.

Donik, C., Kocijan, A., Paulin, I. & Jenko, M. 2009. The oxidation of duplex stainless steel at moderately elevated temperatures. *Materials Technology*, 43**,** 137-142.

Draeger, N. A. *Adsorption of Protein onto a Solid Surface*. Bjorksten.

Economics, T. 2013. *New Zealand GDP annual growth rate* [Online]. New Zealand 2013].

Ehrlich, H. 2010. Byssus: From inspiration to development of novel biomaterials*Biological Materials of Marine Origin.* Springer, Netherlands.

Fahmy, T. 1995. XLSTAT, Software add-in Microsoft Excel

Fant, C., Sott, K., Elwing, H. & Hook, F. 2000. Adsorption behavior and enzymatically or chemically induced cross-linking of a mussel adhesive protein. *Biofouling,* 16**,** 119-132.

Fermi, G., Perutz, M. F., Shaanan, B. & Fourme, R. 1984. The crystal structure of human deoxyhaemoglobin at 1.74 Å resolution. *Journal of Molecular Biology,* 175**,** 159-174.

Flammang, P. 2006. Adhesive Secretions in Echinoderms: An Overview; Biological Adhesives. Smith, A. M. & Callow, J. A. (eds.). Springer Berlin Heidelberg.

Francisco, R. & Heather, S. 2010. Adhesive proteins from mussels*Innovations in Materials Manufacturing, Fabrication, and Environmental Safety.* CRC Press.

Frigerio, F., Coda, A., Pugliese, L., Lionetti, C., Menegatti, E., Amiconi, G., Schnebli, H. P., Ascenzi, P. & Bolognesi, M. 1992. Crystal and molecular structure of the bovine α-chymotrypsin-eglin c complex at 2.0 Å resolution. *Journal of Molecular Biology,* 225**,** 107-123.

Garg, H. G., Linhardt, R. J. & Hales, C. A. 2011. *Chemistry and Biology of Heparin and Heparan Sulfate*, Elsevier.

Gast, K., Zirwer, D., MÜller-Frohne, M. & Damaschun, G. 1998. Compactness of the kinetic molten globule of bovine α-lactalbumin: A dynamic light scattering study. *Protein Science,* 7**,** 2004-2011.

Gieseg, S. P., Simpson, J. A., Charlton, T. S., Duncan, M. W. & Dean, R. T. 1993. Protein-bound 3, 4-dihydroxyphenylalanine is a major reductant formed during hydroxyl radical damage to proteins. *Biochemistry,* 32**,** 4780-4786.

Gillard, M., Chatelain, P. & Fuks, B. 2006. Binding characteristics of levetiracetam to synaptic vesicle protein 2A (SV2A) in human brain and in CHO cells expressing the human recombinant protein. *European Journal of Pharmacology,* 536**,** 102-108.

Goda, T., Maeda, Y. & Miyahara, Y. 2012a. Simultaneous monitoring of protein adsorption kinetics using a quartz crystal microbalance and field-effect transistor integrated device. *Analytical Chemistry,* 84**,** 7308-7314.

Goda, T. & Miyahara, Y. 2012b. Interpretation of protein adsorption through its intrinsic electric charges: A comparative study using a field-effect transistor, surface plasmon resonance, and quartz crystal microbalance. *Langmuir,* 28**,** 14730-14738.

Gray, J. J. 2004. The interaction of proteins with solid surfaces. *Current Opinion in Structural Biology,* 14**,** 110-115.

Haemers, S., Koper, G. J. M. & Frens, G. 2003. Effect of oxidation rate on cross-linking of mussel adhesive proteins. *Biomacromolecules,* 4**,** 632-640.

Hedberg, Y., Lundin, M., Jacksén, J., Emmer, Å., Blomberg, E. & Odnevall Wallinder, I. 2012a. Chromium–protein complexation studies by adsorptive cathodic stripping voltammetry and MALDI-TOF–MS. *Journal of Applied Electrochemistry,* 42**,** 349-358.

Hedberg, Y. S., Killian, M. S., Blomberg, E., Virtanen, S., Schmuki, P. & Odnevall Wallinder, I. 2012b. Interaction of bovine serum albumin and lysozyme with stainless steel studied by time-of-flight secondary ion mass spectrometry and X-ray photoelectron spectroscopy. *Langmuir* 28**,** 16306-16317.

Hellstrom, S. L. 2007. *Introduction to quartz crystal microbalance* [Online]. Stanford University, Autumn 2007.

Hemmerlé, J., Altmann, S. M., Maaloum, M., Hörber, J. K., Heinrich, L., Voegel, J. C. & Schaaf, P. 1999. Direct observation of the anchoring process during the adsorption of fibrinogen on a solid surface by force-spectroscopy mode atomic force microscopy. *Proceedings of the National Academy of Sciences of the United States of America,* 96**,** 6705-6710.

Hiddink, J., Lalande, M., Maas, A. & Streuper, A. 1986. Heat treatment of whipping cream. I. Fouling of the pasteurization equipment. *Milchwissenschaft,* 41**,** 542-546.

Hillier, R. M. & Lyster, R. L. 1979. Whey protein denaturation in heated milk and cheese whey. *Journal of Dairy Research,* 46**,** 95-102.

Hlady, V. & Buijs, J. 1996. Protein adsorption on solid surfaces. *Curr. Opin. Biotechnol.,* 7**,** 72-77.

Höök, F. 1997. *Development of a novel QCM technique for protein adsorption studies.* Dissertation/Thesis, Chalmers University of Technology.

Höök, F., Rodahl, M., Brzezinski, P. & Kasemo, B. 1998a. Energy dissipation kinetics for protein and antibody−antigen adsorption under shear oscillation on a quartz crystal microbalance. *Langmuir,* 14**,** 729-734.

Höök, F., Rodahl, M., Kasemo, B. & Brzezinski, P. 1998b. Structural changes in hemoglobin during adsorption to solid surfaces: Effects of pH, ionic strength,

and ligand binding. *Proceedings of the National Academy of Sciences,* 95**,** 12271-12276.

Höök, F., Vörös, J., Rodahl, M., Kurrat, R., Böni, P., Ramsden, J. J., Textor, M., Spencer, N. D., Tengvall, P., Gold, J. & Kasemo, B. 2002. A comparative study of protein adsorption on titanium oxide surfaces using in situ ellipsometry, optical waveguide lightmode spectroscopy, and quartz crystal microbalance/dissipation. *Colloids and Surfaces B: Biointerfaces,* 24**,** 155-170.

Humphrey, W., Dalke, A. & Schulten, K. 1996. VMD: Visual molecular dynamics. *Journal of Molecular Graphics,* 14**,** 33-38.

Hwang, D. S., Yoo, H. J., Jun, J. H., Moon, W. K. & Cha, H. J. 2004. Expression of functional recombinant mussel adhesive protein Mgfp-5 in *Escherichia coli*. *Applied and Environmental Microbiology,* 70**,** 3352-3359.

Imamura, K., Kawasaki, Y., Nagayasu, T., Sakiyama, T. & Nakanishi, K. 2007. Adsorption characteristics of oligopeptides composed of acidic and basic amino acids on titanium surface. *Journal of Bioscience and Bioengineering,* 103**,** 7-12.

Imamura, K., Shimomura, M., Nagai, S., Akamatsu, M. & Nakanishi, K. 2008. Adsorption characteristics of various proteins to a titanium surface. *Journal of Bioscience and Bioengineering,* 106**,** 273-278.

Incropera, F. P. & DeWitt, D. P. 2001. *Fundamentals of heat and mass transfer,* New York, Wiley.

Irwin, E. F., Ho, J. E., Kane, S. R. & Healy, K. E. 2005. Analysis of interpenetrating polymer networks via quartz crystal microbalance with dissipation monitoring. *Langmuir* 21**,** 5529-5536.

ISSF. 2010. *Stainless steel in the diary industry* [Online]. Belgium: International Stainless Steel Forum Available: www.3-a.org/Resource/pdf/Stainless-Steel-in-the-Dairy-Industry.pdf.

Ito, S., Kato, T., Shinpo, K. & Fujita, K. 1984. Oxidation of tyrosine residues in proteins by tyrosinase. Formation of protein-bonded 3,4-dihydroxyphenylalanine and 5-S-cysteinyl-3,4-dihydroxyphenylalanine. *The Biochemical Journal,* 222**,** 407-411.

Jackler, G., Steitz, R. & Czeslik, C. 2002. Effect of temperature on the adsorption of lysozyme at the silica/water interface studied by optical and neutron reflectometry. *Langmuir,* 18**,** 6565-6570.

Janowski, R., Kozak, M., Jankowska, E., Grzonka, Z. & Jaskólski, M. 2004. Two polymorphs of a covalent complex between papain and a diazomethylketone inhibitor. *The Journal of Peptide Research,* 64**,** 141-150.

Jeurnink, T., Verheul, M., Stuart, M. C. & De Kruif, C. 1996a. Deposition of heated whey proteins on a chromium oxide surface. *Colloids and surfaces B: Biointerfaces,* 6**,** 291-307.

Jeurnink, T. J. M., Walstra, P. & De Kruif, C. 1996b. Mechanisms of fouling in dairy processing. *Nederlands melk en Zuiveltijdschrift,* 50**,** 407-426.

Jeurnink, T. J. M., Walstra, P. & De Kruif, C. 1996c. Mechanisms of fouling in dairy processing. *Dutch Milk and Dairy Journal,* 50**,** 407-426.

Johnson, R. D. & Arnold, F. H. 1995. The temkin isotherm describes heterogeneous protein adsorption. *Biochimica et Biophysica Acta - Protein Structure and Molecular Enzymology,* 1247**,** 293-297.

Jönsson, M. & Johansson, H.-O. 2004. Effect of surface grafted polymers on the adsorption of different model proteins. *Colloids and Surfaces B: Biointerfaces,* 37**,** 71-81.

Jordan, J. L. & Fernandez, E. J. 2008. QCM-D sensitivity to protein adsorption reversibility. *Biotechnology and Bioengineering,* 101**,** 837-842.

Kamphuis, I. G., Kalk, K. H., Swarte, M. B. A. & Drenth, J. 1984. Structure of papain refined at 1.65 Å resolution. *Journal of Molecular Biology,* 179**,** 233-256.

Keckes, J., Burgert, I., Frühmann, K., Müller, M., Kölln, K., Hamilton, M., Burghammer, M., Roth, S. V., Stanzl-Tschegg, S. & Fratzl, P. 2003. Cell-wall recovery after irreversible deformation of wood. *Nature Materials,* 2**,** 810-4.

Khulbe, K. C., Feng, C. & Matsuura, T. 2008. *Synthetic polymeric membranes,* Berlin, Springer.

Kim, D. T., Blanch, H. W. & Radke, C. J. 2002. Direct imaging of lysozyme adsorption onto mica by atomic force microscopy. *Langmuir,* 18**,** 5841-5850.

Kim, J. C. & Lund, D. B. 1998. Kinetics of beta-lactoglobulin adsorption onto stainless steel surfaces. *Biotechnology Progress,* 14**,** 951-958.

King, G. M., Carter, A. R., Churnside, A. B., Eberle, L. S. & Perkins, T. T. 2009. Ultrastable atomic force microscopy: atomic-scale stability and registration in ambient conditions. *Nano Letters,* 9**,** 1451-1456.

Kulik, E. A., Kalinin, I. D. & Sevastianov, V. I. 2008. The heterogeneity of protein/surface interactions and structural alterations of adsorbed albumin and immunoglobulin G. *Artificial Organs,* 15**,** 386-391.

Lalande, M., Tissier, J.-P. & Corrieu, G. 1984. Fouling of a plate heat exchanger used in ultra-high-temperature sterilization of milk. *Journal of Dairy Research,* 51**,** 557-568.

Lee, B., Dalsin, J. & Messersmith, P. 2006a. *Biomimetic Adhesive Polymers Based on Mussel Adhesive Proteins,* Springer Berlin Heidelberg.

Lee, B. P., Messersmith, P., Israelachvili, J. & Waite, J. 2011. Mussel-inspired adhesives and coatings. *Annual Review of Materials Research,* 41**,** 99.

Lee, H., Scherer, N. F. & Messersmith, P. B. 2006b. Single-molecule mechanics of mussel adhesion. *Proceedings of the National Academy of Sciences,* 103**,** 12999-13003.

Lins, L., Thomas, A. & Brasseur, R. 2003. Analysis of accessible surface of residues in proteins. *Protein science* 12**,** 1406-1417.

Liu, S. X. & Kim, J.-T. 2009. Application of Kevin—Voigt model in quantifying whey protein adsorption on polyethersulfone using QCM-D. *Journal of the Association for Laboratory Automation,* 14**,** 213-220.

Lundin, M., Hedberg, Y., Jiang, T., Herting, G., Wang, X., Thormann, E., Blomberg, E. & Wallinder, I. O. 2012. Adsorption and protein-induced metal release from chromium metal and stainless steel. *Journal of colloid and interface science,* 366**,** 155-164.

Lyster, R. 1970. The denaturation of α-lactalbumin and β-lactoglobulin in heated milk. *Journal of Dairy Research,* 37**,** 233-243.

Macakova, L., Blomberg, E., Claesson, P. M., Kemi, Kth & Ytkemi 2007. The effect of adsorbed layer surface roughness on the QCM-D response: Focus on trapped water. *Langmuir*.

MacRitchie, F. 1972. The adsorption of proteins at the solid/liquid interface. *Journal of Colloid and Interface Science,* 38**,** 484-488.

Malmsten, M. 1998. Formation of adsorbed protein layers. *Journal of Colloid And Interface Science,* 207**,** 186-199.

Malmström, J., Agheli, H., Kingshott, P. & Sutherland, D. S. 2007. Viscoelastic modeling of highly hydrated laminin layers at homogeneous and nanostructured surfaces: quantification of protein layer properties using QCM-D and SPR. *Langmuir,* 23**,** 9760-9768.

Manji, B. & Kakuda, Y. 1986. Thermal denaturation of whey proteins in skim milk. *Canadian Institute of Food Science and Technology Journal,* 19**,** 163-166.

Marx, K. A. 2003. Quartz crystal microbalance: a useful tool for studying thin polymer films and complex biomolecular systems at the solution-surface interface. *Biomacromolecules,* 4**,** 1099-1120.

Maurus, R., Bogumil, R., Nguyen, N. T., Mauk, A. G. & Brayer, G. 1998. Structural and spectroscopic studies of azide complexes of horse heart myoglobin and the His-64-->Thr variant. *Biochemical Journal* 332**,** 67-74.

McSweeney, P. L. H. F., Patrick F. (Eds.) 2013. *Advanced Dairy Chemistry* Springer.

Monahan, J. & Wilker, J. J. Specificity of metal ion cross-linking in marine mussel adhesives of Work.

Motulsky, H. 1999. Analyzing Data with GraphPad Prism, 1999. *GraphPad Software Inc., San Diego CA* [Online].

Mulheran, P. & Kubiak, K. 2009. Protein adsorption mechanisms on solid surfaces: lysozyme-on-mica. *Molecular Simulation,* 35**,** 561-566.

Muramoto, S., Graham, D. J., Wagner, M. S., Lee, T. G., Moon, D. W. & Castner, D. G. 2011. ToF-SIMS analysis of adsorbed proteins: principal component analysis of the primary ion species effect on the protein fragmentation patterns. *The Journal of Physical Chemistry C,* 115**,** 24247-24255.

Murray, B. S. & Deshaires, C. 2000. Monitoring protein fouling of metal surfaces via a quartz crystal microbalance. *Journal of Colloid and Interface Science,* 227**,** 32-41.

Nakanishi, K., Sakiyama, T. & Imamura, K. 2001. On the adsorption of proteins on solid surfaces, a common but very complicated phenomenon. *Journal of Bioscience and Bioengineering,* 91**,** 233-244.

Ngadi, N. 2009. *Mechanisms of molecular brush inhibition of protein adsorption onto stainless steel surface.* Dissertation/Thesis, University of Canterbury.

Ngadi, N., Abrahamson, J., Fee, C. & Morison, K. 2008. QCM-D study on relationship of PEG coated stainless steel surfaces to protein resistance. *International Journal of Chemical and Biomolecular Engineering,* 1**,** 126.

Ngadi, N., Abrahamson, J., Fee, C. & Morison, K. 2012. QCM-D study of α-lactalbumin adsorption on stainless steel surface coated with poly ethylene glycol (PEG) nanofilms. *International Journal of Chemical and Environmental Engineering,* 3**,** 167-171.

Otzen, D. E., Oliveberg, M. & Höök, F. 2003. Adsorption of a small protein to a methyl-terminated hydrophobic surfaces: effect of protein-folding thermodynamics and kinetics. *Colloids and Surfaces B: Biointerfaces,* 29**,** 67-73.

Pászti, Z., Keszthelyi, T., Hakkel, O. & Guczi, L. 2008. Adsorption of amino acids on hydrophilic surfaces. *Journal of Physics: Condensed Matter,* 20**,** 224014.

Pessen, H., Kumosinski, T. F., Farrell Jr, H. M. & Brumberger, H. 1991. Tertiary and quaternary structural differences between two genetic variants of bovine casein by small-angle X-ray scattering. *Archives of Biochemistry and Biophysics,* 284**,** 133-142.

Petersen, B., Petersen, T. N., Andersen, P., Nielsen, M. & Lundegaard, C. 2009. A generic method for assignment of reliability scores applied to solvent accessibility predictions. *BioMed Central Structural Biology,* 9**,** 51.

Petrone, L. & McQuillan, A. J. 2011. Alginate ion adsorption on a TiO_2 particle film and interactions of adsorbed alginate with calcium ions investigated by attenuated total reflection infrared (ATR-IR) spectroscopy. *Applied Spectroscopy,* 65**,** 1162-1169.

Premathilaka, S., Hyland, M., Chen, Z., Watkins, L. & Bansal, B. Interaction of whey protein with modified stainless steel surfaces *Proceedings of 7th International Conference on Heat Exchanger Fouling and Cleaning - Challenges and Opportunities,* 2007, Portugal Engineering Conferences International.

Q-Sense. *The QCM-D principle* [Online]. Available: www.biolinscientific.com/q-sense/technologies/.

Rabe, M., Verdes, D. & Seeger, S. 2011. Understanding protein adsorption phenomena at solid surfaces. *Advances in Colloid and Interface Science,* 162**,** 87-106.

Rahn, J. R. & Hallock, R. B. 1995. Antibody binding to antigen-coated substrates studied with surface plasmon oscillations. *Langmuir,* 11**,** 650-654.

Ramachandra, S., Wiehe, S., Hyland, M. & Bansal, B. A preliminary study of the effect of surface coating on the initial deposition mechanisms of dairy fouling. Hans Müller-Steinhagen, M. Reza Malayeri, A. & Watkinson, A. P., eds. *Proceedings of 6th International Conference on Heat Exchanger Fouling and Cleaning - Challenges and Opportunities*, 2005, Germany. Engineering Conferences International.

Ren, J. & Zou, Q. 2014. High-speed adaptive contact-mode atomic force microscopy imaging with near-minimum-force. *Review of Scientific Instruments,* 85**,** 073706-073706-10.

Reviakine, I., Johannsmann, D. & Richter, R. P. 2011. Hearing what you cannot see and visualizing what you hear: Interpreting quartz crystal microbalance data from solvated interfaces. *Analytical Chemistry,* 83**,** 8838-8848.

Rischka, K., Richter, K., Hartwig, A., Kozielec, M., Slenzka, K., Sader, R. & Grunwald, I. 2010. Bio-inspired Polyphenolic Adhesives for Medical and Technical Applications. Byern, J. & Grunwald, I. (eds.) *Biological Adhesive Systems.* Springer Vienna.

Roach, P., Farrar, D. & Perry, C. C. 2005. Interpretation of protein adsorption: surface-induced conformational changes. *Journal of the American Chemical Society,* 127**,** 8168.

Rodahl, M., Höök, F. & Kasemo, B. 1996a. QCM Operation in Liquids: An Explanation of Measured Variations in Frequency and Q Factor with Liquid Conductivity. *Analytical Chemistry,* 68**,** 2219-2227.

Rodahl, M. & Kasemo, B. 1996. A simple setup to simultaneously measure the resonant frequency and the absolute dissipation factor of a quartz crystal microbalance. *Review of Scientific Instruments,* 67**,** 3238-3241.

Rose, P. W., Beran, B., Bi, C., Bluhm, W. F., Dimitropoulos, D., Goodsell, D. S., Prlić, A., Quesada, M., Quinn, G. B. & Westbrook, J. D. 2011. The RCSB

Protein Data Bank: redesigned web site and web services. *Nucleic Acids Research,* 39**,** D392-D401.

Rypniewski, W. R., Holden, H. M. & Rayment, I. 1993. Structural consequences of reductive methylation of lysine residues in hen egg white lysozyme: X-ray analysis at 1.8-A resolution. *Biochemistry,* 32**,** 9851.

Sabban, S. 2011. *Development of an in vitro model system for studying the interaction of Equus caballus IgE with its high-affinity FcεRI receptor.* Dissertation/Thesis, University of Sheffield.

Sakiyama, T., Tomura, J., Imamura, K. & Nakanishi, K. 2004. Adsorption characteristics of bovine serum albumin and its peptide fragments on a stainless steel surface. *Colloids and Surfaces B: Biointerfaces,* 33**,** 77-84.

Sakiyama, T., Toyomasu, T., Nagata, A., Imamura, K., Nakanishi, K., Takahashi, T. & Nagai, T. 1998. Fouling and cleaning of stainless steel surface: Adsorption and desorption behavior of bovine serum albumin and gelatin. *Journal of Chemical Engineering of Japan,* 31**,** 208-213.

Sanni, O. D., Wagner, M. S., Briggs, D., Castner, D. G. & Vickerman, J. C. 2002. Classification of adsorbed protein static ToF-SIMS spectra by principal component analysis and neural networks. *Surface and Interface Analysis,* 33**,** 715-728.

Sauerbrey, G. 1959. The use of quartz crystals for weighing thin layers and for microweighing. *Journal of Physics,* 155**,** 206-222.

Schatzberg, P. 1967. Molecular diameter of water from solubility and diffusion measurements. *The Journal of Physical Chemistry,* 71**,** 4569-4570.

Schmitt, C., Sanchez, C., Lamprecht, A., Renard, D., Lehr, C.-M., de Kruif, C. G. & Hardy, J. 2001. Study of β-lactoglobulin/acacia gum complex coacervation by diffusing-wave spectroscopy and confocal scanning laser microscopy. *Colloids and Surfaces B: Biointerfaces,* 20**,** 267-280.

Schreiber, A. B. & Haimovich, J. 1983. [9] Quantitative fluorometric assay for detection and characterization of Fc receptors. John J. Langone & Vunakis, H. V. (eds.) *Methods in Enzymology.* Academic Press.

Schreiber, L., Franke, R. & Hartmann, K. 2005. Wax and suberin development of native and wound periderm of potato (*Solanum tuberosum L.*) and its relation to peridermal transpiration. *Planta,* 220**,** 520-530.

Scott, T. & Silversides, F. 2000. The effect of storage and strain of hen on egg quality. *Poultry Science,* 79**,** 1725-1729.

Sever, M. J., Weisser, J. T., Monahan, J., Srinivasan, S. & Wilker, J. J. 2003. Metal-mediated cross-linking in the generation of a marine-mussel adhesive. *Angewandte Chemie,* 116**,** 454-456.

Shen, D., Huang, M., Chow, L.-M. & Yang, M. 2001. Kinetic profile of the adsorption and conformational change of lysozyme on self-assembled monolayers as revealed by quartz crystal resonator. *Sensors and Actuators: B. Chemical,* 77**,** 664-670.

Shi, J., Hedberg, Y., Lundin, M., Odnevall Wallinder, I., Karlsson, H. L. & Möller, L. 2012. Hemolytic properties of synthetic nano- and porous silica particles: The effect of surface properties and the protection by the plasma corona. *Acta Biomaterialia,* 8**,** 3478-3490.

Silverman, H. G. & Roberto, F. F. 2007. Understanding marine mussel adhesion. *Marine biotechnology,* 9**,** 661-681.

Stengel, G., Höök, F. & Knoll, W. 2005a. Viscoelastic modeling of template-directed DNA synthesis. *Anal. Chem.,* 77**,** 3709-3714.

Stengel, G., Höök, F. & Knoll, W. 2005b. Viscoelastic modeling of template-directed DNA synthesis. *Analytical Chemistry,* 77**,** 3709-3714.

Stewart, R. J., Ransom, T. C. & Hlady, V. 2011. Natural underwater adhesives. *Journal of Polymer Science Part B: Polymer Physics,* 49**,** 757-771.

Suci, P. A. & Geesey, G. G. 2001. Comparison of adsorption behavior of two *Mytilus edulis* foot proteins on three surfaces. *Colloids and Surfaces B: Biointerfaces,* 22**,** 159-168.

Suen, S. Y. 1996. A comparison of isotherm and kinetic models for binary-solute adsorption to affinity membranes. *Journal of Chemical Technolnology and Biotechnology,* 65**,** 249-257.

Sun, S., Yue, Y., Huang, X. & Meng, D. 2003. Protein adsorption on blood-contact membranes. *Journal of Membrane Science,* 222**,** 3-18.

Székács, A. 2009. Optical waveguide light-mode spectroscopy immunosensors for environmental monitoring. *Applied Optics,* 48**,** B151-B158.

Taniguchi, N. Amino Acids and Proteins. John, W. B. A. & Marek, H. D. (eds.) *Medical Biochemistry.* Elsevier.

Taylor, S. W. 2002. Chemoenzymatic synthesis of peptidyl 3,4-dihydroxyphenylalanine for structure–activity relationships in marine invertebrate polypeptides. *Analytical Biochemistry,* 302**,** 70-74.

Tiefenthaler, K. & Lukosz, W. 1989. Sensitivity of grating couplers as integrated-optical chemical sensors. *Journal of the Optical Society of America B,* 6**,** 209-220.

Trudeau, T. G. & Hore, D. K. 2010. Hydrophobic amino acid adsorption on surfaces of varying wettability. *Langmuir : the ACS journal of surfaces and colloids,* 26**,** 11095-11102.

Tyn, M. T. & Gusek, T. W. 1990. Prediction of diffusion coefficients of proteins. *Biotechnology and Bioengineering,* 35**,** 327-338.

Umpleby II, R. J., Baxter, S. C., Bode, M., Berch Jr, J. K., Shah, R. N. & Shimizu, K. D. 2001. Application of the freundlich adsorption isotherm in the characterization of molecularly imprinted polymers. *Analytica Chimica Acta,* 435**,** 35-42.

Visser, J. & Jeurnink, T. J. M. 1997. Fouling of heat exchangers in the dairy industry. *Experimental Thermal and Fluid Science,* 14**,** 407-424.

Voigt, D. & Gorb, S. 2008. An insect trap as habitat: cohesion-failure mechanism prevents adhesion of *Pameridea roridulae* bugs to the sticky surface of the plant Roridula gorgonias. *Journal of Experimental Biology,* 211**,** 2647-2657.

Vörös, J. 2004. The density and refractive index of adsorbing protein layers. *Biophysical journal,* 87**,** 553-561.

Wahlgren, M. & Arnebrant, T. 1991. Protein adsorption to solid surfaces. *Trends in Biotechnology,* 9**,** 201-208.

Waite, J. H. 1976. Calculating extinction coefficients for enzymatically produced o-quinones. *Analytical Biochemistry,* 75**,** 211-218.

Waite, J. H., Andersen, N. H., Jewhurst, S. & Sun, C. 2005. Mussel adhesion: finding the tricks worth mimicking. *The Journal of Adhesion,* 81**,** 297-317.

Waite, J. H., Housley, T. J. & Tanzer, M. L. 1985. Peptide repeats in a mussel glue protein: theme and variations. *Biochemistry,* 24**,** 5010-5014.

Waite, J. H. & Tanzer, M. L. 1981. Polyphenolic substance of *Mytilus edulis*: Novel adhesive containing L-dopa and hydroxyproline. *Science,* 212**,** 1038-1040.

Waugh, A. & Grant, A. 2010. *Ross and Wilson Anatomy and Physiology in Health and Illness (paperback),* Elsevier Health Sciences.

Wiegemann, M. 2005. Adhesion in blue mussels (*Mytilus edulis*) and barnacles (genus *Balanus*): Mechanisms and technical applications. *Aquatic Sciences,* 67**,** 166-176.

Wilke, P. & Börner, H. G. 2012. Mussel-glue derived peptide–polymer conjugates to realize enzyme-activated antifouling coatings. *American Chemical Society Macro Letters,* 1**,** 871-875.

Wright, A. K. & Thompson, M. R. 1975. Hydrodynamic structure of bovine serum albumin determined by transient electric birefringence. *Biophysical Journal,* 15**,** 137-141.

Wu, J. 2004. *Modeling adsorption of organic compounds on activated carbon: A multivariate approach.* Dissertation/Thesis, Umeå University.

Xu, D.-Y., Chen, J.-Y. & Yang, Z. 2012. Use of cross-linked tyrosinase aggregates as catalyst for synthesis of L-DOPA. *Biochemical Engineering Journal,* 63**,** 88-94.

Yang, H. & Etzel, M. R. 2003. Evaluation of three kinetic equations in models of protein purification using ion-exchange membranes. *Industrial and Engineering Chemistry Research,* 42**,** 890-896.

Yeung, A., Glahn, R. & Miller, D. 2002. Effects of iron source on iron availability from casein and casein phosphopeptides. *Journal of Food Science,* 67**,** 1271-1275.

Yu, H., Eggleston, C. M., Chen, J., Wang, W., Dai, Q. & Tang, J. 2012. Optical waveguide lightmode spectroscopy (OWLS) as a sensor for thin film and quantum dot corrosion. *Sensors,* 12**,** 17330-17342.

Yu, M., Hwang, J. & Deming, T. J. 1999. Role of L-3, 4-dihydroxyphenylalanine in mussel adhesive proteins. *Journal of the American Chemical Society,* 121**,** 5825-5826.

Zou, Q., Leang, K. K., Sadoun, E., Reed, M. J. & Devasia, S. 2004. Control issues in high-speed AFM for biological applications: Collagen imaging example. *Asian Journal of Control,* 6**,** 164-178.

Appendices

Appendix I: QCM-D raw data

Voigt and Sauerbrey mass analysis

This appendix presents the QCM-D raw data analysis.

The masses calculated with the Voigt model (using different overtones) during the initial adsorption on the sensor surface for β-lactoglobulin and haemoglobin are given in Fig A-1 and Fig A-2, respectively. The shear analysis for β-lactoglobulin is given in Fig. A-3.

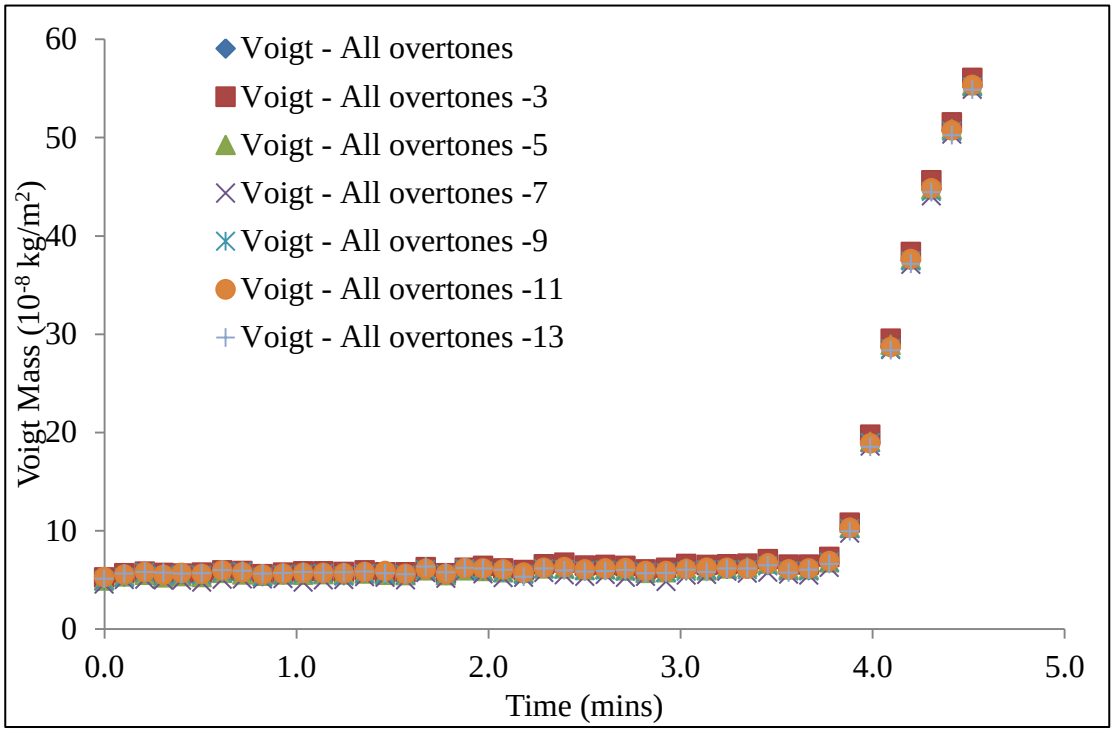

Figure 0-1: Voigt mass analysis for β-lactoglobulin for the first 5 minutes

Figure A-2 represents the Voigt mass for haemoglobin (different overtones) for the first 5 minutes to observe the change in mass that occurred immediately on the surface of the sensor.

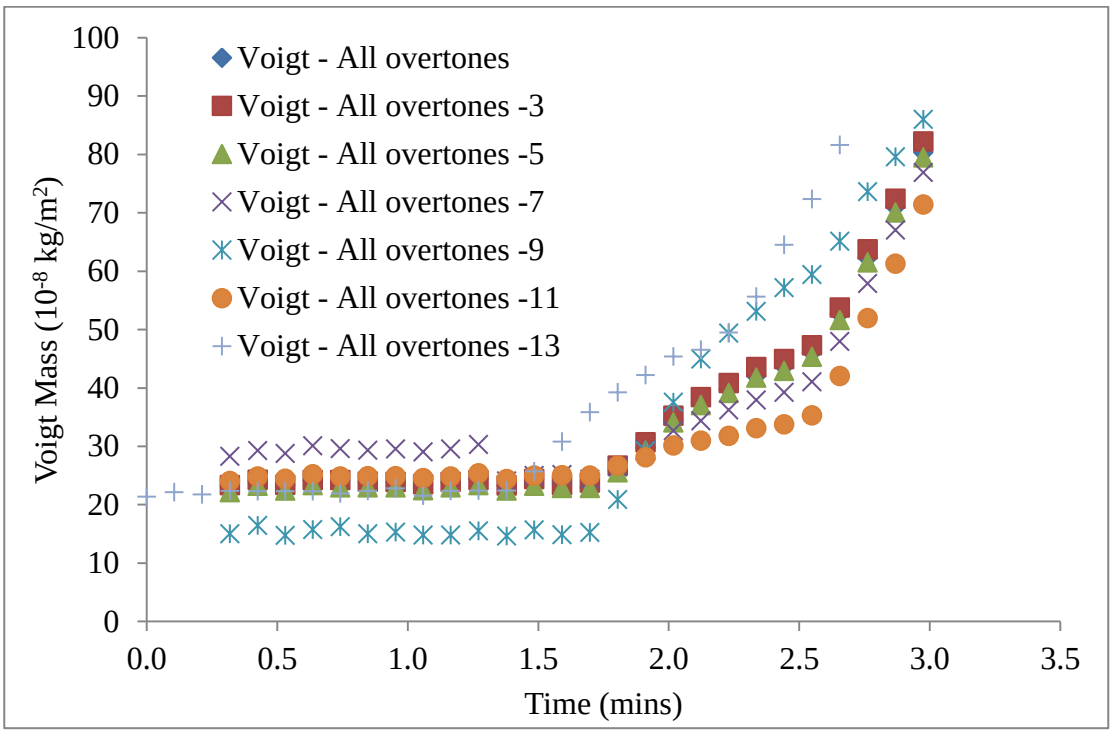

Figure 0-2: Voigt mass analysis for haemoglobin for the first 3 minutes

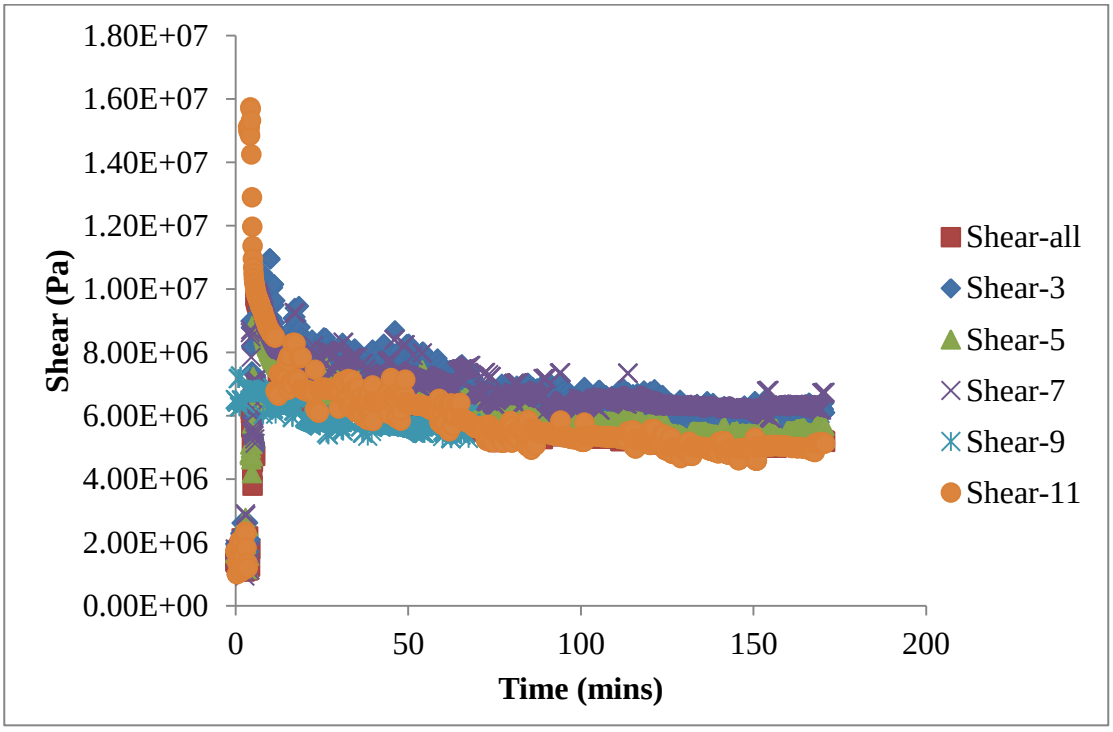

Figure 0-3: Shear analysis for 0.1 mg/mL β-lactoglobulin

The Sauerbrey mass for β-casein at different concentrations tested are predicted in Figs. A-4 – A-9. The mass adsorbed after insulin has been modified with tyrosinase is given in Fig. A-10. Fig A-11 shows the adsorption of myoglobin, taking around 4.5 hours to reach 80% adsorption of the protein on the surface.

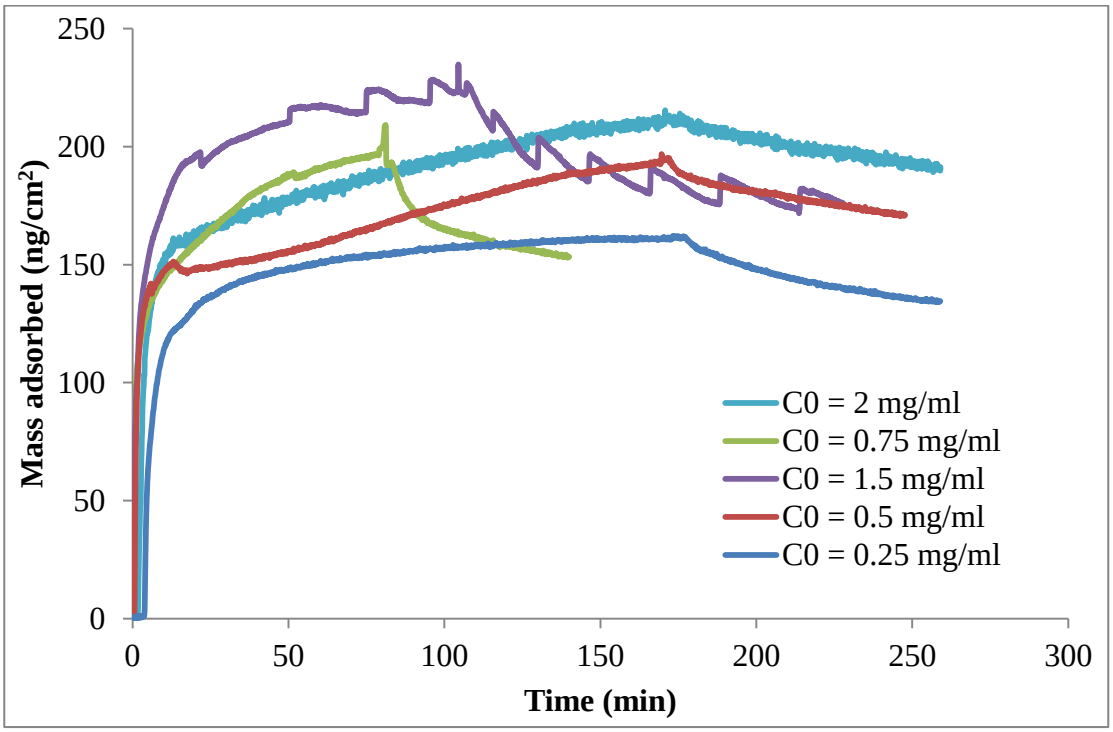

Figure 0-4: Effect of initial β-casein solution concentration on mass adsorbed to SS 316

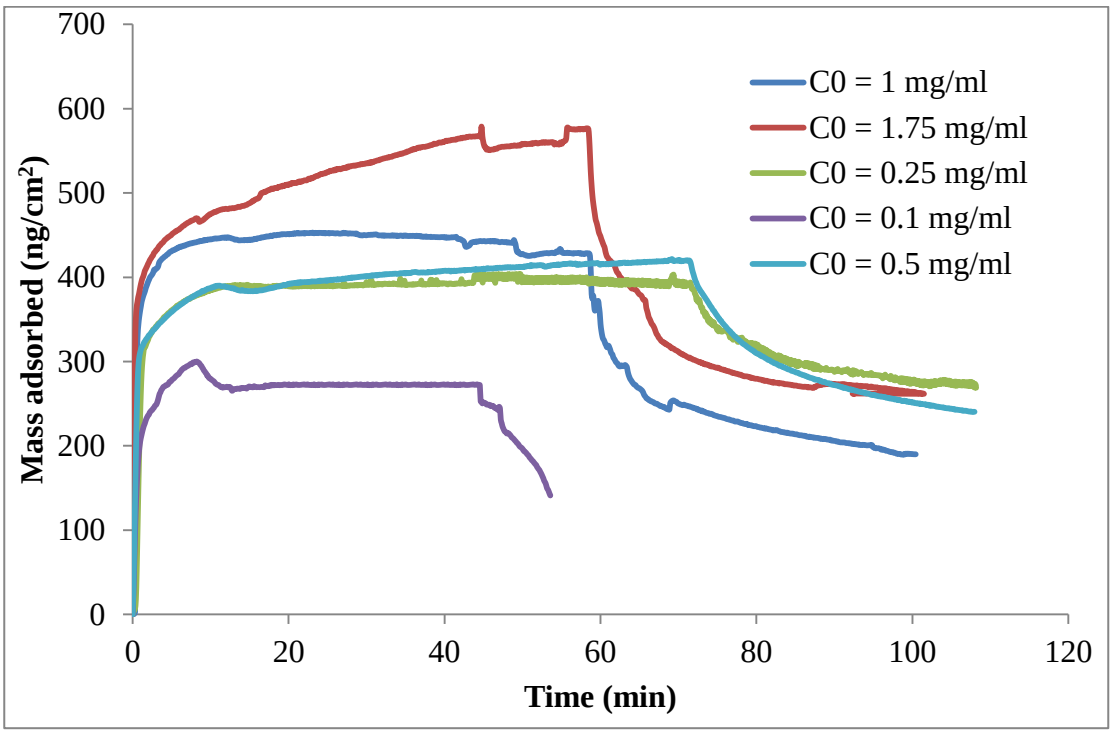

Figure 0-5: Effect of initial α-chymotrypsinogen solution concentration on mass adsorbed to SS 316

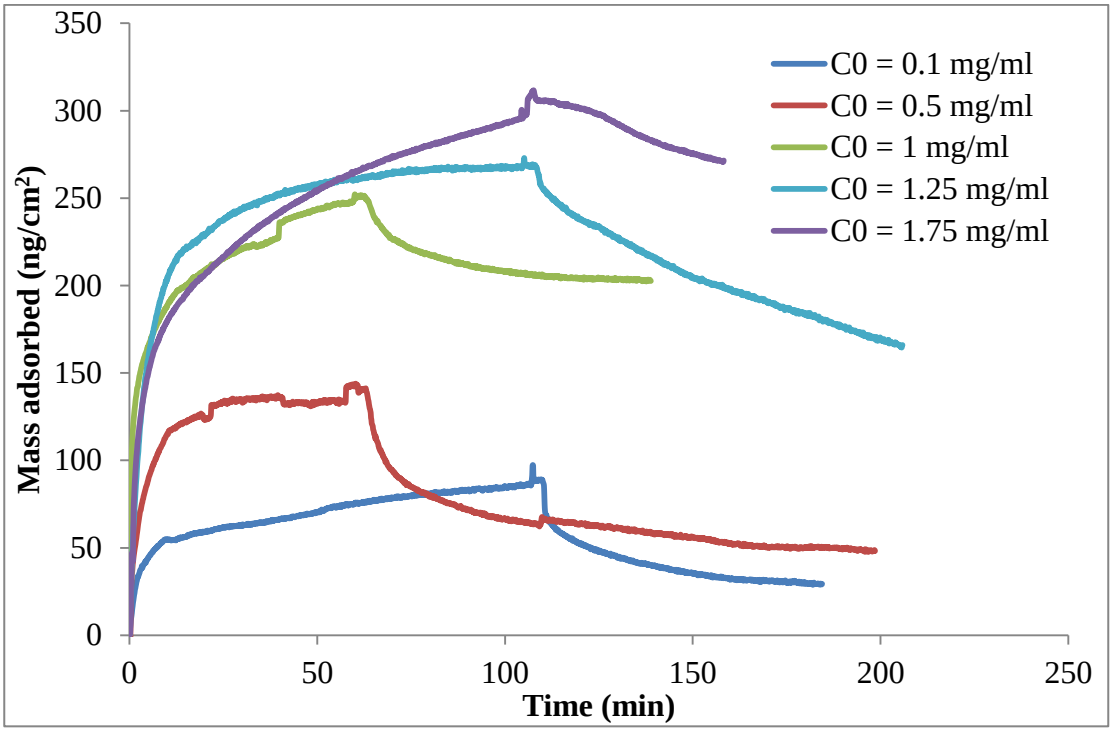

Figure 0-6: Effect of initial α-lactalbumin solution concentration on mass adsorbed to SS 316

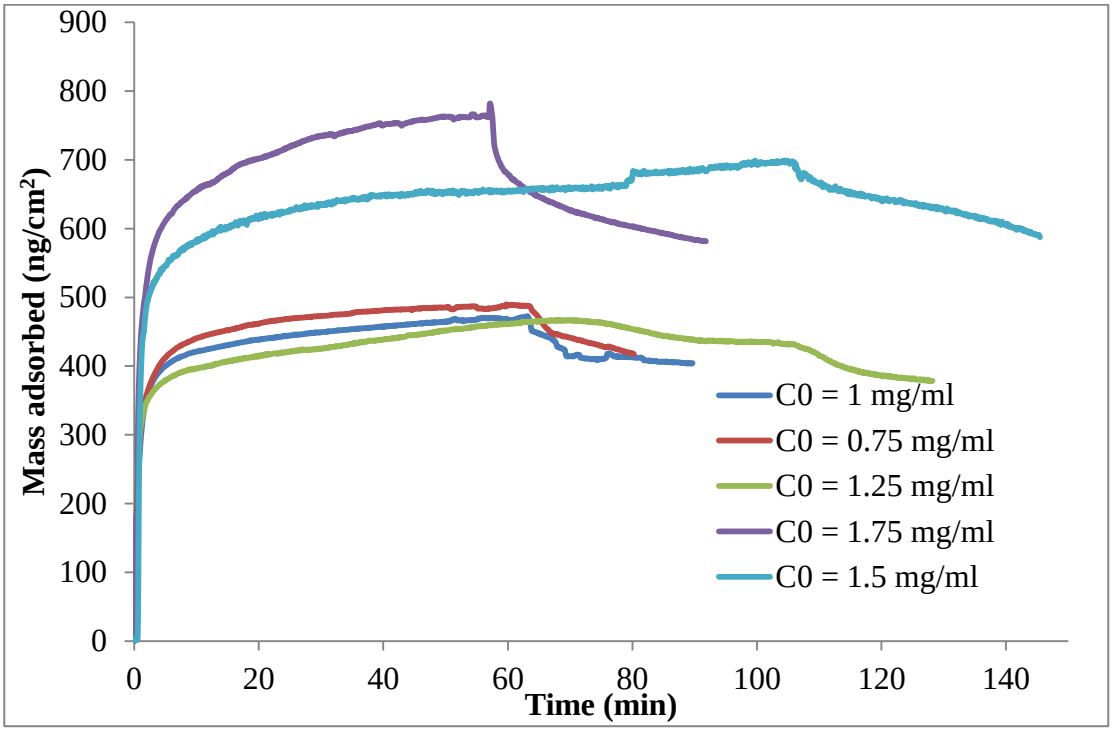

Figure 0-7: Effect of nitial α-casein solution concentration on mass adsorbed to SS 316

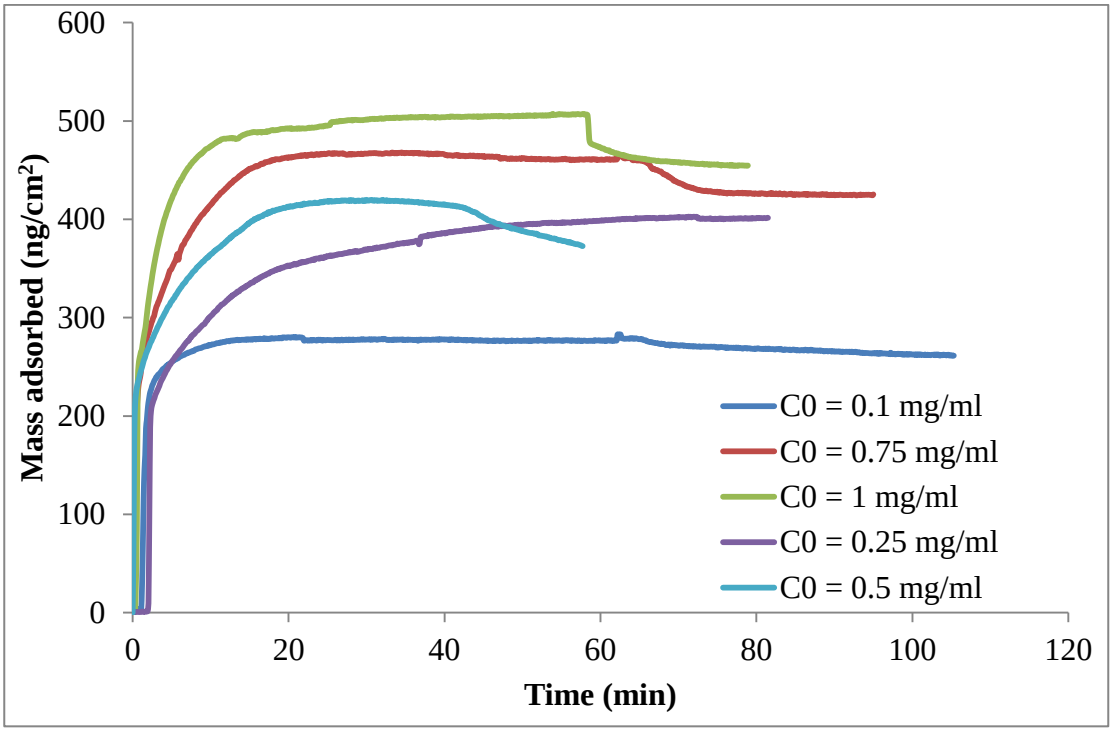

Figure 0-8: Effect of initial lysozyme solution concentration on mass adsorbed to SS 316

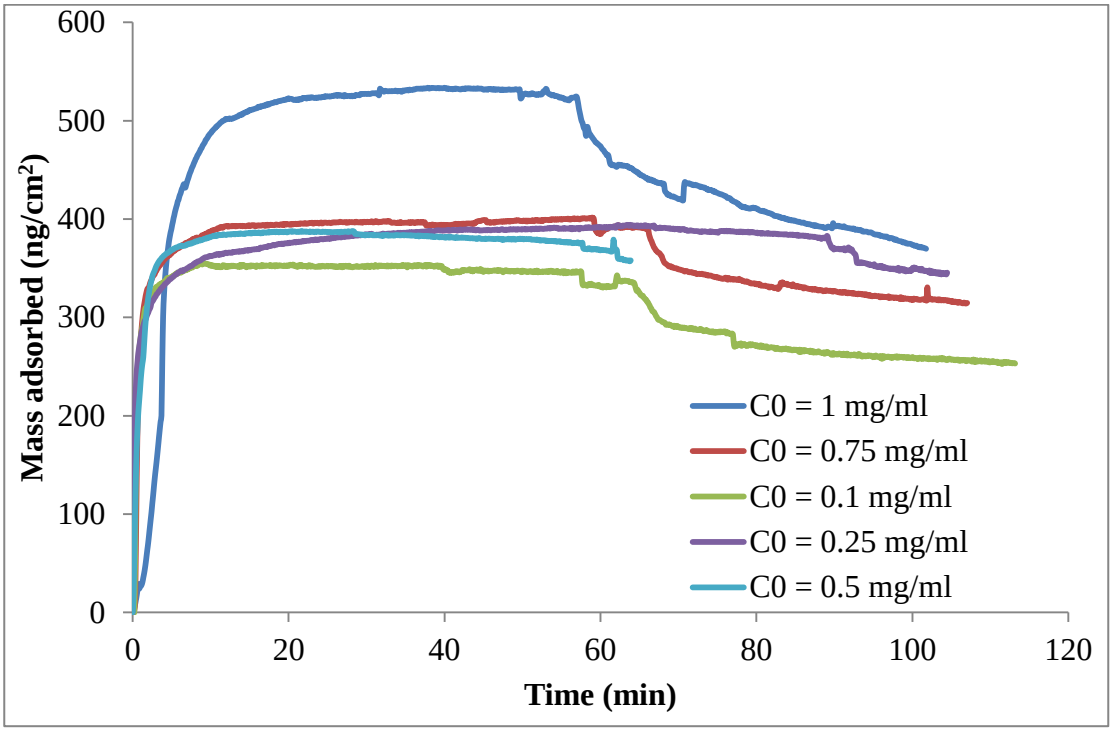

Figure 0-9: Effect of initial haemoglobin solution concentration on mass adsorbed to SS 316

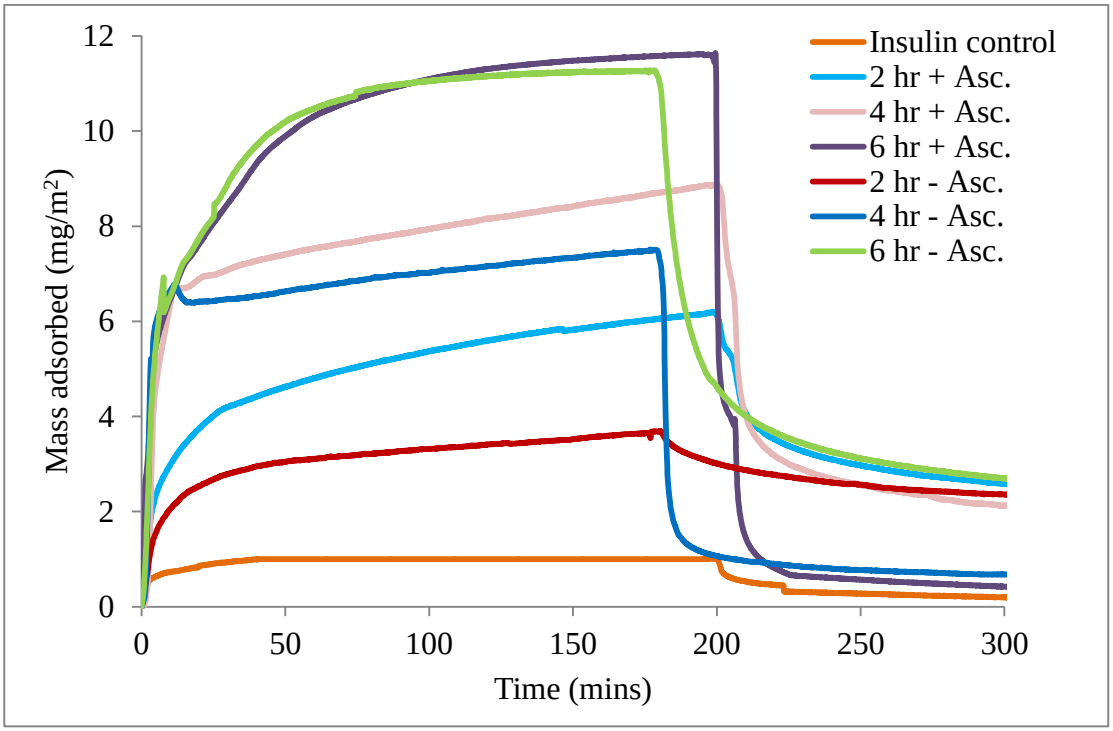

Figure 0-10: Effect of initial human recombinant insulin solution concentration on Sauerbrey mass adsorbed to SS 316

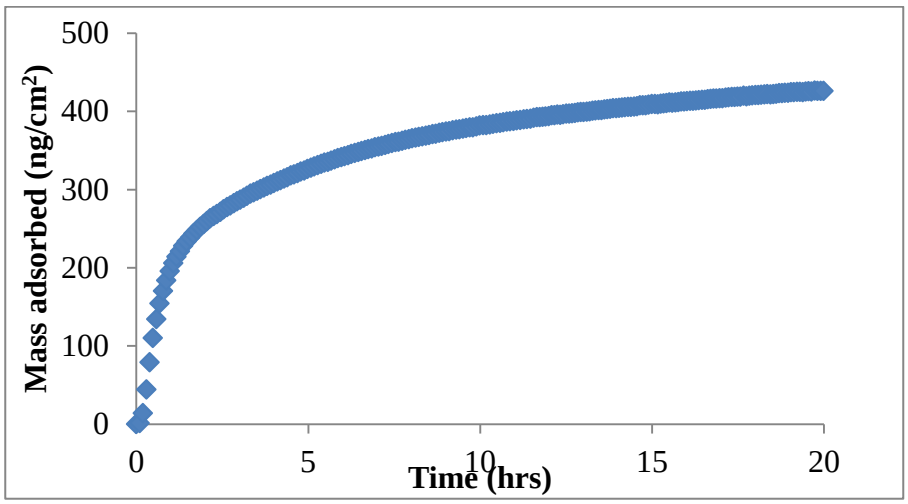

Figure 0-11: Sauerbrey mass for myoglobin at 1 mg/mL adsorbed to SS 316

Table A-1 represents the dimensional ratio for the test proteins at overtone 3 (n=3) and the choice of model for determining the mass adsorbed on SS.

Table 0-1: Effect of protein concentration on frequency, dissipation and dimensional ratio at overtone 3 (n =3).

Protein	Conc. (mg/ml)	Frequency (Hz)	Dissipation (*1E-6)	ΔD/(-Δf/n) (*1E-6)	Rheology of layer	Model used
Haemoglobin	0.10	23	0.8	0.104	Rigid	Sauerbrey
	0.25	22	0.4	0.055	Rigid	Sauerbrey
	0.50	24	1.2	0.150	Rigid	Sauerbrey
	0.75	28	0.2	0.021	Rigid	Sauerbrey
	1.00	28	0.4	0.043	Rigid	Sauerbrey
	1.50	36	1.6	0.133	Rigid	Sauerbrey
	2.00	34	3.4	0.300	Rigid	Sauerbrey
β- lactoglobin	0.10	8	0.5	0.188	Rigid	Sauerbrey
	0.25	10	0.7	0.210	Rigid	Sauerbrey
	0.50	10	0.2	0.060	Rigid	Sauerbrey
	0.75	12	0.4	0.100	Rigid	Sauerbrey
	1.00	14	0.5	0.107	Rigid	Sauerbrey
	1.50	11	0.5	0.136	Rigid	Sauerbrey
	2.00	15	0.8	0.160	Rigid	Sauerbrey
β- caesin	0.10	13.5	0.2	0.044	Rigid	Sauerbrey
	0.25	17	0.9	0.159	Rigid	Sauerbrey
	0.50	24	1.8	0.225	Rigid	Sauerbrey
	0.75	30	2.2	0.220	Rigid	Sauerbrey
	1.00	44	3.2	0.218	Rigid	Sauerbrey
	1.50	48	2.7	0.169	Rigid	Sauerbrey
	2.00	60	2.8	0.140	Rigid	Sauerbrey
Lysozyme	0.10	16	1.5	0.281	Rigid	Sauerbrey
	0.25	18	0.6	0.100	Rigid	Sauerbrey
	0.50	23	0.5	0.065	Rigid	Sauerbrey
	0.75	26	0.1	0.012	Rigid	Sauerbrey
	1.00	24	0.8	0.100	Rigid	Sauerbrey
	1.50	25	0.6	0.072	Rigid	Sauerbrey
	2.00	24	0.6	0.075	Rigid	Sauerbrey

α- chymotrypsin	0.10	16	0.5	0.094	Rigid	Sauerbrey
	0.25	20	2	0.300	Rigid	Sauerbrey
	0.50	22	0.7	0.095	Rigid	Sauerbrey
	0.75	23	1.5	0.196	Rigid	Sauerbrey
	1.00	25	0.8	0.096	Rigid	Sauerbrey
	1.50	24	0.3	0.038	Rigid	Sauerbrey
	2.00	34	2.4	0.212	Rigid	Sauerbrey
α- lactalbumin	0.10	7	1.3	0.557	Non Rigid	Voigt
	0.25	5	0.5	0.300	Rigid	Sauerbrey
	0.50	13	1	0.231	Rigid	Sauerbrey
	0.75	16	0.5	0.094	Rigid	Sauerbrey
	1.00	14	0.7	0.150	Rigid	Sauerbrey
	1.50	14	1.5	0.321	Rigid	Sauerbrey
	2.00	19	1.4	0.221	Rigid	Sauerbrey
α- caesin	0.10	22	0.5	0.068	Rigid	Sauerbrey
	0.25	24	5	0.625	Non Rigid	Voigt
	0.50	32	4	0.375	Rigid	Sauerbrey
	0.75	29	1.4	0.145	Rigid	Sauerbrey
	1.00	34	1.8	0.159	Rigid	Sauerbrey
	1.50	48	2.7	0.169	Rigid	Sauerbrey
	2.00	36	2	0.167	Rigid	Sauerbrey
BSA	0.10	12.5	1	0.240	Rigid	Sauerbrey
	0.25	13	0.8	0.185	Rigid	Sauerbrey
	0.50	20	0.8	0.120	Rigid	Sauerbrey
	0.75	30	1	0.100	Rigid	Sauerbrey
	1.00	30	1	0.100	Rigid	Sauerbrey
	1.50	30	2.2	0.220	Rigid	Sauerbrey
	2.00	30	2.2	0.220	Rigid	Sauerbrey
Myoglobin	0.10	26	0.8	0.092	Rigid	Sauerbrey
	0.25	26	1	0.115	Rigid	Sauerbrey
	0.50	65	12	0.554	Non Rigid	Voigt
	0.75	32	3.2	0.300	Rigid	Sauerbrey
	1.00	75	10.5	0.420	Non Rigid	Voigt
	1.50	32	3.2	0.300	Rigid	Sauerbrey
	2.00	90	11.5	0.383	Rigid	Sauerbrey

Isotherms & Kinetic Modeling

The adsorption isotherms and Conformational Change modelling for the various test proteins are presented in Figs. A-11 – A-30.

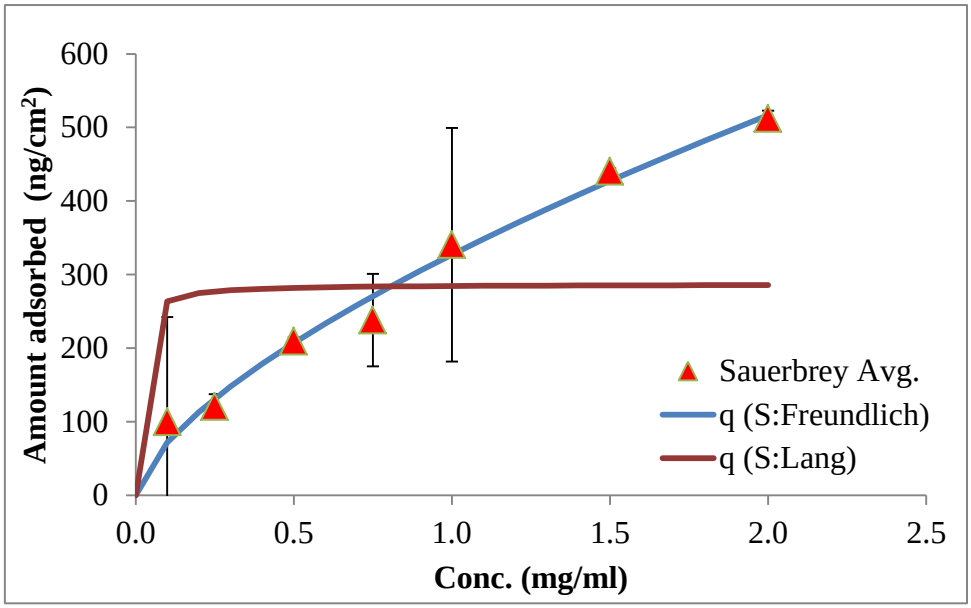

Figure 0-12: Langmuir and Freundlich model isotherms for BSA adsorption

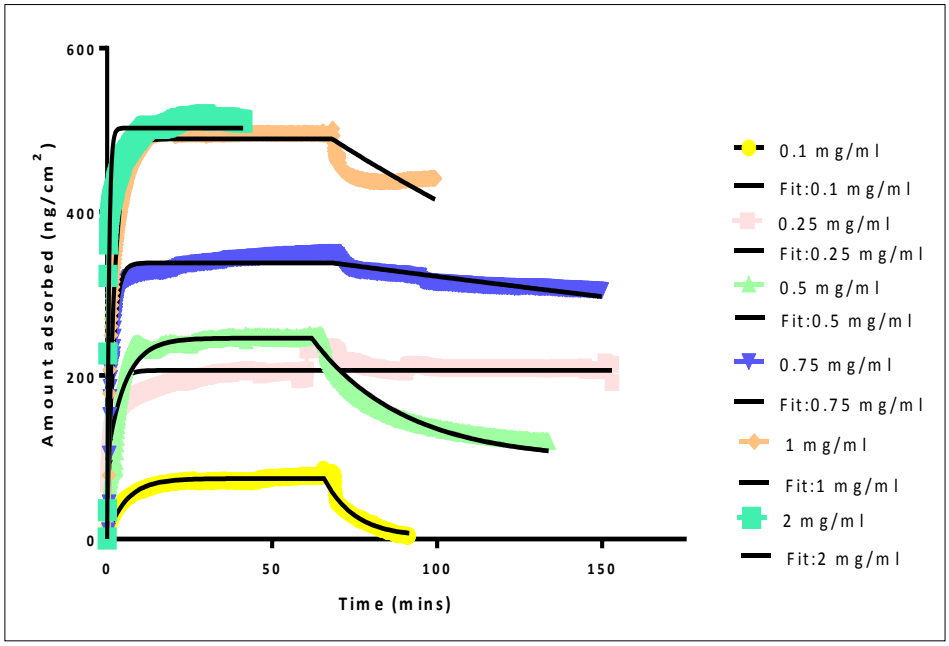

Figure 0-13: Effect of BSA concentration in Conformational Change model kinetics

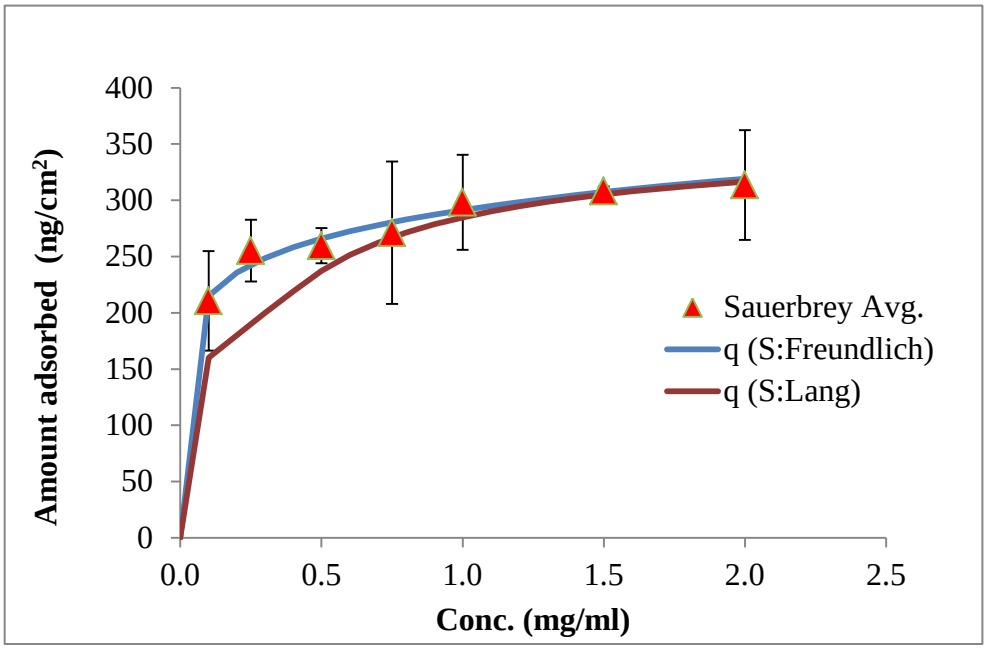

Figure 0-14: Langmuir and Freundlich model isotherms for lysozyme adsorption

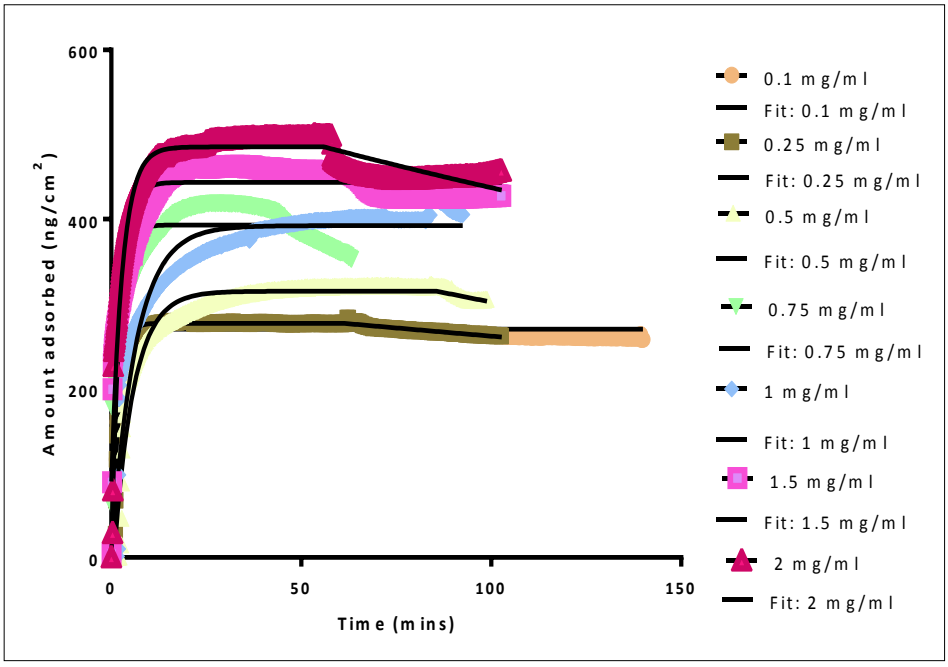

Figure 0-15: Effect of lysozyme concentration in Conformational Change model kinetics

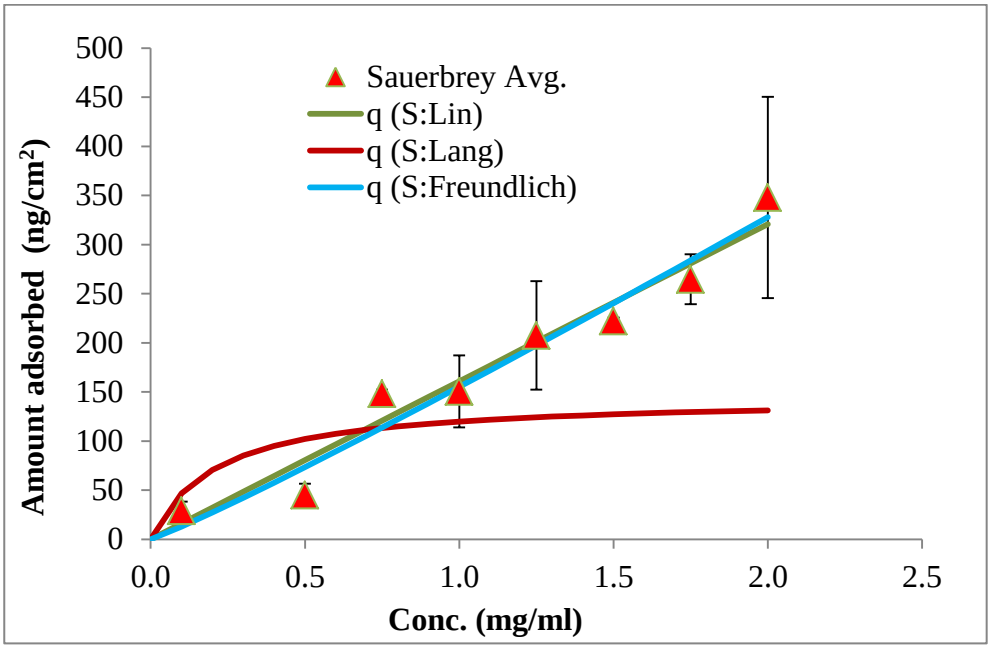

Figure 0-16: Langmuir and Freundlich model isotherms for α-lactalbumin adsorption

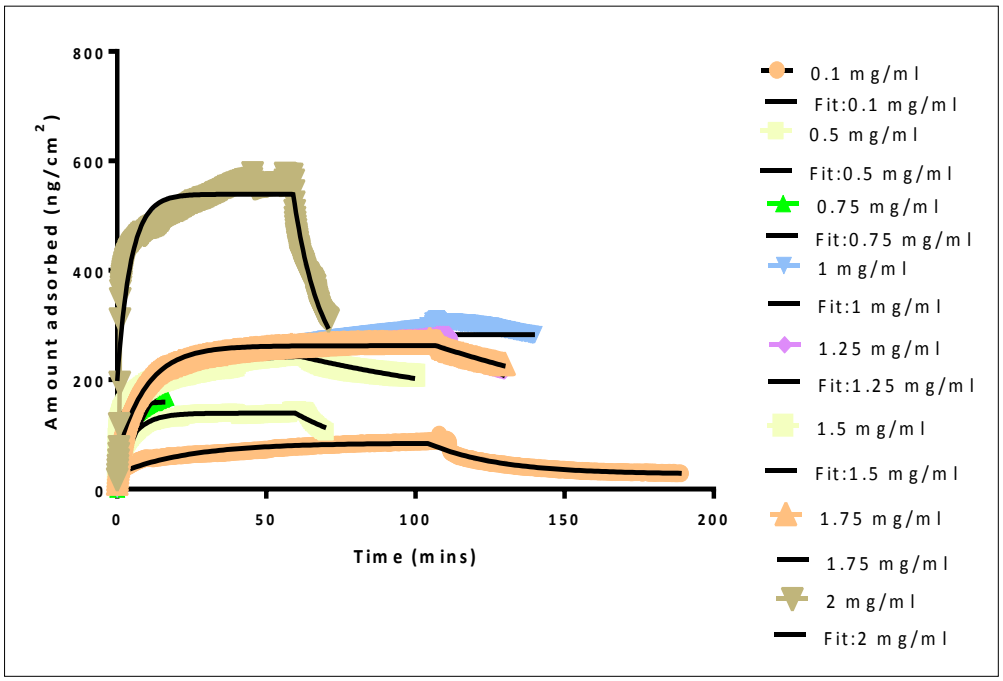

Figure 0-17: Effect of α-lactalbumin concentration in Conformational Change model kinetics

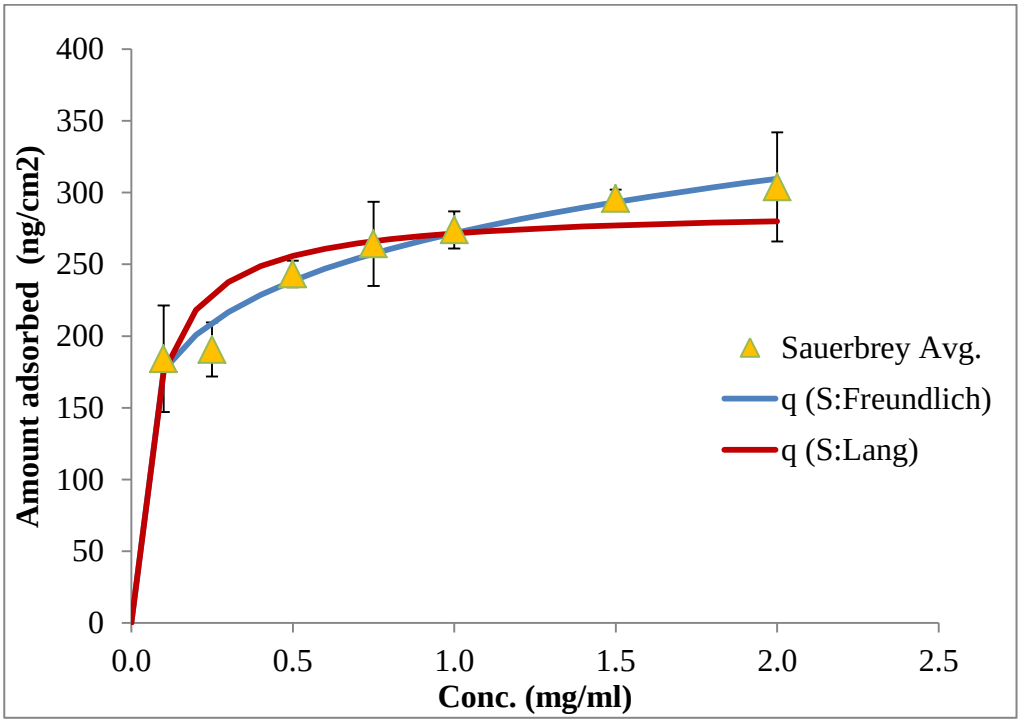

Figure 0-18: Langmuir and Freundlich model isotherms α-chymotrypsinogen adsorption

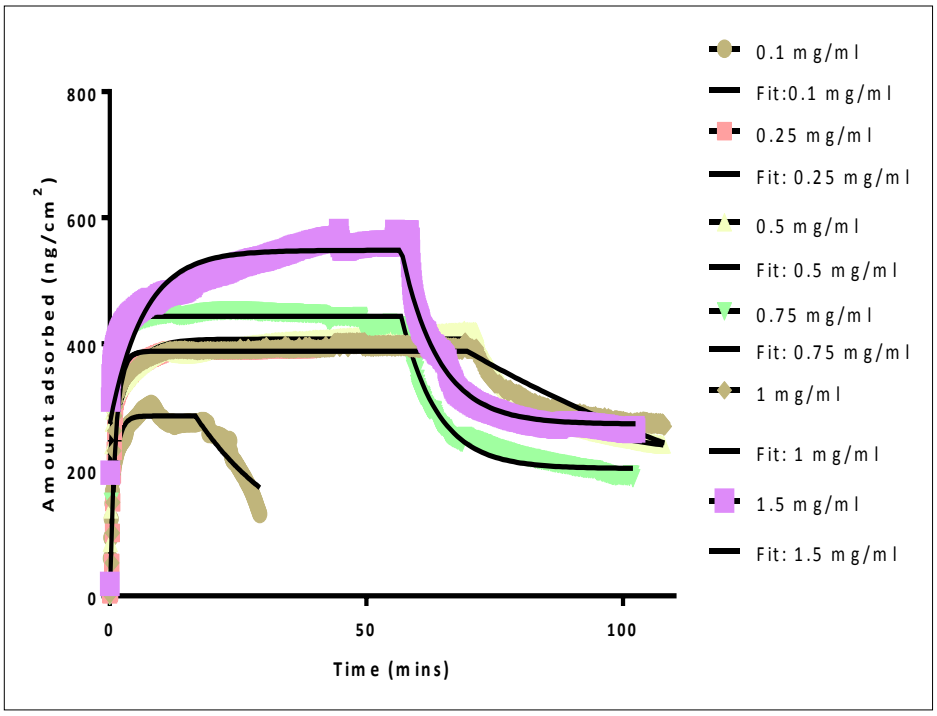

Figure 0-19: Effect of α- chymotrypsinogen concentration in Conformational Change model kinetics

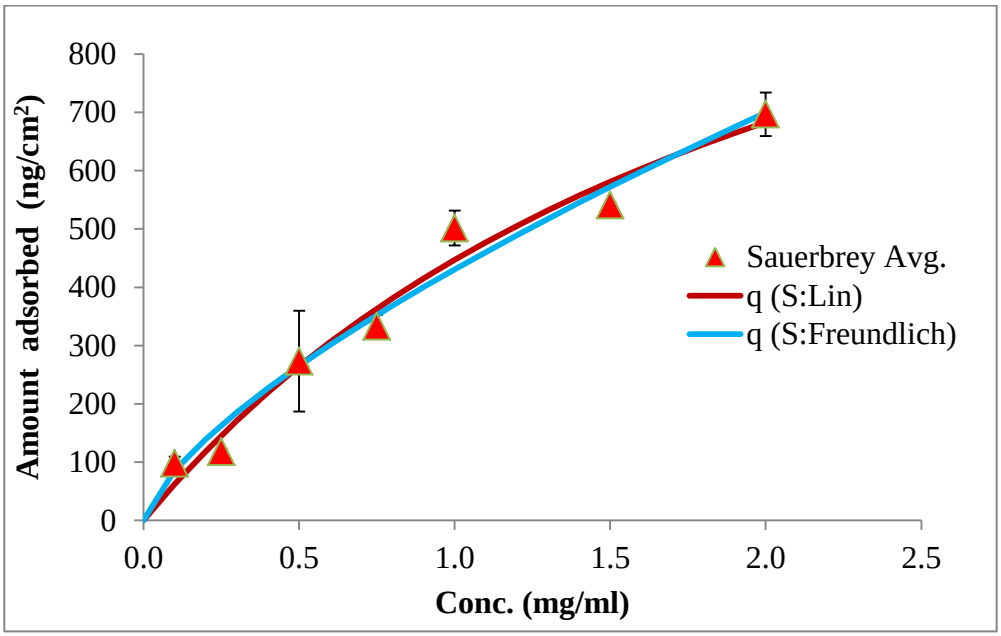

Figure 0-20: Langmuir and Freundlich model isotherms for β-casein adsorption

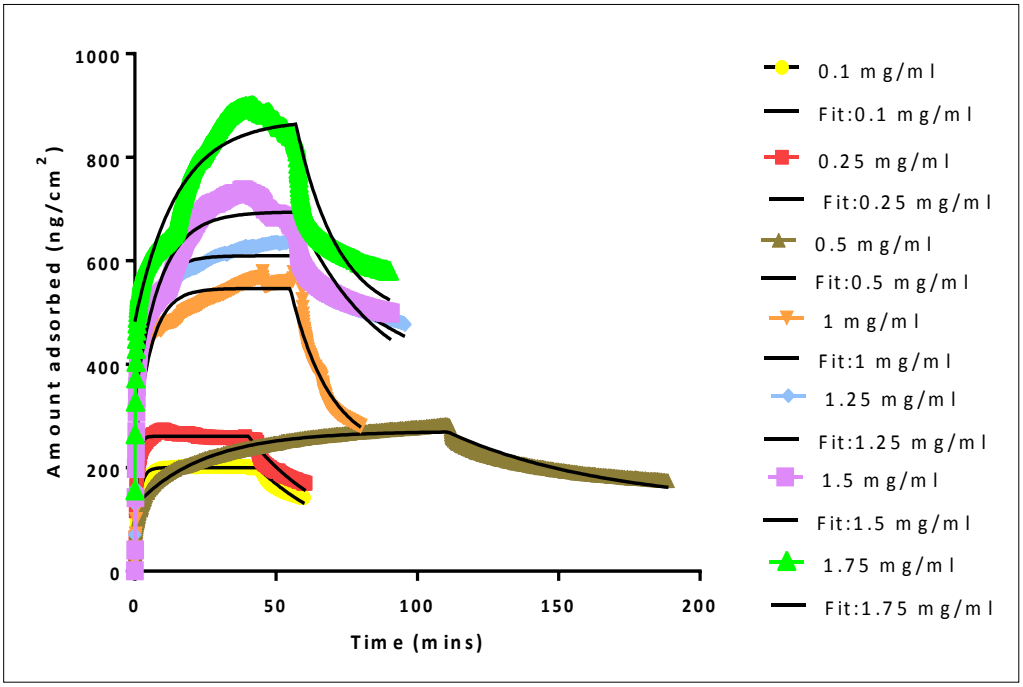

Figure 0-21: Effect of β-casein concentration in Conformational Change model kinetics

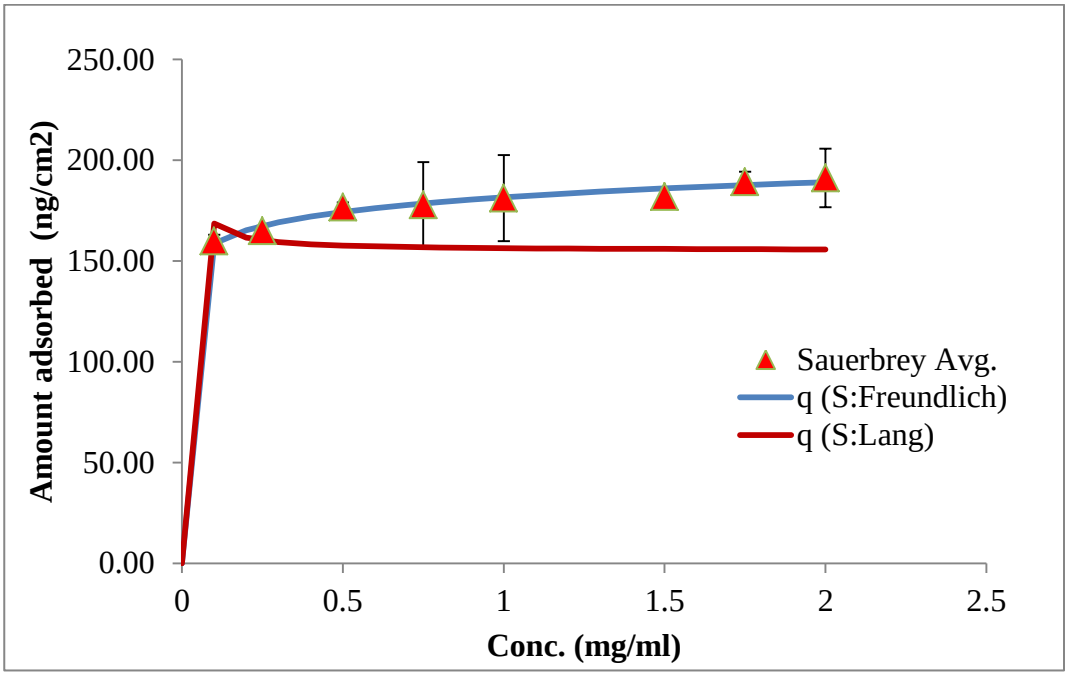

Figure 0-22: Langmuir and Freundlich model isotherms for β-lactoglobulin adsorption

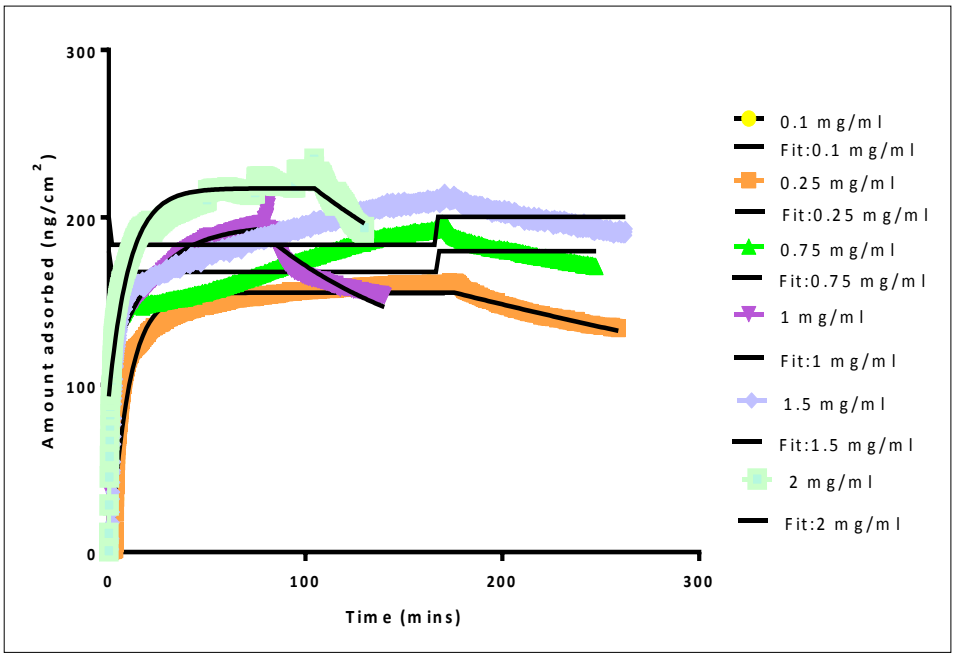

Figure 0-23: Effect of β- lactoglobulin concentration in Conformational Change model kinetics

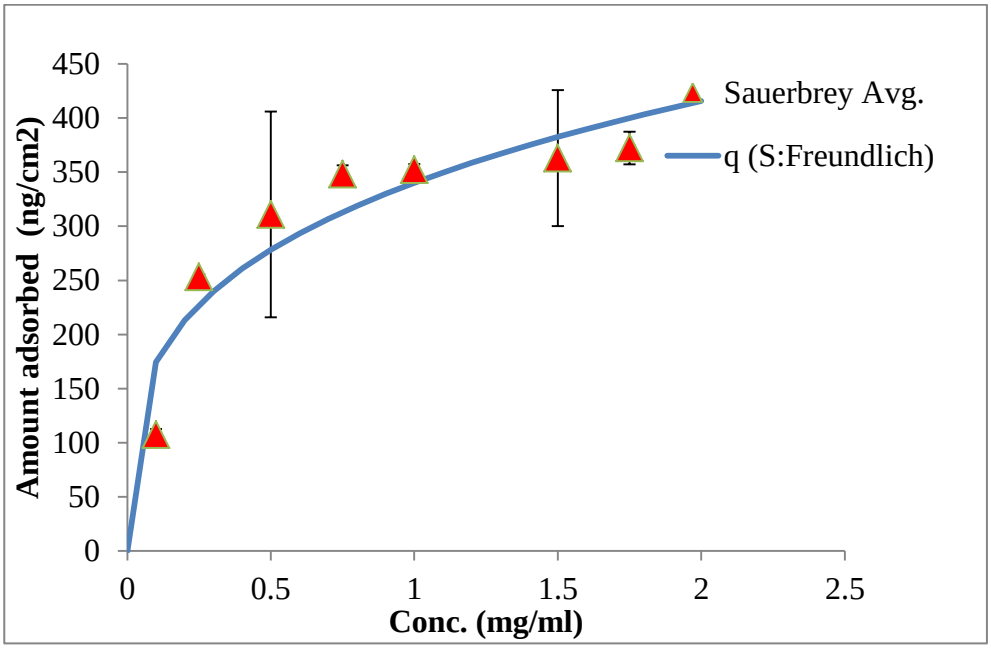

Figure 0-24: Langmuir and Freundlich model isotherms for haemoglobin adsorption

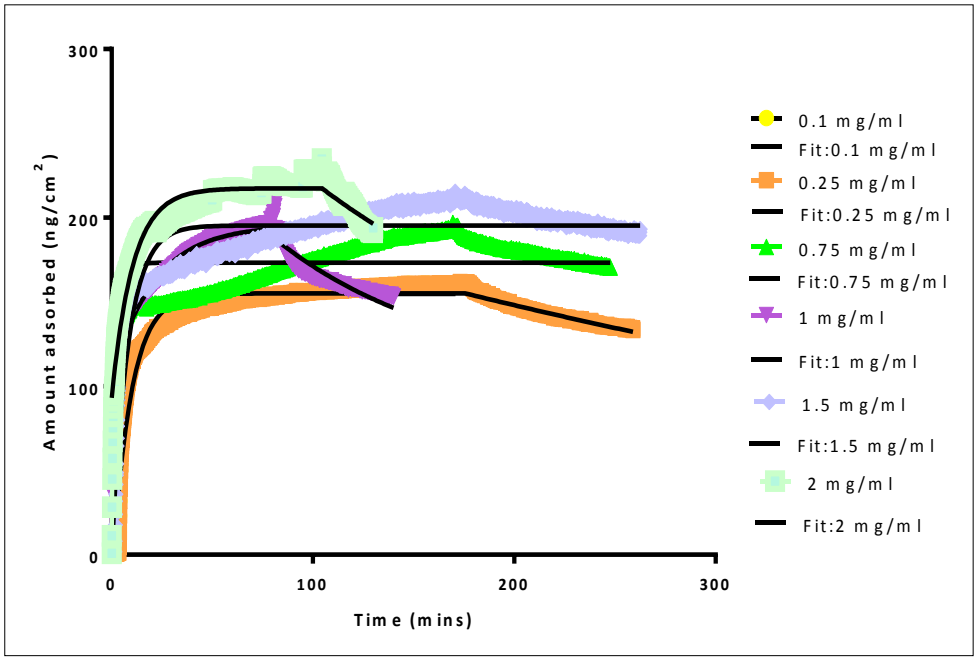

Figure 0-25: Effect of haemoglobin concentration in Conformational Change model kinetics

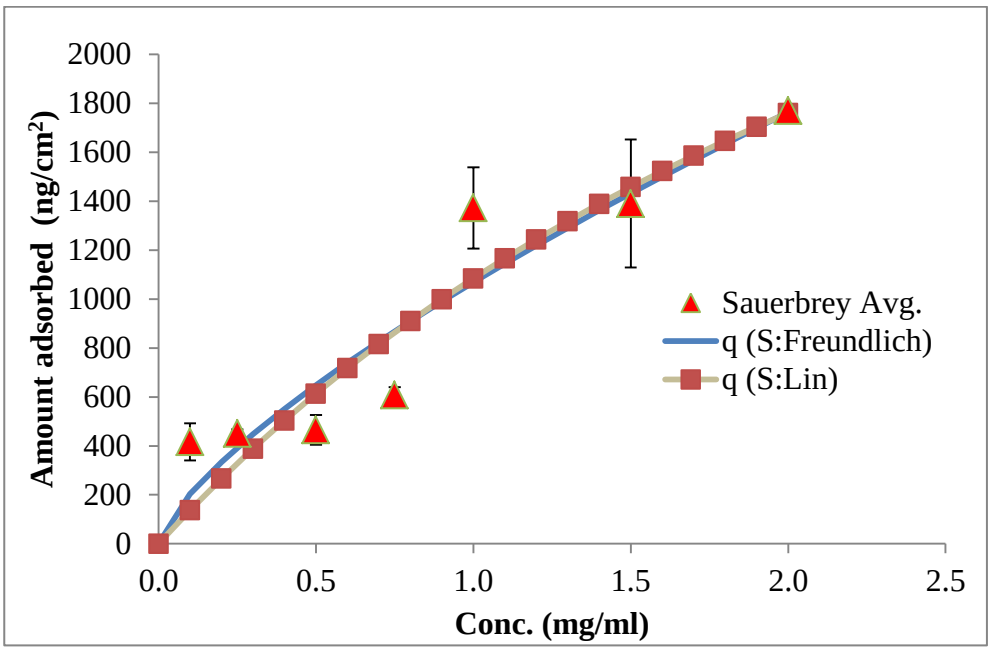

Figure 0-26: Langmuir and Freundlich model isotherms for myoglobin adsorption

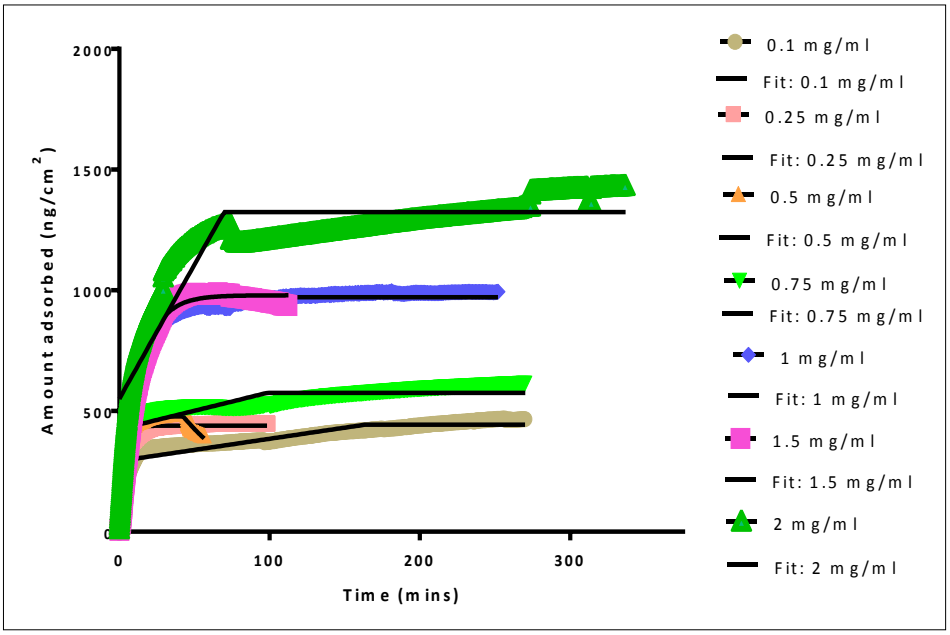

Figure 0-27: Effect of myoglobin concentration in Conformational Change model kinetics

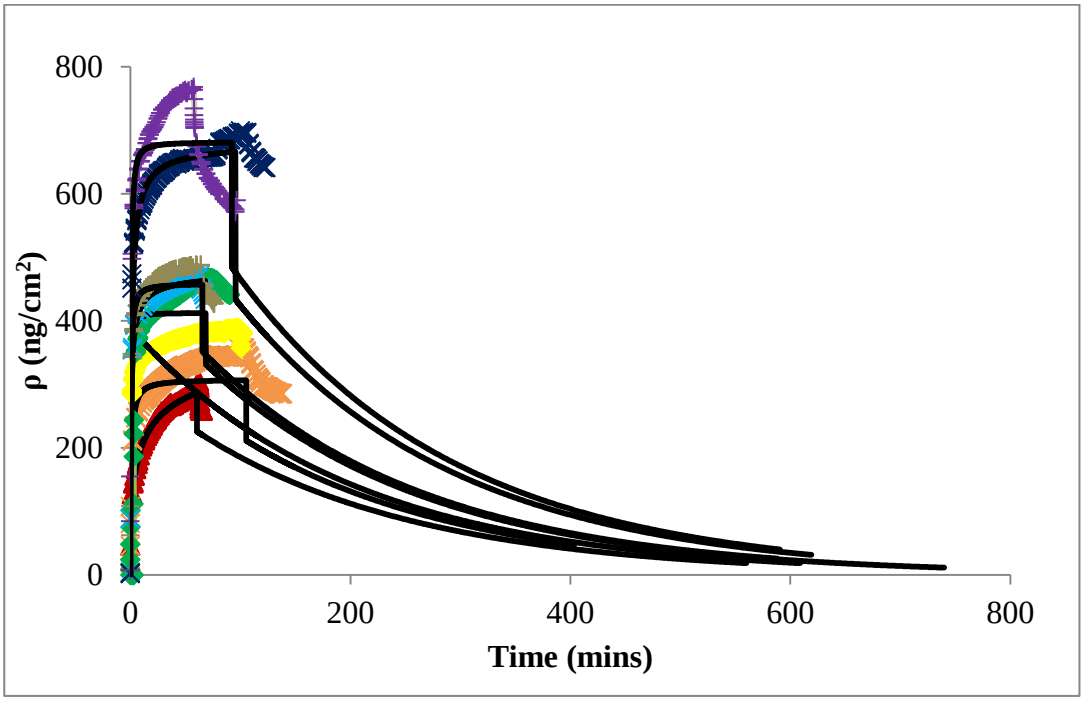

Figure 0-28: Effect of α – casein concentrations in Langmuir model kinetics

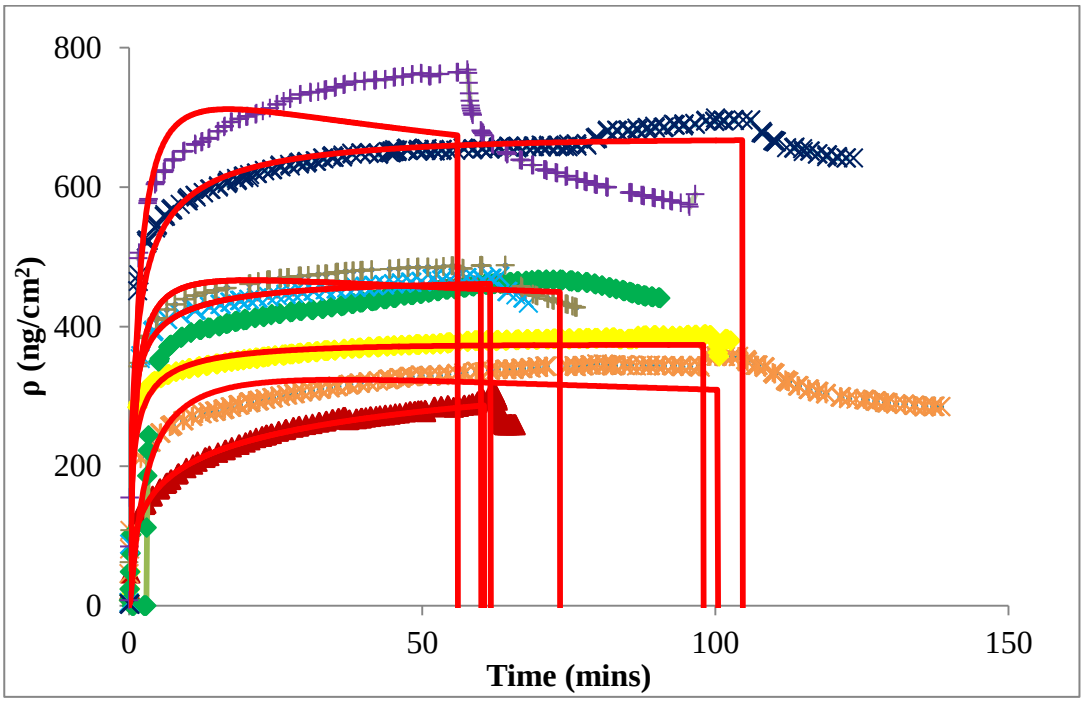

Figure 0-29: Effect of α – casein concentrations on Freundlich kinetic models

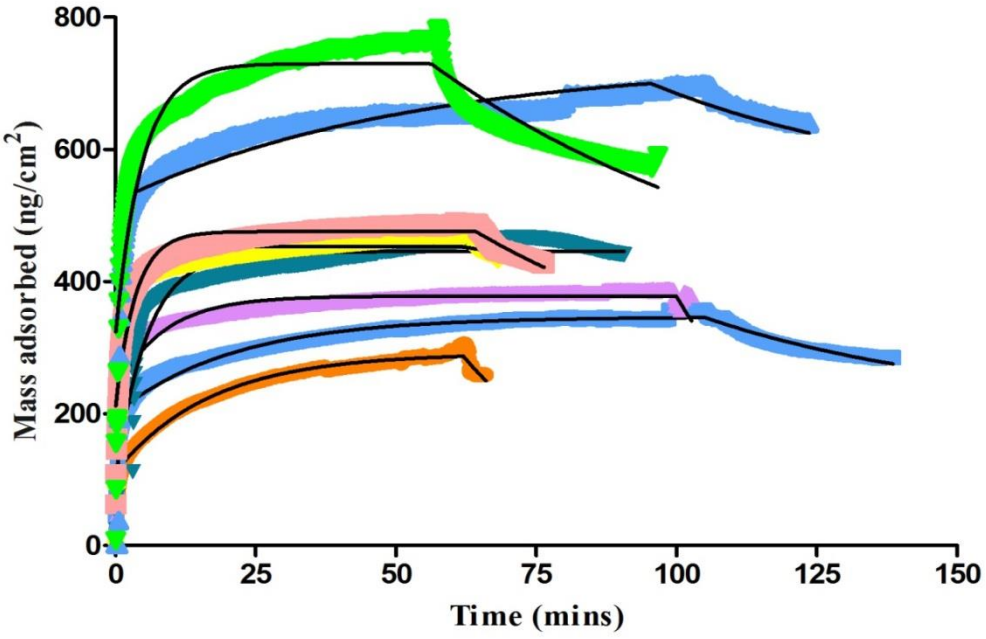

Figure 0-30: Effect of α-casein concentration on the Conformational Change model kinetics

Table 0-2: Adsorption/desorption rate constants obtained for five test proteins by fitting the experimental data with the Langmuir and Freundlich kinetic models

Test Proteins	**Langmuir**			**Freundlich**			
	k_a	**K_D**	**R^2**	**k_a**	**K_D**	**α**	**R^2**
	(1/Ms)	**(M)**		**(1/Ms)**	**(M)**		
BSA	2.0E-03	6.0E-02	0.78	2.0E-3	8.1E-02	0.33	0.88
β-lactoglobulin	3.0E-02	1.3E-02	0.89	4.0E-2	1.0E-02	0.21	0.91
α-lactalbumin	2.2E-02	1.6E-02	0.71	1.2E-2	2.7E-02	0.21	0.79
α- casein	7.0E-02	7.1E-02	0.88	5.0E-2	9.0E-02	0.25	0.87
β-casein	1.6E-01	1.5E-02	0.55	1.5E-1	1.5E-02	0.38	0.52

Table 0-3: Adsorption/desorption rate constants obtained for five test proteins by fitting the experimental data with the Conformational Change model

Test Proteins	**Rate constants values of the Conformational Change Model**			
	k_a (1/M s)	**k_d (1/s)**	**K_D (M)**	**R^2**
BSA	5.0E-01	1.8E-03	3.6E-03	0.95
β-lactoglobulin	8.0E-02	3.0E-03	3.8E-02	0.96
α-lactalbumin	7.0E-02	5.0E-04	7.5E-03	0.97
α- casein	2.5E-01	2.2E-03	8.0E-03	0.96
β-casein	1.6E-01	2.7E-03	1.7E-02	0.97

Rate of adsorption

The different protein adsorption phases onto SS were studied over time. This was done by plotting the rate of adsorption was plotted against the mass adsorbed on the surfaces, as shown in Fig. A-31 – A-38.

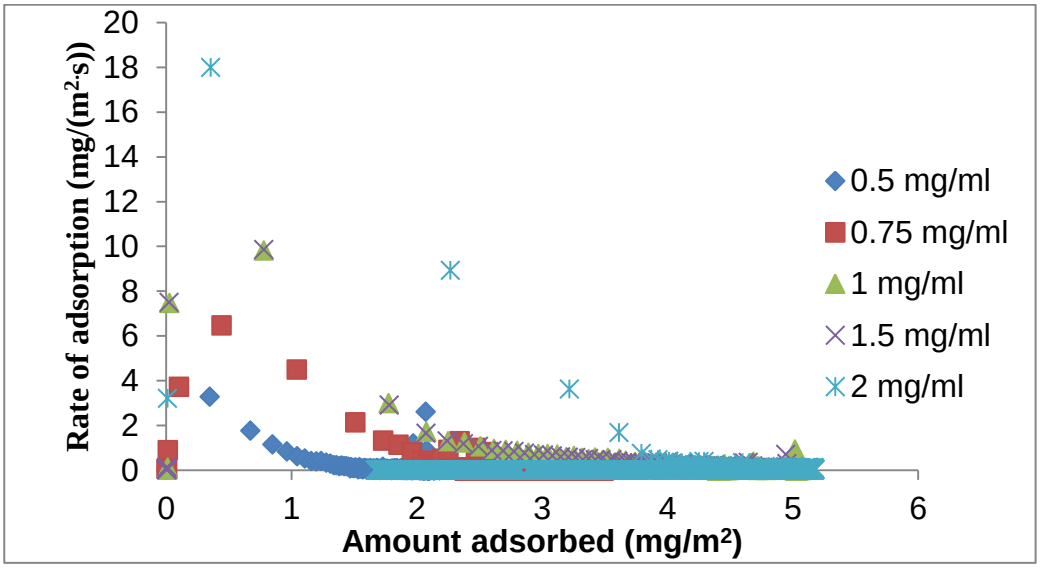

Figure 0-31: Effect of BSA solution concentration on adsorption rate

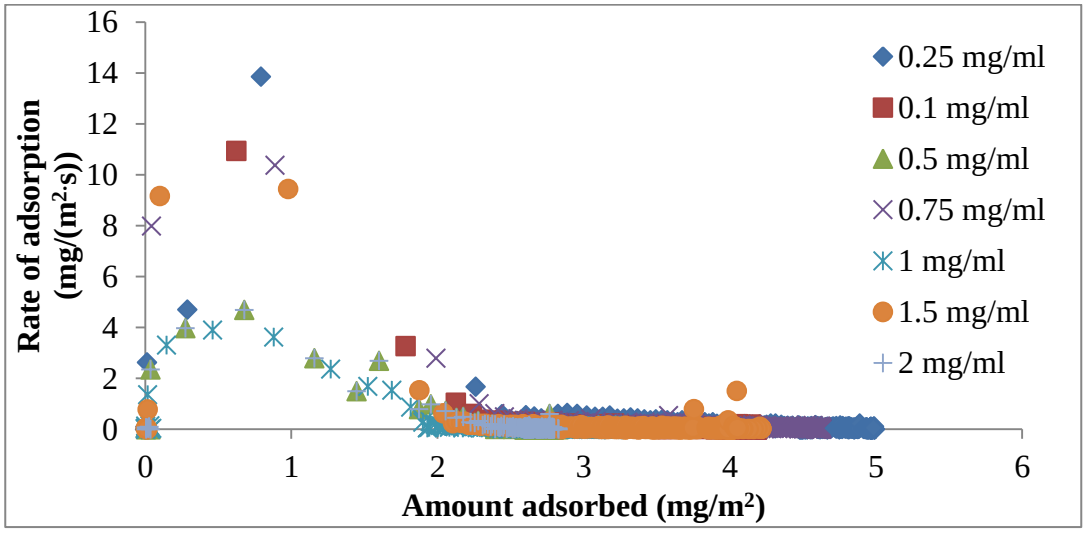

Figure 0-32: Effect of lysozyme solution concentration on adsorption rate

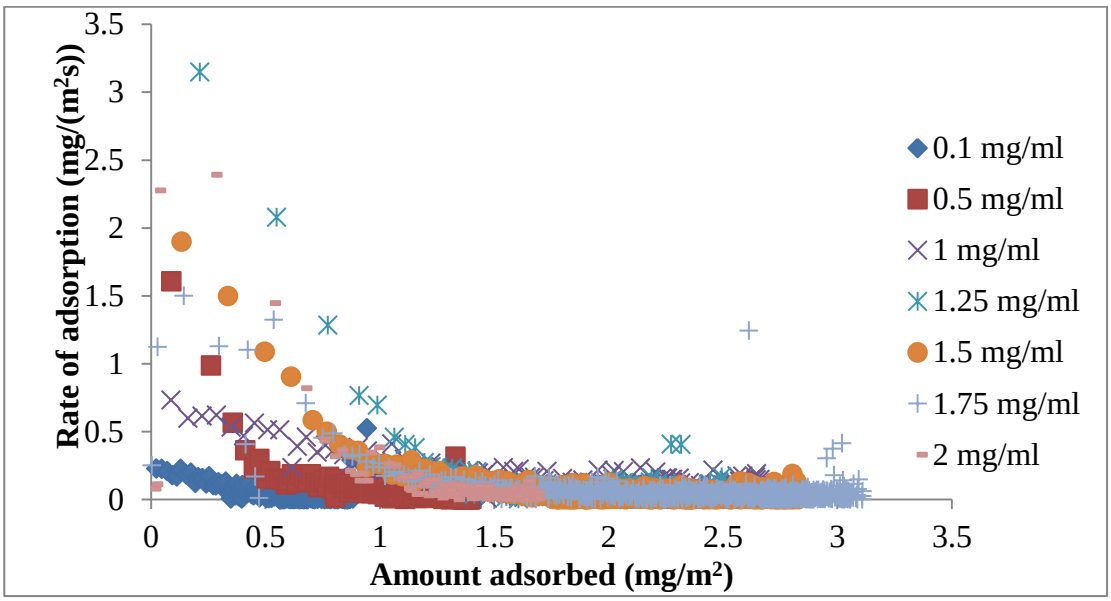

Figure 0-33: Effect of α-lactalbumin solution concentration on adsorption rate

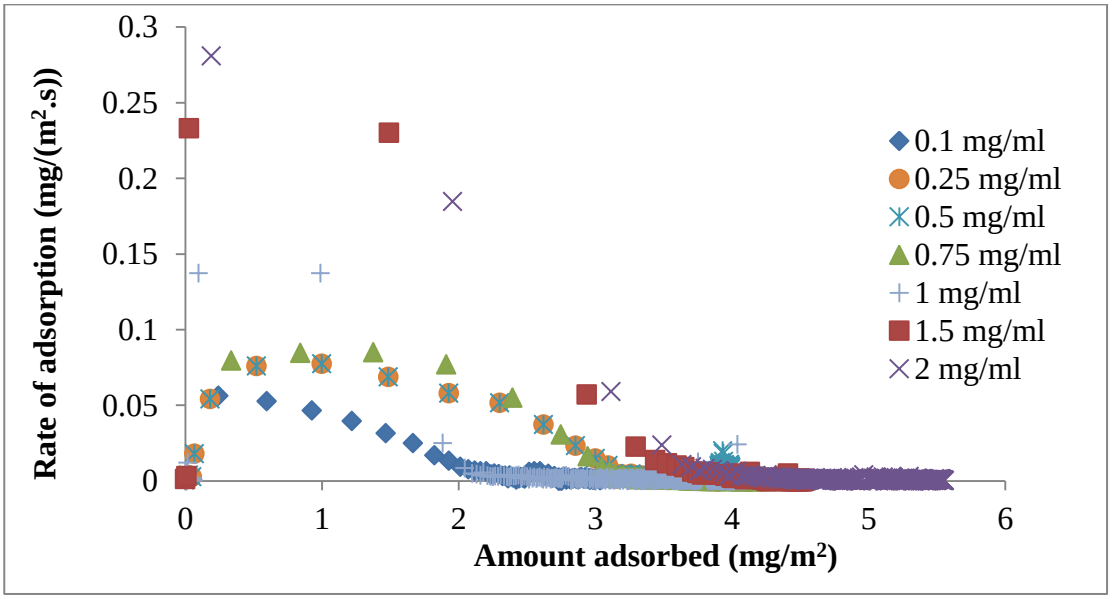

Figure 0-34: Effect of α-chymotrypsinogen solution concentration on adsorption rate

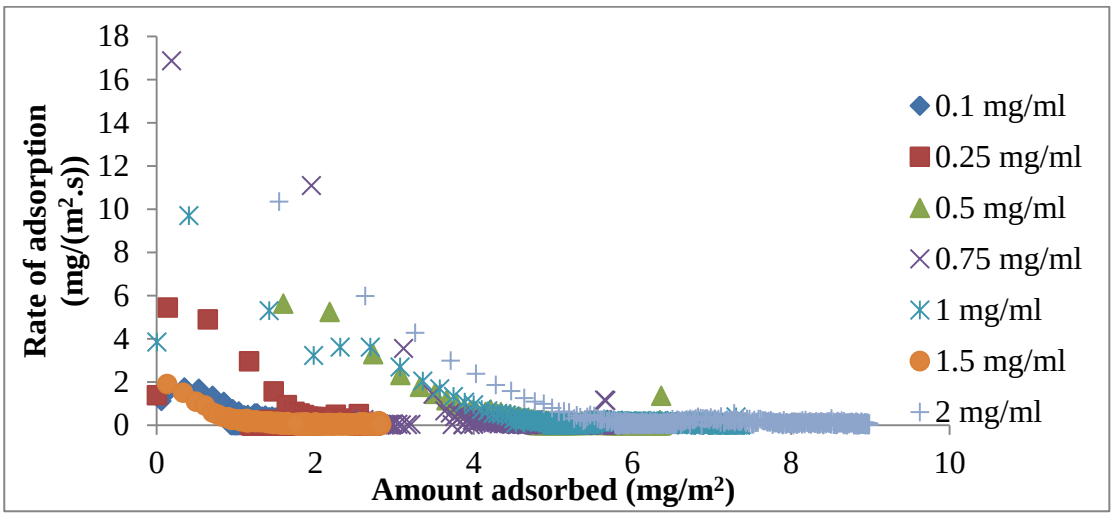

Figure 0-35: Effect of β-casein solution concentration on adsorption rate

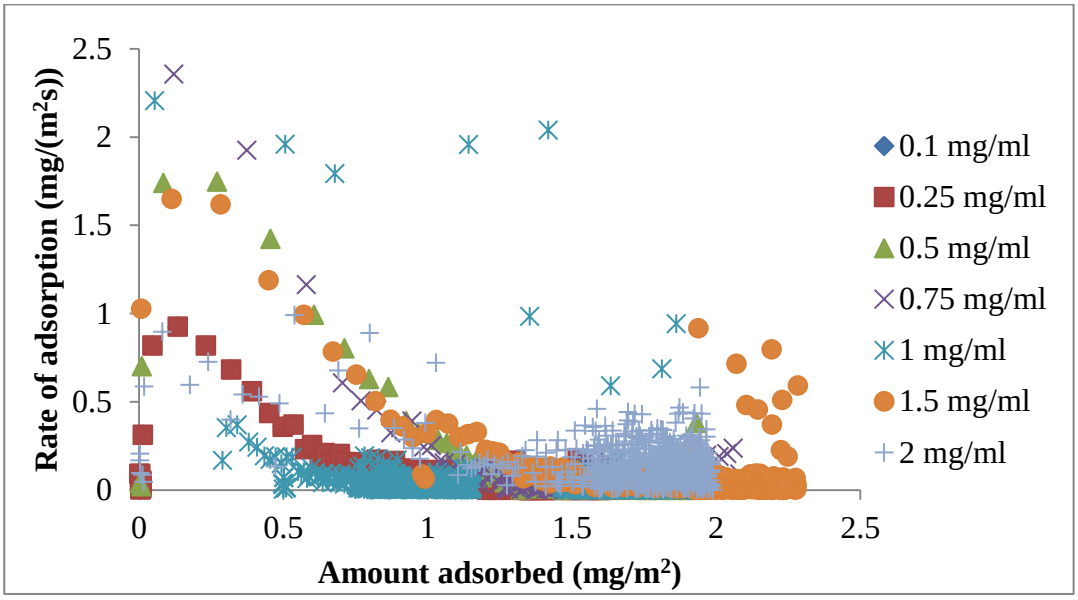

Figure 0-36: Effect of β-lactoglobulin solution concentration on adsorption rate

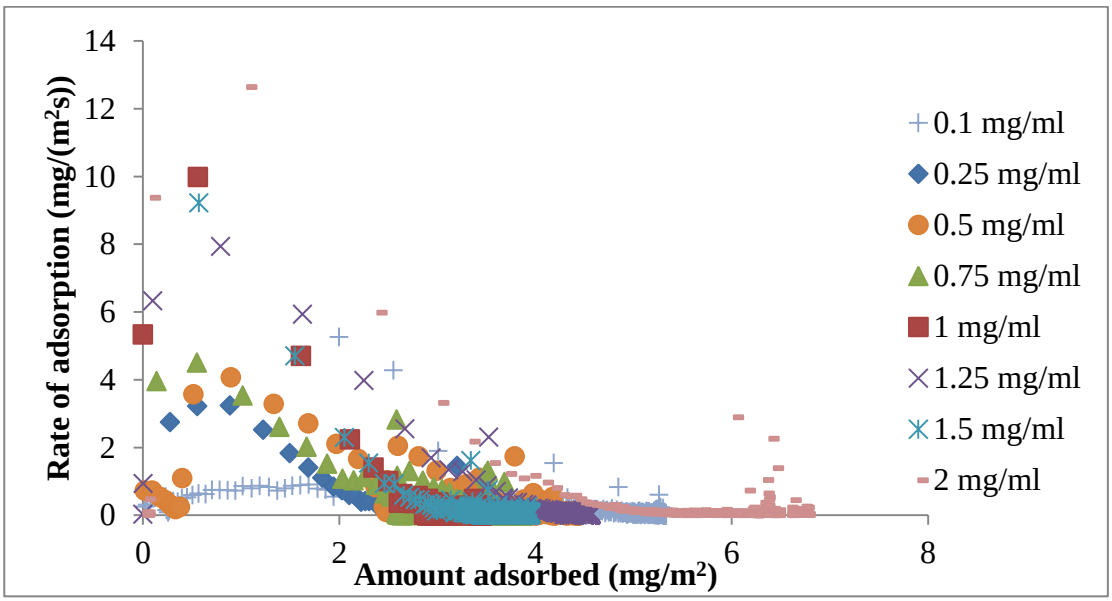

Figure 0-37: Effect of haemoglobin solution concentration on adsorption rate

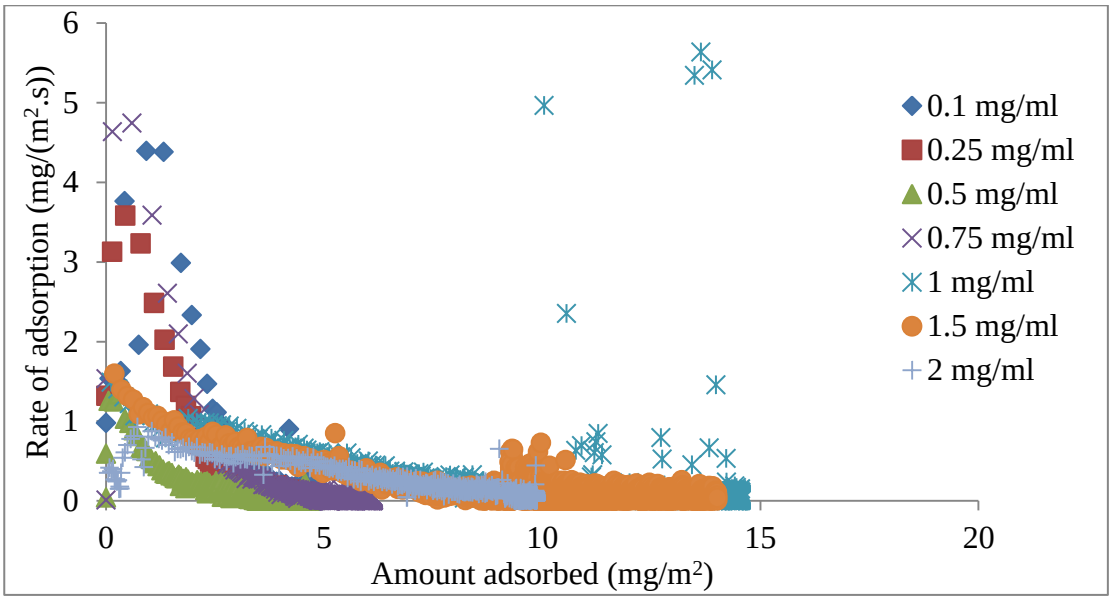

Figure 0-38: Effect of myoglobin solution concentration on adsorption rate

Comparison of β-lactoglobulin adsorption on two surfaces (gold & SS)

Desorption step of β-lactoglobulin from the SS sensor and removal efficiency of the adsorbed protein layer depended on water content of the adsorbed layers. For the gold sensor protein adsorption was high, protein-protein interactions and protein-surface interactions were dominant, and protein removal was limited, as shown in Table A-1.

The buffer wash was conducted for the same time for both surfaces (~100 mins). More protein desorbed from the SS sensor than from the gold sensor. The secondary structure is important when proteins bind strongly to the metal surface (gold) but less important with SS. The removal efficiency of adsorbed protein layers by buffer was affected by (i) destabilizing the protein secondary structure, which increased protein-protein interactions and protein-surface interactions on Au surfaces and (ii) water content adsorbed onto the SS surfaces. The gold surface is inert and the secondary structure of the proteins interacts with other proteins or the surface. The SS surface has negatively charged oxide layers so interaction between surface and water molecules is more prevalent than interaction between the proteins or the protein and the surface. Removal efficiency of protein layers would also be affected by the dominant non-covalent interactions between protein molecules and between them and the surface.

Table 0-4: Concentration of β-lactoglobulin on SS and gold surfaces as a function of solution concentration

Protein conc. (mg/ml)	SS surface (ng/cm^2)		Gold surface (ng/cm^2)	
	Adsorbed mass	Desorbed mass	Adsorbed mass	Desorbed mass
0.10	161±5	121±3	86±5	71±3
0.25	186±3	135±6	114±9	77±5
0.50	198±7	177±5	140±3	82±2
0.75	211±2	178±7	154±2	88±3
1.00	222±8	181±9	168±7	100±8
1.5	231±3	189±2	173±6	101±9
2.0	245±9	191±8	202±6	124±6

Modification of the tyrosine residues in β-lactoglobulin:

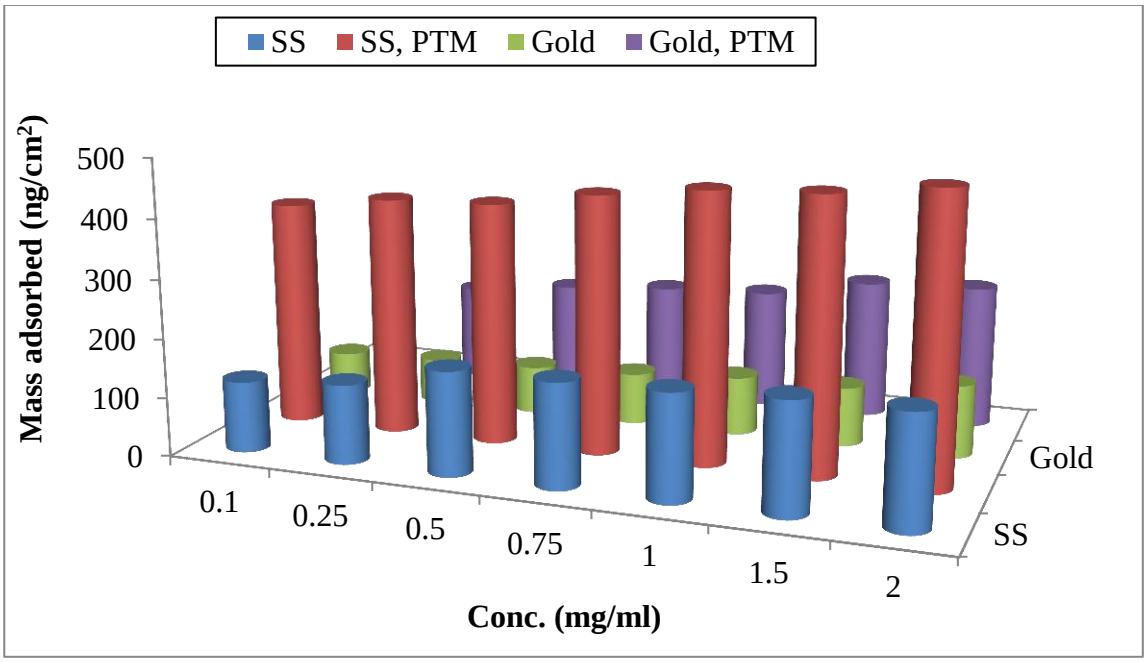

Figure 0-39: Effect of β-lactoglobulin concentration on adsorbed mass of modified and unmodified tyrosine residues in SS and gold surfaces

Table 0-5: Mass of protein adsorbed on SS and Gold, along with post translational modification of protein on SS and gold

Conc. (mg/ml)	SS (± 10 ng/cm^2)	SS, modified (± 15 ng/cm^2)	Gold (± 10 ng/cm^2)	Gold, modified (± 5 ng/cm^2)	Ratio of unmodified b/t Gold & SS	Ratio of modified b/t Gold & SS
0.10	121	383	71	155	59	40.5
0.25	135	405	77	166	57	41
0.50	177	410	81	185	46	45
0.75	178	438	88	198	50	45
1.00	181	458	100	205	55	45
1.50	189	465	101	238	53	51
2.00	191	487	124	244	65	50

Geometrical modeling of proteins:

Formulae:

SA of sphere: $4\pi r^2$ cm^2

SA of cylinder: $2\pi rh$ cm^2

SA of truncated cone: $\pi\left(R^2 + r^2 + (h\tan\alpha(R + r))\right)$ cm^2

where, R= radius of the base of the truncated cone & r is the radius of the top of the cone (=radius of the protein)

Table 0-6: Geometrical modeling data for proteins

Protein	Conc. (mg.ml)	Molecules/SS surface (*E-14)	Model I	Model II	Model III	Model IV	Model V
BSA	0.10	6E-15	1	1	2	3	2
	0.25	2E-14	3	3	5	8	4
	0.50	3E-14	4	4	9	14	7
	0.75	3E-14	5	5	10	16	8
	1.00	4E-14	7	7	14	23	11
	1.50	6E-14	9	9	18	29	14
	2.00	6E-14	11	11	21	34	16
Lysozyme	0.10	2E+13	803	820	948	948	173
	0.25	3E+13	971	992	1147	1147	210
	0.50	1E+13	498	509	589	589	108
	0.75	2E+01	885	904	1045	1045	191
	1.00	2E+13	542	553	640	640	117
	1.50	2E+13	771	788	911	911	167
	2.00	3E+13	960	981	1134	1134	207
α-lactalbumin	0.10	2E+12	94	96	33	33	4
	0.25	2E+12	146	148	51	51	6
	0.50	8E+12	483	489	167	167	21
	0.75	8E+12	491	497	170	170	21
	1.00	1E+13	677	685	235	235	29
	1.50	1E+13	724	734	251	251	31
	1.75	1E+13	863	874	299	299	37
	2.00	2E+13	1134	1149	393	393	49
α-chymotrypsinogen	0.10	1E+13	641	649	242	242	18
	0.25	1E+13	664	672	251	251	18
	0.50	1E+13	847	858	320	320	23
	0.75	1E+13	920	931	347	347	25
	1.00	2E+13	954	966	360	360	26
	1.50	2E+13	1018	1030	384	384	28
	2.00	2E+13	1059	1072	400	400	29

β-casein	0.10	3E+12	710	712	277	277	31
	0.25	4E+12	849	852	332	332	37
	0.50	9E+12	1971	1978	770	770	85
	0.75	1E+13	2402	2411	939	939	103
	1.00	2E+13	3618	3631	1414	1414	156
	1.50	2E+13	3860	3874	1508	1508	166
	1.75	2E+13	5027	5045	1965	1965	216
	2.00	1E+13	2402	2411	939	939	103
β-lactoglobulin	0.10	7E+12	1419	1424	770	770	3
	0.25	7E+12	1452	1457	788	788	3
	0.50	7E+12	1559	1565	846	846	4
	0.75	7E+12	1567	1573	851	851	4
	1.00	8E+12	1598	1604	867	867	4
	1.50	8E+12	1605	1611	871	871	4
	1.75	8E+12	1669	1692	915	915	4
	2.00	8E+12	1686	1692	915	915	4
Haemoglobin	0.10	1E+13	642	652	882	882	37
	0.25	1E+13	789	800	1083	1083	45
	0.50	2E+13	883	895	1212	1212	50
	0.75	2E+13	894	906	1227	1227	51
	1.00	2E+13	920	933	1264	1264	52
	1.50	2E+13	944	958	1297	1297	54
	2.00	2E+13	1111	1127	1526	1526	63
Myoglobin	0.10	2E+13	1201	1216	1062	1062	61
	0.25	2E+13	1301	1317	1150	1150	66
	0.50	2E+13	1342	1359	1187	1187	68
	0.75	6E+13	1754	1775	1550	1550	89
	1.00	6E+13	3955	4004	3497	3497	202
	1.50	0E+00	4008	4057	3543	3543	204
	2.00	8E+13	5102	5165	4511	4511	260

Protein adsorption factors

Tables A-7 represents the protein adsorption factors for five test proteins at various percentages of primary adsorption.

Table 0-7: Protein adsorption factor, *K* (*1E-6) (cm/s) for five milk proteins at 50% 60%, 70%, 80%, 50%<x<70% and 50%<x<80% of the first 10 minutes of adsorption

	α-chymotrypsinogen	β-casein	α-casein	β-lactoglobulin	α-lactalbumin
50%	0.07±0.03	0.01±0.04	0.02±0.01	2.40±0.03	0.02±0.06
60%	0.09±0.02	0.04±0.04	0.03±0.05	2.40±0.04	0.03±0.09
70%	0.11±0.04	0.20±0.03	0.09±0.02	4.30±0.09	0.03±0.01
80%	0.11±0.02	0.50±0.01	0.14±0.01	10.00±1.50	0.04±0.01
50%<x<70%	0.13±0.05	0.64±0.30	0.02±0.04	10.10±1.60	0.24±0.04
50%<x<80%	0.20±0.05	0.64±0.04	0.40±0.03	12.00±1.44	0.30±0.02

Appendix II: QTools Tutorial

Fit Analysis

Step 1: Once the QTools software is running, the first step would be to split the four sensors into different sheets to evaluate the data more easily

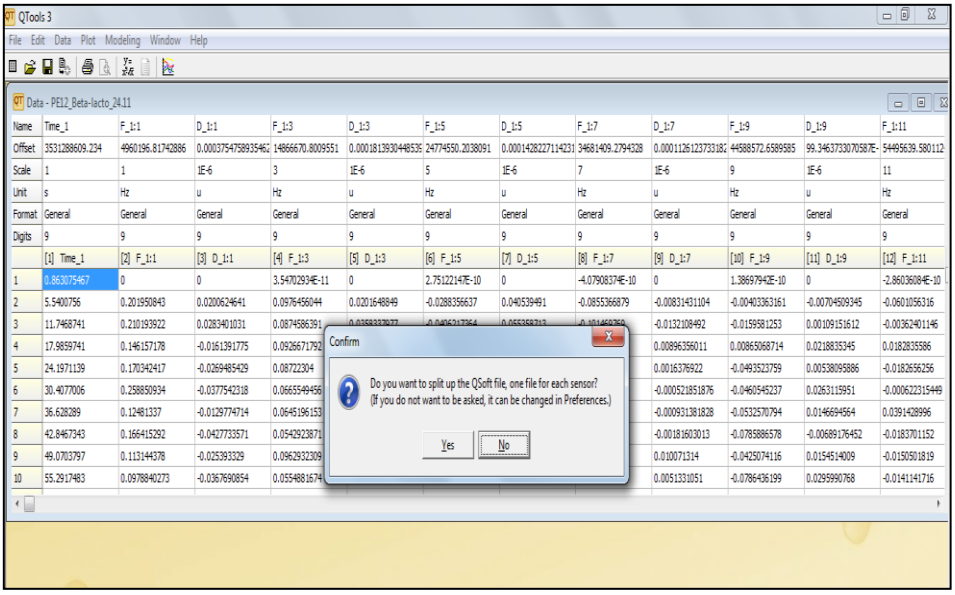

Figure 0-40: *Step I* in QTools – Split of 4 sensors into different worksheets

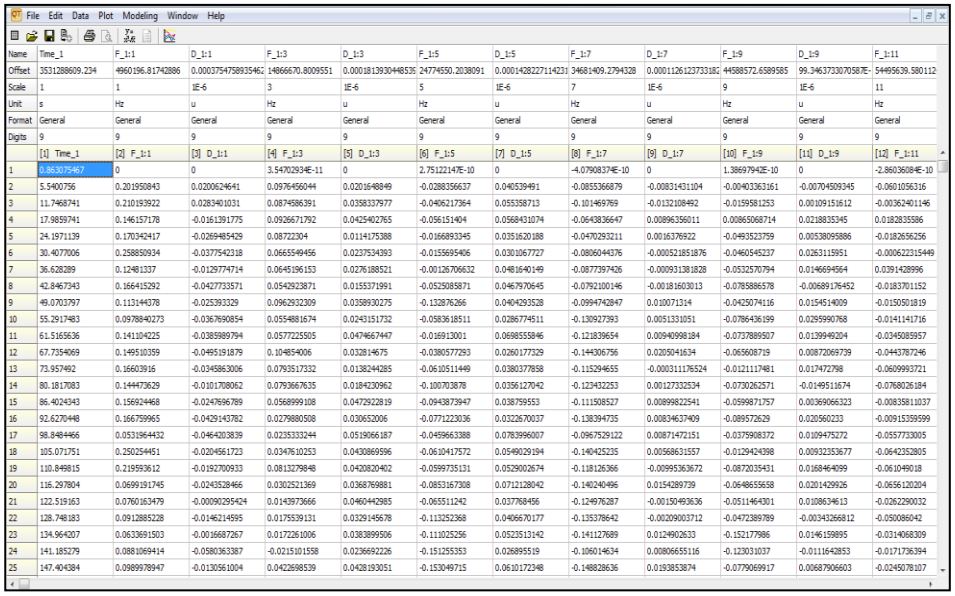

Figure 0-41: Representation of a worksheet

Step 2: **Voigt Model Analysis:** For the Voigt model analysis, shift from the Data Sheet to the Modeling Centre is performed.

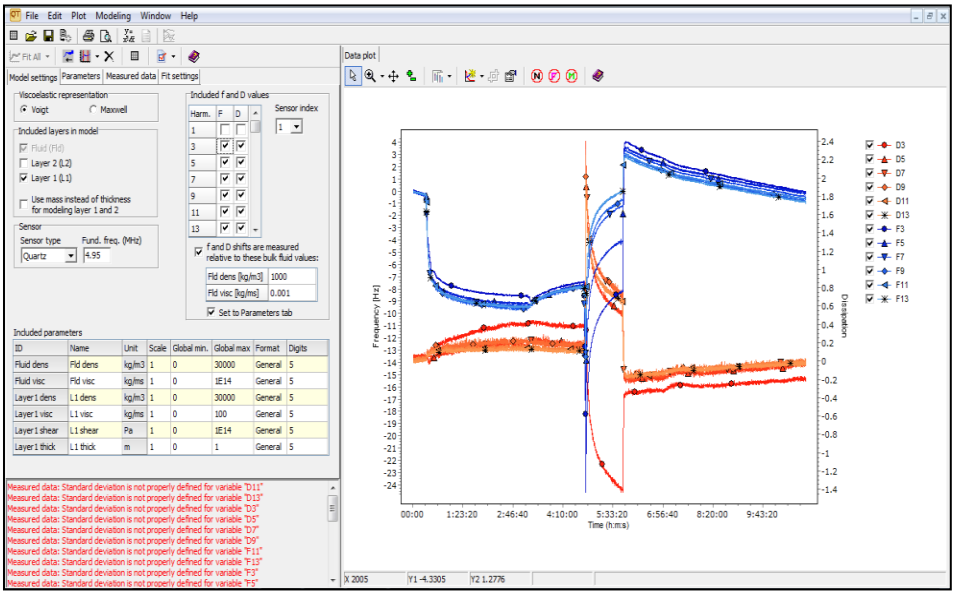

Figure 0-42: Modeling center for analysis of the Voigt Model

Step 3: Initialize of parameters for Voigt Analysis: Selection frequencies to be included for the analysis. (Usually the first frequency because it is too noisy). Select either a mass adsorption analysis or thickness to be analysed. (Chosen mass for the data evaluation).

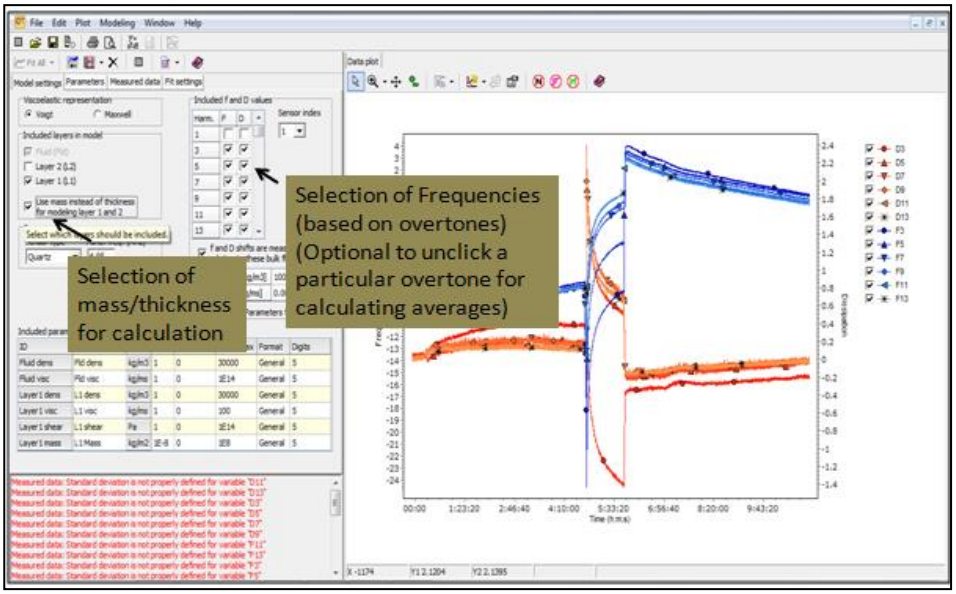

Figure 0-43: Voigt Analysis- Initialization of parameters

Step 4: In the Measurement tab, the standard deviation values for all the frequencies and dissipation are calculated.

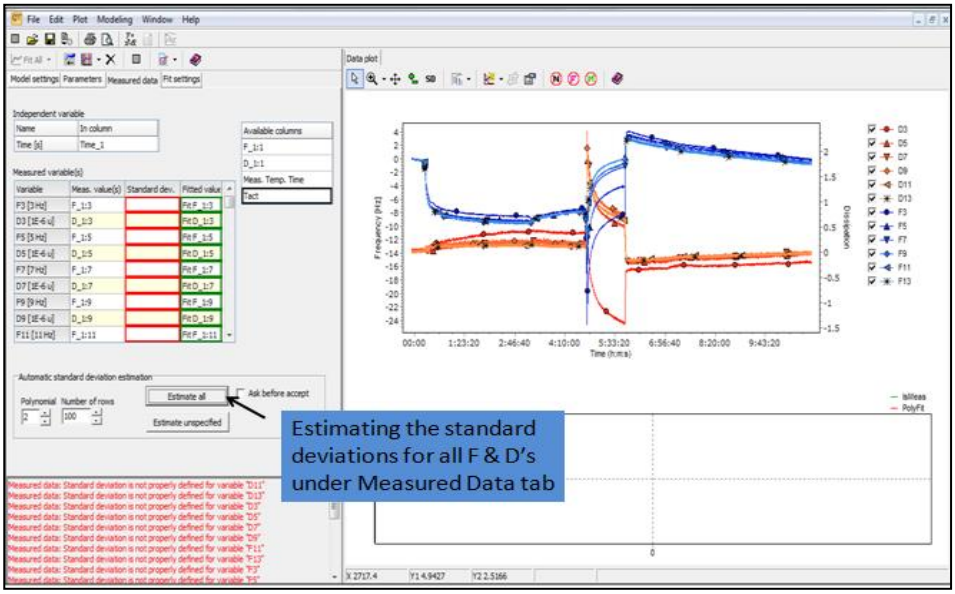

Figure 0-44: Measurements

Step 5: Fit parameters under the Fit Settings tab, check the option for limiting the x-values is. In the data side of the analysis column the offsets are marked as shown.

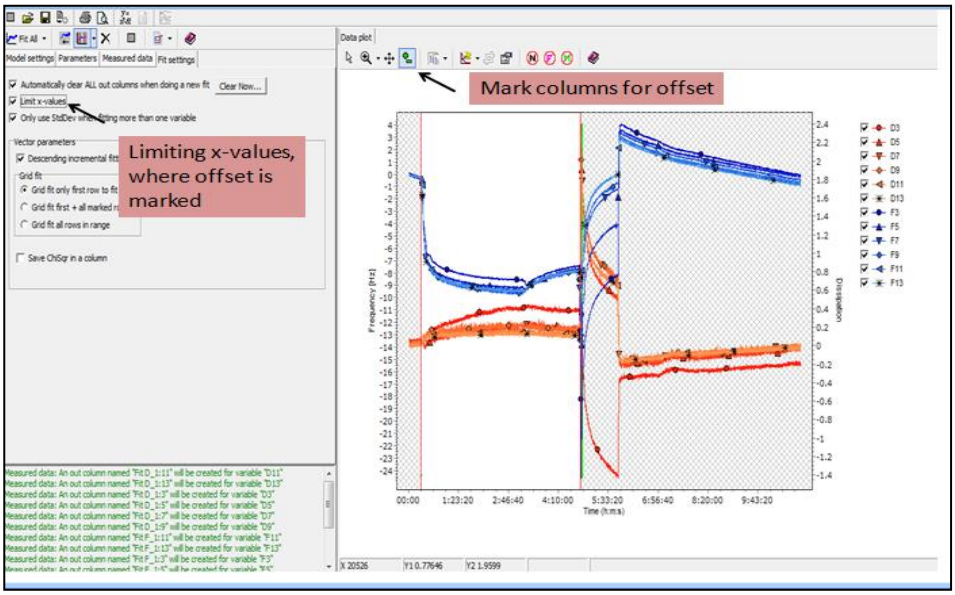

Figure 0-45: Fitting parameters

Step 6: Initialize parameters for vector parameter and data plots, and performed the fitting.

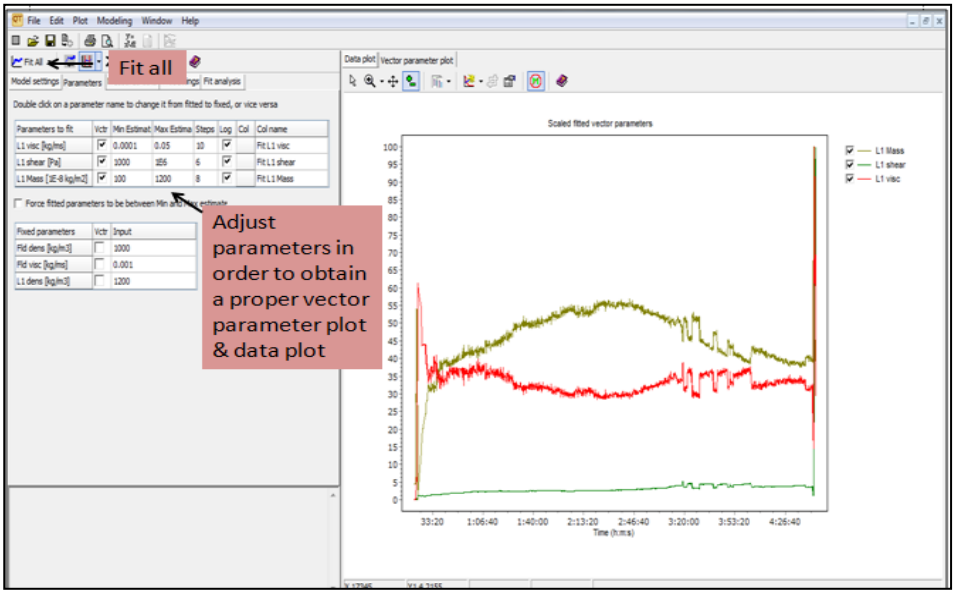

Figure 0-46: Initializing parameters

Step 7: Once the fitting is performed, the fit analysis tab is displayed showing the results of the fit. Figure A-46 is the datasheet. The fitting results are updated simultaneously. Figure A-47 displays the Fit L1 (layer 1) mass plotted against time.

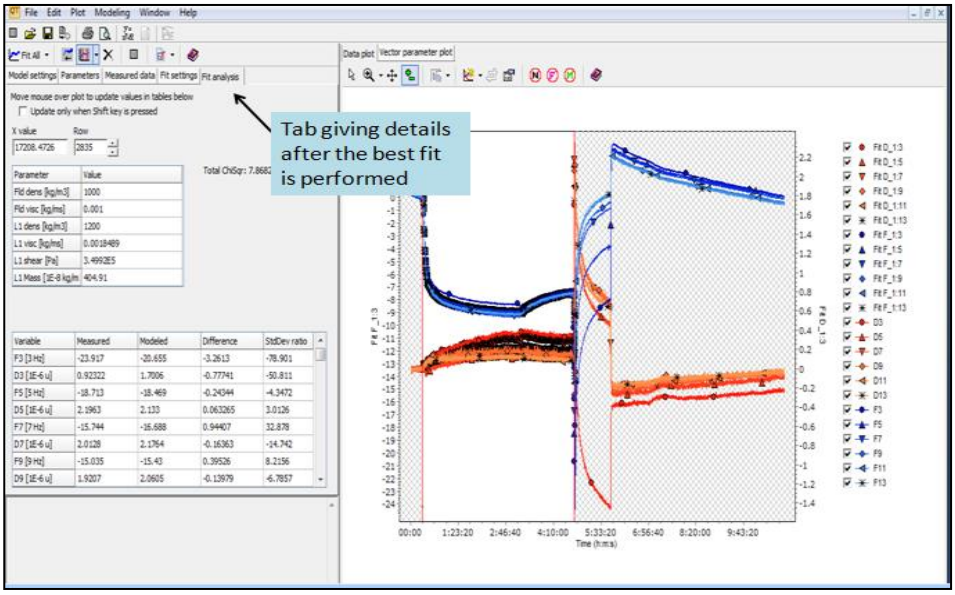

Figure 0-47: Fit Analysis

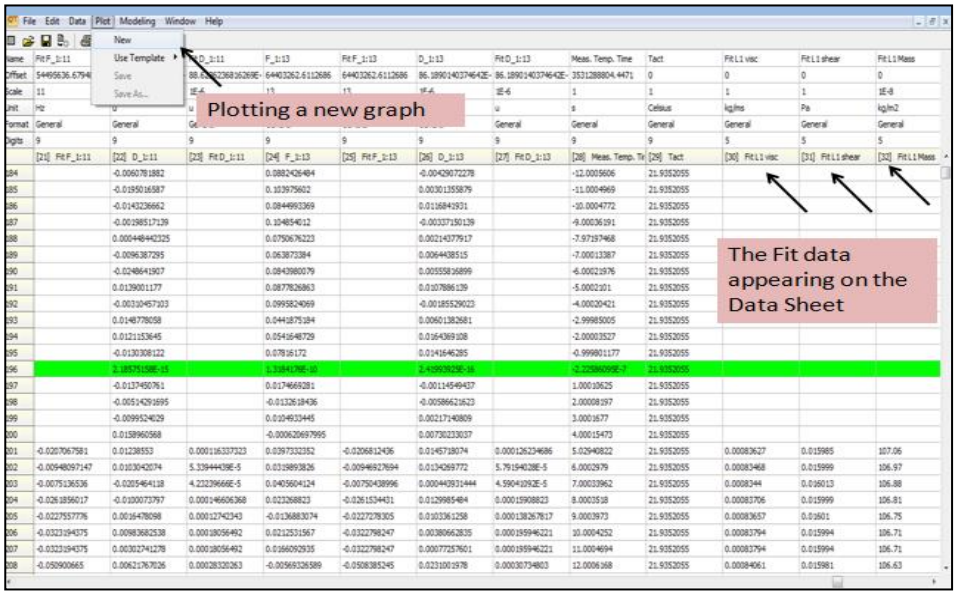

Figure 0-48: Data Sheet with Fitting results

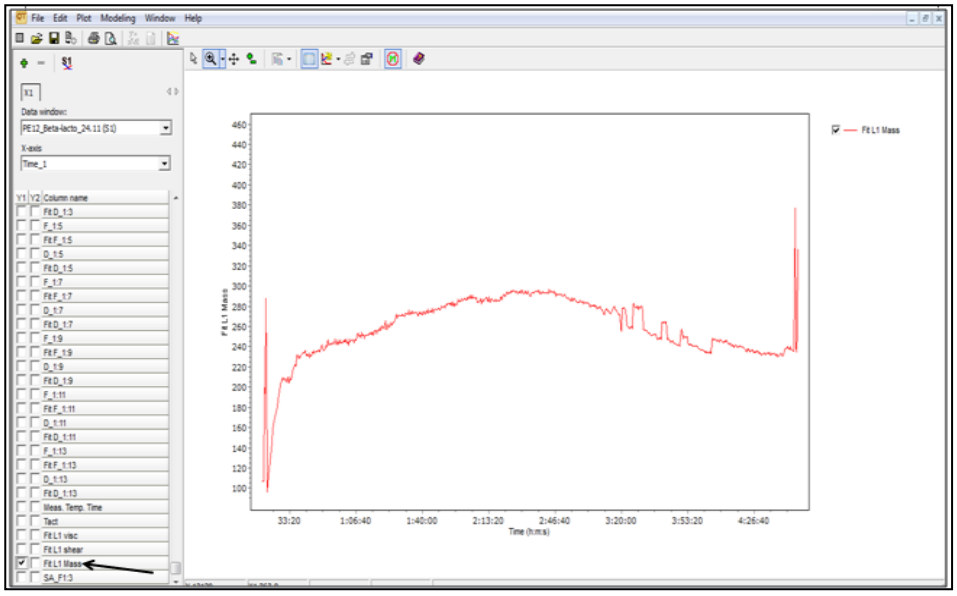

Figure 0-49: Graph depicting Fit L1 mass

Step 8: **Sauerbrey Analysis**

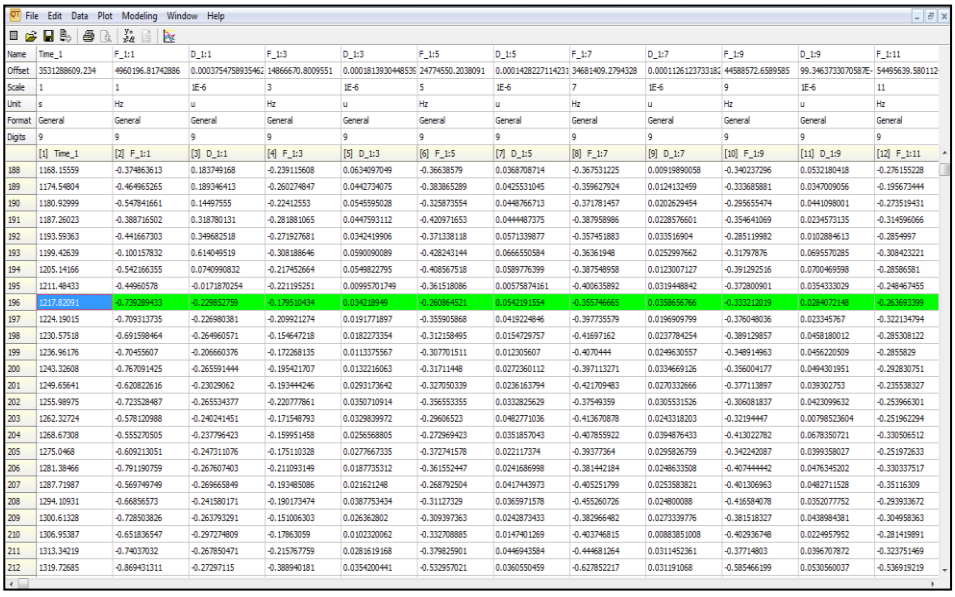

Figure 0-50: Representation of Data Sheet after offset of columns in the Modeling tab

Step 9: In this step, the marked columns are offset at the point, excluding time, temperature and tact.

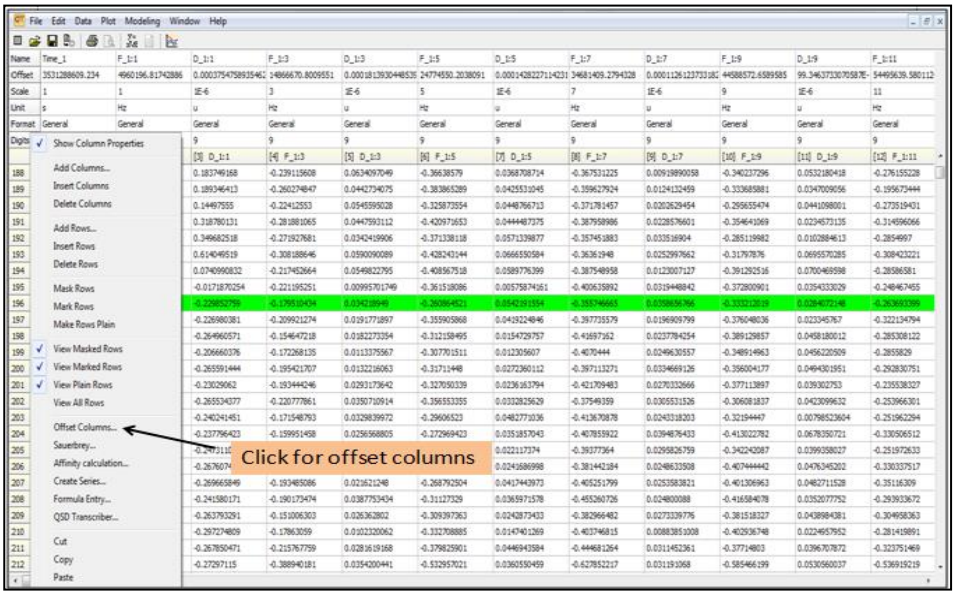

Figure 0-51: Offset of marked columns

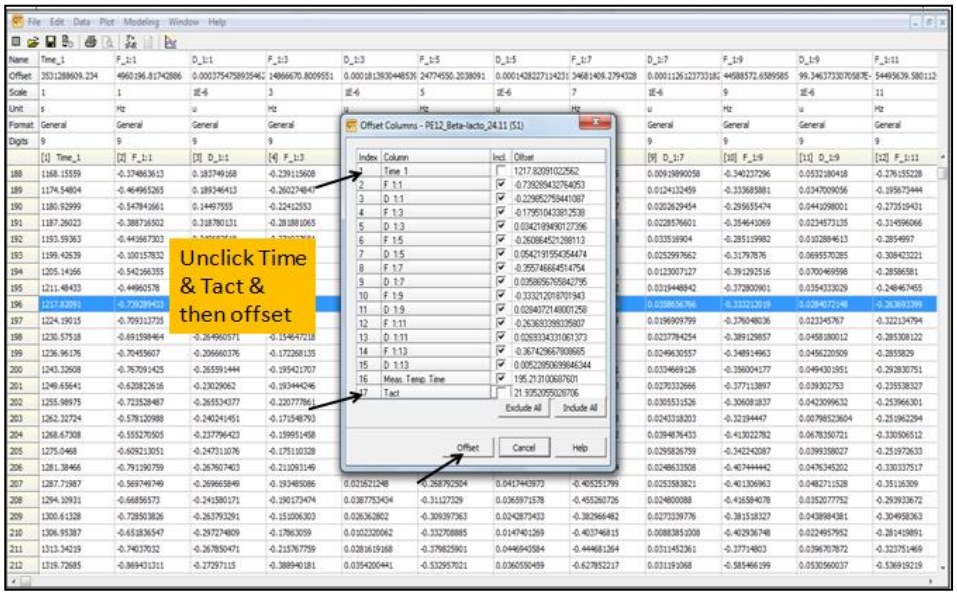

Figure 0-52: Offset excluding temperature, time and tact.

Step 10: Sauerbrey analysis to determine the mass absorbed on the surface of the sensor.

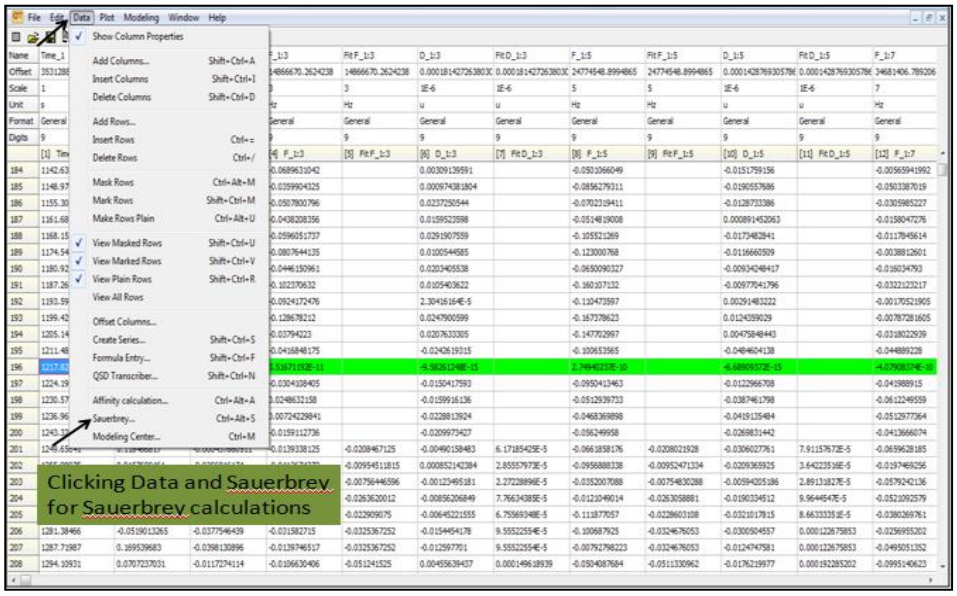

Figure 0-53: Sauerbrey Analysis

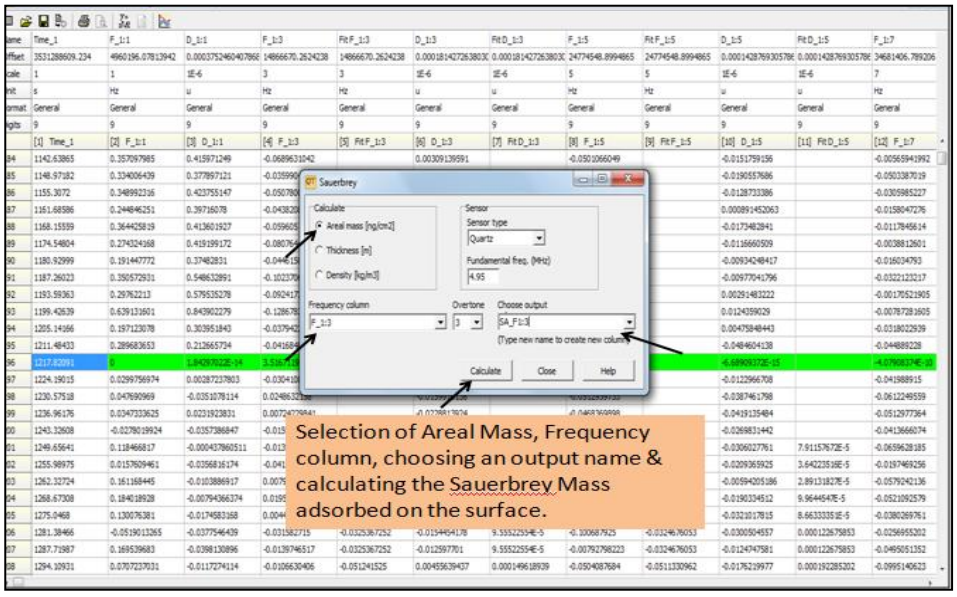

Figure 0-54: Initializing parameters for Sauerbrey Analysis

Step 11: Plotting data from Sauerbrey Analysis

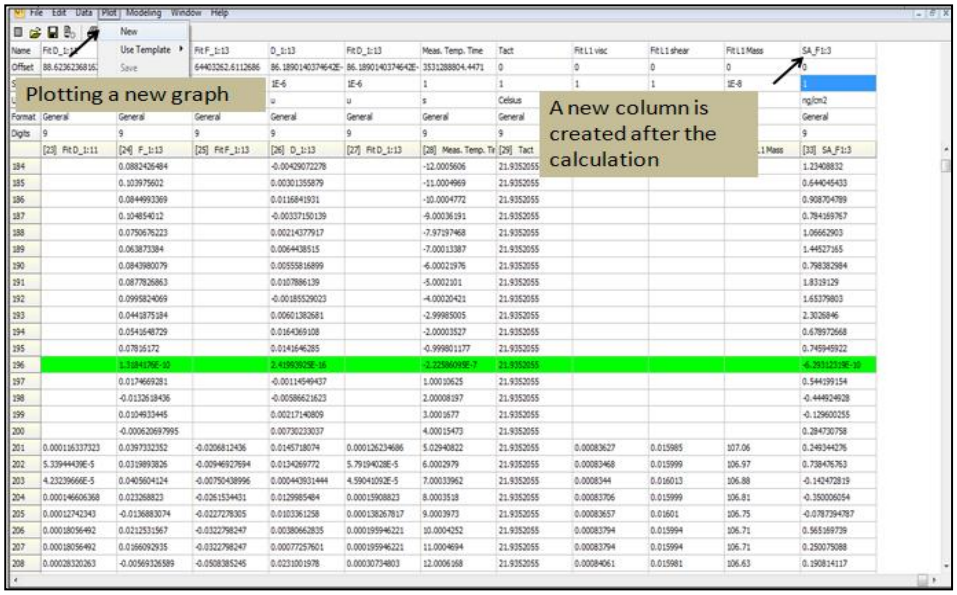

Figure 0-55: Plotting of Sauerbrey Data after analysis

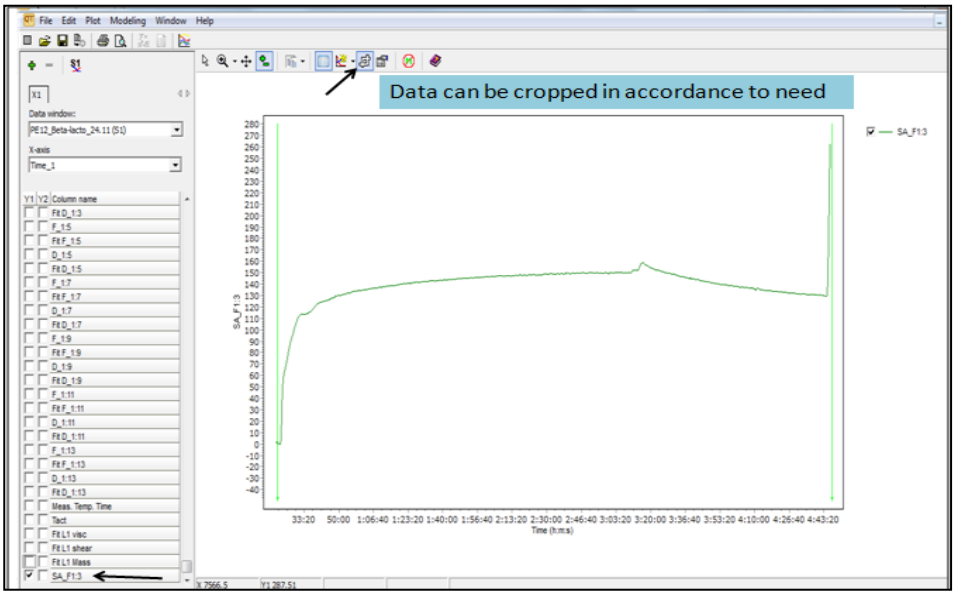

Figure 0-56: Graph of mass calculated by the Sauerbrey Model

Appendix III: Fluorescent labelling and peptide structure

Influence of salt in buffer on protein adsorption on stainless steel

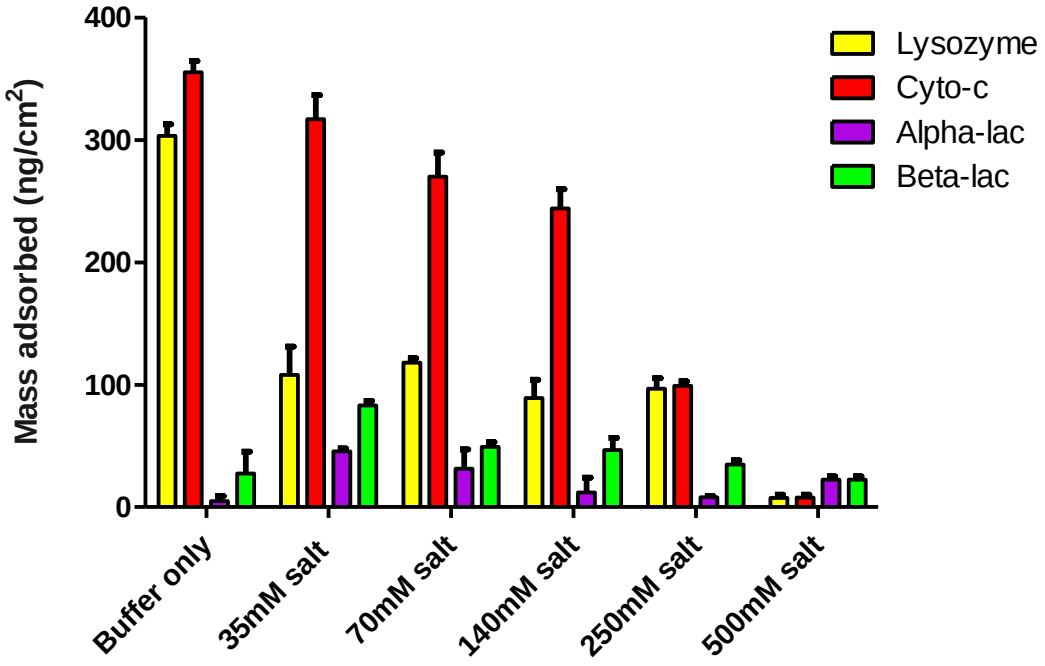

Figure 0-57: Effect of salt in the buffer on protein adsorption on SS (for fluorescent labeling)

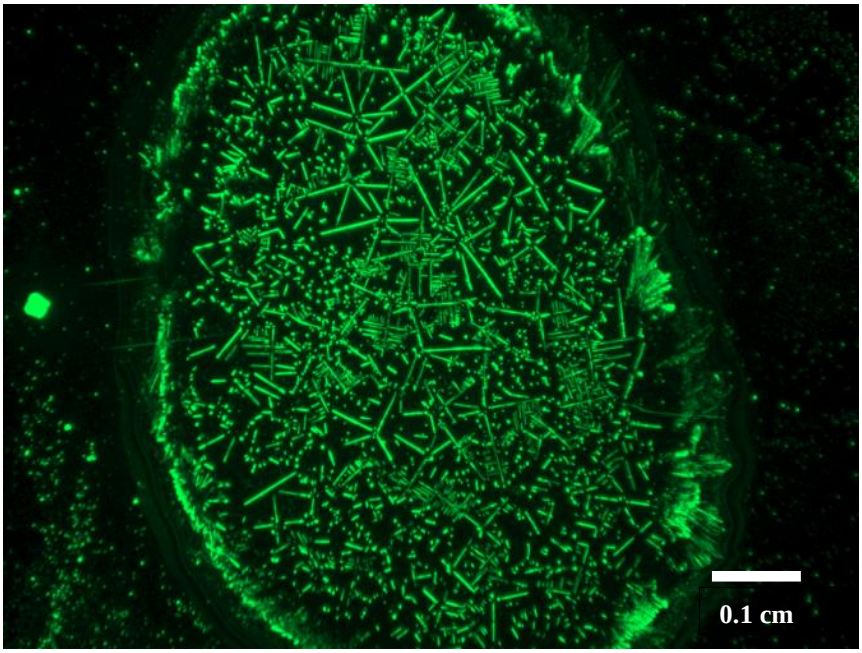

Figure 0-58: Formation of salt crystals (in dried) in β-lactoglobulin spot

DOPA structure

The adhesion of modified and unmodified peptide fragments and proteins were studied (Chapter 4). The structure of peptide I fragment (developed in Yasara, molecular modeling software package, YASARA Biosciences, http://www.yasara.com) shows there are two tyrosine residues near each other. The third tyrosine residue is oriented in opposite direction. Two hypotheses are proposed here for the interaction with the surface. In the first, the catechol moiety of two tyrosine residues close to each other once converted to DOPA have their catechol moiety attached to the metal surface forming DOPA-metal interactions. The third DOPA moiety could form a cohesive bond to another DOPA moiety. In the second hypothesis, all three molecules of DOPA bind to the surface separately, giving strong DOPA-metal interactions and hence increased adsorption to SS.

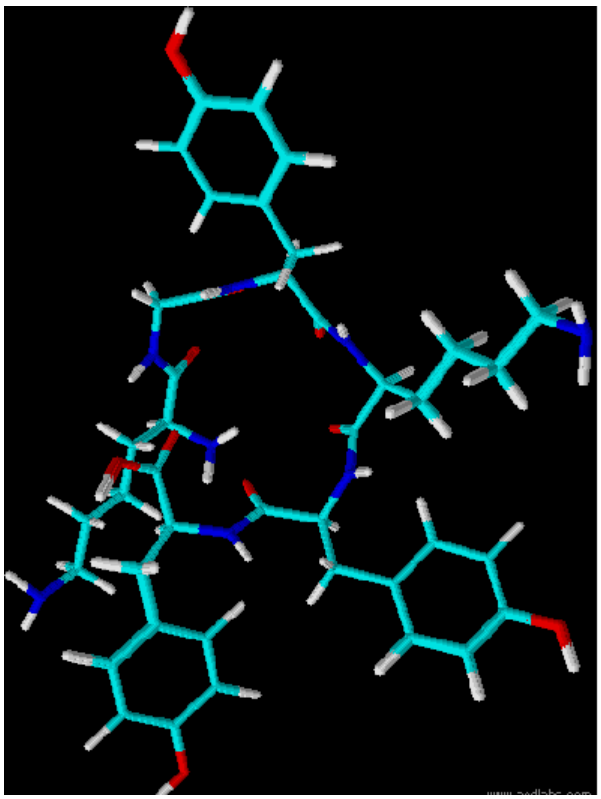

Figure 0-59: Structure of Peptide I fragment

Appendix IV: Phage Display Technique

A trial using phage display technique using stainless steel beads to adhesion of peptide sequences was performed as trial at AIBN, Brisbane. The peptide sequences are expressed in a phage virion then boundto SS. This work should be investigated further to check adsorption on beads.

Introduction

Phage display is a selection technique where a library of peptide or protein variants is expressed on the outside of a phage virion, while the genetic material encoding each variant resides on the inside. This creates a physical linkage between each variant protein sequence and the DNA encoding it, which allows rapid partitioning based on binding affinity to a given target molecule (antibodies, enzymes, cell-surface receptors, etc.) by an *in vitro* selection process called 'panning'. In its simplest form, panning is done by incubating a library of phage-displayed peptides on a plate (or bead) coated with the target, washing away the unbound phage, and eluting the specifically bound phage. The eluted phage are then 'amplified' and taken through additional binding/amplification cycles to enrich the pool in favor of binding sequences. After three to four rounds, individual clones are characterized by 'DNA sequencing and ELISA'. The Ph.D.™ (phage display) system is based on a simple M13 phage vector, modified for pentavalent display of peptides as N-terminal fusions to the minor coat protein pIII.

(a)

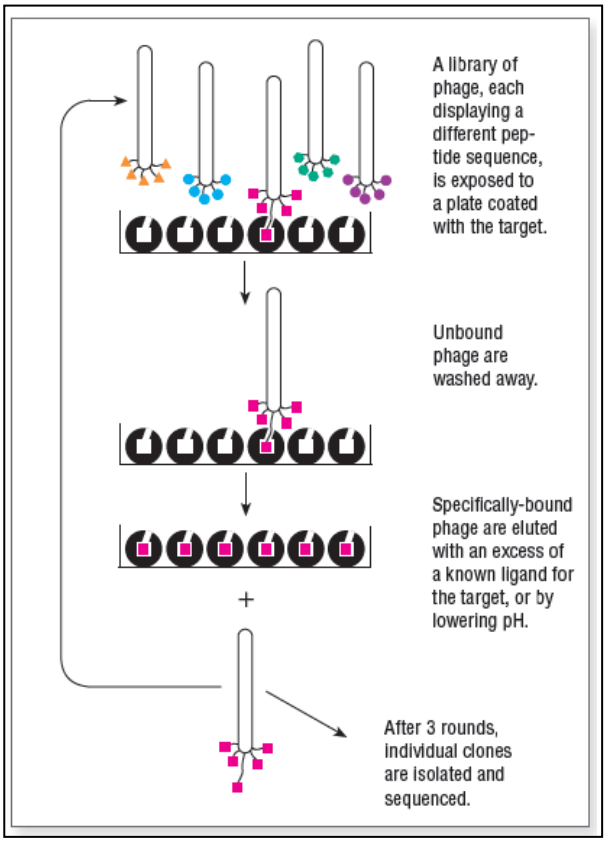

(b)

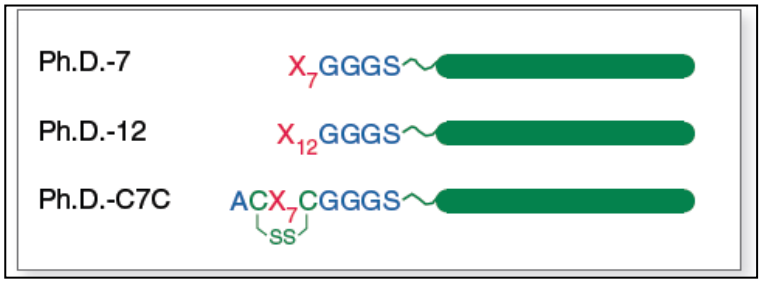

Figure 0-60**:** (a) Phage Display - Panning with a pentavalent peptide library displayed on pIII and (b) Peptide libraries from New England Biolabs (Ipswich, MA)

The premade libraries consist of linear heptapeptide (Ph.D.-7) and dodecapeptide (Ph.D.-12) libraries, as well as a loop-constrained heptapeptide (Ph.D.-C7C) library. The randomized segment of the Ph.D.-C7C library is flanked by a pair of cysteine residues, which are oxidized during phage assembly to a disulfide linkage, resulting in the displayed peptides being presented to the target as loops. All the libraries have

complexities for about 10^9 independent clones, which is sufficient to encode most if not all of the possible 7-mer (1.28×10^9) peptide sequences, but only a tiny fraction (less than 1 millionth) of the 4.1×10^{15} possible 12-mer sequences. The Ph.D.-12 library can thus be considered of as having the equivalent diversity of the Ph.D.-7 library, but spread out over 12 residues. In both the Ph.D.-7 and the Ph.D.-12 libraries, the first residue of the peptide-pIII fusion is the first randomized position, while the first randomized position in the Ph.D.-C7C library is preceded by Ala-Cys. All the libraries contain a short linker sequence between the displayed peptide and pIII: Gly-Gly-Gly-Ser.

Materials and methods

Autoclave, Laminar Air Flow chamber, water bath (50°C), Incubator (static, 37°C), Shaking incubator (250 rpm, 37°C), ELISA plate reader, Fridge: 4,20,-80°C, Centrifuge (14000 rpm, 4°C), Falcon tubes, micro centrifuge tubes, UV Visible Spectrophotometer (OD 600), mini lab roller, weigh balance, magnetic stirrer, oven (60-70°C), microwave, pH meter, ultrasonic bath, pippetors, ice machine, nanodrop, vacuum, Elisa plate washer, vortex mixer, multichannel pipettors (5-50µl and 50-300µl).

Protocol for phage display technique

The following steps were performed to check adsorption on stainless steel beads. Although proteins were not adsorped on the beads, this work could be futureexplored in the future, with modifications, to observe adsorption on the bead surfaces.

Day One: Surface panning procedure (direct target coating)

The most straightforward method for affinity partitioning (panning) involves directly coating stainless steel beads with the target of interest (by nonspecific hydrophobic and electrostatic interaction), washing the excess, and passing the pool of phage over the target-coated surface.

Step 1: 10 ml LB + 10 µl of Tet was inoculated with 0.1 ml of an overnight culture of ER2738 until it reaches an OD of 0.5 in a shaking incubator at 37°C

Step 2: Fill an eppendorf tube completely with blocking buffer and incubated for at least 1 hour at 4°C.

Step 3: Discard the blocking buffer and wash five times with TBST (Tween 0.1% for first round of panning and 0.5% for the remaining).

Step 4: Place the beads in the Eppendorf and wash with TBST another five times.

Step 5: Incubate the beads with 1 ml of TBS + 100 fold representation of the library in rocking for 1 hour at room temperature. Tween is not added in this step.

Step 6: Discard the solution in and wash beads with TBST. The eppendorf tube containing the beads wasis washed about 20 times.

Step 7: The beads are amplified directly in the Erlenmeyer flask containing 20 ml LB+ 20 µl Tet+ 200 µl of an overnight culture of ER2738 in a shaking incubator at 37°C for 4.5 to 5 hours

Step 8: Transfer the culture to a centrifuge tube and spun for 10 minutes at 12,000 g at 4°C. Transfer the supernatant to a fresh tube and re-spun (discarding the pellet).

Step 9: Transfer the supernatant to a fresh tube and re-spun

Step 10: Transfer the upper 80% of the supernatant (~15-18ml) into a fresh tube and add 1/6 volume of 20% PEG/2.5 M NaCl (~2.5-3ml). The phage is allowed to precipitate at 4°C for at least 2 hours, preferably overnight.

Day Two: Phage purification and titration

Step 1: Spin PEG precipitate at 12,000 g for 15 minutes at 4°C. Decant the supernatant. Spin the tube was spun briefly, and residual supernatant with a pipette. The phage pellet isas a white finger print sized smear on the side of the tube.

Step 2: Suspend the pellet in 1 ml of TBS then transfer. The suspension was transferred to a micro centrifuge tube and spin at maximum (14,000 rpm) for 5 minutes at 4°C to pellet residual cells.

Step 3: Transfer the supernatant to a fresh micro centrifuge tube and re-precipitate by adding 1/6 volume of 20% PEG/2.5 M NaCl (~150-170µl). It was incubated on ice

for 15–60 minutes. Then, micro centrifuge at 14,000 rpm for 10 minutes at 4°C, discard the supernatant, re-spin briefly and remove residual supernatant with a micropipette.

Step 4: Suspend the pellet was suspended in 200 µl of TBS then micro centrifuge for 1 minute to pellet any remaining insoluble material. Transfer the supernatant to a fresh tube. This is the amplified eluate.

Phage Titering

Step 5: 10 ml LB with ER2738 from a plate is inoculated and incubated with shaking for 4.5 to 5 hours (until it reaches an OD of 0.5).

Step 6: While the cells are growing, melt top Agar in the microwave and deispense 3 ml into sterile culture tubes, one per expected phage dilution. Maintain tubes at 50°C.

Step 7: Prewarm one LB/IPTG/Xgal plate per expected dilution at 37°C until ready for use.

Step 8: Prepare 10 to 10^3-fold serial dilutions of phage in LB; 1 ml final volumes were convenient. (Suggested dilution range are: 10^8–10^{11} for amplified phage culture supernatants, and 10^1–$10^4$for unamplified panning eluates,). Aerosol-resistant pipette tips are used to prevent cross-contamination.

Step 9: When the culture in Step 1 reached the mid-log phase, dispense 200 µl was dispensed into microfuge tubes, one for each phage dilution.

Step 10: To carry out infection, add 10 µl of each phage dilution was added to each tube, vortexed quickly and incubated at room temperature for 1–5 minutes.

Step 11: Transfer the infected cells, as one infection at a time to culture tubes containing 45°C Top Agar, vortexed briefly and *immediately* and pour the culture onto a pre-warmed LB/IPTG/Xgal plate.

Step 12: Allow the plates to cool for 5 minutes, invert, and incubate overnight at 37°C.

Step 13: Count plaques on plates that have approximately 100 plaques. Multiply the count number by the dilution factor for that plate to get phage titer in plaque forming units (pfu) per 10 μl.

Day Three: Amplication of plaques

Step 1: Dilute an overnight culture of ER2738 1:100 in LB. Dispense 1 ml of diluted culture into culture tubes, one for each clone to be characterized. 10–20 clones from the third round are usually sufficient to detect a consensus binding sequence.

Step 2: Use a sterile wooden stick or pipette tip to stab a blue plaque from a titering plate (important: plates should be <1–3 days old, stored at 4°C and have <100 plaques) and transfer to a tube containing the diluted culture. Pick well-separated plaques to ensure each plaque contains a single DNA sequence.

Step 3: Incubate the tubes at 37°C with shaking for 4.5–5 hours (no longer).

Step 4: Transfer the cultures to micro centrifuge tubes, and microfuge at 14,000 rpm for 30 seconds (see next section to purify sequencing template). Transfer the supernatant to a fresh tube and re-spin. Using a pipette, transfer the upper 80% of the supernatant to a fresh tube. This is the amplified phage stock and can be stored at 4°C for several weeks with little loss of titer.

Step 5: For long-term storage (up to several years), dilute 1:1 with sterile glycerol and store at –20°C.

Day Four: Purification of DNA

Step 1: Carry out the plaque amplification procedure described above. After the first centrifugation in Step 4, transfer 500 μl of the phage-containing supernatant to a fresh micro centrifuge tube.

Step 2: Add 200 μl of 20% PEG/2.5 M NaCl ,mix well and let to stand for 10–20 minutes at room temperature.

Step 3: Micro centrifuge at 14,000 rpm for 10 minutes at 4°C and discard the supernatant . Phage pellet may not be visible at this stage.

Step 4: After re-spinning, carefully pipette away and discard any remaining supernatant.

Step 5: Suspend the pellet thoroughly in 100 µl of Iodide buffer by vigorously tapping the tube. Add 250 µl of ethanol and incubate for 10–20 minutes at room temperature. Short incubation at room temperature will preferentially precipitate single-stranded phage DNA, leaving most phage protein in solution.

Step 6: Micro centrifuge at 14,000 rpm for 10 minutes at 4°C, and discard the supernatant. The pellet is dissolved with 0.5 ml of 70% ethanol (stored at –20°C), re-spun, discarded the supernatant, and briefly dried the pellet under vacuum.

Step 7: Suspend the pellet was suspended in 30 µl of TE buffer.

Day Five: ELISA (Enzyme linked immunosorbent assay)

Step 1: Carry out the plaque amplification procedure was carried out.

Step 2: Dilute an overnight culture of ER2738 was diluted as 1:100 in 20 ml of LB.

Step 3: Add 5 µl of phage stock from Step 1 (or a single phage plaque) to a 20 ml culture for each clone to be characterized for each culture and incubate with vigorous aeration for 4.5–5 hours at 37°C.

Step 4: Transfer the culture to a centrifuge tube and spin at 12,000 g for 10 minutes at 4°C. Transfer the supernatant to a fresh tube and re-spun (discarding the pellet).

Step 5: Transfer the upper 80% of the supernatant (~15-18ml) to a fresh tube and add 1/6 volume of 20% PEG/2.5 M NaCl (~2.5-3ml). Allow the phage to precipitate at 4°C for at least 2 hours or overnight.

Step 6: Spin the PEG precipitation at 12,000 g for 15 minutes at 4°C. Decant and discard the supernatant, re-spin the precipitate briefly, and remove any residual supernatant with a pipette.

Step 7: Suspend the pellet in 1 ml of TBS, and transfer to a micro centrifuge tube. Spin the sample at 14,000 rpm for 5 minutes at 4°C to pellet residual cells.

Step 8: Transfer the supernatant to a fresh micro centrifuge tube and re-precipitate with 1/6 volume of 20% PEG/2.5 M NaCl (150-170µl). Incubated for 15–60 minutes on ice. Spin at 14,000 rpm for 10 minutes at 4°C,discarding the supernatant, and re-spin briefly. Remove residual supernatant with a micropipette.

Step 9: Suspend the pellet in 50 µl of TBS. Phage tittering is done as describeed in Amplification of plaques

Step 10: Block the ELISA plate with the blocking buffer for 1-2 hours at 4°C

Step 11: Remove the blocking buffer and wash each plate was six times with TBST. The percentage of Tween should be the same as the concentration used in the panning wash steps.

Step 12: Place the beads in the wells.

Step 13: Add fourfold serial dilutions of phage in 200 µl of TBS/Tween per well, starting with 10^{12} virions in the first well of a row and ending with 2 x 10^{5} virions in the 12th well.

Step 14: Use a multichannel pipettor to transfer, 100 µl from each row of diluted to a row of target-coated wells, and transferred 100 µl to a row without target. Incubate at room temperature for 1–2 hours with agitation.

Step 15: Wash the plate six times with TBST as in Step 12.

Step 16: Dilute HRP-conjugated anti-M13 monoclonal antibody (GE Healthcare. #27-9421-01) in blocking buffer to the final dilution recommended by the manufacturer. Add 100 µl of diluted conjugate was added to each well and incubate at room temperature for 1 hour with agitation.

Step 17: Repeat Step 12.

Step 18: Add 100 µl of substrate solution (TMB) to each well, and incubated for 10–60 minutes at room temperature with gentle agitation.

Step 19: Transfer the coloured solution to a flat bottomed ELISA plate and an equal volume of sulphuric acid.

Step 20: Read the plates using a micro-plate reader set at 405–415 nm. Compare the signal for each phage concentration, with and without target protein.